Loughborough University

This item was submitted to Loughborough's Institutional Repository (https://dspace.lboro.ac.uk/) by the author and is made available under the following Creative Commons Licence conditions.

creative commons

COMMONS DEED

Attribution-NonCommercial-NoDerivs 2.5

You are free:

- to copy, distribute, display, and perform the work

Under the following conditions:

BY:

Attribution. You must attribute the work in the manner specified by the author or licensor.

Noncommercial. You may not use this work for commercial purposes.

No Derivative Works. You may not alter, transform, or build upon this work.

- For any reuse or distribution, you must make clear to others the license terms of this work.
- Any of these conditions can be waived if you get permission from the copyright holder.

Your fair use and other rights are in no way affected by the above.

This is a human-readable summary of the Legal Code (the full license).

Disclaimer

For the full text of this licence, please go to:
http://creativecommons.org/licenses/by-nc-nd/2.5/

DETERMINING IMPACT INTENSITIES IN CONTACT SPORTS

by

Felix Tsui

A Doctoral Thesis

Submitted in partial fulfilment of the requirements for the award of Doctor of
Philosophy of Loughborough University

September 2010

© by Felix Tsui, 2010

ABSTRACT

Determining Impact Intensities in Contact Sports

Felix Tsui, Loughborough University

Most sports Personal Protective Equipment (PPE) consist of varying levels of foam – more foam equals more protection. This has led to bulky, cumbersome PPE which restricts user movement. However, before existing PPE can be modified, their performance must be assessed and a baseline for necessary protection must be explicitly determined. This is a major limitation since current techniques for assessing PPE performance and impact intensity measurements from sport have used surrogate anvils and impactors which were not validated for the sports-related impact they tried to replicate. Through a series of independent studies, a better understanding of human impact response in sporting impacts was sought. This included investigating methods for improving the measurement of impact intensities in sports and the assessment of PPE performance.

Human impact response revealed that tensed muscle led to a significant increase in impact force but was associated with less perceived discomfort. At low impact intensities common to sport, the increased local stiffness helped to dissipate impact energy and reduce soft tissue compression. As previous anvils omitted this soft tissue response, modifications were made to a martial arts dummy, BOBXL, to increase its biofidelity. This anvil was validated using *in vivo* kicks and an impact force – impact velocity relationship. Using this validated anvil, existing methods of assessing PPE performance were evaluated. Current methods were found to create artificially comparable levels of force but did so by using an incorrect effective mass and impact velocity. In all tests, PPE performance was found to depend on weight providing evidence of the 'more protection, more foam' concept. As it is impractical to use *in vivo* kicks to assess PPE performance, kick kinematics were investigated to assess its variability in terms of the impact force – impact velocity relationship and its accuracy. This aided in the development of a mechanical kicking robot which could more properly assess PPE performance. This research was applied to the design of form-fitting, impact-mitigating sports PPE with the capability for integrated technology. Proposed amendments to the current methods of assessing PPE will help to develop better testing and better performing PPE in the future.

PUBLICATIONS

Journal Papers:

Pain, M.T.G., Tsui, F., and Cove. S. (2008). *In vivo* determination of the effect of shoulder pads on tackling forces in rugby", *Journal of Sports Sciences*, 26 (8), 75-82.

Conference presentations:

Tsui, F. & Pain, M.T.G. (2009). Effects of testing techniques on the performance of chest protectors in Tae Kwon Do. *Proceedings of the* 33rd *Annual Meeting of the American Society of Biomechanics*, The Pennsylvania State University, USA.

Tsui, F. & Pain, M.T.G. (2009). *In vivo* measurements required for assessing the effectiveness of personal protective equipment in Tae Kwon Do." *Proceedings of the 4th European Conference on Protective Clothing (ECPC) and Nokobotef 9*. Arnhem, Netherlands.

Tsui, F. & Pain, M.T.G. (2008). The effects of muscle tension on human biomechanical response and perceived impact intensity. *Proceedings of the 4th North American Congress on Biomechanics,* Ann Arbor, USA.

Tsui, F. & Pain, M.T.G. (2008). The effects of muscle tension on human impact response and injury. *Proceedings of the Biomechanics Interest Group of the British Association of Sport and Exercise Sciences*, 24, University of Wales Institute, Cardiff, p. 40.

ACKNOWLEDGEMENTS

First and foremost, I would like to thank my supervisor, Dr Matthew Pain, for his guidance, expertise and, most of all, his patience. I could not have asked for a better mentor and truly appreciate all of his efforts.

I would also like to recognise Prof Roy Jones whose thoughts, advice and humour have been invaluable during my research. In addition, I would like to thank everyone associated with the SCUTA project without whom this research may have never been made possible: the lecturers: Richard, Chris T, Andy, Jon, James F; Research Associates: Dan P, Chris H, Ruth; and fellow researchers: James C, James W, Paul W and James B-C.

I would also like to express my gratitude towards the Sports Biomechanics and Motor Control Group, past and present, for their camaraderie and humour: Matt, Fred, Mike, Mark, Steph, Sam, Mikael, Felipe, Dave J, Emma R, Chris M, Helen, Idafe, Jono, Pete, Martin, Neale, Phil, Monique, Michael, Andy, Behzat, Dave B, George, Sarah, Jo, Bob, Lesley, Jon, Dave H, Akiko, Paul, Ciaran, Mark and Adam. An honourable thank you also goes out to the researchers of the STI group, past and present, who have always accepted me as one of their own.

Last, but not least, I would like to thank my family and friends for their unwavering support, faithful love and endless laughter throughout my time here.

DEDICATIONS

To my family and my friends.

TABLE OF CONTENTS

ABSTRACT i
PUBLICATIONS iii
ACKNOWLEDGEMENTS iv
DEDICATIONS v
TABLE OF CONTENTS vi
TABLE OF FIGURES xi
TABLE OF TABLES xiv

Chapter 1 Introduction 1
- 1.1 Chapter Overview 1
- 1.2 Research Motivation 1
- 1.3 Background 2
- 1.4 Statement of Purpose 5
- 1.5 Research Questions: 5
- 1.6 Chapters Summary 8

Chapter 2 Car Crash and Ballistics Literature Review 11
- 2.1 Chapter Summary 11
- 2.2 Anatomy 11
  - 2.2.1 Thorax 11
    - 2.2.1.1 Skeletal Structure 11
    - 2.2.1.2 Muscles 12
    - 2.2.1.3 Organs 12
  - 2.2.2 Abdomen 13
    - 2.2.2.1 Structure 13
    - 2.2.2.2 Muscles 13
    - 2.2.2.3 Organs 13
  - 2.2.3 Tibia 13
    - 2.2.3.1 Structure 13
    - 2.2.3.2 Muscles 14
- 2.3 Injuries 14
  - 2.3.1 Chest 15
    - 2.3.1.1 Injury Mechanisms 15
    - 2.3.1.2 Ribs 16
    - 2.3.1.3 Lungs 16
    - 2.3.1.4 Heart 17
  - 2.3.2 Abdomen 17
    - 2.3.2.1 Injury Mechanisms 17
    - 2.3.2.2 Organs 18
  - 2.3.3 Tibia 19
    - 2.3.3.1 Injury Mechanism 19
    - 2.3.3.2 Contusions 19
- 2.4 Experimental Models 20
  - 2.4.1 Human Volunteers 20
  - 2.4.2 Human Cadavers 20
  - 2.4.3 Animal Surrogates 22
  - 2.4.4 Mechanical Models 23

2.4.5 Computer (Mathematical) Models 24
2.5 Measurements 25
2.5.1 Acceleration 26
2.5.2 Force 26
2.5.3 Deformation 27
2.6 Injury Criterions 28
2.6.1 Abbreviated Injury Scale 28
2.6.2 Acceleration-Based 29
2.6.2.1 Thoracic Trauma Index (TTI) 29
2.6.3 Force-Based 30
2.6.4 Compression-Based 30
2.6.5 Velocity- and Compression-Based 31
2.7 Biomechanical Response 32
2.7.1 Biomechanical Response Corridors 33
2.7.2 Chest 33
2.7.3 Abdomen 35
2.7.4 Tibia 35
2.7.5 Influential Factors 36
2.7.5.1 Age 36
2.7.5.2 Loading Condition 36
2.7.5.3 Gender 38
2.7.5.4 Muscle Tension 39
2.8 Injury Tolerance Levels 41
2.8.1 General 41
2.8.2 Probit Analysis 43
2.8.3 Chest 43
2.8.3.1 Frontal 43
2.8.3.2 Lateral 44
2.8.4 Abdomen 44
2.8.5 Tibia 44
2.8.6 Influential Factors 45
2.8.6.1 Effect of Age 45
2.8.6.2 Loading Condition 47
2.8.6.3 Gender 49
2.8.6.4 Muscle Tension 49
2.9 Summary 50

Chapter 3 Impacts in Sports Literature Review 61
3.1 Introduction 61
3.2 Injuries in Sport 61
3.2.1 Cricket 62
3.2.2 Football (Soccer) 64
3.2.3 Tae Kwon Do (TKD) 67
3.3 Impact Intensities in Sport 69
3.3.1 Impact Measurement in Sports 69
3.3.2 Cricket 70
3.3.3 Football (Soccer) 71
3.3.4 Tae Kwon Do (TKD) 72
3.3.5 Boxing 73
3.3.6 Fight Science 75

3.4 Current Preventative Measures 75
  3.4.1 General 75
  3.4.2 British Standards 76
    3.4.2.1 Cricket – Batting Leg Pads and Chest Protector 76
    3.4.2.2 Football - Shin Guards 78
    3.4.2.3 Taekwondo – Shin Guards and Chest Protectors 78
    3.4.2.4 Criticisms of British Standards 79
  3.4.3 Cricket Batting Pad Performance 80
  3.4.4 Shin Guards Performance 81
  3.4.5 Trunk Protectors 82
3.5 Special Case Study: Commotio Cordis 83
  3.5.1 Overview 83
  3.5.2 Animal Surrogates 84
  3.5.3 Mechanical Models 85
  3.5.4 Prevention of Commotio Cordis 85
    3.5.4.1 Safety Baseballs 86
    3.5.4.2 Chest Protectors 86
3.6 Comparison of Impacts 87
3.7 Conclusion 93

Chapter 4 Equipment & Measurement Systems 94
4.1 Chapter Overview 94
4.2 Force Measurement Systems 94
  4.2.1 Kistler Force Plate 94
    4.2.1.1 General 94
    4.2.1.2 Calibration 95
  4.2.2 Tekscan 95
    4.2.2.1 General 95
    4.2.2.2 Calibration 98
  4.2.3 Custom Force Plate (CFP) 102
    4.2.3.1 General 102
    4.2.3.2 Calibration 103
4.3 Motion Analysis Systems 104
  4.3.1 Vicon 105
    4.3.1.1 General 105
    4.3.1.2 Calibration 106
  4.3.2 Phantom High-Speed Camera 106
    4.3.2.1 General 106
    4.3.2.2 Calibration 107
4.4 Summary 107

Chapter 5 Influence of Muscle Tension on Biomechanical Response 108
5.1 Chapter Overview 108
5.2 Introduction 108
5.3 Methods 112
  5.3.1 Subjects 112
  5.3.2 Trial Protocol 113
  5.3.3 Instrumentation 113
  5.3.4 Impactor Properties 114
  5.3.5 Impact and Rebound Velocity 115

- 5.3.6 Calculations and Statistics 115
- 5.3.7 Muscle Mass Estimation 116
- 5.4 Results 117
  - 5.4.1 Impactor Properties 117
  - 5.4.2 Impact Intensity Measurements 117
  - 5.4.3 Impact Characteristics 119
  - 5.4.4 Subject Normalisation 122
- 5.5 Discussion 125
  - 5.5.1 General 125
- 5.6 Conclusion 131

Chapter 6 Biofidelity of Human Surrogates 132
- 6.1 Chapter Overview 132
- 6.2 Introduction 132
- 6.3 Pilot Testing 135
- 6.4 Methods 136
  - 6.4.1 Trial Protocol 136
  - 6.4.2 Assessing Biofidelity 138
  - 6.4.3 Customised ATD Impacts 139
  - 6.4.4 Impact Velocity 140
- 6.5 Results 141
- 6.6 Discussion 146
- 6.7 Conclusion 150

Chapter 7 Evaluation of Hogu Performance 151
- 7.1 Chapter Overview 151
- 7.2 Introduction 151
- 7.3 Methods 154
  - 7.3.1 Introduction 154
  - 7.3.2 Method 1: British Standards (BStan) 154
  - 7.3.3 Method 2: Modified British Standards (MBS) 155
  - 7.3.4 Method 3: Competition 156
  - 7.3.5 Analysis 156
- 7.4 Results 157
  - 7.4.1 Method 1: BStan 157
  - 7.4.2 Method 2: Modified British Standards (MBS) 158
  - 7.4.3 Method 3: Competition 159
- 7.5 Discussion 161
- 7.6 Conclusion 164

Chapter 8 Determining Human Impactor Variation 165
- 8.1 Chapter Overview 165
- 8.2 Introduction 165
- 8.3 Methods 168
  - 8.3.1 General 168
  - 8.3.2 Trial Protocol 168
  - 8.3.3 Kick Trials 169
  - 8.3.4 Determining Kick Location & Consistency 170
  - 8.3.5 Kinematic Analysis of Kick 170
  - 8.3.6 Statistical Analysis 171

8.4 Results 171
  8.4.1 Impact Force & Velocity 171
  8.4.2 Impact Location 174
  8.4.3 Kick Consistency 175
  8.4.4 Kinematic Analysis of the Kick 175
8.5 Discussion 178
8.6 Conclusion 183

Chapter 9 Development of a Computer Simulation Model of an Impactor 184
9.1 Chapter Overview 184
9.2 Introduction to Kicking Models 184
  9.2.1 Mechanical Models of Soccer Kicks 184
  9.2.2 Mathematical Models of Martial Arts Kicks 186
  9.2.3 Chapter Aims 187
9.3 Mechanical Model of a Roundhouse Kick 187
  9.3.1 Overview 187
  9.3.2 Mechanical Model Discussion 191
9.4 General Simulation Model Parameters 193
  9.4.1 Constraints from the Mechanical Model 193
  9.4.2 Computer Simulation Anvil 194
9.5 Single-Segment Model (*1-SM*) 195
  9.5.1 Design & Model Parameters 195
  9.5.2 Performance 196
  9.5.3 Discussion 196
9.6 Three-Segment Model (*3-SM*) 197
  9.6.1 Design & Model Parameters 197
  9.6.2 Performance 201
  9.6.3 Comparison: 1-SM and 3-SM 203
  9.6.4 Discussion 205
9.7 Conclusion 207

Chapter 10 Conclusion 208
10.1 Chapter Overview 208
10.2 Research Aims 208
10.3 Research Questions 209
10.4 Research Limitations 213
10.5 Future Directions 214
  10.5.1 Product Design Specification (PDS) 214
  10.5.2 Automated Scoring in TKD 215
  10.5.3 Multi-segment Kicking Robot 215

REFERENCES 216

APPENDIX A MEASUREMENT SYSTEMS SPECIFICATIONS 234
APPENDIX B SUBJECT CONSENT FORMS 244
APPENDIX C SOFT TISSUE RATIOS 250
APPENDIX D VICON BODYBUILDER CODE 251
APPENDIX E CALCULATION OF IMPACT ACCURACY 254
APPENDIX F CALCULATION OF RMSE, RESIDUALS AND 95% CIs 256

TABLE OF FIGURES

Figure 1.1	Work package interactions	2
Figure 1.2	Load-injury model	3
Figure 2.1	Transition in injury type as a function of compression and velocity of deformation	15
Figure 2.2	Injury mechanisms	16
Figure 2.3	Decay of muscle response after death	22
Figure 2.4	Lobdell model	32
Figure 2.5	Contributions of inertia, elastic and viscous resistances in forming biomechanical response from an external loading	34
Figure 2.6	Influence of loading condition on deformation at impact	37
Figure 2.7	Influence of loading condition on biomechanical response curves	38
Figure 2.8	Effect of shift and un-shifted corridors on the validity of response in ATDs	41
Figure 2.9	Compression and viscous tolerance as a function of impact velocity	43
Figure 2.10	Influence of age on rib fractures for a given force	46
Figure 2.11	Probability injury risk functions for 30- and 70-year olds	47
Figure 3.1	Models used to represent the kicking leg	73
Figure 3.2	Protection zones on a cricket leg guard	77
Figure 4.1	Tekscan set-up	96
Figure 4.2	Tekscan sensor with individual sensels	97
Figure 4.3	Tekscan calibration curves for 4-kg and 10-kg medicine balls	99
Figure 4.4	Calibration coefficient as a function of the number of impacts	101
Figure 4.5	95% CI for Tekscan sensor calibration	102
Figure 4.6	Custom Force Plate (CFP) linked to PCB signal conditioner routed to Vicon	103
Figure 4.7	Force transducer calibration curve	104
Figure 5.1	Influence of force and work required to deform the thorax as a function of chest deflection	110
Figure 5.2	Experimental set-up showing load cell, ankle strap, high speed camera and Tekscan	113
Figure 5.3	Sample frame taken from high-speed camera	114
Figure 5.4	Power curve equation required to determine energy required to deform the medicine ball	117
Figure 5.5	Average group impact force (± SD)	118
Figure 5.6	Average energy absorbed by the thigh at each drop height	118

Figure 5.7 Impact force and energy absorption as a function of perceived impact intensity 119
Figure 5.8 Representative trial from player 1comparing relaxed and tensed impacts 121
Figure 5.9 Perceived impact intensity as a function of muscle mass-to-length (MML) ratio 123
Figure 5.10 Force as a function of MML ratio at three different heights: 100, 130 and 160 cm 124
Figure 5.11 Theoretical curve for the relationship between force and MML in relaxed and tensed muscle 129
Figure 6.1 Front- and side-on view of BOBXL 134
Figure 6.2 Image from high speed camera (*left*) and normalised force as a function of impact velocity (*right*) 135
Figure 6.3 Set-up of the Vicon MX cameras 137
Figure 6.4 Set-up of MBOBXL 140
Figure 6.5 Regression curves from custom ATD impacts (*top*) and comparing these regression curves to in vivo impacts (*bottom*) 142
Figure 6.6 95% Confidence Intervals (CIs) for each *in vivo* trial 144
Figure 7.1 Blue confor CF45 insert hogu 154
Figure 7.2 Electromagnetic dropper 155
Figure 7.3 Set-up for each hogu evaluation method (left-to-right): British Standards, Modified British Standards (MBS) and Competion 155
Figure 7.4 Surface and transmitted forces for BStan test 157
Figure 7.5 Surface and transmitted forces for MBS test 158
Figure 7.6 Surface and transmitted forces for competition method for both players 159
Figure 8.1 Motion capture volume 169
Figure 8.2 Marker locations on the player’s leg, MBOBXL and the wall behind MBOBXL 169
Figure 8.3 Average normalised impact force as a function of velocity separated by kick style 173
Figure 8.4 Relationship of impact velocity and normalised impact force 173
Figure 8.5 Kick location for player 1 174
Figure 8.6 Average hip, knee, and ankle angles for each type of kick on separate plots 176
Figure 8.7 Average hip, knee and ankle angles for an average *hard* kick 177
Figure 8.8 Schematic showing relationship between joint angles and segments 177
Figure 9.1 Two mechanical models: Schempf et al. (1995) robot and STI robot 185
Figure 9.2 Model of thrust and swing kicks 186
Figure 9.3 CAD of TKD kicking robot 188
Figure 9.4 Interaction between kicking robot and anvil 190

Figure 9.5	CAD of mechanical anvil of torso	191
Figure 9.6	Computer simulation anvil	194
Figure 9.7	Plot of hip, knee and ankle joint angles for an average *hard* kick	201
Figure 9.8	Schematic showing relationship between joint angles and segments	201
Figure 9.9	Plot of hip and knee angles produced during a 16 ms^{-1} kick using the computer simulated kicking model	202
Figure 9.10	Schematic of 3-SM with anvil just prior to impact	202
Figure 9.11	FE-analysis of 1-SM and 3-SM	205

TABLE OF TABLES

Table 2.1	Abbreviated Injury Scale	28
Table 2.2	Stiffness in the AP and LM directions	36
Table 2.3	Comparison of thoracic stiffness in relaxed and tensed muscle	41
Table 2.4	Tibial injury tolerances chance of injury in 30- and 70-year olds	48
Table 2.5	Biomechanical response of frontal thorax	52
Table 2.6	Biomechanical response of lateral thorax	54
Table 2.7	Biomechanical response of frontal abdomen	55
Table 2.8	Biomechanical response of lateral abdomen	56
Table 2.9	Frontal thoracic tolerances	57
Table 2.10	Lateral thoracic tolerances	58
Table 2.11	Frontal abdominal tolerances	59
Table 2.12	Lateral abdominal tolerances	60
Table 3.1	Injury incidence in cricket by body region	63
Table 3.2	Injury prevalence in cricket by position	64
Table 3.3	Football injury rates	66
Table 3.4	Football injury types as a % of all injuries	67
Table 3.5	Tae Kwon Do (TKD) injury rates	68
Table 3.6	Injuries identified at the 2006 UK TKD Championships	69
Table 3.7	Reduction in cricket ball speeds from release	70
Table 3.8	Impact forces measured in TKD	72
Table 3.9	Impact velocities in TKD	73
Table 3.10	Impact forces measured in boxing	74
Table 3.11	Fight Science impact force measurements	75
Table 3.12	Maximum transmitted forces for the let guard and chest protector in cricket	77
Table 3.13	Testing conditions for protectors in TKD	79
Table 3.14	Reduction in peak force and deceleration from soccer shin guards	82
Table 3.15	Summary of tibial impacts	89
Table 3.16	Comparison of impact forces in the chest and abdomen	90
Table 3.17	Summary of impact velocities used in automobile, ballistics and sport impacts	92
Table 4.1	Sensel dimensions	97
Table 4.2	Regression calibration coefficients from repeated impacts	101
Table 5.1	Increase in stiffness from muscle tension	109
Table 5.2	Summary of athletes	112
Table 5.3	Ratios used for muscle mass estimation	116
Table 5.4	Impact characteristics at each drop height and separated by muscle condition	120
Table 5.5	MVI and drop height variation	120
Table 5.6	Subject inertial parameters and two correction factors	122

Table 5.7	Bone, fat and muscle mass for 15% fat	123
Table 5.8	Summary of impacts for player 1	127
Table 6.1	Breakdown of impact conditions with anvils and impactors defined	137
Table 6.2	Summary of forces and velocities for *in vivo* and custom ATD trials	141
Table 6.3	RMSE values obtained from comparing custom ATDs to *in vivo* impacts	142
Table 6.4	Residuals obtained from comparing custom ATDs to *in vivo* impacts	143
Table 6.5	Significance values for the comparison of contact times (CTs) between custom ATD and *in vivo* impacts	145
Table 6.6	Significance values for the comparison of Times to Peak Force (TTPFs) between custom ATD and *in vivo* impacts	145
Table 7.1	Summary of commercially available hogus	152
Table 7.2	Confor foam material properties	154
Table 7.3	Summary of both athletes	156
Table 7.4	Significance values from repeated measures ANOVA comparing hogus in MBS test	158
Table 7.5	TTPF and CT for each hogu in BStan and MBS methods	159
Table 7.6	Impacts summary for athlete 1	160
Table 7.7	Impacts summary for athlete 2	160
Table 8.1	Athlete summary	168
Table 8.2	Summary of impact characteristics for each athlete showing velocity, force, CT, TTPF	171
Table 8.3	Statistical comparison between each style of kick in terms of impact velocity, force, CT and TTPF	172
Table 8.4	Mean kick location for each athlete	174
Table 8.5	Kick consistency for each athlete separated by kick style	175
Table 9.1	Inertial parameters for 50th and 95th percentile male	189
Table 9.2	Interaction between kicking robot and anvil	190
Table 9.3	Model parameters for 1-SM model	196
Table 9.4	Joint angles and overall change in knee angle for *hard* kicks	198
Table 9.5	Summary of joint angular velocities from literature	199
Table 9.6	Component characteristics for the 3-SM	200
Table 9.7	Comparison of impact forces and TTPF between 1-SM and 3-SM	204

Chapter 1

Introduction

1.1 Chapter Overview

The motivation for this research and its applications to industry are first presented. A background into sports impact injury, its causal factors and reasons for further study into the roundhouse kick are then examined. Research questions are then posed with brief explanations into its importance and how they will be investigated. The chapter concludes with a chapter-by-chapter summary which addresses the manner in which these questions were answered.

1.2 Research Motivation

SCUTA (latin for '*shield*') is a multi-disciplined project which aims to design custom-tailored, impact-mitigating Personal Protective Equipment (PPE) garments for sport. It considers current PPE garments to be over-engineered and cumbersome while, at times, offering sub-optimal protection. As such, its main motivations are attributed to:

1. Changes in rules and regulations in specific sports which necessitate the use of PPE;
2. A lack of knowledge into how existing PPE can affect the comfort and mobility of an athlete;
3. A lack of understanding into the levels of protection required to prevent an acute impact injury; and,
4. Recent advances in rapid manufacturing that allow shapes of different sizes, strength and flexibility to be easily constructed.

Through direct research of these key areas, in conjunction with work on human conformal data and computer simulation, it was hoped that many of the shortcomings that exist within current PPE could be eliminated. Six individual but inter-linking work packages (WPs) were developed to address these specific areas (Fig 1.1). While there are many sports (and many body parts within a given sport) which required PPE, SCUTA focused mainly on chest protectors in Tae Kwon Do, batting pads in cricket and shin guards in Association Football (FA).

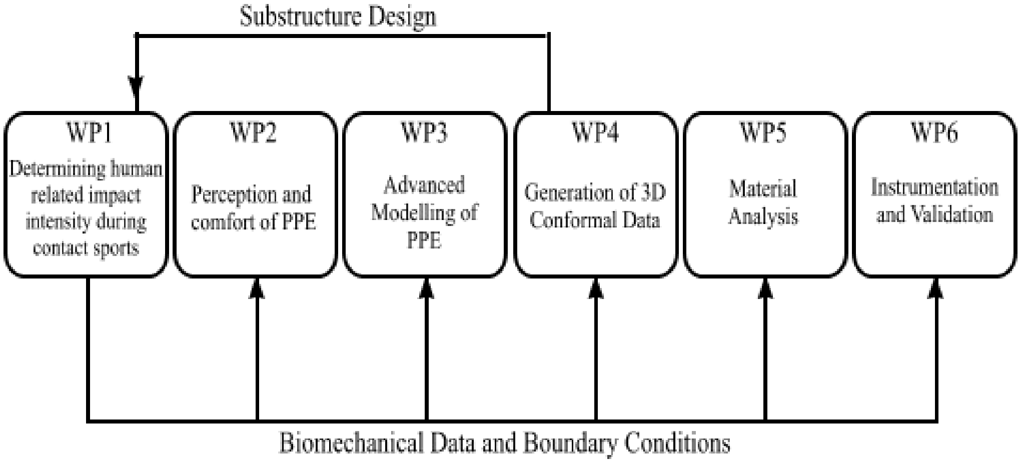
Substructure Design
WP1
Determining human related impact intensity during contact sports
WP2
Perception and comfort of PPE
WP3
Advanced Modelling of PPE
WP4
Generation of 3D Conformal Data
WP5
Material Analysis
WP6
Instrumentation and Validation
Biomechanical Data and Boundary Conditions

Figure 1.1 Work package interactions for the SCUTA Project. WP1 provides the underpinning for all the other WPs.

These WPs combine recent advances in materials and rapid manufacturing, along with data on human movement, geometry, impact response and comfort, to design and possibly construct an optimal piece of protective equipment. This technique allowed for custom-tailored, form-fitting and impact resistant PPE. The research conducted within this document is an investigation into WP1 entitled, "*Determining human-related impact intensity during contact sports*". More specifically, it deals with the identification and protection of injuries in the human anvil during contact sport; that is, the main focus was on the player being impacted and not the player delivering the impact.

1.3 Background

Injuries in sport are typically the result of overuse and/or acute overload (McIntosh, 2005). While overuse injuries are very common, the risk for severe damage is much higher in accidental or acute-overload injuries. These latter injuries occur in sports such as ice hockey, American football and lacrosse which feature high-mass, low-velocity, body-to-body collisions or low-mass, high velocity, object-to-body impacts (Caswell & Deivert, 2002). In certain cases, these sports injuries are similar to those observed in car crash or blunt ballistic impacts. From an injury prevention perspective, this is advantageous since knowledge gained from car crash and ballistic impacts research can provide insight on impact injuries in sport. This field of research is known as injury biomechanics.

Injury biomechanics focuses on understanding injury processes and developing ways of reducing or eliminating structural and functional damage that occur during impact through the identification of their injury mechanisms (Viano et al., 1989). Its study aids the development of specific methods for preventing injury, whilst helping to improve the overall understanding of human tolerances to impact (McIntosh, 2005). In the automotive industry, it has led to the development of more compliant steering wheels, improved force-limiting seat belts, and more effective side and front airbags. Applying this strategy to sports, though, can lead to a modification in playing rules, playing surfaces, equipment (i.e. balls, bats) and PPE. While rules, surfaces and equipment generally remain unchanged, the design and function of PPE is constantly evolving. As such, it is an area which deserves more attention as it can mitigate the causation of injuries.

In general, when a body is subjected to an external loading, it deforms and triggers a biomechanical response which varies between and within people. If the response is not ‘strong’ or ‘fast’ enough, an injury tolerance level will be exceeded leading to a specific injury which is a function of its injury mechanism. The stages of injury causation or the factors that govern its severity are outlined in the Load-Injury Model (Fig 1.2).

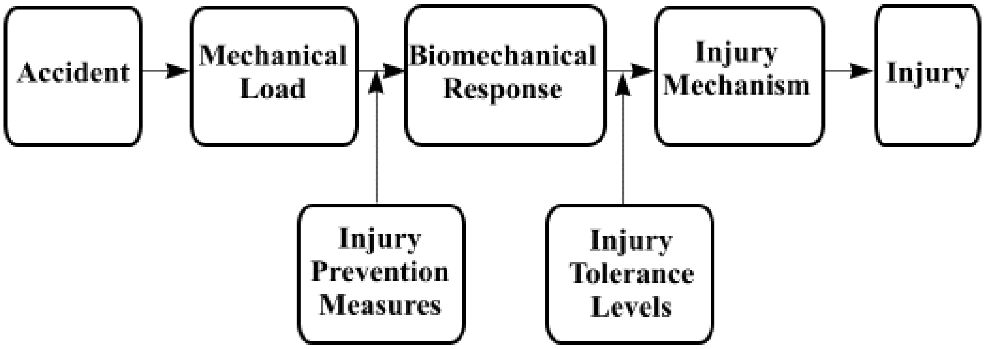

Figure 1.2 Load-Injury Model (Wisman, 2001).

Identifying injury mechanisms and the injuries they cause may be a relatively simple task, but assigning meaningful and relevant mechanical values or variables to describe the other parameters in the Load-Injury Model are not. This is an inherently difficult task because the body does not respond in a predictable manner; it is composed of anisotropic, non-homogeneous structures whose material properties and responses vary between subjects and across impact conditions. As such, a single variable is unable to describe the human impact response or predict the onset of all injuries. In fact, variables which have been used in past research include, but are not limited to: force, rate of force development, deformation, rate of deformation, contact time, pressure, energy absorption and/or rate of energy absorbed. Therefore, it is more relevant to talk in terms of an '*impact intensity*' which refers to an impact's positive correlation for injury risk from a specific impact (i.e. greater intensity implies higher injury potential) measured using any mechanical variable. As such, it is important to collect data on as many variables as possible, in a given impact, so that a reliable correlation using any of these variables may be made to the injuries caused.

The SCUTA project outlined three areas for PPE improvement, but this research will be based on Tae Kwon Do with specific focus on the roundhouse kick. While there has been limited research into the study of injury potential of a roundhouse kick (Serina & Lieu, 1991, Chuang & Lieu, 1992), there has not been any research into the design and development of chest PPE garments (i.e. hogus). Instead, previous studies in martial arts have focused on differentiating between types of kicks (Tsai et al., 1999; Kong et al., 2000; Lan et al., 2000; Kim & Hinrichs, 2006) and how to maximise velocity and/or force in each (Sorensen, 1996; Boey & Xie, 2002; Pedzich et al., 2006; Falco et al., 2009; O'Sullivan et al., 2009). A common issue exhibited within these studies and similar sports impact research (e.g. boxing) was the absence of validation for the surrogate anvils used to mimic the human body response and, as a result, its biofidelity was not assessed. This lack of validation was also present when rigid masses were used to represent the kicking leg in TKD (BS EN 13277-1: 2000, BS EN 13277-3: 2000) or soccer (Philippens & Wismans, 1989; Bir et al.. 1995; Francisco et al., 2000 Ankrah & Mills, 2002, 2003a). Using impactors and/or anvils of low biofidelity were likely to produce inaccurate measures of impact intensity leading to incorrect conclusions about potential injury risk and PPE performance. This implied that very little was actually known about the threats posed from a roundhouse kick and how to properly protect the human body.

1.4 Statement of Purpose

The aim of this research was to increase the biofidelity – the ability to mimic human impact response under a set of similar impact conditions – of current testing techniques used to measure impact intensities, determine injury potential and assess PPE performance for roundhouse kicks. With these techniques, more meaningful insight into the human impact response can be obtained, the variability of roundhouse kicks can be assessed and modifications in PPE design can be proposed. Past research from automobile, ballistics and sports impacts have helped identify and summarise general injury tolerances, injury mechanisms and potential injuries to the abdomen and thorax. In this research, in-depth investigations of *in vivo* impacts are used to assess the influence of kick kinematics and kinetics and anvil impact properties on impact intensities and biomechanical response. These parameters are then applied to the design of mathematical and mechanical impactor and anvil surrogates to aid in the design and evaluation of PPE. Ultimately, whilst the current anvils and impactors may require improvements to their design, it is only the impact intensity of the anvil which is of primary concern for the prevention of injury.

1.5 Research Questions:

Q1. *How do the impact properties of an anvil change its biomechanical response and predictions for injury?*

Previous studies on roundhouse kicks have all used different anvils to measure impact responses. This has made it difficult to compare results across studies as the response was primarily dependent on the load-transfer mechanisms of each anvil. This partially explained the wide range of impact intensities measured despite the small range in impact mass and velocity. As these anvils were not typically validated to human impact response, it was also likely that the conclusions about injury risk and causation were incorrect. This was further exacerbated by not only the differences between individuals, but also within individuals since their level of muscle tension also likely affected the impact properties, injury risk and injury tolerance of the human anvil. Therefore, the effect of muscle tension should also be investigated and accounted for when validating surrogate anvils in future studies. This research should lead to more accurate measures of biomechanical response, an improvement in the identification of injury predictors and enhance future PPE development.

Q2. *What effect does test equipment (i.e. impactor, anvil) have on assessing Personal Protective Equipment (PPE) performance?*

At present, there have not been any studies conducted to assess the performance of chest protectors in TKD. British Standards tests specify the use of a rigid impactor and rigid anvil which sandwich each individual PPE garment. The importance of a high biofidelity anvil was already discussed in Q1, but the biofidelity of using a single rigid mass to represent the kick has yet to be assessed. It is assumed that this mass is of low biofidelity since it likely does not mimic the co-ordination of joint and muscle activation in the leg to create the correct effective mass at impact. Furthermore, the impact velocity ($\sim 2.5\ \mathrm{ms}^{-1}$) used for this mass is much lower than the kick velocities reported within the literature. However, this assumption needs to be verified and its implications must be discussed. Furthermore, additional parameters are required to assess PPE performance since its current measure, force attenuation, has only been shown to capably predict skeletal injury and not soft-tissue injury. Therefore, an in-depth investigation should lead to a more suitable assessment of PPE performance and an improved ability to protect against injury in the future.

Q3. *How can the surrogate anvil and/or impactor be improved to produce an impact of higher biofidelity?*

Through the investigation of Q1 and Q2, the shortcomings of existing surrogate anvils and impactors should be evident. Impactors can be improved by obtaining the proper impact properties of the foot, correct effective mass at and during contact, and the correct impact velocity. Similarly, correct effective mass at impact and load-transfer properties will lead to improvements of the anvil. Improvements in impactor and anvil can be achieved by first obtaining measurements during *in* *vivo* impacts (i.e. human impactor and human anvil). These responses can then be compared to *human* impacts delivered on surrogate anvils and modifications to these anvils can be proposed. The modified surrogates are then re-evaluated against the original *in vivo* impacts until a suitable anvil is constructed. These *in vivo* tests will also provide increased knowledge on the kicking leg, such as its kinematics, to improve strategies for developing a computer and mechanical model of the kicking leg can be obtained. High biofidelity surrogate impactors and anvils are advantageous since more rigorous testing can be conducted which may lead to improved injury prevention through optimised PPE designs. Moreover, it is generally impractical to use human impactors and anvils to provide information about either injury causation or PPE performance for ethical and repeatability issues.

Q4. *Can the impact intensity of a roundhouse kick be obtained with non-invasive modes of measurement during competition?*

Currently, roundhouse kicks have been investigated using surrogate anvils to re-create competition-style kicks within a lab-setting. This method can be effective at producing a range of impact intensities observed within competition, especially when improved surrogate or human anvils were used. However, it did not provide a true measure of impact intensity for kicks which caused injury or scored points during competition. These thresholds were important for the prevention of injury, the consistency of the sport and in the development of future automated scoring systems. As such, a means for obtaining impact intensity non-invasively was necessary. With assistance from research conducted within WP6, it may be possible to embed sensors with sufficient technology into PPE garments. This would require impact intensity thresholds with sufficient spatial accuracy and sampling frequencies to be specified for each sensor which can be obtained from laboratory experimentation. This is a common technique that has been employed in the development of helmets in American football and ice hockey. Alternatively, kinematic data from motion analysis systems may also display a high-strength relationship with these impact intensities. As kinematic data can be obtained non-invasively through video, this may provide another method for measuring impact intensity during competition.

1.6 Chapters Summary

The following provides a chapter-by-chapter summary of the research conducted.

Chapter 2: Car Crash and Blunt Ballistics Literature

A review of the relevant anatomical regions and the injuries and injury mechanisms caused by car crash and ballistics impacts within these regions is conducted. The main variables and criteria used for predicting injury are identified. A summary of measured biomechanical responses and injury tolerances in frontal and lateral impacts to the chest and abdomen are presented and the factors which influence the determination of both are discussed.

Chapter 3: Literature Review: Sports Impacts

The most common injuries within cricket, soccer and TKD are identified. Impact intensities representative of the impacts in these sports are summarised. A review of PPE performance (i.e. batting pads, shin guards and chest protectors), including the testing guidelines set by British Standards and a case study on Commotio Cordis are presented. Impact forces measured within the car crash, ballistics, and sports industry are compared for the tibia, chest and abdomen, as are the impact velocities used in these studies.

Chapter 4: Equipment and Measurement Systems

A summary of measurement systems used in each experimental chapter are presented with a brief description of its technology and calibration methods. Where applicable, the manner in which each system is used and/or modified to help obtain *in vivo* measurements was discussed. These reviews for each system are split into two categories: force and motion analysis.

Chapter 5: Influence of Muscle Tension on Biomechanical Response

This chapter examines the influence of muscle tension on the human biomechanical response. A compliant medicine ball is dropped on the thigh of relaxed and tensed muscle from different heights while various intensity measures are measured. These are then compared to subjective ratings of impact intensity and potential pain mechanisms to infer the risk of injury. Inertial parameters of each participant are obtained to investigate the variability in impact intensity despite the use of a single impactor. Implications for future surrogate anvil design are discussed.

Chapter 6: Biofidelity of Human Surrogates

A review of past anvils or Anthropometric Test Devices (ATDs) is made and the importance of developing a high-biofidelity model is discussed. After pilot testing, an existing martial arts training device is modified to create three models and impacted with roundhouse kicks from four separate athletes. The impact response of each model is compared to the intensity measured from *in vivo* impacts using a human anvil to determine the model of highest biofidelity.

Chapter 7: Evaluation of Hogu Performance

An overview of commercially available hogus is presented and the techniques used to assess its viability as a protector are outlined. Four separate hogus are tested using three techniques: a *British Standards* method, a *Modified British Standards* method which increased the biofidelity of the anvil, and a *Competition* method which couples *in vivo* kicks with the high-biofidelity anvil. Hogus are found to be sensitive to the testing type and that the implications of these findings on the assessment of hogu performance are discussed.

Chapter 8: Determining Human Impactor Variation

The importance of a consistent impactor is discussed. The mechanics behind the roundhouse kick and other relevant kicking literature are reviewed. Nine athletes performed three variations of the front roundhouse kick (hard, fast and consistent) to develop relationships between variables and to assess the variation in kick performance. While certain styles of kick are shown to be generally more consistent, rationale for the development of a more consistent surrogate anvil are discussed.

Chapter 9: Development of a Mathematical and Mechanical Kicking Model

A review of past mathematical and mechanical kicking models is conducted. A description of the models to be developed is presented. Inertial, kinematic and kinetic parameters are summarised from performances in previous chapters. Parameters for mechanical components are obtained by matching model performance to human performance. Validation of the surrogate anvil is also performed and the results are discussed.

Chapter 10: Conclusion

A summary of the major aims and findings, with specific reference to specific experimental chapters, from this research is presented. The applications of this research to industry are discussed. Future areas of work resulting from this research are outlined.

Chapter 2

Car Crash and Ballistics Literature Review

2.1 Chapter Summary

The anatomy for the thorax, abdomen and tibia is presented. Injuries and their associated injury mechanisms caused by car crash and ballistics impacts are discussed. Models and mechanical variables used to determine biomechanical responses and injury tolerances – in addition to the factors which influence their measurement – resulting from these impacts are reviewed. The chapter concludes with a summary of studies which assessed the biomechanical response and injury tolerances for the frontal and lateral regions of the thorax and abdomen and the tibia.

2.2 Anatomy

All tissues within the human body are visco-elastic, non-linear and anisotropic materials whose response are dependent on the amplitude, rate and direction of loading. As such, it is vital to identify the anatomy of the thorax, abdomen, and lower leg to understand the impact response in each region.

Skin covers the entire body and helps hold the underlying muscles in place, whilst protecting against superficial injuries such as cuts. Below its surface, soft tissues such as muscle and fat help protect the skeletal system and provide a solid barrier to guard the body's vital organs in the head, thorax and abdomen. Overall, human impact response is a function of the underlying soft (muscles, organs) and hard tissues (bones) and the interaction between them.

2.2.1 Thorax

2.2.1.1 Skeletal Structure

The thorax or chest is part of the axial skeleton, which joins the bones that lie along the axis of the body's midline. It sits below the clavicles and just superior to the diaphragm. Twelve pairs of ribs articulate posterior to the body of the thoracic vertebrae, ten of which attach to the sternum's anterior, forming the thoracic cage. Its size depends on the rib's curvature (i.e. costal angle), length, shape and orientation, all of which vary from superior to inferior providing the thorax with variable mechanical properties depending on its rib level (Chapon, 1984). The role of the ribcage is to protect and provide space for vital structures whilst facilitating lung and diaphragm function (Nahum, 1973).

Each individual rib features a counter-clockwise longitudinal twist while its curvature has been found to vary along its length, with larger curvatures found posteriorly (Mohr et al., 2007). Costal (hyaline) cartilage attaches the first to seventh ribs (*true* ribs) directly to the sternum, while the cartilage of the eighth through to tenth ribs (*false* ribs) connects to the cartilage of the seventh rib. The cartilage of the two most inferior ribs is without sternal attachments.

2.2.1.2 Muscles

Like most flat bones, the ribs provide considerable protection and extensive areas for muscle attachments. Three functional muscle groups originate or insert on the ribs: *Anterior Thoracic*, *Erector Spinae* and the *Scalenes* muscles. The deepest layer of chest muscle, the external and internal intercostals, run at right angles to each other and connects the ribs together allowing for opposite actions during breathing. Each act to either contract or relax the diaphragm, which provides the power for breathing and originates at the sternum.

2.2.1.3 Organs

Organs in the thorax are critical due to their important roles within the respiratory and circulatory systems. The thoracic cage is divided into three separate cavities: the pericardial cavity, which surrounds the heart, and two pleural cavities encasing the lungs. The fluid within these cavities reduces friction and allows the viscera to slide during movements such as breathing. Whilst the lungs occupy the left and right side of the thoracic cavity, the mediastinum, which contains the heart, esophagus, trachea, thymus and several large blood vessels, is positioned in the centre. The sternum lies directly in front of the heart providing maximal protection.

2.2.2 Abdomen

2.2.2.1 Structure

Similar to the thorax, the abdomen houses vital internal organs, but is considered to not have a bony skeleton. Anatomically, the diaphragm separates the inferior thoracic region from the superior abdominal cavity. However, since the diaphragm is not flat, there is an overlap between cavities as organs of the abdomen are protected by the most inferior ribs. The lower abdominal cavity is bordered by the pelvic bones.

2.2.2.2 Muscles

The abdomen relies on four pairs of muscles to protect and contain the abdominal viscera. The external oblique, internal oblique and transversus abdominis extend in different directions forming three layers of muscle around the abdomen. The fourth layer, the rectus abdominis, is the most anterior and spans the entire length of the abdominal wall. Abdominal muscles of greater cross-sectional area offer more protection.

2.2.2.3 Organs

The organs of the abdomen are either hollow or solid. Hollow organs have large cavities relative to their size and are air-filled and include the bladder, stomach, intestines and appendix. In contrast, solid organs have fluid-filled vessels (i.e. blood) and include the liver, kidneys and spleen. Whilst some of these organs are part of the urinary tract, their main function is in the role of digestion. The liver and diaphragm protect the gall bladder and pancreas and are protected laterally by the overlapping false ribs of the thoracic cage. Other organs in the abdominal cavity include the spleen and small and large intestines. These organs rely on muscle for support and protection as this region lacks a skeleton.

2.2.3 Tibia

2.2.3.1 Structure

The tibia, or shin bone, is the larger and more medial bone of the lower leg which bears the weight of the body. The tibia articulates with the femur proximally forming the tibiofemoral (knee) joint and distally with the medial malleolus of the talus bone. The fibula runs parallel to the tibia and attaches laterally on both of its ends. The tibia lacks a prominent soft tissue layer on its anterior face and is therefore not afforded much natural protection.

2.2.3.2 Muscles

The muscles covering the anterior leg are similar, in function, to the muscles of the forearm. The four anterior lower leg muscles combine to dorsiflex the foot at the ankle joint and extend the phalanges. The muscles run just laterally to the tibia and do not offer protection to the most anterior part of the leg.

2.3 Injuries

Injuries occur when tissues are deformed past their recoverable limit and are the result of one or more injury mechanisms. These mechanisms are the factor(s) which most consistently produce a specific type of injury as obtained through hypothesis-testing (King, 2000). In general, the elastic stiffness protects the chest from crush injuries at low velocities, whilst inertial and viscous properties determine the force and deformation developed in high-speed impacts (Viano & King, 2000). Moreover, as deformation rates increase, the contributions of compression to injury decrease and the injury severity is governed primarily by the deformation velocity (Fig 2.1). In sports though, impacts rarely occur at very low deformation rates and thus injury due purely to crushing is rare. Instead, impacts from kicks in Tae Kwon Do or soccer are more prone to viscous injury, whilst projectiles in ball sports (i.e. baseball or cricket) may lead to blast injury. The close proximity of internal organs in the chest and abdominal region also suggest that not only are multiple injuries possible in a single loading, but the impact responses would be difficult to determine. This change in injury mechanism with increasing deformation velocity is discussed further in the next section.

Figure 2.1 Transition in injury types for crushing, viscous and blast injury (p=0.50) in terms of deformation velocity and compression (Lau et al. (1986).

2.3.1 Chest

2.3.1.1 Injury Mechanisms

Chest trauma is especially dangerous due to the vital organs located in this region (King, 2000) and is categorised as “blunt” or “penetrating”. Penetrating injuries are caused by high-energy impacts which load the body past their tolerances in very short contact times. In contrast, blunt impact injuries vary with loading rate and are the result of three following injury mechanisms.

At low loading rates (< 3 ms^{-1}), injury is caused by deformation or crushing of the rib cage when elastic tolerances are exceeded reducing the distance between the ribs and spine forcing the underlying organs to forcefully compress or shift (King, 2000). This can cause internal organs and vessels to be contused or burst and supporting ligaments to tear as organs become displaced (Fig 2.2a).

In medium velocity impacts (3 – 30 ms^{-1}), viscous injuries become more prominent. These occur when a shock load exceeds the viscous tolerance and transfers significant kinetic energy to the underlying organs. These occur as a function of the magnitude of compression and the rates of deformation and internal injuries can occur before maximum deflection is achieved or in the absence of skeletal injury (Fig 2.2b).

In high speed impacts (> 30 ms^{-1}), inertial loads cause blast injuries. This causes tearing of internal structures due to significant body deceleration or through the acceleration of internal organs that is greater than the acceleration of the body (Fig 2.2c). In BABT, energy is transferred at contact by a short duration stress wave which propagates through the armour or the bullet penetrates the armour causing large deformations (Grimal et al., 2004). Giacobbe et al. (1997) proposed that if the dynamic hardness of the impactor is below the natural chest wall frequency, the bulk of impact energy would be transferred into vibration of the internal organs, thus exciting the internal soft tissues into resonance causing thoracic injury (Nicholls et al., 2004). In the most extreme case, high-speed blunt impacts (i.e. baseballs) can cause the heart to go into ventricular fibrillation causing death in the majority of cases (King, 2000).

Figure 2.2 Injury Mechanisms: (a) Compression (Crushing); (b) Viscous Shock; (c) Inertial (Acceleration).

2.3.1.2 Ribs

Rib fractures are common injuries in thoracic trauma and occur when the amount of bending in the rib exceeds its tolerance. They generally originate at the point where the greatest force is applied, but may also fracture at their weakest point – the site of the greatest curvature just anterior to the costal angle (Chapon, 1984). The failure of ribs (and other bones) was also thought to be strain-controlled as lower failure strains can reduce its energy absorption capacity (Stitzel et al., 2004). When at least four consecutive ribs are fractured at two points, a segment of the chest wall “floats” causing a condition known as a ‘flail chest’. In ‘open’ fractures, exposed ends of bones can also lacerate or rupture the underlying vessels which can lead to a loss of blood into the thoracic cavity.

2.3.1.3 Lungs

Injuries to the lungs are very frequent in chest trauma as it occupies a large area of the thorax. The two most severe injuries are pneumo- and hemo-thorax. Pneumothorax occurs when the visceral pleura is ruptured allowing air to penetrate the pleural cavity during inhalation. In severe cases, air enters the pleural cavity but cannot escape during expiration. This creates an increased interpleural pressure leading to a deviation of the mediastinum and disturbing ventilation in the other lung (Chapon, 1984). Therefore, the lungs begin to progressively deflate. In contrast, the disruption of blood vessels causes hemothorax leading to blood accumulation in the pleural cavity, blood loss and loss of respiratory capacity through decreased lung expansion (Nahum, 1973). Of the two, hemothorax is considered to be much more severe.

Other common injuries include contusions and lacerations. In general, contusions were more common than fractures and sometimes occurred in the absence of rib fractures (Chapon, 1984). In contrast, lacerations were most often produced from the penetration of a broken rib fragment, but also occurred from bursting due to instantaneous pressure changes or when the lung was compressed followed by forceful exhalation post-impact.

2.3.1.4 Heart

The difficulty in identifying heart injuries was that they could occur without sternum or rib fractures (Lau & Viano, 1988). In severe impacts, the sternum may push into the heart causing cardiac rupture and lacerations particularly to the aortic vessels which may lead to rapid and fatal losses in blood volume. As the space between the sternum and spine is small, the heart may also rapidly displace causing tears in points of attachment such as arteries and ligaments. The right ventricle was also found to be at risk due its position directly behind the sternum and its thin myocardial wall (Chapon, 1984). When an impact has sufficient energy to bruist the heart, direct myocardial contusion can damage the electrical conducting system of the heart (Nahum, 1973). This can cause ventricular fibrillation, a defective heart rhythm, in the form of Commotio Cordis.

2.3.2 Abdomen

2.3.2.1 Injury Mechanisms

As the abdomen is not encased by a skeletal cage, the range of injuries caused by blunt trauma are greater due to the lack of ribs, the dynamic response of the many organs in this small region and the low friction between them (Snyder, 1973). This may lead to higher deformations at the site of impact. Increased compression of underlying organs can cause a dangerous pressure build-up which bursts or ruptures organs. This may also cause high accelerations of the abdominal viscera which forcefully stretch the ligaments until they potentially tear or shear. In seat-belt loads, a phenomenon known as 'submarining' can occur where the belt presses into the abdominal cavity but does not puncture the organs.

Injury mechanisms caused by blunt trauma depend on the impact intensity, impact location, overlying muscle layers and on the fullness of the organs at the time of impact (Walt & Wilson, 1973). The actual organ location at the time of impact may influence the severity as well; e.g., if the organ rests against the spine, it is more likely to experience a crushing injury or may be afforded more protection if underneath the ribs. This has made it very difficult to obtain consistent responses and accurately predict the injury potential of a given impact. In frontal impacts, the main impactor is the seat belt in belted passengers and the steering wheel and airbag in unbelted passengers. In lateral impacts, injuries are mainly caused by the side structures of the vehicle deforming inwards toward the cabin with the liver and spleen the most vulnerable to injury (Stalnaker et al., 1973).

2.3.2.2 Organs

The majority of injuries to the abdominal organs are caused by blunt trauma. In general, hollow organs can withstand a higher load and are not injured as much as the solid organs (Stalnaker, 1973; Cavanaugh et al., 1986). However, injuries are more fatal in solid organs because of the higher blood supply as Bondy (1980) reported that 32% of all fatal injuries to the abdomen were accounted for by the kidneys, liver and spleen (Cavanaugh et al., 1996).

Due to its location within the abdominal cavity and its overall size, the liver has been found to be the most commonly injured solid organ. Liver injuries accounted for 20% of severe abdominal traumas, 30% of which result in mortality and 65% occurring in the right lobe (Chapon, 1984). It is prone to lacerations or punctures from the lower ribs when they are open fractured or compressed between the ribs or overlying abdominal muscles and spinal column (Walt & Wilson, 1973). This latter mechanism, on its own, can cause intrahepatic pressure in the liver to increase generating high tensile or shear strains (Viano, 2001).

2.3.3 Tibia

The majority of tibial injuries found in car crashes have been caused by axial loads transferred from the pedal to the tibia through the ankle. This resulted in tibial plateau and pilon fractures which lead to joint degeneration and long-term arthritis (Funk et al., 2004). Injuries to the tibia were considered less serious than in the chest and abdomen due to the absence of organs. However, its slenderness and lack of protection on the antero-medial side made it vulnerable to a high risk of infection in an open injury (Funk et al., 2004). Other injury risks include contusions and lacerations of soft tissue.

2.3.3.1 Injury Mechanism

The main injury mechanism in the tibia was found to be produced by bending or a sharp concentrated load causing a fracture when elastic tolerances were exceeded (Funk et al., 2002). A bending moment can occur either from an eccentric axial load or through direct trauma perpendicular to the orientation of the bone causing compressive stress on the loading side and tensile stress on the opposing side (Funk et al., 2002; Phillipens & Wismans, 1989). In direct impacts perpendicular to the length of the bone, loads to the middle third of the tibia were found to be more susceptible to fracture than its ends (Wong et al., 2010)

2.3.3.2 Contusions

Soft tissue contusions, or bruising, were found to be caused by localised damage to blood vessels leading to a leakage of blood into extracellular spaces (Cavanaugh et al., 1986). It was usually caused by blunt impact causing the underlying soft tissue to be damaged by compression and shearing forces (BS EN 13061, 2001). Unfortunately, contusions were not well understood and its severity was highly variable between subjects. There have been many attempts in the literature to develop a validated model for producing contusions in animals (Crisco et al., 1996; Sherman et al., 2005) and biomechanical models (Bush & Challener, 1989), but the results obtained from these models were inconclusive.

2.4 Experimental Models

Five separate models are used to study and develop the biomechanical response of the human body to impact. These are summarised in the following.

2.4.1 Human Volunteers

It is implicit that the best experimental models for studying and developing human impact responses are human volunteers. They allow researchers to consider the *in vivo* response, even if the impact was isolated to a body part or region, without having to make assumptions about skeletal structure, soft tissue composition and possible organ distribution and pressure. In addition, it allows the effects of muscle tone and pre-bracing on the dynamic skeletal, soft tissue and internal organ response to be studied *in vivo* (Wismans, 2001). However, impact forces on deformable surfaces are not easily measured making soft tissue impact responses difficult to obtain (Verriest, 1984). Moreover impact intensities are constrained, particularly to the sternum, to avoid rapid movement or crushing of the underlying organs. Therefore, potentially injurious impacts have been avoided due to the underlying ethical issues. This is a major limitation since it creates a void in human response data at a critical level when injuries were typically found.

Another major limitation with using human volunteers was the decrease in experimental control and repeatability. The variability and complexity of the human body made it difficult to formulate injury mechanisms, understand the body response and establish injury tolerances. In addition, initial studies were conducted with military personnel who were not representative of the entire population, with experimentation also being costly and time-consuming.

2.4.2 Human Cadavers

To study more severe impacts, human cadavers or Post-Mortem Human Subjects (PMHS) have been used as surrogates to study the human impact response. In terms of anatomy and mass distribution, they best represented the human *in vivo* (Snyder, 1973; Verriest, 1984). However, this only allowed structural injuries to be observed. Without working physiological components, major vascular trauma and pulmonary contusions could not be assessed. Variability between cadaver models also led to less reliable and repeatable tests.

The validity of identified causes of skeletal injury and injury severity is dependent on the similarity between mechanical properties of living and PMHS tissues (i.e. bones, muscle). Post-mortem, bone, ligament and tendon have not been found to significantly alter in properties (Van Ee et al., 2000). Similarly, in the first eight hours post-mortem, a change in modulus and no-load strain of passive skeletal muscle was not reported (Van Ee et al., 2000). However, injury severity has been found to be lower in living than in PMHS. Patrick (1981) reported similar load-deflection characteristics between live humans and pigs, but noted higher injury severities in pig cadavers. Viano (1977) found at a given level of chest deflection, the number of fractures for live animals was roughly 25 % lower than that for the post-mortem animals. Similarly, Foret-Bruno (1978) noticed an increase of 3 to 5 rib fractures in cadavers when compared to real crashes under belt loading. These response differences in cadavers were found to stem from the absence of muscle tension, the age of the specimen, cadaver preparation and a memory effect in cadavers produced plastic deformation (Wismans, 2001; Van Ee et al., 2000; Kent, 2004). To diminish these limitations, the cardiovascular system and organs have been pressurised to restore their inertial properties as the thoracic response was also dependent on the underlying viscera (Verriest, 1984).

Early studies embalmed cadavers to not only preserve their composition, but to also increase the cadaver stiffness to mimic the effects of muscle tension. Embalming consisted of submersing the specimen in a formaldehyde-concentrated solution. Whilst the effective stiffness of cadaveric tissue increased, the degree to which this represented *in vivo* muscle tensing was unknown (Kent et al., 2006). Thoracic stiffness of embalmed cadavers, though, have been reported to be approximately three times greater than that of living subjects, whilst compression characteristics were similar in fresh cadavers and living humans (Lee, 1994). However, it was difficult to compare across studies due to differences in embalming technique, preparation, age, and quality of cadaver (Snyder, 1973).

Another strategy used to reproduce muscle tension effects involved electrically stimulating individual muscles or muscle groups to full contraction (i.e. tetanus). This was difficult because cadavers cannot be obtained, screened and prepared for testing prior to the onset of rigor mortis (Kent et al., 2004). This was important because after the onset rigor mortis, failure stress levels were significantly decreased (Van Ee et al., 2000). Jones et al. (1995) found that the level of electrical muscle stimulation was heavily dependent on the time post-mortem. After 10 minutes, muscle response rapidly declined until a short plateau at 30 to 40 minutes, where generated force was just 20 to 35% of the maximum (Fig 2.3). As such, the mechanical properties of tensed muscle may not be adequately modelled due to a lack of electrical excitability.

Figure 2.3 Decay of muscle response with time after death (Jones et al., 1995).

A major limiting factor, especially in predicting skeletal injuries, was the age of cadaver specimens. Typically, the PMHS used were much older than the population found in competitive sport. This must be accounted for since the mechanical properties (i.e. tolerance) of bone decline with age (see § 2.7.5.1). However, young PMHS subjects were difficult to find – especially those that were free from disease. In spite of this, PMHS may still provide the most useful insight into the human response in impact conditions too severe for the living population.

2.4.3 Animal Surrogates

A principal advantage of animal surrogates was that physiological responses could be monitored, especially in injury-inducing or fatal impacts. This included investigating injuries to organs and identifying the effects of muscle tension on stiffness. It was unclear, however, whether these injury mechanisms applied to humans because of the size and structural differences in animal surrogates (Wismans, 2001). In spite of this, animal surrogates provided an underlying relationship between living and dead specimens that can potentially be applied to human cadaver results (Beckman et al., 1970; Verriest, 1984; Wismans, 2001). Another advantage was that experimental procedures were generally more controlled as the subject was anaesthetised, though this may also have a detrimental effect to the transferability of results. Finally, it was much easier to gather subjects as ethical clearance was easier to obtain than in human testing.

Swine are the most commonly used in thoracic impacts because their chest anatomy and organ distribution were quite similar to humans (Bir et al., 2004; Bir & Eck, 2005). However, differences in cross-sectional shape, skeletal structure (less sloped) and muscle distribution (more pronounced thoracic musculature on the dorsal thorax) may have limited their applicability to humans (Lau et al., 1993; Kent et al., 2004; Kent et al., 2006). While other animal models (rats, primates, rabbits) have been used, only specific body parts from each have been analysed since each was based on structural and physiological likeness.

2.4.4 Mechanical Models

Mechanical models attempt to match components of the human body in terms of size, shape, mass and kinematics. They are instrumented to measure parameters such as acceleration, force and deflection during impact. These variables are used to provide insight into impact severity and potential injury risk through comparison with a validated injury criterion. The measured response, however, was dependent on its biofidelity; that is, how accurate it mimicked the human response. This was dependent on results obtained from human volunteer and cadaver testing so the complexity of this type of model, and its results, were limited (Kimpara et al., 2006). For example, the effects of muscle tension could not be included because its role was still not fully understood. Another limitation was that only the risk of skeletal fractures can be examined as the absence of soft tissue and internal organs suggested that their injuries cannot be assessed. In general though, these results were unreliable as structural components of the body are living organisms and respond to stress and strain biologically (i.e. non-uniformly and inconsistently) not just mechanically (Bedewi, 2001).

Despite many limitations, mechanical models still offered considerable advantages to volunteer testing as it eliminated the risk of injury. This absence of ethical issues allowed for more extreme testing in terms of the magnitude and frequency of impact. There was also less preparation time involved and, although more expensive, subjects did not have to be recruited. The variability between models was also less than human and PMHS subjects which allowed within-tests to be more repeatable and between-tests to be more accurately compared.

The most frequently used mechanical model in car crash safety tests was the Hybrid III but other models included the EuroSID, WorldSID, THOR and Toyota's THUMS model. Each model was biofidelic for thoracic impacts but had not been validated for abdominal traumas (Elhagediab & Rouhana, 1998). More recently, Roberts et al. (2005) described a model, GELMAN, which consisted of anatomically shaped surrogate organs (e.g. heart and lungs). As each bone and organ had different material properties, it was assumed to have a higher biofidelity to a variety of loadings. However, whilst the full-body response matched the experimental results, the timing and amplitudes of peak pressures for each individual organ were different to those measured experimentally. This implied that its high biofidelity was artificially created.

2.4.5 Computer (Mathematical) Models

Similar to biomechanical models, a major limitation of computer (or mathematical) models was that its accuracy and reliability strongly depended on the (biomechanical) information available and the assumptions made in formulating the model (Snyder, 1973; Wismans, 2001). Therefore, a model's complexity and biofidelity was a function of the responses that could be reliably measured in living and cadaver specimens. While hard and soft tissue geometries may be easy to obtain, material properties, particularly of soft tissue, were difficult to classify (Van Loocke et al., 2006). Kimpara et al. (2006) varied the stiffness and mass density of the ribcage, internal organs, and superficial muscles by ±50 % in an FE model of thoracic pendulum impacts. Significant changes in chest stiffness, force-deflection response and rib fractures were observed, demonstrating that the assumptions of specific material parameters had a significant effect on the human response. Model sensitivity was further exacerbated by limitations in formulating precise mathematical expressions to describe the body's biological responses. Therefore, even simplified models may take a long time to develop and may never achieve the desired level of accuracy.

The major advantage of computer models is that they allowed for more extreme and variable experimental conditions whilst producing consistent results. It is also a cheaper option than biomechanical models since impactors and test rigs did not need to be obtained for each specific loading condition and the risk of damaging equipment is avoided. Instead, tests are solely dependent on the mathematical code used to describe the impact. Since iterations of different impact conditions can be computed without technical supervision, an expansive amount of testing can be conducted in limited time. Therefore, if the accuracy and validity of mathematical models can be improved, it will be an effective and efficient method for obtaining impact responses under different loading conditions.

To date, the most influential mathematical model was the Lobdell model (1973), which is a lumped-mass model of the anteroposterior thoracic impact response of the human thorax. It is the mechanical analog of the human chest composed of two masses with connecting springs and dashpots and its force-deflection response was validated against blunt impact data from literature. This model is described in more detail in § 2.7. Finite-Element (FE) models are also commonly used and function by representing surfaces and volumes with a finite number of elements connected by nodes. The response of the model is then governed by its material properties and the displacement between nodes. A few FE models used for investigating thorax injuries include Grimal et al. (2004), Ward et al. (2005), Kimpara et al. (2006) and Forbes et al. (2006).

2.5 Measurements

The strategies and instrumentation used to obtain objective measures of impact intensities are outlined in this section. These measurements are then used to develop injury criterion, biomechanical responses and injury tolerances, while helping to develop and validate surrogate models.

2.5.1 Acceleration

Acceleration due to impact can be easily obtained using accelerometers which measure whole body motion and kinematics, but must be placed on rigid masses such as bone (Snyder, 1973). The use of an accelerometer also made it possible to determine relative motion within a body by placing accelerometers on two surfaces. Viano (1987) fixed accelerometers on the sternum and spine and found the relative difference between both to determine anterior thoracic movement. However, this was not the most accurate method due to errors associated with integration. Accelerometers have also been placed on the impact sled to control impact severities and match impact conditions to real car crashes (Kallieris et al., 1982; Cavanaugh et al., 1990; Kallieris et al., 1998; Kent et al., 2001). Whilst simple to measure, the main issue with acceleration as an indicator of injury was that some authors believed that it was not a causal factor in soft tissue injury in the chest and abdomen (Kroell et al., 1974).

2.5.2 Force

There are four separate ways in which force has been measured to indicate impact severity in car crashes. Early studies placed an accelerometer on the impactor and, with knowledge of the impactor mass, were able to calculate impact force using Newton's 2nd Law (Kroell et al., 1971; Kroell et al., 1974; Patrick, 1981; Cavanaugh et al., 1986; Viano et al. 1989a; Yoganandan et al., 1997). A disadvantage of this method was that it limited measuring force to instances where rigid impactors were used since the effective mass in non-rigid impactors would have been constantly changing. Furthermore, this technique only applied to studies in which the subject was stationary and was impacted with a known moving object, which did not account for all impact conditions. Forces have also been measured using load cells and transducers instrumented in impactors (Beckman et al., 1970; Cavanaugh et al, 1996; Lee et al., 1994; Kent et al., 2003; Kent et al., 2006) and in the ground for cadaver drop tests, particularly when investigating side-impact response (Stalnaker, 1979). They have also been measured from the tension of seatbelts in volunteer (L'abbe et al, 1982; Backaitis & Laurent, 1986) and cadaver (Foret-Bruno et al., 1978; Troseille et al., 2002; Duma et al., 2005) testing to help investigate submarining injuries.

The main issue with force was that its tolerance may vary with impact environment, stiffness of impact interface, impactor size in addition to impact severity (Lau & Viano, 1986). Furthermore, it did not delineate between the mechanisms of injury fully because of variable contributions of inertial, elastic and viscous components (Lau & Viano, 1986). In spite of this, it continues to be used as a popular measure of impact intensity since it can be easily obtained.

2.5.3 Deformation

Deformation is usually presented as a percentage of the original thorax or abdominal thickness along the axis of impact. In side impacts, it is measured as the compression of the struck-side (at the T5) divided by half the chest width. Early research used three methods to obtain these deformations: directly using a gauge on the impactor typically in the form of a string potentiometer (Kroell et al., 1981), digitising high-speed video (Kroell et al., 1971; Kroell et al., 1974, Lobdell et al., 1974; Viano, 1989) or integrating accelerometer data (Lau et al., 1993). The method chosen was generally a function of the set-up. With the back restrained, only the sternal deflection needed to be measured and each method could be used independently. In unrestrained or free-fall impacts, spinal kinematics were also necessary. Therefore, a gauge on the impactor had to be used together with either an accelerometer or high speed video – both of which had their associated errors. Accelerometers had errors due to integration, whilst the resolution of video footage made it difficult to accurately identify between subject and impactor.

In the 1980s, the External Peripheral Instrument for Deformation Measurement (EPIDM) (i.e. chestband) was developed. It is a high-strength steel alloy consisting of strain gauges placed at known distances apart and has been used in various studies (Yoganandan et al., 1997; Kent et al., 2001; Shaw et al., 2006) to measure temporal thoracic deformations. Its main advantage was that deformation along anywhere on the band could be determined (Yoganandan et al., 1997). However, there were usually not enough strain gauges to accurately account for the discontinuities in the ribcage surface thus affecting its accuracy (Shaw et al., 2006). In spite of these limitations, it was the only method available to measure dynamic chest deformation and has been found to be reliable in distributed (i.e. airbag) loadings (Kent et al., 2001).

2.6 Injury Criterions

Injury criterions identify the mechanical variables which are considered to cause a specific type of injury from a given loading based on engineering principle. The internal response of any mechanical structure, regardless of size or material composition, are uniquely governed by the structure's geometric and material properties and the forces and motions applied to its surface (Eppinger et al., 1999). Biomechanical responses and injury tolerances were then based on the developed criterion. For example, if the injury criterion was based on force and deflection, the force-deflections measured produced the biomechanical response. Specific injuries were then identified at a certain level of force-deflection to create an injury tolerance or threshold. As such, it was important that the correct criterion was selected as this ultimately determined the injury potential of future impacts.

2.6.1 Abbreviated Injury Scale

The Abbreviated Injury Scale (AIS) is a method of easily quantifying injury severity to indicate a "threat-to-life" (Table 2.1).

Table 2.1 Abbreviated Injury Scale for skeletal and soft tissue injury in the thorax and abdomen.

AIS	Injury Severity	Skeletal Injury	Soft Tissue Injury
0	*no injury*		
1	*minor*	Single rib fracture	Superficial Abdominal wall laceration
2	*moderate*	2 - 3 rib fractures Sternum fracture	Laceration of Spleen, Kidney, Liver Contusion of Spleen, Kidney, Liver
3	*serious*	4 or more rib fractures 2 - 3 rib fractures with hemo-/pneumothorax	Major laceration of kidney, spleen Lung/Minor Heart Contusion
4	*severe*	4 or more rib fractures with hemo-/pneumothorax 4 or more rib fractures on each side	Major Liver Laceration Bilateral Lung/Minor Heart laceration Major Heart contusion
5	*critical*	Bilateral flail Chest	Major aortic laceration Lung laceration w/ pneumothorax
6	*unsurvivable*		Aorta rupture & haemorrhage not confined to mediastinum
9	*unknown*		

Each score is a six-digit code which identifies the body region, type and specific anatomical structure, injury type followed by a decimal number indicating the AIS level. This ranges from 0 to 9, but the relationship is not linear; that is, AIS=2 is not doubly more severe than AIS=1. Instead, each AIS level indicates a more severe injury relative to that particular anatomical region. As such, a fracture in the leg may have the same AIS level as a flail chest. In general, though, chest and abdominal injuries of AIS≥4 are considered to be life-threatening. The primary criticism of the AIS scale was that it did not address such issues as quality of life, cost incurred by an injury, the extent of disability, or cumulative effect of multiple injuries (Bedewi, 2001).

2.6.2 Acceleration-Based

This criterion measures the whole-body acceleration generated in a given impact. It relies on a sustainable amount of acceleration within a specific time and its magnitude has been found to decrease as the duration of the exposure increased (Lau & Viano, 1986). Its main limitation was that it could only measure the acceleration of bony structures and did not account for deformation. Since injury has been induced well before the peak in acceleration response (Lau & Viano, 1986), this criterion was restricted to predicting mainly skeletal injuries. In spite of this, it has also been widely used in the determination of injuries during head impacts and is the main parameter of the Head Injury Criterion (HIC) which has been instrumental in identifying serious head injuries. The main acceleration-based criteria for thoracic injuries are the Average Spinal Acceleration (ASA) which is measured directly, the Thoracic Trauma Index (TTI) which was formulated from cadaver experimentation and the Combined Thoracic Index (CTI) which combines acceleration and thoracic deformation.

2.6.2.1 Thoracic Trauma Index (TTI)

The Thoracic Trauma Index (TTI) is the most well-known acceleration-based criterion (Equation 2.1). It is based on the lateral acceleration of either the 4th rib or 8th rib (whichever is greatest) and the 12th thoracic vertebra (T12) and is one of the only criterions to adjust for age.

$$TTI = 1.4\,Age + 0.5(RIB_y + T12_y) * \frac{M}{M_{50}} \qquad (2.1)$$

Where,
Age: subject's age
RIB_y: maximum absolute acceleration on struck side
$T12_y$: maximum absolute acceleration of 12th vertebrae
Mass: Subject mass
M_{50}: Mass of a 50th percentile male

2.6.3 Force-Based

The foundation of force-based criterions are on Newton's 2nd Law (F=ma). Forces are measured using the product of impactor mass and acceleration and then correlated to a specific level of injury. As such, these tolerances are also related to (a change in) momentum – upon contact, the impactor accelerates the body or body region until both reach a common velocity. The time required to achieve this common velocity is proportional to the effective mass of both colliding objects and their velocities at impact. Whilst force may provide repeatable results for skeletal (i.e. ribs) impacts, measuring it has been particularly complicated in abdominal injuries and has not been considered to be a good predictor for injury in this region (Rouhana, 1987). Its main issue was that it did not delineate between the contributions of inertial, elastic and viscous components in the mechanisms of injury (Lau & Viano, 1986). As such, force correlated well with skeletal fractures and very serious injuries (AIS = 4+), but could not be used to predict soft tissue injuries. Force-based tolerances were also more sensitive to changes from impact environment, stiffness of the impact interface and impactor size (Lau & Viano, 1986). As such, it may be more useful if the magnitude of force, the area of impact (i.e. pressure) and impact locations, were known for predicting injury.

2.6.4 Compression-Based

Compression-based criteria are based on measurements of deformation as defined in § 2.5.3. Early research by Kroell (1971, 1974) demonstrated that compression was an important indicator of thoracic trauma severity, particularly at impact velocities below 3 ms^{-1}. Chest compression was observed to trigger the onset of rib fracture, whilst spinal acceleration and force were observed to be poor indicators of injury. Despite its inability to predict injury severity, force has been used to determine the dynamic stiffness of the chest when coupled with compression. This provided insight into the human response before fracture aiding in the development of surrogate models. A major issue not addressed in this criterion, though, was that most soft tissue injuries have been found to occur well before maximum compression (Lau & Viano, 1986). Therefore, compression may not be the most accurate indicator for all injuries and impact parameters.

2.6.5 Velocity- and Compression-Based

Through experimentation, it has been suggested injuries cannot only be compression-dependent, but also rate-sensitive. Kroell (1981) reported increasing trauma severity with increasing compression in swine subjected to mid-sternal impacts at a constant velocity. In contrast, Viano & Lau (1986) conducted tests on internal rabbit organs and found:

- Injury severity increased with increasing impact velocity and fixed maximum compression within the liver (16%)
- in the lung, injury severity increased with increasing compression at impact velocities of 5, 10 and 18 m/s; also less compression was required to produce the same level of injury at a given velocity

Therefore, at high impact velocities, maximum compression did not reflect the viscous and inertial properties of the chest or the time of greatest soft-tissue injury risk. This led to the development of the Viscous Criterion by Viano & Lau (1988).

The viscous response, VC, is calculated as the product of the velocity of deformation, V, and compression, C. This parameter was thought to physically represent the absorbed energy in a viscous dashpot under impact loading (Viano & King, 2000). It was suggested that, in impacts above 3 ms^{-1}, peak VC was a better indicator of serious injury than maximum compression. Viano & Lau (1988) showed that peak viscous response occurred earlier (10 ms after initial impact) than maximum compression (30 ms) and was roughly when Kroell (1976) found rib fractures to occur (9-14 ms) – more than half the time before max compression.

A caveat of this criterion was that it was near impossible to measure the VC of internal organs in living human impacts. Therefore, published values often referred to the compression and compression rate of the body as a whole and not the individual organ itself. Nevertheless, it has been found to correlate well with the onset of injury (Viano et al., 1989; Lau et al., 1993) and be a consistent predictor of abdominal injury (Johannsen & Schindler, 2007).

2.7 Biomechanical Response

When subjected to an external (mechanical) load, the body or body region produces a change in position and shape (due to deformation) during the course of contact (Wismans, 2001). This load-deformation relationship is known as the *Biomechanical Response*. These responses are difficult to establish as they are not only dependent on the object's mass, velocity and material properties, but are influenced by the impactor shape and the location of impact. In addition, Kent et al. (2004) suggested that the thoracic and abdominal response may be influenced by the particular anatomical structures that bear the load rather than the area of load application due to the non-homogeneity of the region. Whilst impact responses can be expressed using force, deformation or acceleration as a function of another relevant independent variable (King, 2000), force-deflection curves were found to provide the best biomechanical representation of the impact response of the thorax (Viano & King, 2000).

The characteristics of all biomechanical response curves from external impact loadings were described by three distinct components as developed by Lobdell (1973) and shown in Fig 2.4:

(1) **inertial** resistance $[m_2 y_2]$ by acceleration of body masses;

(2) **elastic** resistance $[k_{23}(y_3 - y_2)\,\text{and}\,\text{k}_{\text{ve23}}(y_4 - y_2)]$ by compression of stiff structures and tissues; and

(3) **viscous** resistance $[c_{23}(y_3 - y_2)]$ by rate-dependent properties of tissue.

Figure 2.4 Lobdell Model (Viano & king, 2000)

In addition to the springs and dashpots shown here, a secondary spring (not shown) has been included to simulate a bilinear increase in thoracic stiffness for chest deflections beyond 38 mm (Viano, 1987a).

This section will first examine how biomechanical responses were calculated and expressed. It will then look at the general trends in responses for each body region and conclude with the factors which influence the response. Measured responses appear at the end of this chapter.

2.7.1 Biomechanical Response Corridors

Combining all the response curves for a given impact condition can be used to form *Biomechanical Response Corridors*. These describe how a body responds (deforms) to a given impact (force) and provides data for the development of biomechanical, mathematical and computer surrogates (Bir et al., 2004; Bir & Eck, 2005). If the force-deflection profile of the surrogates lay within the corridor, then it was assumed that the surrogate response was accurately reproducing the human response. This provided a means for assessing a surrogate's biofidelity. For a given impact condition (i.e. same mass, velocity, etc;), the upper- and lower-bounds of the corridors have been established in three separate ways:

1) Calculated from taking +/- 15% of the average from all response curves (Lobdell et al., 1973)
2) Calculated using +/- 1 SD from the average of all curves (Cavanaugh et al., 1986)
3) Maintaining the general effect of the impact by including the majority of individual responses of all specimens within the corridor and segregating outliers (Bir & Eck, 2005).

A caveat of these response corridors was that, not only must the model response fall within the upper and lower bounds, but it must also exhibit a similar trend in shape (Morgan et al., 1986).

2.7.2 Chest

Kent et al. (2004) described the impact response as having an initial force spike with very little displacement developing from the inertia required to accelerate the body (i.e. sternal mass in chest impacts) to impactor velocity and from the high rates of deformation producing viscous forces. The response plateaus as contributions from viscous forces gradually decreased (due to decreasing deformation velocity as the body decelerates the impactor) and elastic forces from tissue compression increased (Fig 2.5). Melvin (1988) modelled the force-deflection response in frontal impacts with the initial rise in stiffness as A = 0.26 + 0.60(V – 1.3) and the plateau as B = 1.0 + 0.75(V – 3.7), where A was in kN/cm, B was in kN and V was in m/s (King, 2000). After unloading, the body will attempt to return to its original state, but will do so under different force-deflection properties. This hysteresis effect represented the energy absorbed by the body during contact and it has been speculated that minimising this energy absorption could lead to a significant decrease in injury (Viano et al., 2000). As the front and side of the thorax have different in terms of structure, musculature and underlying organs, the kinematics during side impacts are also different (Viano et al., 1974; Viano, 1989). Chest compliance in lateral impacts to the ribs was found to be softer due to the flatter arch of the ribs as opposed to the narrower and symmetric rib cage geometry encountered in frontal impacts (Viano, 1989).

Figure 2.5 Contributions of inertial, elastic and viscous resistances in forming a biomechanical response curve caused from an external impact loading on the chest (Kent et al., 2004).

Frontal and lateral stiffness for the thorax appear in Table 2.5 and 2.6, respectively, at the end of the chapter.

2.7.3 Abdomen

In general, the abdomen has been found to be more compliant than the chest with much higher deflections measured for a given force (King, 2000). Viano et al. (1989) also found the viscous response to be higher for a given impact condition with the difference in stiffness' and VC attributed to the lack of skeletal structure to resist low-level deflection. Similar to chest impacts, energy was absorbed by the abdomen during impact, but the difference in the amount of hysteresis upon unloading appeared to be a function of the impact location and size of the impactor (Hardy et al., 2001).

Within the abdomen itself, Cavanaugh et al. (1986) suggested that there may be a transition in response from the upper to lower abdomen. The upper abdomen response has been found to be similar to the chest; that is, it showed a linear increase to peak force, followed by a plateau, then a small rise before unloading. In contrast, the lower abdomen did not seem to show a discernable transition between each of these three phases and has shown a much different response. This was attributed to the lack of rib contact, lack of muscle tone and less stiff response causing the lower abdomen to bottom out (i.e. fail) later. In addition, injury occurrence and intensity also depended on the direction of loading. Laterally, rib deflection deformed the lung which can cushion the heart from rib cage loading while the heart and great vessels can displace laterally against the compliance of the opposite lung (Viano, 1989a). Therefore, the impact response will depend on the structures in series directly behind the direction of impact.

Frontal and Lateral stiffness' for the abdomen appear in Table 2.7 and 2.8 at the end of the chapter.

2.7.4 Tibia

Unlike the thoracic and abdominal cavities, scant research has been conducted on the dynamic impact response of the tibia. Nyquist et al. (1985) tested the tibia, with the fibula still attached, in three-point bending. Dynamic loads were applied in the antero-posterior (A-P) and latero-medial (L-M) direction with a 32-kg impactor at velocities between 2.1 to 6.9 ms^{-1}. It was found that the tibia was much stiffer in the AP direction than in the LM direction (Table 2.2). This difference was accounted for by the inclusion of the fibula which was proposed to be stronger in the A-P direction.

Table 2.2 Stiffness of Tibia in antero-posterior (A-P) and latero-medial (L-M) directions from 3-point bending tests (Nyquist et al., 1985).

Direction	Stiffness
A-P	282 ± 92 kN/m
L-M	105 ± 36 kN/m (initial) 265 ± 70 kN/m (prior to fracture)

2.7.5 Influential Factors

2.7.5.1 Age

With age, humans undergo a slow, progressive loss of skeletal muscle mass that was replaced largely by fibrous connective tissue and adipose tissue (Tortora & Grabowski, 2003). As such, the mechanical properties of bone change significantly due to this increased porosity and demineralisation (Zhou et al., 1996). Furthermore, Currey (1979) found age-related changes in impact energy absorption of human bone, which were connected to changes in density, porosity and calcium content of bone (Zhou et al., 1996). It was also proposed that the slope of ribs in the sagittal plane decreased with age (Kent, 2003). These factors implied that the biomechanical response of the body changed with age.

2.7.5.2 Loading Condition

Loading conditions can be varied in terms of its surface area, the type of impactor and the anatomical regions targeted. Most impactors were blunt (i.e. steering wheel or airbag) or quasi-static (i.e. seatbelt), whilst the body was positioned with the back restrained or free with arms either overhead or by their side. Altering these parameters has shown to have a significant effect on the response measured. Larger contact areas in thoracic impacts resulted in a higher stiffness as more ribs were available to absorb the impact (Lau & Viano, 1986). Loads to the superior thorax generated a greater stiffness, but smaller inertia when compared to the 7th and 8th ribs, with larger crush injuries in the inferior ribs (Verriest, 1984). Diagonal belts resulted in a substantially stiffer response than loading from a hub (Kent et al., 2004). Similarly, blunt ballistic impacts showed a much higher stiffness (i.e. higher impact forces and smaller chest compressions) compared to typical car crash impacts (Bir et al., 2004; Bir & Eck, 2006).

Kent & Crandall (2001) found that thoracic deformation of cadaver and ATD subjects were sensitive to three separate restraint systems (i.e. boundary conditions). When solely restrained by an airbag, the thorax exhibited an evenly distributed deformation with minimal chest deflection. Conversely, the two belt-airbag conditions caused more local deformations, with higher deflections in the standard belt than in the force-limiting belt (Fig 2.6). A similar trend has been observed by Patrick (1981) and Kent et al. (2006).

Figure 2.6 The airbag-only show a distributed loading whilst the other two show a localised deflection illustrating the dependence of loading condition on chest deflection

The loading condition also influenced the overall shape and magnitude of the biomechanical response curves (Fig 2.7). First, belt loads suggested that the body acted as a more compliant system requiring less energy to deform the chest. Second, the impact response from each loading condition received contributions from different response elements. Blunt impacts formed a curve that featured an initial spike caused by the inertia of the impactor followed by a plateau as the viscous force decreased with increasing elastic force. In contrast, belt loads featured a force-deflection response that was constantly increasing. As the belt pressed against the body, contributions from inertial resistances was negligible since the relative velocity between the belt and subject was zero. Furthermore, since belt velocity was constant, viscous forces also remained relatively constant throughout impact. As such, the thorax was pinched between the belt and the seat in restrained loadings thus generating lower force and acceleration magnitudes when compared to blunt loading (Patrick, 1981).

Figure 2.7 Shape of biomechanical response curve produced in blunt and belted impact loadings due to the initial spike in inertial resistance and the viscous response (Kent et al., 2006).

In general, the interpretation of the thorax deflection data for injury assessment purposes must reflect the type of restraint system used to contain the occupant (Backaitis & St-Laurent, 1986). In car crashes, however, the loading condition can rapidly change from belt to airbag or belt to steering wheel. As such, ATDs must be able to accurately predict injury risk to rapid changes in loading conditions (Kent et al., 2004). To ensure that models are validated for a wide-range of impact conditions, each model must be within pre-established corridors and the shape of the curve must be similar for that specific impact type.

While safety devices were intended to decrease the impact severity, a change in loading condition may reduce the risk of one injury but increase the risk of another. Deng et al. (1989) reported an increase in padding thickness reduced thoracic accelerations but increased thoracic deflection and VC_{max} due to reduced peak force but concomitant occupant to door contact duration (Kent & Crandall, 2003). Viano (1987) found that varying levels of side protection, energy-absorbing material would change the measureable VC. If the crush force of the material was too high, it would act like a rigid surface; if it was too low, there would not be enough energy absorbed by the material to provide adequate protection.

2.7.5.3 Gender

Due to differences in anatomy and height between men and women, it is necessary to distinguish between impacts response measured in each. Duma et al. (2005) found that the onset of rib fractures in male cadavers occurred at higher forces, yet lower deflections compared to female cadavers. Moreover, males showed much lower force-deflections (2000-3000 N at 10-20 % compression) for left rib fractures than right rib fractures (5500-7000 N at 27-33 %), whilst rib fractures in females occurred over the same force-deflection ranges on both sides. These results suggested two things: 1) male cadavers were much stiffer than female cadavers; and 2) the fracture response from changed laterally in male cadavers, with no difference in female cadavers. This knowledge has been reflected within the industry as different ATDs have been used to represent the morphology and impact response between males and females.

2.7.5.4 Muscle Tension

A major caveat of biomechanical response curves was that most have been developed using cadavers which lacked a muscular response. This was critical since muscle tension can effectively alter the stiffness and mass of a body segment or region (Kent et al., 2006). Furthermore, muscle tensing was thought to cause a more rapid unloading and a concomitant reduction in hysteresis (Lobdell et al., 1973). As a result, muscle tensing would likely change the shape and magnitude of the cadaver-developed response curves. It was proposed that muscle contraction increases the stiffness in two ways (Kent et al., 2006):

1) cross-fibre modulus of muscle tissues increase when stimulated (more force required to deform); and
2) stimulating the muscle tissue generate an isometric tensile force, which pre-stress the thoracic cage and underlying viscera

As soft tissue has shown to dissipate significant amounts of impact energy in falls (Robinovitch et al., 1995) and drop landings (Pain & Challis, 2002), changing its impact properties could have a considerable effect on injury potential. In contrast, Lobdell et al. (1973) proposed that increases in chest diameter caused by tensing had a greater influence on the impact response than the increase in stiffness.

Substantial research has focused on comparing responses in contracted and relaxed muscle states in human volunteers to provide *in vivo* data (Table 2.3) which was used to develop and validate the biofidelity of mechanical and mathematical models. Upon examination, Neathery (1974) suggested adjusting the thoracic biofidelity response corridors to account for the perceived increase in stiffness due to muscle tensing. However, these impacts were restricted to deflections < 20% to maintain non-injurious levels. As such, it was unknown whether this increase in stiffness would remain at larger deflections or impact velocities (Lobdell et al., 1973). It was also difficult to compare results as each study used their own conditions. Stalnaker et al. (1973) halted the impactor after a pre-determined amount of travel set pre-trial by the subject. Lobdell et al. (1973) rested the thorax against a flat backrest creating a squeeze-type loading instead of an inertial loading whilst Patrick (1981) adjusted the stiffness in both conditions by estimating tissue thickness and the force required to compress this soft tissue.

Table 2.3 Comparison of thorax stiffness in relaxed and tensed conditions in human volunteers.

			Average Thoracic Stiffness			
	Model (# subjects)	**Method**	**Relaxed (N/cm)**	**Tensed (N/cm)**	**% increase**	**% deflection**
Lobdell et al. (1973)	Human Volunteers (7)	Static Hub Loading	70	236	337	11
Stalnaker et al. (1973)	Human Volunteers (2)	Dynamic Test	403	1138	282	8
Patrick et al. (1981)	Human Volunteers (1)	10 kg Padded Hub @ 2.4 m/s	570	790	139	18
Backaitis & St-Laurent (1986)	Human Volunteers (10)	Diagonal belts	1336	1613	121	-
Lee et al. (1999)	Human Volunteers (17)	Wooden Plate with 120 N load	-	105 (m) 84 (f)	-	-

Since significant injuries cannot be induced in human volunteers, research has resorted to the use of animal models with mixed results. Beckman et al. (1970) impacted Rhesus monkeys in the chest with a 1” flat plate and found the embalmed cadaver, which simulated muscle tension, to be stiffer than an anaesthetised living monkey. Crisco et al. (1996) suggested that impact stiffness in contracted muscle was decreased due to the decreased contribution from the underlying bone when impacting the gastrocnemius in rat models. Kent et al. (2003) found that muscle tetanus had no measurable effect on the structural response of the thorax in supine swine. Kent et al. (2006) proposed that as chest deflection approached injurious levels, thoracic stiffness would be dominated by the mechanical properties of the rib cage and internal organs with minimal influence on peak force from superficial tissues.

The conclusion from these experiments was that an upwards shift of 667 N in the biomechanical corridors did not accurately capture the effect of muscle tension. This value was estimated at sub-injurious levels using limited quantitative data (Lobdell et al., 1973) and a simple vertical shift did not consider the effect of tensing on the work performed by the deforming thorax (Kent et al., 2006). As such, it may be better to understand how the shape of the whole biomechanical response curve was affected by muscle tensing at all levels. This was relevant when validating ATDs as it was important that its response curve fell within the most correct biomechanical corridor to ensure the greatest biofidelity (Fig 2.8).

Figure 2.8 The effect of shifted and un-shifted corridors on the validity of response from the Hybrid III and THOR ATDs. (Kent et al., 2006)

2.8 Injury Tolerance Levels

2.8.1 General

As the intensity of an impact increases, the overall biomechanical response also increases until an Injury Tolerance Level (ITL) is reached. Whilst these can be expressed numerically as a single value or probability, it is important to first define what is meant by an ITL. In this context, an ITL is an acceptable level of impact intensity measured subjectively or through mechanical variables that are associated with a certain level of discomfort, pain, injury or range of injuries. Three types of tolerances have been identified (Snyder, 1973):

1) a *subjective*, voluntary loading threshold;
2) a *reversible* injury threshold tolerance level; and
3) a *survivable* limits tolerance

Reversible and survivable tolerances were generally used in car crash testing, but their use was dependent on the models used and the intensity of impacts.

Subjective tolerance levels have only been used in studies with human volunteers as it relied on subjective feedback. Individual tolerances were set - by each participant in a given impact condition - as the limit at which intensities could not be exceeded due to perceived pain or injury risk. While this varied between test type and subject, a distinct limit could always be obtained from a group of participants. As this method was biased towards avoiding injury, this tolerance level was considered to be lower than the actual injury threshold level.

The next tolerance limit refers to the level of injury that was *reversible*. Typically, this tolerance was used to determine the threshold for recoverable injuries such as contusions or bone fracture. The severity of similarly-typed injuries, however, can depend on the anatomical region affected; that is, rib fractures were more severe than leg fractures though they are the same type of injury. As such, an injury score of AIS ≤ 3 was generally used to establish which injuries were considered to be ‘recoverable’. This also reduced ambiguity in defining what was meant to be severe and allowed tolerances to be developed for skeletal and soft tissue injury which have different injury mechanisms. Lastly, due to the potential for severe and long-term injury, cadavers and animal surrogates must be used to infer the corresponding living human tolerance.

The last injury tolerance was the maximum *survivable* limit. This identified the threshold for irrecoverable severe injury. Again, due to the severity of the impact intensities, only cadavers and animal surrogates have been used to develop these tolerances. In automobile safety design, this threshold has been used to design energy-absorbing hubs or force-limiting belts to ensure that severe or fatal injuries were prevented. Whilst impact intensities of this nature in sport were rare, Commotio Cordis, a potentially fatal injury, has been identified in certain ball sports. As such, much research has been dedicated to understanding the triggers of this condition and methods of prevention (§ 3.5).

2.8.2 Probit Analysis

In human injury, tolerances rarely governed the entire population. As such, it was more appropriate to consider a probability for injury (Mills & Hobbs, 1984). As such, the most effective method of obtaining injury probabilities is to use Probit Analysis. This is a regression analysis technique which can be used to relate the frequency of an all-or-nothing, quantal response to a quantifiable dose or stimulus (Mills & Hobbs, 1984). This produces a sigmoidal relationship between variables such as force or compression and probability. Lau & Viano (1988) suggested that the actual threshold region for injury was between probability levels of 25% and 75% with those outside the regions considered to be the weaker and stronger samples of the population, respectively. Therefore, threshold levels often appear as a single value with an associated probability for injury (usually 25% or 50%).

2.8.3 Chest

2.8.3.1 Frontal

From early human and cadaver testing, the onset of skeletal injury was found to occur at a compression of 20% with a flail chest occurring at 40%. However, this did not account for the visco-elasticity of the ribs or the age of the cadavers tested. Eppinger and Marcus (1985) found that the severity of injury is proportional to the amount of specific energy that the thorax must absorb (Zhou et al., 1996). This implied that for a given mass, the severity of injury will change depending on the impact velocity (Lau & Viano, 1988) and contact duration, with shorter times allowing for greater tolerances (Snyder, 1973; Bir et al., 2004). Injury tolerances as a function of velocity are shown in Fig 2.9.

Figure 2.9 Viscous and compression tolerance for blunt frontal impact (Lau & Viano, 1988)

Frontal injury tolerances are summarised and appear in Table 2.9.

2.8.3.2 Lateral

The National Accident Sampling System (NASS) and National Crash Severity Study (NCSS) found that side impacts represented 47% of fatal car crashes and that 52% of these impacts were to the chest and abdomen (Viano et al., 1989). As the anatomy between the left and right side are different, separate injury tolerances have been developed for lateral impacts. Morgan et al. (1986) found that the right side seemed to have a higher probability of skeletal injury than the left. Chapon (1984) found soft tissue injuries to be more prominent in right side impacts due to the relative size of the liver compared to the other abdominal organs. In general, Cavanaugh et al. (1989) found that compression was a good indicator of injury in lateral impacts at all velocities. Lateral injury tolerances are summarised and appear in Table 2.10.

2.8.4 Abdomen

The major problem with establishing a single tolerance for the abdomen, as discussed previously, was that the abdominal organs differed in structure and strength, especially between hollow and solid organs (King, 2000). However, individual organs were rarely impacted individually as their responses were influenced by neighbouring structures. As such, tolerances are mainly displayed by region and are separated into left and right upper, middle and lower sections. Abdominal injury tolerances are summarised appear in Table 2.11 and 2.12.

2.8.5 Tibia

Whilst biomechanical responses of the tibia were scarce, considerable research has been conducted on injury tolerances of the tibia. In the tibia, the most serious injury was skeletal fracture. Therefore, lower leg tolerances indicated the threshold at which non-fatal fractures occurred. Generally, published tolerances reflected results obtained from testing on an isolated tibia, despite injury tolerances being greater in conditions where the tibia and fibula were tested together. Furthermore, testing methods and injury criterions varied among tests making it difficult to compare tolerances across each condition. A summary of tibia tolerances to fracture appears in Table 2.4.

Table 2.4 Tibial injury tolerances using force, bending moments and stiffness.

Study	Type	Measure	Impactor	Tolerances
Kramer (1973)	Pendulum	Force (kN)	145-mm cylinder	4.3 (7.1 ms^{-1}, p=0.50)
			216-mm cylinder	3.3 (6.3 ms^{-1}, p=0.50)
Stalnaker (1976)		Bending Moment (Nm)	8 - 13 ms^{-1}	560 -1760
		Peak Force (N)		7517 - 22241
Nyquist (1985)		Moments (Nm)	25-mm cylinder	304 ± 90 (male, AP) 330 ± 89 (male, LM) 288 ± 37 (female, AP) 264 ± 14 (female, LM)
		Force (kN)		4.57 ± 1.59 (male, AP) 5.03 ± 1.37 (male, LM) 4.70 ± 0.74 (female, AP) 4.16 ± 0.22 (female, LM)
Francisco et al. (2000)	Drop Tests (1.2 - 2.5 m/s)	Avg Peak Force (N)	3.81-cm diameter, 4.2 kg	2980 ± 208 (male) 2873 ± 768 (female)
		Strain (με)		5744 ± 745 (male) 6832 ± 148 (female)
Heiner & Brown (2001)	Bending (*Anterior* Tension)	Bending Stiffness (Nm^2)		215 (Motoshima, 1960) 217 (Cristofolini, 2000)
	Bending (*Lateral* Tension)	Bending Stiffness (Nm^2)		182 (Motoshima, 1960) 193 (Cristofolini, 2000)

2.8.6 Influential Factors

2.8.6.1 Effect of Age

Age has been found to be a major influence on changes in tissue properties and the occurrence of injury. Zhou et al. (1996) reported that the mechanical properties of bone changed between 60 and 70 years old. Moreover, Kroell et al. (1971) showed that cadavers obtained from the older population were more susceptible to rib fracture whilst Eppinger (1976) found that for a given belt force, the number of fractures increased with age (Verriest, 1984). In spite of this, injury tolerances were often published as a single value or equation to represent the mean age of the population. Patrick (1976) advised that formulating a single tolerance equation for all age groups did not accurately predict injury risk (Zhou et al., 1996) but the relationship between tolerance and age was not well understood.

This was particularly important in sport, where elite athletes are physiologically different from the cadavers generally used to predict their injury tolerance.

Zhou et al. (1996) analysed thoracic injury data previously collected from cadavers and human subjects to examine trends in injury tolerance with increasing age. Subjects were split into six age categories and fractures were normalised by the total fractures within the youngest age group. A dramatic decrease in tolerances was observed in adults aged 36 and 66 (Fig 2.10). Based on these results, adults were divided into three groups (16-35, 36-65 and 66+) and reduction ratios were formulated for belt, frontal blunt and side impact loads for injuries under AIS-3 using linear regression to adjust existing injury tolerances. This eliminated the use of a single equation which underestimated the tolerance in the young group and overestimated the tolerance in the elderly group.

Figure 2.10 Influence of age on fracture (left) and fracture tolerance (right) (Zhou et al., 1996).

Kent & Patrie (2005) further expanded the data set from Zhou et al. and developed closed-form continuous functions that expressed thoracic injury risk as a function of age. Using logistic regression, injury probability risk functions were developed which established a relationship between the number of rib fractures, and parameters such as maximum deflection, age, loading condition, gender and a gender x age interaction term. The two most significant parameters, chest deflection and age, were then used to produce a reduced injury probability model (Fig 2.11). For a given chest deflection, the probability of a single rib fracture and severe rib fracture significantly increased with age. In other words, the deflection required for the onset of a single rib fracture and severe rib injury decreased with age, implying that older subjects were more susceptible to skeletal injury (Table

2.8). As a result, Cavanaugh et al. (1990) proposed adjusting the predicted AIS using the equation AIS – 0.025*(Age-45), while Verriest (1984) proposed that an increase in age from 40 to 65 corresponded to a degree on the AIS scale.

Figure 2.11 Probability injury risk functions for 30- and 70- year olds. The probability of minor and severe rib fractures significantly increased with age (Kent & Patrie, 2005).

It has been suggested that there were many reasons for the decrease in chest deflection tolerance as age increased (Kent & Patrie, 2005):

1) Failure strain of both cortical and trabecular bone decreased with age
2) Geometric changes associated with aging may predispose ribs to fracturing for older subjects under conditions where they might deflect non-injuriously in a younger subject (decrease in proportion of rib cross-section that is cortical bone)
3) Material changes such as calcification of the costal cartilage and decreased bone mineral density.

2.8.6.2 Loading Condition

As loading condition was found to have a significant effect on the human biomechanical response, it was also expected to have an effect on injury tolerances as well. Patrick et al. (1965) reported that in order to produce similar injuries, the loading condition would affect the maximum tolerable load; e.g. a hub load (3.3 kN) on the sternum caused minor trauma, whilst an 8.8 kN force distributed over the chest was required to generate a similar trauma. As the energy absorbing properties, shape and surface characteristics of the impacted material can greatly affect the individual's chance of injury or survival (Snyder, 1973), it was likely that this could have an effect on the injury criteria as well.

The major issue with assuming a single injury tolerance across all loading conditions was that each impact condition caused different injury severities and injury patterns. Airbags were found to fracture ribs anteriolaterally at the axillary line, whilst belt loads caused fractures that were concentrated along the belt path and area of loading (Kallieris et al., 1982; Kallieris et al., 1998; Kent & Crandall, 2001; Kent et al., 2002). Furthermore, fractures were found to occur more often in the lower left ribs in an occupant with an upper right to lower left belt (Duma et al., 2005). As such, Morgan et al. (1994) proposed that there were different injury criteria for each loading type from which an injury tolerance can be established.

Zhou et al. (1996) found that reduction ratios (Fig 2.10) for injury tolerances were not only dependent on age, but on whether the body was subjected to a belt load or blunt impact. That is, while loading condition affected injury tolerance, the extent of its influence was dependent on the age of the subject. Similarly, Kallieris et al. (1998) found that the 3-point belt initiated the highest frequency and severity of injury (rib fractures) when compared to a 3-point belt plus airbag loading and an airbag-only condition. Interestingly, the deceleration values (i.e. the injury criterion used) in the airbag-only condition would have indicated that this loading condition had the highest injury potential. Maximum and 3-ms mean decelerations were, on average, highest in the airbag-only condition but produced the least severe injuries. This supported the need to reconsider, not only the changes in injury tolerance, but the injury criterion used as well.

In contrast, Kent & Patrie (2005) found that the age-related risk for thoracic injury was insensitive to the loading condition on the sternum. Four separate blunt anterior loadings were examined: blunt hub, seatbelt, distributed (i.e. airbag) and a combined belt-and-bag loading. Using the same logistic regression developed for age-effects, the loading condition was found to be the least significant parameter. Moreover, the injury predictive ability of a reduced model, which did not include loading condition as a parameter, was not found to be significantly different than the injuries predicted from a full model which included all parameters. It was suggested that this would simplify injury risk assessments as the maximum chest deflection could be used as the only injury criterion for a given age, irrespective of loading. Kent et al. (2001) suggested that the soft tissue may re-distribute the load negating any affects of loading condition on deformation.

Whilst each study produced contrasting conclusions, neither examined the influence of loads to other parts of the thorax or abdomen or the effect on soft tissue injury. Zhou et al. (1996) cautioned that an injury assessment based on rib fractures may underestimate the injury severity of young people, overestimate their injury tolerance and exaggerate the reduction of tolerance in older age groups. In addition, rib fractures have been shown to be a poor indicator of soft tissue injury and the two injury types appeared to be unrelated (Lau et al., 1993).

2.8.6.3 Gender

The issue with establishing gender specific tolerances was that most of the cadavers used in previous studies had been male. As such, there has been limited data collected on female cadavers. In limited research, Duma et al. (2005) reported that for an AIS ≤ 3 injury, male cadavers were found to have a threshold of 13% chest deflection while females showed 23%. Similarly, Nyquist (1985) and Francisco et al. (2000) found different tolerances for tibial impacts across gender. This limited research supported the need for gender-specific tolerances to help determine the potential for injury risk.

2.8.6.4 Muscle Tension

It was previously shown that muscle tensing effectively increased the body stiffness in human volunteers at sub-injurious levels. A body which increased in stiffness would produce greater impact forces and stresses within the body as predicted by the *Elastic Impact Theory* (Crisco et al., 1996). This implied that injury patterns would change as the stress distribution in tissues were altered as external forces were applied (Kent et al., 2006). Crisco et al. (1996) proposed that if higher forces and stresses were associated with a higher risk of injury, then the tensed living thorax may actually be much more susceptible to injury than indicated by a cadaver. In contrast, Funk et al. (2002) argued that muscle tensing acted to reduce the risk of injury through the re-distribution of stresses through the muscles. Therefore, while it may be common practice to brace (i.e. tense) before an impact, its role in reducing the injury potential was very unclear.

Crisco et al. (1996), which reported a decrease in stiffness with muscle tension, proposed that contracted muscle decreased the viscous response of the limb. This acted to reduce the severity of contusion injury by decreasing the impact energy and time to peak force. While injury potential decreased, it was unclear whether this was accomplished through a reduction in impact intensity or through an increase in the reversible injury tolerance. In contrast, Hyrosomallis et al. (1996) found tensed muscle to develop significantly greater peak decelerations and shorter rise times, causing a greater rate of force development. Total contact times in muscle states were not significantly different implying that higher impulses were also generated in tensed muscle conditions. From a purely mechanical perspective, these variables or their derivatives suggested a higher likelihood of injury when muscles were tensed. However, tensed subjects reported less discomfort. Thus, it was suggested that at low level impacts on living soft tissue, higher peak decelerations of a striking mass may not necessarily reflect a higher level of discomfort.

Typically, research into muscle tension effects, particularly at high impact intensities, has only focused on its influence on the biomechanical response. As such, it was not generally known how it altered the reversible injury tolerance. However, there was compelling evidence to suggest that muscle tensing actually served to reduce the subjective injury tolerance.

2.9 Summary

While the loading conditions between car crash and blunt ballistic impacts and sports are different, the injury mechanisms, biomechanical responses and injury tolerances are likely to be similar. These variables have all been found to vary with age, loading condition, gender, muscle tension and is important to consider when examining the potential for injury in sporting impacts.

Nomenclature and headings explained for the following tables:

C: Compression [%]
F: Force [kN]
G3ms: Average acceleration over 3-ms [g]
GT8-7: Acceleration of Thorax [g]
GT12-Y: Acceleration of Lower Ribs [g]
ED: Probability [%]; probability of injury according to the logist function used to determine the injury tolerances
Level: Plateau of initial force spike
m: Mass [kg]
MT: Muscle Tension; indicates whether muscle tension was present in each trial. '-' denoted studies which were N/A.
P: Pressure [kPa]
TTI: Thoracic Trauma Index [TTI]; see 2.6.2.1
VC: Viscous Criterion [m/s]

NB:

- '*' denotes estimates taken from graphs
- All tolerances were for injuries of AIS-4 or MAIS-4 severity or higher

Table 2.5 Biomechanical Response of the frontal thorax (continued onto next page)

Author	Model	Test	Area	Impact	MT	Stiffness (N/cm)					
						Lower	Level	Upper	Level	Average	Level
Kroell et al. (1971)	Unembalmed Cadavers	Carrier/Striker (m=19.54-23.64)	Sternum	6.71 - 7.38 ms^{-1}	-	1080*	2742.7 N*	10077*	3335 N*	5578.5*	
Lobdell (1973)	Human Volunteers	bar	Mid-Sternum	Quasi-dynamic	Yes					236	
					No					70	
Stalnaker (1973)	Unembalmed Cadavers	m = 10	4th intercostal space	6 ms^{-1}	-					122.6	6227 N
	Human Volunteers				Yes					1138	1512 N
					No					403	667 N
Kroell et al. (1974)	Unembalmed Cadavers	Guided Mass m = 19.5/23.1	4th intercostal space	6.71 - 7.38 ms^{-1}	-	1167*	2770 N*	9403*	3310 N*	5285*	
Neathery (1974)	Summary Paper of Kroell et al. (1971), Stalnaker (1973)		4th intercostal space	5.33 - 6.67 ms^{-1}	-	315.3	3115 N	788.6	6120 N	551.95	
Fayon (1975)	Cadavers	Belt Loading	Sternum		-	175		263		219	
			R2R		-	175		350		262.5	
			R9R		-	88		175		131.5	
		Disc Loading	Sternum		-	88		175		131.5	
		Belt Loading	Mid-Sternum		-					1664	
Walfisch (1980)	Reviewed by King (2000)	Belt Loading			-	700		1611		1194	
Patrick (1981)	Single Volunteer	Bar Pendulum (m = 10)	Chest	2.4 ms^{-1}	Yes					790	1100 N
					No					570	
				4.6 ms^{-1}	Yes					2500	1340 N

						Stiffness (N/cm)					
Author	**Model**	**Test**	**Area**	**Impact**	**MT**	**Lower**	**Level**	**Upper**	**Level**	**Average**	**Level**
L'Abbe et al (1982)	Volunteer	Belt Loading	Mid-Sternum	m = 45 kg h = 0.40	No					1375	3.2 kN
			7th Rib		No					1232	
			Clavicle		No					2000	
			Mid-Sternum		Yes					1400	4 kN
			7th Rib		Yes					1250	
			Clavicle		Yes					2700	
Backaitis & St-Laurent (1986)	Human Volunteers	Belt Loading	L. Clavicle	3 KN	Yes					2513	
					No					2036	
			Mid-Sternum		Yes					1618	
					No					1342	
			Right 7th Rib		Yes					1256	
					No					1018	
Schneider (1992)	Unembalmed Cadavers	Quasi-static	Upper-Mid Sternum		-	86		123			
			Lower Sternum		-	57		114			
			2nd Rib		-	56		73			
			5th		-	51		84			
			7th Rib		-	34		52			
Yoganandan (1997)	Unembalmed Cadavers	Pendulum (m = 23.4)	Right 8th Rib	4.3 ms^{-1}	-					2276.7	1300
King (2000) (Review)	Nahum (1970), Kroell (1971)	Pendulum (6" impactor)		4.9 ms^{-1} (19.5 kg)	-	3430	2179 N	4692	2980 N	4062	2580 N
				7.2 ms^{-1} (23.2 kg)	-	5323	3380 N	7144	4537 N	6304	4003 N
Duma et al. (2005)	Human Cadavers	Dynamic Belt Test		1.5 ms^{-1}	-					19.5 kN/% (male) 6.6 kN/% (female)	

Table 2.6 Biomechanical Response of the lateral thorax

						Stiffness (N/cm)					
Author	**Model**	**Test**	**Area**	**Impact**	**MT**	**Lower**	**Level**	**Upper**	**Level**	**Average**	**Level**
Stalnaker (1973a)	Unembalmed cadavers	Flat Impactor (m = 10)	Thorax	6.1 ms^{-1}	-	2736		4378			
				8.8 ms^{-1}	-	4378		7900			
Viano (1989)	Unembalmed cadavers	Pendulum (m = 23.4)	Thorax	4.42 ms^{-1}	-	214	1.5 kN	640	3.2 kN		
				6.52 ms^{-1}	-	400	2 kN	1000	3.0 kN		
				9.33 ms^{-1}	-	434.8	5 kN	1400	7.0 kN		
Viano et al. (1989)	Unembalmed cadavers	Pendulum (m = 23.4)	Thorax	4.76 ms^{-1}	-					447*	
				6.83 ms^{-1}	-					830*	
				9.4 ms^{-1}	-					667*	
Viano et al. (1989a)	Swine	Pendulum (m = 23.4)	Lower Thorax	4.3 ms^{-1}	-					1167.3*	
				6.7 ms^{-1}	-					1464.8*	
				8.2 ms^{-1}	-					1489*	
Talantikite et al. (1998)	Cadavers	Horizontal Impactor (m = 12 or 16)	xiphoid process	6 ms^{-1} (12 kg)	-	469	1.5 kN	1325	2.65 kN	666.7	2 kN
				6 ms^{-1} (16 kg)	-	933.3	1.4 kN	1880	2.35 kN	1200	1.8 kN
				8.5 ms^{-1} (12 kg)	-	1150	2.3 kN	2400	3.6 kN	1666.7	3 kN
Shaw et al. (2006)	Fresh Cadavers	6" diameter m = 23	Thorax		-					2667*	1.6 kN*

Table 2.7 **Biomechanical response for the frontal abdomen.**

						Stiffness (N/cm)					
Author	**Model**	**Test**	**Area**	**Impact**	**MT**	**Lower**	**Level**	**Upper**	**Level**	**Average**	**Level**
Cavanaugh et al. (1986)	Unembalmed Cadavers	Rigid Bar (m = 32/64)	L3	6.1 ms^{-1}	-	202		1012		208	
				10.4 ms^{-1}	-					703	
Hardy et al. (2001)	Unembalmed Cadavers	Free-back Rigid Bar (m = 48)	Mid-Abdomen (L3)	6 ms^{-1}	-	190		350		270	
				10 ms^{-1}	-	500		750		625	
		Fixed-back Rigid Bar	Mid-Abdomen	3 ms^{-1}	-					100	restricted to 200 mm
		Belt Loading	Mid-Abdomen (Umbilicus)	3.0 - 5.0 ms^{-1}	-					1200	
		Air Bag		13 ms^{-1}	-	5000		20000		12500	
Troseille et al. (2002)	Fresh Cadavers	Belt Loading	Lower		-					129	
King (2004) (review)	Nusholtz (1988)		Lower		-					527	
	Stalnaker & Ulman (1985)		Lower		-					230	

Table 2.8 Biomechanical response for the lateral abdomen.

						Stiffness (N/cm)					
Author	**Model**	**Test**	**Area**	**Impact**	**MT**	**Lower**	**Level**	**Upper**	**Level**	**Average**	**Level**
Viano (1989)	Unembalmed cadavers	Pendulum (m=23.4)	Abdomen	4.79 ms^{-1}	-	176.5	1.5 kN	1000	1.5 kN		
				6.83 ms^{-1}	-	352.9	3.0 kN	750	3 kN		
				9.4 ms^{-1}	-	346.1	4.5 kN	1285.7	4.5 kN		
Viano et al. (1989)	Unembalmed cadavers	Pendulum (m = 23.4)	Abdomen	4.76 ms^{-1}	-					537*	
				6.83 ms^{-1}	-					758.9*	
				9.4 ms^{-1}	-					1232*	
Viano et al. (1989a)	Swine	Pendulum (m = 23.4)	Upper Abdomen	4.3 ms^{-1}	-					1076.9*	
				6.7 ms^{-1}	-					1464.8*	
				8.2 ms^{-1}	-					1489*	

Table 2.9 **Frontal thoracic tolerances**

					Tolerances (AIS 4+)								
Author	**Model**	**Test**	**Impact**	**Area**	**VC**	**C**	**GT8-7**	**GT12-Y**	**F**	**G3ms (g)**	**TTI (g)**	**P**	**ED**
Kroell et al. (1974)	Unembalmed Cadavers	Guided Mass m = 19.5/23.1	6.71 - 7.38 ms^{-1}	Sternum		39%			4.83				
Walfisch (1980)		Belt Loading		Thorax	1.4								
Lau & Viano (1986)	Cadavers	Analysed past papers	5- 15 ms^{-1}	Thorax	1 1.3								p = 0.25 p = 0.50
Lau & Viano (1988)	Swine (liver)	Steering Wheel	6, 9, 12 ms^{-1}	xiphoid process	1.24	35.0%							p = 0.50
Ridella & Viano (1990)	Cadavers	pendulum	2.42 - 8.91 ms^{-1}	Thorax	1.09	35.9%							p =0.25
	Swine	Driven impactor	15 – 30 ms^{-1}		0.65	7.5%							
Foret-Bruno (1998)		Seatbelt							6.9				p = 0.50
Lau et al. (1993)	Swine	airbag	15 kPa/ms	xiphoid process	2.0-3.0	72 mm			11				
Viano & King (2000) (summary)					1	34%				60	85-90		p = 0.25
King (2001) (review)	PMHS Patrick (1965)			Sternum					3.3				
				Clavicle + Sternum					8				
	Rhesus Monkeys (Melvin et al., 1973)			liver								310	

Table 2.10 Lateral thoracic tolerances

					Tolerances (AIS 4+)									
Author	**Model**	**Test**	**Impact**	**Area**	**VC**	**C**	**C(half)**	**GT8-7**	**GT12-Y**	**F**	**G3ms**	**TTI**	**P**	**ED**
Morgan et al. (1986)	Cadavers, Computer SID	vehicle crash	40 - 60 km/h	4th/8th rib								R: 129 L: 149		p = 0.25
Viano (1989)	Unembalmed cadavers	Pendulum (m = 23.4 kg)	4.42 ms^{-1} 6.52 ms^{-1} 9.33 ms^{-1}		1.47	38.4%		45.2	31.6	5.48				p = 0.50
Viano et al. (1989)	Unembalmed cadavers	Pendulum (m = 23.4 kg)	4.42 ms^{-1} 6.52 ms^{-1} 9.33 ms^{-1}		1.0	33.9%		28.5	20.4	3.19				
Viano et al. (1989a)	Swine	Pendulum (m = 23.4 kg)	4.3 ms^{-1} 6.7 ms^{-1} 8.2 ms^{-1}		1.01	32.5%				3.9	81.3	140		p = 0.50
Ridella & Viano (1990)	Cadaver	pendulum	2.2 - 7.6 ms^{-1}		1.47	50.0%								p = 0.25
	swine		2 - 7 ms^{-1}		0.89	26.7%								
Viano & King (2000) (review)	Summary Paper			Chest + Shoulder	1.47	38.0%				10.2				

Table 2.11 **Frontal abdominal Tolerances**

					Tolerances (AIS 4+)								
Author	**Model**	**Test**	**Impact**	**Area**	**VC**	**C**	**GT8-7**	**GT12-Y**	**F**	**G3ms**	**TTI**	**P**	**ED**
Lau, 1981	Rabbits				1.9 (liver) 2.2 (kidneys)								
Stalnaker (1985)	Monkeys			Upper	3.02								
				Mid	3.83								
				Lower	8.03								
Cavanaugh et al. (1986)	Unembalmed Cadavers	Rigid Bar (m = 32/64)	6.1 ms^{-1} 10.4 ms^{-1}	L3	< 3.38 (liver) < 5.58 (ribs)								
Ridella & Viano (1990)	Swine	Seatbelt	1.5 - 6.0 ms^{-1}		1.12	50%							
Lau & Viano (1986)	Cadavers	Analysed past papers	5 - 15 ms^{-1}		1.4								p =0.25
Viano & King (2000) (review)	Summary Paper				1.4	48%			3.9			216	
King (2001) (review)	rabbits (Lau & Viano, 1986)	fixed back		liver					0.24				
	Cadavers (Horsch et al., 1985)	steering wheel		liver	0.72								
	Swine (Miller, 1989)	belt loa		lower		48.3%			3.76				p = 0.25
Hardy et al. (2001)	Unembalmed Cadavers	Free-back Rigid Bar (m = 48 kg)	6 ms^{-1}	Mid-Abdomen (L3)					4.5				
Steffan (2002)	Human Cadavers	Belt Loading		Lower					6 - 7.1				
Troseille et al. (2002)	Fresh Cadavers	Belt Loading		Lower	1.6				7.5				

Table 2.12 Lateral Abdominal Tolerances

					Tolerances (AIS 4+)									
Author	**Model**	**Test**	**Impact**	**Area**	**VC**	**C**	**C(half)**	**GT8-7**	**GT12-Y**	**F**	**G3ms**	**TTI**	**P**	**ED**
Stalnaker (1973a)	Monkey Cadavers	Flat Impactor (m = 10 kg)		~9th rib			Right: 0.54 Left: 0.60			3.11		220 (Upper)		
Stalnaker (1985)	Monkey & Human Cadavers	Review			right: 3.53 left: 4.69									
Viano (1989)	Unembalmed cadavers	Pendulum (m = 23.4 kg)	4.79 ms^{-1} 6.83 ms^{-1} 9.4 ms^{-1}		1.98	43.7%		30.7	39	6.73				p = 0.25
Viano et al. (1989)	Unembalmed cadavers	Pendulum (m = 23.4 kg)	4.79 ms^{-1} 6.83 ms^{-1} 9.4 ms^{-1}		2.01	51.2%		28.2	30.1	6.1				
Viano et al. (1989a)	Swine	Pendulum (m = 23.4 kg)	4.3 ms^{-1} 6.7 ms^{-1} 8.2 ms^{-1}	Upper Abdomen	1.01	32.5%				3.9	81.3	140		p = 0.50
Cavanaugh et al. (1996)	Cadavers	Sled	6.7 ms^{-1}						72			143		
Viano & King (2000) (review)	Summary Paper				1.98	47.0%				6.7				
King (2000) (review)	Rabbits (Rouhana et al., 1986)			liver right left	3.15 2.71 3.31									p = 0.50

Chapter 3
Impacts in Sports Literature Review

3.1 Introduction

The chapter begins by identifying the most common injuries within cricket, football and Tae Kwon Do and summarising the impact intensities that have been measured. Next, it discusses preventative measures that have been implemented to reduce or prevent these injuries. Next, a case study on identifying the causes of Commotio Cordis and the development of relevant prevention methods is presented. Finally, a comparison between impacts in sports, and car crash and ballistics is made. This was the main aim of this chapter; that is, to disseminate the difference between the injuries and risk of injury observed in automobile accidents and blunt ballistic impacts to those found in sport.

3.2 Injuries in Sport

Clinical observation of injury showed that those incurred in sport are generally less severe than car crash or ballistic injuries. This is likely due to the difference in loading condition as collisions in sport have much lower impact energies; that is, they are either low mass-high velocity (i.e. cricket) or high mass-low velocity (tackle). Car crash victims are generally subjected to a single impact event from a combination of the seatbelt, airbag or steering wheel, whereas an athlete can experience multiple loads to the same body part throughout the duration of a match or competition. This suggests that sports injuries may not be caused by a single acute trauma, but rather from a small number of moderate traumas leading to failure or a series of micro-traumas leading to an overuse injury (Kazemi et al., 2005).

To determine which areas of the body need further protection, it is important to assess an individual athlete's injury risk. This is inherently difficult, however, because injury definitions vary within and between sports as well as amongst researchers. As such, injury rates are not consistently defined across studies making conclusions hard to formulate. Using different injury definitions with the same raw data will lead to drastically different implications in terms of injury risk and severity.

Brooks & Fuller (2006) summarised the most common ways of reporting injuries are: (i) the absolute number of injuries; (ii) the proportion of injuries; and (iii) the incidence of injuries. These authors argued that reporting injury data in terms of incidence was considered to be the most accurate because absolute and proportional injury rates did not provide information about injury risk and did not account for the different levels of exposure to various risk factors. As such, injury incidence rates are typically discussed in *injuries per athlete exposure* (A-E). However, this is dependent on how an 'athlete-exposure' was defined; it can be based on each player-hour of exposure, per athlete-exposure or match. Of the three, the player-hour of exposure is considered to be the most valuable because per-athlete exposure does not account for the time exposed and per match does not account for the number of competitors.

3.2.1 Cricket

Cricket is a relatively safe game that has lower rates of injury risk and severity when compared to other professional sports (Orchard et al., 2002). At present, an official cricket injury is defined as:

> "any physical injury or medical condition that either prevents a player from being fully available for selection for a major match or causes a player to be unable to bat, bowl or keep wicket when required by either the rules or the team's captain during a major match" (Orchard et al., 2005).

This definition includes players who were available for limited action, but were not selected (i.e. all-rounders who were not selected as batsman when their injury affected their bowling), and did not include players that were withheld from matches for injury prevention reasons. Injuries were also classified into acute (rapid onset), chronic (slow changes over longer duration) and acute on chronic (slow developing and long in duration, but caused by rapid movements) to describe the causes of injury (Stretch, 2003).

The two main measures of injury risk and severity are *injury incidence* and *injury prevalence*. Injury incidence measured the number of injuries over a given period (1), while the prevalence analysed the average number of squad members unavailable for selection due to injury (2). A caveat of injury incidence rates was that they were generally separated by body region and were calculated as the ratio of injury for that body region to the total number of recorded injuries (3).

$$\text{(1)} \qquad \text{injury incidence} = \frac{\text{total \# of injuries}}{\text{total \# of matches}} \text{ or } \frac{\text{total \# of injuries}}{\text{season}} \text{ (overall)}$$

$$\text{(2)} \qquad \text{injury prevalence} = \frac{\text{total \# of missed player games}}{\text{total \# of games} \times \text{total \# of squad members}}$$

$$\text{(3)} \qquad \text{injury incidence} = \frac{\text{total \# of injuries per body region}}{\text{total \# of injuries}} \text{ (body region)}$$

Table 3.1 Summary of injury incidence in cricketers separated by body region and divided by total injuries to indicate overall injury risk.

Study	Summary	Injury Incidence (%)				
		Head & Neck	Upper Limb	Back & Trunk	Lower Limb	Other
Leary & White (2000)	English County Club	5.7	29.4	20	44.9	-
Orchard et al. (2002)	State/National Australian	3.4	19.7	19.5	49.1	8.2
Newman, D. (2003)	England & Wales 1st Class County	4.3	22.6	23	46	2.7
Stretch, RA (2003)	Provincial & National South African	4.1	23.3	22.8	49.8	-
Orchard et al. (2005)	State/National Australian	2	24.5	13.2	49	7.3
Mansingh, A et al. (2006)	West Indies International Team	12	28	28	28	4

The most frequent injury site to cricketers was the lower limbs, followed by the upper limbs, and back and trunk (Table 3.1). Injuries in these regions were commonly hamstring strains, hand fractures and dislocations, and lumbar stresses and strains, the last of which contributed roughly 15.3 – 27.2% of the total missed player games (Orchard et al., 2002; Newman, 2003; Stretch, 2003; Orchard et al., 2005). These injuries occurred most frequently when bowling and fielding, whilst batting produced the least number of injuries (Stretch, 2003) suggesting that most injuries in cricket were not impact-related. However, recent studies have observed an increase in the number of injuries to the hands of batsmen caused by a pinching effect between the bat and ball (Orchard et al., 2005; Mansingh et al., 2006). While this supported the re-designing of batting gloves to better mitigate and absorb this impact (Newman, 2003), it also suggested that current cricket PPE are generally adequate in protecting the batsman from projectile ball impacts.

In terms of playing position, bowlers, especially pace bowlers, were at particular risk for severe injury (Table 3.2). Pace bowlers consistently accounted for the highest percentage of missed match selection due to injury. As such, the bulk of research into cricket injuries has focused on the bowling action. Whilst injuries to batsmen have steadily increased over time, the main cause of injury was from the acts of fielding and catching and not direct cricket ball impacts (Mansingh et al., 2006).

Table 3.2. Injury prevalence in cricketers separated by position. Data from Orchard et al. (2005) includes seasons from 2002-03 to 2004-05.

Study	Injury Prevalence by Position					
	Batsmen	**Wicketkeeper**	**Pace Bowler**	**Medium Pace**	**Spinner**	**All-rounder**
Leary & White (2000)	4.9%	4.7%	7.0% (all bowlers)			5.5%
Orchard et al. (2002)	4.0%	1.6%	13.7%	-	4.0%	-
Newman, D (2003)	7.0%	6.7%	18.0%	15.0%	8.9%	-
Orchard et al. (2005)	3% 7.1% 9.5%	0.9% 3.7% 3.2%	16.6% 18.3% 9.5%	-	3.8% 6.9% 4.2%	-

3.2.2 Football (Soccer)

With over 250 million players registered in the Federation Internationale de Football Association (FIFA), soccer is the world's most popular organised sport. With steadily increasing participation and more intense competition, the likelihood for severe injury has increased as the athletes have grown stronger and faster. These injuries affect not only the performance of the player and their club, but also carry with it a substantial economic cost. As such, there has been a lot of pressure to conduct injury surveillance studies to identify and describe the risks, mechanisms and incidences of injury. This information can then be used to develop effective treatment to reduce the effects of injury and prevention strategies to decrease the occurrence of injury.

An official soccer injury is officially defined as “any physical complaint sustained by a player that result from football match or training” and was developed by the FIFA Medical Assessment and Research Centre (F-MARC) (Fuller et al., 2006). An injury that results in a player receiving medical attention is a *medical attention* injury, whilst a *time-loss* injury results in a player being unable to take full part in future football training or competition.

Injury rates in soccer have been found to be generally higher than most professional sports. Male soccer players participating in the most elite-level of matches (e.g. World Cup) were at particular risk due to the intensity, pressure and the high rewards for victory (Wong & Hong, 2005; Rahnama, 2007). Injury rates in the World Cup have reached up to 80.96 injuries per 1000 match hours (Dvorak et al., 2007) – an injury rate comparable to those observed in rugby, which was more of a full-on contact sport (Hawkins & Fuller, 1999). Female players also had a high risk of injury, but this was attributed to their lower level of skill and inability to avoid injury-provoking events (Giza & Micheli, 2005; Wong & Hong, 2005).

In general, the greatest site of injury was the lower extremity, accounting for 60-90% of all soccer-related injuries (Table 3.3). Knee injuries, particularly to the ACL, were more significantly common amongst females (Wong & Hong, 2005; Giza et al., 2005; Jacobson & Tegner, 2007). Knee injuries also resulted in the highest frequency of cases where females missed 28+ days of action (Jacobson et al., 2007) and males were forced out of practices and games for 10+ days (Agel et al., 2007). Other injuries causing significant time-loss in males were lower leg contusions and ankle sprains (Dvorak et al., 2007), despite the thigh having the highest injury incidence. Lower leg fractures, which take between 18-40 weeks for full recovery (Boden et al., 1999), and concussions both had low injury incidences, but were recognised as two of the most severe injuries that can occur. As such, shin guards were made mandatory to the uniform and rules were set in place to reduce actions in soccer that were thought to cause contusions. However, over 80% of injuries to the shin occurred while the victim was wearing a shin guard, suggesting that more research into their design was necessary, particularly in protecting the middle and distal thirds of the tibia and fibula (Cattermole et al., 1996; Boden et al., 1999).

Table 3.3 Summary of football injury rates from literature.

Study		**Jacobson et al. (2007)**	**Dvorak et al. (2007)**		**Agel et al. (2007)**	**Giza et al. (2005)**	**Junge et al. (2004)**	**Elias (2001)**		**Hawkins et al. (2001)**	**Hawkins & Fuller (1999)**
Level		Women's Swedish Premier League	2006 World Cup	2002 World Cup	NCAA 1988-89 to 2002-03	WUSA	FIFA & Olympics 1998-2001	USA Female U12 - U19	USA Male U12 -U19	English Premier League	English Premier League
Head & Neck		10.3	9.0	14.6	12.8	10.4	15.0	12.4	12.3	6.9	3.3
Upper Extremity		1.7	7.0	4.7	6.8	-	-	10.2	11.7	2.7	2.3
Torso & Back		2.6	6.4	3.5	10.5	-	-	7.1	8.1	2.9	6.4
Lower Extremity	**Total**	81.2	72.4	76.6	67.3	60.0	-	57.2	61.4	87.1	88.0
	Groin	4.3	2.8	5.3	-	-	-	-	-	6.2	10.7
	Hip		0.7	1.2	-	-	-	-	-	2.2	2.6
	Thigh	19.0	14.5	17.5	-	-	16.0	-	-	24.2	22.8
	Knee	25.9	12.4	12.9	-	31.8	12.0	18.0	16.8	16.6	15.1
	Shank	7.8	20.7	17.0	-	-	15.0	-	-	12.3	
	Ankle	16.4	16.6	14.6	-	9.3	17.0	-	-	18.6	17.6
	Foot	7.8	9.7	8.2	-	9.3	-	-	-	6.9	7.2

The major injury mechanism found in football was from either receiving or making a slide tackle accounting for 16 - 31.8% of all injuries (Hawkins & Fuller, 1999; Hawkins et al., 2002; Agel et al., 2007). In a small sample, Rahnama (2007) reported that 70% of all injuries were caused from a player receiving a slide tackle. As both receiving and making a tackle involve the kicking leg, the dominant side has been found to be significantly more injured than the non-dominated side, registering between 52.3 - 56.5% of recorded injuries (Hawkins & Fuller, 1999). These actions mainly caused contusions, strains and sprains, making up between 60 – 90 % of all injuries (Table 3.4).

Table 3.4 Summary of football injury types (as a % of total injuries).

Study	**Hawkins & Fuller (1999)**	**Hawkins et al. (2001)**	**Giza et al. (2005)**	**Dvorak et al. (2007)**		**Jacobson et al. (2007)**
Contusion	24.0	16.0	16.2	49.1	51.0	8.4
Strain	37.1	35.0	30.7	20.5	13.1	28.7
Sprain	21.2	20.2	19.1	14.0	16.6	24.5
Overuse	5.1	1.2	-	-	-	31.2
Fracture	3.8	4.9	11.6	1.8	0.7	1.3
Laceration	2.0	1.6	-	7.0	4.1	1.3
Concussion	-	-	2.9	2.3	0.7	3.8
Other	6.6	21.1	-	5.3	13.8	0.8

3.2.3 Tae Kwon Do (TKD)

Tae Kwon Do (TKD) is a full contact sport which awards points for forceful punches to the torso and kicks to the head, face and torso. As bouts are decided by points or knock-outs, TKD competitions encourage physical contact between competitors. This places considerable injury risk on each competitor as the emphasis is on fast, powerful kicks with the potential for causing severe injury (Serina & Lieu, 1991). In fact, the risk of injury and injury severity in TKD has been found to be much higher than other martial arts such as shotokan karate, aikido and kung fu (Zetaruk et al., 2005), despite the protective equipment worn by the competitors. This extra padding, however, may ultimately benefit the athlete who performed the attack rather than the one absorbing the blow (Zemper & Pieter, 1989).

Injuries in TKD are defined as any event that required an athlete to cease competition (Burke et al., 2003), including situations where:

1) the participant was forced to leave the competition;
2) the referee or athlete had to stop the competition; or
3) the athlete requested medical attention under any circumstance

(Kazemi & Pieter, 2004; Kazemi et al., 2005).

Using these definitions, injury incidence rates from competition have been defined in terms of *athlete-exposures* (AE), *athlete-exposures per hour* (AE/h) and *per athlete* (PA) as shown in Table 3.5.

Table 3.5 Incidence of injury rates for various TKD championships (AE: Athlete-exposure; AE/h: Athlete-exposure per hour; PA: per athlete).

Study	**Competition**	**Injury Rates**	
		Male	**Female**
Zemper & Pieter (1989)	1988 US Olympic Trials	12.74 % AE	9.01 % AE
Pieter et al. (1995)	1993 Taekwondo Cup	13.95 % AE	9.65 % AE
Pieter et al. (1998)	Open British Tournament	5.13 % AE	4.76 % AE
Pieter et al. (1999)		9.51 % AE	10.55 % AE
Beis et al. (2001)	Greek National Championships	2.06 % AE	3.64 % AE
Phillips et al. (2001)	African National Championships	8.66% AE (combined)	
Kazemi & Pieter (2004)	1997 Canadian Taekwondo Championships	79.9 % AE 16 % PA	25.3 % AE 5.1 % PA
Kazemi et al. (2005)	Canadian National Tournament	Training: 35.4 % AE Competition: 16.67 % AE Training: 3.25 % AE/h	
Zetou et al. (2006)	Greek National Taekwondo Division	Training: 0.66 % AE/h Competition: 0.9 % AE/h	

The most commonly reported sites of injury were the head, neck and the lower extremities. The injury mechanism of head and neck injuries were from receiving kicks, particularly roundhouse kicks, whereas the lower extremities were usually injured while attacking specifically with the instep of the foot when striking the elbow (Kazemi & Pieter, 2004). The most common injury types were found to be contusions, lacerations and sprains (Kazemi & Pieter, 2004; Zetou et al., 2006). Furthermore, injury risk did not seem to fully correlate with gender, but the majority of studies had reported higher levels of injury risk amongst male competitors.

In the 2006 UK Taekwondo Championships, a total of 11 injuries were reported to the medical staff (Table 3.6). All but one injury occurred from kicks, with the majority of injuries suffered by the competitor who was kicked. These injury trends reflected those reported in literature and suggested that PPE designs have not yet addressed the specific needs of the competitors.

Table 3.6. Summary of reported injuries at the 2006 UK TKD Championships (courtesy of Ben Aherne, UK TKD).

Total Number of Reported Injuries: 11		
Attacking	**Receiving**	**Other**
* Top of right foot (kick to elbow) * Left foot tissue damage	* Kick to right knee & ankle * Kick to jaw (soft tissue injury) * Kick to left elbow * Kick to 1/2 metatarsal * Kick to head * Kick to right eye & nose bleed * Kick to C spine * Kick to 5th metatarsal	* 3rd finger (bent in match)

3.3 Impact Intensities in Sport

Before PPE can be designed to properly protect areas of high injury risk, whether it is due to susceptibility or severity, it is important to establish the common impact intensities experienced within each specific sport. However, this has been an inherently difficult task due to limitations in technology and for ethical reasons. The following summarises these sporting impact intensities.

3.3.1 Impact Measurement in Sports

Impact intensities in sport were traditionally obtained by recreating match-like conditions within a controlled laboratory environment. Test rigs were designed to match the inertia of a specific body part and instrumented to measure variables such as force, contact area and pressure, whilst high speed or automatic motion capture systems helped to calculate the velocity and acceleration of the impactor. However, these rigs were generally constructed of materials whose properties were not representative of the human body. As such, its measurements were thought to overestimate the actual impact intensities due to their low biofidelity. Moreover, input impact energies and forces derived from the impactor were thought to be inaccurate as establishing the correct effective mass is difficult (Falco et al., 2009). Therefore, meaningful results were likely only to be obtained during real match play.

3.3.2 Cricket

Scant literature exists regarding the intensity of ballistic impacts during cricket matches as most injuries are chronic and recurring. In spite of this, impact intensities can be estimated using knowledge of the inertial parameters of the ball and the velocities at impact. The ball consists of a core of cork covered by leather with a raised sewn seam, having a mass of 155-163 g and a diameter between 224 – 229 mm. In terms of velocity, Penrose et al. (1976) found that there was a significant decrease between release velocity out of the bowler's hand and the velocity when it reached the batsmen (Table 3.7). Furthermore, release speeds could be fairly consistent, but end speeds were more highly variable. Whilst factors such as temperature, humidity and the pitch condition also affect the end velocity, the most influential variable was likely to be the length of bowl. A 'full' bowl will encounter less reduction in velocity, so it is possible that batsmen may experience a bowl approaching 100 mph.

Table 3.7 Reduction in cricket ball velocity as it reaches the batsman (Penrose et al., 1976)

Bowler	Release Speed (mph)	Speed at Batting End (mph)
J. Thomson (Australia)	99.7	80.73
A. Roberts (West Indies)	93.62	80.71
K. Boyce (West Indies)	85.24	75.6

Using these measured match velocities and the adjustments from Penrose et al., an estimate of the energy upon impact can be easily obtained. A full toss delivered at 100 mph (44.7 ms^{-1}), was roughly equivalent to 155 J of energy. However, as full tosses were quite rare, the impact energy was more likely to be around 112 J representing a velocity of 85 mph (38 ms^{-1}).

3.3.3 Football (Soccer)

Despite the high frequency of slide tackles and kicks to the leg during matches, there is very little information available regarding their intensity. Instead, data has been obtained from estimating the velocity of each impact and using the inertia or effective mass of the impactor to estimate the impact energy. Straight-legged slide tackles have been reported at 1-5 ms^{-1} (Francisco et al., 2000) with a kinetic energy of 992 J when the full bodyweight was utilised (Woods, 1994; as cited in Ankrah & Mills, 2002). In contrast, an opponent's foot velocity during a kick was found to range from a minimum of 8 ms^{-1} (Philippens & Wismans, 1989) up to 18-24 ms^{-1} (Francisco et al., 2000). Ankrah & Mills (2003b) suggested that the impact energy was 10 J for a 16 ms^{-1} kick, with an effective mass of 0.1 kg, onto an ankle with an effective mass of 0.2 kg. In contrast, stud impacts have been administered with impact energies between 0.9 - 3.7 J (Ankrah & Mills, 2002; Ankrah & Mills, 2003a) and velocities of 1.2 - 2.5 ms^{-1} (Francisco et al., 2000).

Football impacts have been modelled as a single mass from a free-swinging pendulum (Bir et al., 1995), a guided drop rig consisting of tubes covered in rubber (Francisco et al., 2000) and football studs with a weighted mass (Ankrah & Mills, 2003). Ankrah & Mills (2003) suggested that these simplifications were acceptable because of the flexibility in the ankle, which did not allow the body's full inertia to be involved. However, there has not been enough research to prove that these impacts were best modelled as a point mass; that is, it is possible that the peak impact force or pressure may not occur until the inertia of the body is involved. If there is evidence of an inertial component, the impactor should be modelled as a multiple-mass system, where contact is made by an initial mass with increasing force or pressure as the additional mass(es) also made contact. However, force and pressure measurements have yet to be measured, despite being a good indicator of skeletal fracture and soft tissue contusion and very useful in developing models of the impactor for biomechanical and mathematical testing. As such, more research should be devoted to the instrumentation of football shin guards or novel force or pressure-sensing elements which can help create more realistic models for future testing.

3.3.4 Tae Kwon Do (TKD)

In Olympic TKD, the most effective form of scoring points is through the delivery of a fast and forceful kick. The majority of research has focused on the linear foot velocity at contact which was used to improve form or competitive performance (Table 3.8). This research was conducted to determine the characteristics of different TKD kicks (Kong et al., 2000; Kim & Hinrichs, 2006; Pedzich et al., 2006; Tang et al., 2007), the role of the non-kicking leg in producing velocity and power (Tsai et al., 1999) and the influence of distance, height and a target on kick performance (Nien et al., 2007; Falco et al., 2009; O'Sullivan et al., 2009). A few studies have attempted to measure the force at impact, but all used different anvils making comparisons between studies difficult (Table 3.9).

Table 3.8 Impact velocities of selected kicks in Taekwondo.

Study	**Technique**	**Participants [Experience] (number)**	**Kicks** (ms^{-1})		
			Roundhouse	**Axe**	**Back**
Serina & Lieu (1991)	High Speed Video (500 Hz)	Black Belt [1st dan +] (3)	15.9	-	8.8
Tsai et al. (1999)	High Speed Camera (120 Hz)	High School [avg: 6.7 yrs] (7)	6.382	6.183	6.015
Pieter & Pieter (1995)			15.54		
Boey & Xie (2002)			13.32 (females) 18 (males)		
Kim & Hinrichs (2006)	CCD Cameras (200 Hz)	University [min: 3 yrs] (6)	13.9 ± 0.72	-	~ 10.5
Roosen (thesis)	Vicon (250 Hz)	Taekwondo	14		
O'Sullivan et al. (2009)	Vicon	Taekwondo (5)	17.66		

Table 3.9 Impact forces measured in TKD kicks

Study	Technique (frequency)	Participants [number]	Force (N) [level]	Velocity (ms^{-1})
Pedzich et al. (2006)	Force Plate [800 Hz]	WTF players [5]	9015	-
Chiu et al. (2007)	Air Pressure	TKD players [3]	8410	23.46
Falco et al. (2009)	Piezoresistive Sensors	TKD players [31]	3482 [expert] 1478 [novice]	-
O'Sullivan et al. (2010)	Accelerometers	TKD players [5]	6400	17.66

Serina & Lieu (1991), and adopted by Chuang & Lieu (1992), calculated foot velocities and inertial parameters to determine the injury potential caused by thrust and side kicks. Swing kicks were modelled with the thigh and knee fixed and the foot rotating about the knee, whilst thrust kicks were modelled as a slider-crank linkage with the foot as a point mass at the end of the link (Fig 3.1). These linkages were simplified into effective masses and used to drive a Lobdell Chest Model. Thrust kicks were found to cause reversible skeletal damage (C_{max} = 22%), while swing kicks had the potential to cause severe internal organ and soft tissue damage (VC_{max} = 1.53 ms^{-1}). Whilst it was unclear whether the calculation of effective mass (based upon kinetic energy equivalence) was accurate, this was the first attempt to determine the injury potential of attacks within TKD.

Figure 3.1 Models used to represent thrust and swing kicks (Chuang & Lieu, 1992)

3.3.5 Boxing

Boxing is not a focus in this research, but the impact intensities found during bouts can be compared to those found in TKD. It is a research area which has received substantial attention to first identify injury potential and then design instrumented head gear to prevent head injuries. However, most of the literature has focused on striking objects of low biofidelity. Targets such as water-filled punching bags (Joch et al., 1981), padded metal targets suspended as a ballistic pendulum (Atha et al., 1985), head-forms from biomechanical surrogates such as the Hybrid III (Walilko et al., 2005) and punching bags instrumented with tri-axial accelerometers (Smith et al., 2000) have been used. Whilst the expertise of the boxers varied, the different measurement techniques would have also contributed to a wide range of measured forces (Table 3.10).

Table 3.10 Impact forces measured from punches in boxing.

Study	Technique (Frequency)	Participants [Number]	Force (N) [level]	Velocity (ms^{-1})	Impact Time (ms)
Joch et al. (1981)	Dynamometer	Elite [24] National [23] Novice [23]	3453 [elite] 3023 [Nat] 2932 [Nov]		
Atha et al. (1985)	High Speed Camera (500/1400 Hz)	Professional Boxer [1]	4096 [pad] 6320 [head]	8.9	14
Smith & Hamill (1986)	High Speed Camera (100 Hz)		6000 [exp] 3998 [int] 4234 [nov]	12.34 (exp) 11.67 (int) 10.48 (nov)	~ 10
Smith & Dyson (2000)	Dynamometer	Elite Boxers	4800 [rear] 2847 [front]		
Walilko et al. (2005)	TekScan (1.4 kHz) & High Speed Video (1 kHz)	Olympic Boxers [7]	1990 - 4741	9.14	
Pierce et al. (2006)	BestShot Force System	Professional Boxing Match [6]	1571 - 5358		

Pierce et al. (2006) argued that most of these forces were only representative of the maximum potential force that could be generated by a punch where the player did not have to worry about a counter-attack. Therefore, these measurements were most likely over-estimates and did not replicate actual match-like conditions. As such, his study instrumented the gloves of amateur boxers with capacitive force sensors to measure punch force during actual matches. These authors had hoped that future research would be able to adopt a similar approach with improved technology.

3.3.6 Fight Science

Fight Science (2005), a programme televised by National Geographic, examined human impact intensities in various martial arts and determined their injury potential. Engineers combined martial arts with knowledge and technology of car crash safety testing, biomechanics and motion analysis. A modified Hybrid III model was used to examine the force of kicks and punches from various martial arts disciplines (Table 3.11). Punches were delivered to the head-form, whilst kicks were targeted at the chest with potential injuries to the skull and chest were based on the measured impact intensities. Punches were found to potentially fracture facial bones or produce concussions in the most extreme case, while kicks were strong enough to cause rib fracture and damage internal organs.

Table 3.11 Impact intensities, in terms of force [N], for punches and kicks in Kung Fu, Karate, TKD and Boxing.

Attack		Kung Fu	Karate	Taekwondo	Boxing
Punch	**Style**	1" punch	Straight		
	Force (lb.f.)	612	816	917	993
	[N]	[2722]	[3629]	[4079]	[4417]
Kick	**Style**	Side	Flying	Spinning Back	-
	Force (lb.f.)	1023	981	1572	-
	[N]	[4550]	[4364]	[6992]	

3.4 Current Preventative Measures

3.4.1 General

Preventative measures can change the biomechanical response of the body by altering how an applied load is distributed. In sports, preventing injury, aside from avoiding impact, was likely only to be achieved by wearing PPE since changes to other equipment were rare. PPE must adhere to the British Standards which set criteria for how it must perform (i.e. minimising force transfer) under prescribed test conditions. While this provides a baseline for comparison between PPE garments, it was argued that these testing protocols were developed to protect the test rig from breaking and not to match the impact intensities encountered in sport (Ankrah & Mills, 2003).

Martin et al. (1994) suggested that the mechanical properties of the pad should be adjusted to match the mass and velocity of the impacting object; if there was insufficient mass, the pad may not deform and a reduction in acceleration may not be achieved. Even with sufficient mass, the PPE may deform in a point-elastic manner and may not spread the load or protect against the injury mechanism (Pain et al., 2008). Nevertheless, PPE must follow British Standards regulations and these are summarised in the following.

3.4.2 British Standards

British Standards, henceforth known as *BStan*, provide general requirements for all aspects of a PPE garment including the ergonomics, size and coverage. Furthermore, it outlines testing methods that should be used to assess the overall performance of PPE and allows pads within the same sport to be compared directly. In general, all PPE are to be visually and manually inspected for hard or sharp edges or any other protuberances sticking out of the PPE that could potentially injure the user. All PPE are to remain in place at all times during sporting movements and be designed to minimise discomfort and impediment. PPE should also allow for normal ranges of movements within the protected area and specific sport. The following summarises the impact testing protocol for each PPE.

3.4.2.1 Cricket – Batting Leg Pads and Chest Protector

Cricket pads are governed by two standards: BS 6183-1 and BS 6183-3. After testing, each protective zone (Fig. 3.2) is given a value which rates its overall performance and the level of cricket for which it is suitable. This ranges from pre-adolescents with limited physical strength (Level 1) to the most physically trained cricketer competing at the highest level (Level 3).

Leg pads were intended to reduce pain and injury from accidental impacts by cricket balls or in instances when used to deliberately intercept cricket balls. Protection was provided to the knee and the anterior, medial and lateral sides of the shank, with more protection on the lateral side of the forward batting leg and medial side of the rear batting leg. Chest pads were intended to protect the heart and lateral portion of the torso facing the bowler.

Figure 3.2 Protection zones for cricket batting leg guard and chest protector; (a) 1K: outer knee area; 1S: outer shin area; 2K: knee inner area; 2S: inner shin area. (b) hatch marks represent protection zones 1 and 2.

All protectors are to be impact-tested with a steel striker mounted on a guided falling mass (2.5 ± 0.1 kg) designed to simulate a cricket ball impact. The height of the hemispherical striker (72 ± 2 mm) must be adjustable to produce impact energies between 5 – 40 J (Table 3.12). The protector should rest on an anvil mounted directly on a stiff load cell or force transducer capable of measuring up to 50 kN at a minimum of 10 kHz. The batting pad is tested on two different anvils (leg and knee) whilst the chest protector has its own anvil. Prior to testing, garments are placed in a 20 ± 2 ℃, 65 ± 5% relative humidity environment for 48 hours. Five impacts at each location are to be conducted with the impact centres at least 60 mm apart and 30 mm from the edge. The maximum transmitted force in each impact is to be recorded and mean force values calculated and reported.

Table 3.12 Maximum Transmitted Force must not exceed the values provided for the given performance level and energy input.

Protector	**Performance Level**			**Maximum Transmitted Force (kN)**
	1 (J)	**2 (J)**	**3 (J)**	
Leg:				
outer shin (zone 1)	5	10	20	5
inner shin (zone 2)	10	20	40	5
outer knee (zone 1)	5	10	20	6
inner knee (zone 2)	10	20	40	6
Chest:				
outer (zone 1)	5	5	10	4
heart (zone 2)	7.5	10	15	4

3.4.2.2 Football - Shin Guards

Shin guards are governed by BS EN 13061 (2001), which explicitly states that, "shin guards cannot always prevent serious injuries but are intended to significantly reduce the severity of laceration, contusion and puncture caused by impacts". For testing, guards are subjected to stud and blunt impacts while rested on a leg form cone that is made either of metal, wood or hard plastic.

In stud impacts, the inner surface of the pad should not tear or perforate and the outer surface should not shatter. Three areas must be tested with the shin guard firmly attached to the cone. A 10 ± 0.5 mm diameter stud, at least 16 mm long, needs to be attached to a 1-kg block and released from 1.5 m (~5.4 ms^{-1}) with an appropriate guidance mechanism to produce impact. All damage is to be assessed visually and the test repeated for a condition where the guard orientation is 10° from the vertical.

When subjected to blunt impacts, the mean peak transmitted force should not exceed 2.0 kN in the central or lateral tests areas. A guided mass (1-kg, width: 14 ± 0.5 mm, length: 65 mm) with rounded edges needs to be positioned to strike the guard at roughly 90°. Force (threshold <10 kN at > 5 KHz) is to be measured with load cells or force transducers on an anvil placed on the inside of the leg form. Similarly, three separate areas will be tested, which include areas that have local discontinuities in material or geometry. Impact velocities are set at 2 ms^{-1} centrally and 1.75 ms^{-1} laterally.

3.4.2.3 Taekwondo – Shin Guards and Chest Protectors

Taekwondo equipment is governed by a three-part standard formulated for all disciplines of martial arts (BS EN 13277-1/2/3, 2000). It states that protective equipment for martial arts should "protect the wearer against contusion, abrasion, laceration, fractures and physical injuries". Furthermore, no part of the protector shall break, split or be deformed irreversibly (i.e. plastically) at any time.

The striker ($m = 2.5 \pm 0.025$ kg) is an 80±2 mm diameter cylindrical shaft with a dome-shaped end with a 100 ± 2 mm radius of curvature. Impacts are delivered in free-fall at the prescribed range of impact energies and should not exceed the maximum allowable peak force (Table 3.13). Testing is conducted at an ambient temperature of 20 ± 2 °C and relative humidity of 65 ± 5%.

Table 3.13 **Testing Conditions for shin and chest protector in Taekwondo PPE.**

Protector	Minimum number of positions to be tested	Impact Energy of the Striker (J)	Peak Force (kN)
Shin Protector	3	3	2
Chest Protector	3	12	3

The shin guard is to rest on a rigid half-cylinder (length ≥ 150 mm, 90 ± 5 mm) made of aluminium, wood or rigid plastic. Resting centrally inside the support is an anvil mounted on a load cell. To fix the guard on to the support, the two straps of the leg guard are to be pre-loaded to 50 N. Test positions should then be directed towards the weakest parts of the protector.

The chest guard must be placed on a horizontal steel plate (width ≥ 300 mm, length ≥ 350 mm, thickness ≥ 20 mm) with an anvil, resting on a load cell, in the middle of the plate. A compression ring, made of steel (m = 10 ± 0.1 kg, 140 ± 0.1 mm internal and 260 ± 4 mm external diameter) is used to fix the support. Test positions are to be situated no closer than 20 mm to the limit of zone of protection or 70 mm from the edge.

In general, the load cell or force transducer within each anvil must sample at a minimum of 2000 Hz and measure a maximum load of 10 kN. Impacts at each location are to be tested at least 3 times at the same impact energy in intervals of 60 ± 10 seconds. Moreover, each impact location is not to be tested within 80 mm of the prior test location unless an alternative protector is used. After each test, the testing apparatus must remain stationary while the pad is moved to its new location.

3.4.2.4 Criticisms of British Standards

A major shortcoming of these standards is that they were formulated without proper scientific assessment or justification. Impact conditions were often significantly lower than the levels observed regularly in sport or required to cause injury. While certain researchers may actually want to limit these impact intensities (to protect the test rig from breaking) it meant that PPE were not adequately scrutinised to the level required to protect against significant injury. This is addressed further in § 3.7. Also, the response of PPE may be non-linear;

that is, the level of force reduction at more severe intensities may not be the same as shown in these impacts.

Secondly, all tests were conducted on test rigs with low biofidelity. For example, test rigs for testing football shin guards could be constructed of metal, wood or hard plastic. While neither of these materials represented the human leg, the guidelines did not provide material property constraints to ensure that testing was similar in all cases. This was important as impacts to a leg of low biofidelity will create false load transfer mechanisms and changing the leg-form will alter the values of force transmitted. The trade-off in using such a rigid test rig was that it was easier to analyse a shin guard's force-deflection response on a rigid anvil, despite having an increased impact severity relative to a real body impact.

Lastly, certain clauses were too subjective, particularly those regarding its fit and comfort. In all cases, PPE were intended to 'minimise discomfort', but it was not inherently clear how this was to be objectively assessed. Similarly, PPE were to allow for a normal range of movements, but the restriction between athletes was sure to change if the equipment itself was generic. Moreover, PPE was intended to remain in place at all times, though observation from the 2006 UK Taekwondo Championships suggested that this remained a major issue. Competitors were found to be constantly adjusting their PPE after each attacking or defending action, ruining the overall continuity of the bout.

3.4.3 Cricket Batting Pad Performance

As the main role of the batting pads was to prevent injury and injuries to the lower leg in cricket were quite rare, they have always been considered to be functionally adequate. As such, very little research has been conducted on the performance of batting pads. However, it has been postulated that they may be too cumbersome, bulky while leading to significantly increased body temperatures.

Hyrosomallis (1996) tested 11 leg guards from a free-fall height of 40 cm with a 5-kg metal striker having a hemispherical impact surface (7.3 cm diameter). Tests were conducted at two different temperature conditions: 1) 20 °C and 65% relative humidity (RH) and; 2) 25 °C and 85% RH. In general, the leg guards offered adequate shin and ankle impact resistance but more than half were inadequate at the knee roll, particularly in cases at higher temperatures and humidity. This implied that under hot and humid conditions, pads would not provide the expected levels of protection necessary for the most elite players. Furthermore, a correlation between protective performance of these pads and price was not found.

Stretch (1998) found that the different structure and composition of pads affected the impact kinetics at various impact speeds. Pads made of polyurethane offered the most protection by effectively absorbing impact forces. Current traditional pads, however, were found to decrease the ball rebound distance by reducing the ball-pad coefficient of restitution. While players may not select pads based solely on their restitution, it may influence their decision as it can decrease the likelihood of being caught ‘bat-pad’. Therefore, controlling the rebound characteristics remains an important design consideration and it is suggested that more research is needed to understand the impact properties of different material combinations.

3.4.4 Shin Guards Performance

Shin guards needed to be sufficiently flexible to not restrict movement, yet stiff enough to absorb or dissipate energy (Ankrah & Mills, 2003). Whilst shin guards were capable of absorbing large quantities of energy, it was unlikely that they were able to prevent fractures from potential high-energy blows. In spite of this, the majority of research into shin guards focused on protecting against tibial fractures (Philippens & Wismans, 1989; Francisco et al., 2000) mainly because biomechanical information was not available on contusions, abrasions and cuts. These tests were performed on biomechanical surrogates such as wooden legs (Philippens & Wismans, 1989; Lees & Cooper, 1995), the Hybrid III leg-form (Bir et al., 1995) or composite bones (Francisco et al., 2000; Ankrah & Mills, 2003). The main advantage of these models was they allowed for consistent testing across all pads though fracture thresholds were much higher than actual bone to avoid the costs of replacing the test rig. While cost-effective, the low biofidelity of the models affected the ability to transfer these results to the human leg. Nevertheless, all tested shin guards showed the ability to significantly reduce peak transmitted force (Table 3.14).

Table 3.14 Performance of shin guards in reducing peak force and deceleration.

Study	Model	Impactor	Input	Measured Variable	Reduction
Philippens & Wismans (1989)	Wooden Leg	70 mm hemisphere	Kinetic Energy (5.3 J)	Peak Force	28 - 53 %
Bir et al. (1995)	Hybrid III	38 mm cylinder radius	Force (2.3 kN)	Peak Force	40 - 77 %
Lees & Cooper (1995)*	Wooden Leg	70 mm hemisphere	Energy (19.6 J)	Peak Deceleration	40 - 60 %
Francisco et al. (2000)	Padded Sawbones Tibia	38-mm radius cylinder with 12.7-mm rubber cover	Energy (4.1 - 16.5 J)	Peak Force	11 - 17%
Ankrah & Mills (2003)	Sawbones Tibia & Senflex 435	Stud attached to falling 4.1-kg mass	Impact Energy (< 5 J)	Peak Force	27-73 %

The main design problem of shin guards was that their role as guards were not well understood; that is, they were either intended to transfer energy across the length of the guard (Francisco et al., 2000) or transfer load from a central impact, away from the bone to the muscles at the side of the tibia (Ankrah & Mills, 2003). Nevertheless, the injury criteria used to assess the performance of shin guards in all studies was the peak transmitted force to the surrogate leg. Whilst Bir et al. (1995) showed that the protective performance decreased with temperature, Francisco et al. (2000) proposed that design and performance of shin guards were dependent on three points:

1) fibreglass shells were better than other materials in distributing impact force, but not attenuating force;
2) increasing the compliance (i.e. by using air bladders), ratio of padding material to guard material, attenuated peak forces;
3) increased foam thickness was more important than increased guard length, though length governs coverage.

3.4.5 Trunk Protectors

In spite of the vital organs located in the chest and abdomen, very little research has been conducted on the design and performance of trunk protectors. In fact, the majority of research has only focused on preventing Commotion Cordis, specifically in baseball, because of its potentially lethal effects. In designing chest protectors, Viano et al. (2000) outlined three ways in which a chest protector can reduce the energy transfer to the chest:

1) Spread the impact load over a greater area of the chest lowering the local pressure of impact and reducing chest deflection;
2) Absorb a portion of the kinetic energy of impact; and
3) Increase the mass of the chest as the local mass of the vest must also be accelerated until the ball reaches a common velocity with the interface.

While the impact intensities in baseball are similar and transferable to cricket, the loading conditions in TKD are much different. TKD has low-velocity, high-energy impacts which can cause a much wider range of injuries than impacts from a cricket ball or baseball. Furthermore, multiple impacts can be delivered to the same area in short time durations making competitors more susceptible to injury. As such, more research is required into TKD-specific impacts.

3.5 Special Case Study: Commotio Cordis

3.5.1 Overview

Impacts to the chest hold a potentially lethal effect due to the sensitive nature of the vital organs encased within the thorax. A sudden collapse and death caused from a low-energy, non-penetrating blunt thoracic trauma in the absence of cardiac abnormality is known as *Commotio Cordis (CC)*. This results in a disturbance of the heart's rhythm (i.e. arrhythmia) usually in the form of Ventricular Fibrillation (VF). While VF has other causes, CC is uniquely characterised by a lack of structural cardiac damage separating it from other heart traumas (Bir & Viano, 1999). It had previously been thought to be an unexplainable sudden death, but, reports of CC have steadily increased in frequency particularly in sport. It is prevalent in sports that feature solid projectiles such as baseball, hockey and lacrosse. Young athletes may hold the most risk because of a more pliable chest wall that facilitates the transmission of chest impact energy directly to the heart (Link, 2002; Link, 2003; Link & Maron, 2005). The associated impact velocities and energies, though, were not found to be irregular for a given sport (Link, 2003). The following identifies research into CC to establish its causes and motivation.

3.5.2 Animal Surrogates

Link et al. (1998) designed an experimental animal model suitable for low-energy chest impacts to replicate the clinical syndrome of CC. Juvenile swine *(Sus scrofa*) were selected because their organ distributions were similar to humans and any differences were not thought to have a measurable effect (Link et al., 2003). These swine were generally 4 - 8 weeks old with ranging in mass between 2 - 25 kg. A wooden object, similar in size and mass to a baseball, was used to strike onto the chest perpendicularly at different points in the cardiac cycle. The exact period of the cardiac cycle was measured with a cardiac stimulator timed which accounted for the 130 ms delay between release and impact. Electrophysiological consequences of chest-wall impacts were found to be time-dependent on the cardiac cycle. Impacts during the QRS-complex produced heart blockage, but strikes 15 to 30 ms before the T-peak induced VF significantly more than at any other time. Link (2003) found this critical window to occur from 30 to 10 ms. Using this impact timing window, key mechanical determinants of CC which maximised its likelihood were examined. Link et al. (2001) reported that chest wall impacts directly over the anatomical centre of the heart were more dangerous than those at its periphery. This precordial location was classified as the ‘cardiac silhouette’ and strikes to this region were required to trigger VF but did not necessarily do so. By targeting all projectiles at the silhouette, impacts below the threshold velocity (25 mph) did not induce VF establishing a clear relationship between the velocity of impact and the probability of VF (Link et al., 2003). The greatest risk occurred at 40 mph with the probability decreased for VF at velocities above and below this peak. As such, the timing and location of impact as well as the hardness of the impactor was found to have an important role in inducing CC.

The main limitation with using animal surrogates was that, ultimately, pigs and humans were different. While their anatomies were quite similar, the force of chest-wall impacts may have been relatively greater in pigs than in humans due to their size difference (Link, 2003). In each case, however, impact was positioned perpendicular to the chest completing a full strike on the heart keeping the conditions as similar as possible (Link et al., 2003). This also minimised the variability in chest contours between humans and swine (Weinstock et al., 2006).

The only other concern was that anaesthesias may have reduced the threshold for induced arrhythmias (Link et al., 1998).

3.5.3 Mechanical Models

Using the experimental swine model by Link et al. (1998) and logist functions, the probability of inducing VF was related to the Viscous Criterion (VC) with reference to the AIS. VC was subsequently validated as being the most relevant biomechanical response to accurately assess the risk of CC using this particular model (Bir & Viano, 1999). It has also been proven to measure the risk of soft tissue and organ injuries to the body (Janda et al., 1992) and the energy dissipated by soft tissues during high-speed impact (Bir & Viano, 1999).

Two main biomechanical models, the Hybrid III dummy and a 3-rib Chest Structure (3-RCS), were designed to calculate the VC response by measuring the maximum deflection and rate of deformation. The Hybrid III dummy was considered to be suitable because of its role in car-crash testing. Alternatively, the 3-RCS was specially developed to create a surrogate with high biofidelity to low-mass, high-velocity chest impacts (Viano et al., 2002).

Despite attempts to design biomechanical models which mimicked human response, biofidelity still remained the main limiting factor. These models did not test for, produce, or mimic this complex phenomenon while the contact phase at impact may not be well modelled to reflect the different absorptive properties of the human body (Weinstock et al, 2006). Instead, these models were heavily reliant on the VC response. This would indicate that faster impact velocities increased the vulnerability of the body to VF. From the experimental model, it was already proven that the highest risk occurred at ~ 40 mph and susceptibility decreased as the velocity increased. Therefore, it has been proposed that VC may not be the most accurate predictor of CC (Link, 2003).

3.5.4 Prevention of Commotio Cordis

Preventative techniques were tested using impacts that delivered a maximum likelihood of inducing VF, thus scrutinising protectors in a worst-case impact scenario. In the experimental model, this meant aiming baseballs to strike the centre of the heart at 10 to 30 ms before the T-wave peak at a velocity of 40 mph. To protect against this condition, softer ‘safety’ baseballs and chest protectors were designed and developed. These changes were thought to decrease the amount of energy transferred to the heart reducing the occurrence of CC (Link et al., 2002).

3.5.4.1 Safety Baseballs

The most consistent finding showed that safety baseballs have been proven to decrease sternal accelerations at impact, but did not reduce the likelihood for CC (Janda et al., 1992). The effectiveness of safety baseballs in reducing cases of this lethal condition have varied and appear to be test-dependent. Janda et al. (1992) found that softer baseballs did not reduce the likelihood for VF in experimental models. However, impacts were aimed at 95 mph, an unusually high velocity that has not been shown to cause the highest level of vulnerability. Significant differences were also not found between regular baseballs and the least-hard ball when impacts were geared towards the most susceptible point in the cardiac cycle (Link et al., 1998). Conversely, when the ideal experimental model was used, safety baseballs, up to a rating of 10 on the Reduced Injury Factor (RIF), reduced the risk of VF significantly (Link et al., 1998). Risk was found to be linearly correlated with baseball hardness clearly establishing a direct relationship between projectile hardness and the susceptibility for VF. Link et al. (2002) suggested that softer baseballs coupled with effective chest wall barriers and improved coaching could lead to a successful prevention of CC.

3.5.4.2 Chest Protectors

The role of a chest protector was to dissipate or absorb the impact energy and re-distribute it allowing the person wearing the protector to experience less of the impact (Viano et al., 2000). However, more than 25% of fatal events that occurred during organised competitive sport have involved athletes that were wearing commercially available chest protectors (Doerer et al., 1997; Weinstock et al., 2006). Link et al. (2003) suggested that chest protectors may actually increase the incidence of CC by reducing the amount of energy transmitted at higher velocities to more dangerous levels. For example, if 40 mph impacts maximised risk, a chest protector capable of lowering the energy from a 60 to 40 mph strike would actually increase the incidence of CC.

Viano et al. (2000) examined the performance of five different baseball chest protectors using the 3-RCS. When VC was used to predict the incidence of VF, only one of the chest protectors significantly reduced CC across all velocities when compared to the control condition where no protection was used. When the lab results were linked to VF occurrence in baseball, chest protectors were shown to dramatically reduce the incidence of VF (~61%). In contrast, Weinstock et al. (2006) found that commercially available chest protectors (7 baseball and 5 lacrosse) did not significantly reduce the triggering of VF. Only a "Brine Pro" lacrosse pad exhibited a trend towards decreasing VF incidence which was attributed to its unique design (a layer that contained sleeves of expanded propylene beads instead of the regularly used high-density foam). These authors suggested that these protectors served as adequate protection against soft tissue and bone injury, but not against the more lethal VF.

There were other possible reasons why chest protectors may not be effective. Existing protectors significantly reduced the local accelerations at impact, but this correlated poorly with the occurrence of CC (Viano et al., 2000). This implied that bruising and pain may decrease, but there was no protection against a more lethal outcome. Furthermore, the protection zone may shift during movement affecting the protective covering over the left chest wall (Link, 2003). Therefore, it was imperative that the padding cover the entire silhouette regardless of body movement or position (Link et al., 2001). Past protectors did not work because they did not cover the precordium during all blows or did not attenuate the force of the blow when the projectile struck the chest barrier (Link & Maron, 2005). Future designs may need to use novel materials and/or designs that are more effective in dissipating impact energy than those used to protect against tissue injury (Weinstock et al., 2006) and place considerable thought into maintaining protection during typical sporting movements.

3.6 Comparison of Impacts

In § 2.7and § 2.8, biomechanical responses and injury tolerances were summarised for the chest, abdomen and tibia for automobile and blunt ballistic impacts. Similarly, biomechanical responses obtained from sport were analysed in § 3.3. In addition, the standards for PPE equipment were outlined in § 3.4. This section compares the impact characteristics from these tests.

Tibial impacts are summarised in Table 3.15. Impacts used to assess the performance of soccer shin guards were all below the lowest threshold for tibial fracture. This was also true for *BStan* tests, which had starting impact conditions which were not severe enough to cause injury. For example, tests for soccer shin guards were set at 2 J, though impact energies have been estimated to be as high as 10 J. As such, these tests cannot be considered to be an accurate assessor of shin guard performance – at least for protection against tibial fracture. In contrast, *BStan* testing for cricket leg guards were severe enough to cause fracture, despite these tests being limited to 40 J – equivalent to a bowl of ~ 22 m/s – and tibial fractures having never been reported. It was likely that the threshold was higher because of the assumed to decrease in effective impact mass and contact time (Bir et al., 2004) and to account for the false load-transfer mechanism of the anvil.

Among all the forces measured within sport, automobile and ballistics impacts to the chest and abdomen, the standards for the chest protector seemed to underestimate sports impact intensity, especially when its load-transfer mechanism was considered (Table 3.16). Whilst at first glance it would seem that the relationship between impact response and tolerance was inconsistent, this table re-affirmed the sensitivity of human impact response to different impact conditions. It also supported the argument that force may not be the most accurate predictor for injury. However, force remained one of the easier variables to measure and, as such, was measured in the most studies for cross-comparison.

A comparison of all impact velocities used in the assessment of PPE, and in the determination of biomechanical responses and injury tolerances was also formulated (Table 3.17). Velocities shown are the maximum average velocities reported within each study. Whilst velocities in sport cover the same range of automobile and ballistic impacts, *BStan* testing was found in the lower part of the velocity range. Therefore, to obtain comparable forces shown in previous tables, either the impact mass was higher or the anvil was of low bio-fidelity or a combination of both which suggested that the assessment of PPE was not representative of a real-life condition.

Table 3.15 Summary of Tibial impacts across all conditions[1] organised by force.

Study	Type[2]	Model	Condition	Input	Force [kN]	Injury?	Reference[3]
Ankrah & Mills (2003)	**R**	Foam-Covered Tibia	Guarded	3.5 J	1.07	-	T 3.14
Ankrah & Mills (2003)	**R**	Foam-Covered Tibia	Unguarded	3.5 J	1.23	-	T 3.14
Phillipens & Wismans (1989)	**R**	Dummy leg	Unguarded	3.6 m/s	1.25	-	T 3.14
Bir et al. (1995)	**R**	Hybrid III leg	Guarded	2.3 kN	1.47	-	T 3.14
Ankrah & Mills (2003)	**R**	FE model (stud impact)	Unguarded	10 J	1.60	-	T 3.14
***BStan* Soccer Shin Guard (Lateral)**	**S**	Leg Form	Guarded	1.53 J	2	-	§ 3.4.2.2
***BStan* Soccer Shin Guard (Central)**	**S**	Leg Form	Guarded	2 J	2	-	§ 3.4.2.2
***BStan* TKD Guard**	**S**	Leg Form	Guarded	3 J	2	-	T 3.13
Francisco et al. (2000)	**T**	Rubber Synthetic leg	Bare	4.1 - 16.5 J	2.98 (male) 2.87 (female)	Fracture	T 2.7
Kramer (1973)	**T**	Tibia	Bare	6.3 m/s	3.3 (p = 0.50)	Fracture	T 2.7
Kramer (1973)	**T**	Tibia	Bare	7.1 m/s	4.3 (p = 0.50)	Fracture	T 2.7
Nyquist (1985)	**T**	Tibia (A-P direction)	Bare	0 - 4 m/s	4.57 (male) 4.7 (female)	Fracture	T 2.7
Blum (1977)	**T**	Mathematical	-	static	4.7	Fracture	none
***BStan* Cricket Leg Guard**	**S**	Leg Form	Bare	40 J	5	-	T 3.12
Nyquist (1985)	**T**	Tibia (L-M direction)	Bare	0 - 4 m/s	5.03 (male) 4.16 (female)	Fracture	T 2.7
Yang (1997)	**T**	MADYMO 3D	Bare	13.78 m/s	5.5	Fracture	none
Stalnaker (1976)	**T**	Tibia	Bare	8 - 13 m/s	7.5 - 22.2	Fracture	T 2.7

---

[1] Colours refer to the overall impact type of the study (applies for all tables):
- Sports: yellow, BStan: Grey, Automobile/Ballistics: White

[2] Type: column refers to the motive of the study; R: Response, S: Standard, T: Tolerance;
- the difference between response and tolerance was that response was the highest force measured without causing injury

[3] Reference: column refers to where more information about the particular study can be found

Table 3.16 Comparison of impact forces measured in the chest and abdomen.

Study	Type	Model	Condition	Input	Force [kN]	Injury?	Reference
Lee et al. (1994)	R	Human	frontal	plate	0.12	none	T 2.7
Beckman et al. (1970	R	Monkeys	frontal	Metal Plate	0.9	none	T 2.2
Patrick (1981)	R	Human	frontal	bar	1.4	45.2 mm deflection	§ 2.8.6.2
Stalnaker et al. (1973)	R	Human	frontal	plate	1.51	16.7 mm deflection	T 2.7
Shaw et al. (2006)	T	PMHS	lateral	ram	1.85	Fracture	T 2.4
Yoganandan et al. (1997)	R	PMHS	frontal	pendulum	2.9	AIS = 2	T 2.2
***BStan* Chest Protector**	S	Anvil	-	cylinder	3	-	T 3.13
Backaitis & St. Laurent (1986)	R	Human	frontal	seatbelt	3.2	18.5 mm deflection	T 2.7
Patrick et al. (1965)	T		Sternum	hub	3.3	fracture	T 2.8
Joch et al. (1981)	R	Water-filled bag	-	punch	3.45	-	T 3.10
Falco et al. (2009)	R	Modified Dummy	guarded	kick	3.48	-	T 3.8
L'abbe et al. (1982)	R	Human	unguarded	belt	3.6		T 2.2
Talantikite et al. (1998)	R		lateral	plate	3.94		T 2.4
Fight Science	R	Hybrid III	unguarded	punch	4.08		T 3.11
Atha et al. (1985)	R	Pad	-	punch	4.1		T 3.10
Cavanaugh et al. (1996)	R	SID Dummy	lateral	sled	4.1	TTI = 181	T 2.4
Walilko et al. (2005)	R	Hybrid III	-	punch	4.74	-	T 3.10
Bir & Eck (2005)	R	PMHS	ballistics	projectile	4.74	22 mm deflection	T 2.2
Smith et al. (2000)	R	Boxing Dynanometer	unguarded	punch	4.8	-	T 3.10
Viano et al. (1989a)	R	PMHS	lateral	pendulum	5.01	rib fractures	T 2.4
Pierce et al. (2006)	R	in vivo	guarded	punch	5.36	-	T 3.10
Kent et al. (2006)	R	FE human model	frontal	plate	5.4	20% deflection	T 2.2
Lobdell et al. (1973)	R	PMHS	frontal	plate	5.56	none	T 2.2
Smith & Hamill (1986)	R		unguarded	punch	6	-	T 3.10

Study	Type	Model	Condition	Input	Force [kN]	Injury?	Reference
Atha et al. (1985)	R	Metal Mass	unguarded	punch	6.32	-	T 3.10
O'Sullivan et al. (2009)	R	Sandbag	unguarded	kick	6.4	-	T 3.8
Viano (1989)	R	PMHS	frontal	pendulum	6.94	fractures	T 2.2
Fight Science	R	Hybrid III	unguarded	kick	6.99	-	T 3.11
Kroell et al. (1974)	T	PMHS	frontal	plate	7.94	AIS = 6	T 2.8
Chiu et al. (2007)	R	Air bag	unguarded	kick	8.25		T 2.2
Patrick et al. (1965)	T		Shoulders/ Sternum	hub	8.8	fracture	§ 2.8.6.2
Pedzich et al. (2006)	R	Force Plate	unguarded	kick	9.01		T 3.8
Cavanaugh et al. (1986)	T	PMHS	lateral	aluminium bar	10.2		T 2.8
Troseille et al. (2002)	R	PMHS	abdominal (frontal)	belt	10.29	MAIS = 6	T 2.4
Bir et al. (2004)	R	PMHS	frontal	projectile	10.62	52.3 mm deflection	T 2.2
Kroell et al. (1973)	T	PMHS	frontal	plate	11.65	fracture	T 2.8
Bierman et al. (1946)	R	Human	frontal	four-point belt	13.3	none	-

Table 3.17 Summary of impact velocities used in all automobile, blunt ballistics and sports impacts.

Study	Study Motivation	Type	Velocity [ms^{-1}]	Reference
Duma et al. (2005)	Chest Tolerance (frontal)	Seatbelt	1.5	-
Ankrah & Mills (2003)	PPE Performance	4.1-kg drop	1.56	T 3.13
Shaw et al. (2006)	Chest Tolerance (lateral)	Penumatic Ram	2.5	T 2.9
Francisco et al. (2000)	PPE Performance	4.2-kg drop	2.7	T 3.13
***BStan* TKD Chest Protector**	Standard	2.5-kg drop	3.1	T 3.13
Patrick (1981)	Chest Response (frontal)	10-kg cylindrical bar	4.2	T 2.2
Yoganandan et al. (1997)	Abdominal Response (frontal)	23.5-kg pendulum	4.3	T 2.4
Hrysomallis et al. (1996)	Injury Potential	Drop	4.43	-
***BStan* Soccer Shin Guard**	Standard	5-kg drop	5.42	§ 3.4.2.2
***BStan* Cricket Leg Guard**	Standard	2.5-kg drop	5.66	T 3.12
Stalnaker et al. (1973)	Chest Response (frontal)	10-kg plate	6.22	T 2.7
Tsai et al. (1999)	TKD Kinematics	Kick	6.38	T 3.9
Talantikite et al. (1998)	Chest Response (lateral)	16-kg plate	7.16	T 2.4
Viano et al. (1989a)	Chest Response (lateral)	23.4-kg pendulum	8.2	T 2.4
Cavanaugh et al. (1996)	Abdominal Tolerance (lateral)	Sled	8.9	T 2.9
Atha et al. (1985)	Punch Kinematics	Punch	8.9	T 3.13
Walilko et al. (2005)	Punch Kinematics	Punch	9.14	T 3.13
Viano et al. (1989)	Chest Tolerance (lateral)	23-kg Pendulum	9.4	T 2.9
Viano (1989)	Chest Response (lateral)	23.4-kg pendulum	10.2	T 2.9
Cavanaugh et al. (1986)	Abdominal Tolerance (Frontal)	Sled	10.4	T 2.3
Kroell et al. (1974)	Chest Tolerance (frontal)	22.86-kg plate	10.9	T 2.7
Link et al. (1998)	Commotio Cordis	0.15-kg ball	13.33	§ 3.5
Link et al. (2001)	Commotio Cordis	baseball	13.33	§ 3.5
Kroell et al. (1971)	Chest Tolerance (frontal)	5.5-kg plate	13.73	T 2.7
Kim & Hinrichs (2006)	TKD Kinematics	Kick	13.9	T 3.9
Roosen (2008, thesis)	TKD Kinematics	Kick	14	T 3.9
Kroell et al. (1981)	Chest Tolerance (swine)	10.4-kg striker mass	14.5	T 2.7
Conkel et al. (1988)	TKD Kinematics	Kick	14.6	-
Kallieris et al. (1998)	Chest Tolerance (frontal)	Seatbelt	15.28	T 2.7
Pieter & Pieter (1995)	TKD Kinematics	Kick	15.54	T 3.9
Serina & Lieu (1991)	TKD Kinematics	Kick	15.9	T 3.9
Lees & Nolan (1988)	TKD Kinematics	Kick	16	-

Study	Study Motivation	Type	Velocity [m/s]	Reference
Kent et al. (2002)	Chest Tolerance (frontal)	Seatbelt	16.39	T 2.7
O'Sullivan et al. (2009)	TKD Kinematics	Kick	17.66	T 3.8
Weinstock et al. (2006)	Commotio Cordis	baseball	17.78	§ 3.5
Boey & Xie (2002)	TKD Kinematics	Kick	18	T 3.8
Beckman et al. (1970)	Chest Response (frontal)	0.35-kg Metal Plate	19.5	T 2.2
Viano et al. (2000)	Commotio Cordis	baseball	31.1	§ 3.5
Link et al. (2003)	Commotio Cordis	baseball	31.1	§ 3.5
Bir et al. (2004)	Chest Response (frontal)	Ballistics	40	T 2.2
Penrose et al. (1976)	Cricket Ball Kinematics	-	44.7	§ 3.32
Bir & Eck (2005)	Chest Response (frontal)	Ballistics	60	T 2.2

3.7 Conclusion

This chapter showed that despite the existence of PPE for cricket, football and TKD, impact injuries continue to occur. Whilst some PPE are shown to actually increase the probability of injury (e.g. protecting against CC), some are ineffective due to inadequate methods of assessing their performance (i.e. British Standards). As such, there is more scope for research into PPE, particularly in developing higher biofidelity ATDs and impactors, which can then aid in the development and assessment of current and future PPE.

Chapter 4

Equipment & Measurement Systems

4.1 Chapter Overview

This chapter describes the equipment used in each experimental section conducted within this research. It is divided into two types of measurement systems: force and motion analysis. For each system, its technology, method of calibration and intended use within this research are discussed.

4.2 Force Measurement Systems

Research in each experimental section is concerned with obtaining *in vivo* measures of impact intensity, such as force, so it is necessary to have a flexible device that could obtain measurements on surfaces of varying contours and compliance. In addition, it needs to have the ability to conform to various parts of the human body yet still be robust enough to withstand multiple loading conditions. As such, classical force measuring devices such as a force plate cannot be relied upon to provide these values. Instead, these devices are mainly used for the calibration of apparatus' with novel technology that can be adopted and modified for obtaining measurements on deformable human structures. The following provides the specification of the plate used, outlines the selection process for the flexible sensor and examines sensor performance.

4.2.1 Kistler Force Plate

4.2.1.1 General

The Kistler 9821B12 force plate is 0.6 m long x 0.4 m wide and has four piezoelectric sensors located 0.1 towards the centre of plate in length and width from each of the plate's four corners. Each sensor measures three forces by taking advantage of the compressive properties of quartz crystal and combines with the other three sensors to measure nine moments. When a load is applied to the crystal, an electric charge is produced with minimal deflection (in the order of microns) due to the high rigidity of quartz under compression. The charge is amplified and converted to voltage using a Kistler Type 9865 8-channel charge amplifier (*Appendix A*). The exact relationship between the load and the electric charge (or voltage) produced is dependent on the specific properties of the quartz and is determined from the manufacturer's calibration. The main uses of the Kistler plate are to help calibrate the Tekscan sensors and to help replicate specific impact tests.

4.2.1.2 Calibration

The calibration of each force sensor is conducted singly in each axis and recorded by the manufacturer. Upon installation, the calibration is checked by an engineer and a calibration certificate is provided (*Appendix A*). The main parameters of the force plate are:

Sensitivity: Fz = -3.87 pc/N

Range: Fz = -10 to 20 kN

Whilst the range is controlled by the amplifier, it is always set at 'Range 4' to provide the maximum force range. Prior to each trial, a quick calibration is conducted. The software records the voltage during a static period and uses this to 'zero' the plate (i.e. recorded voltage corresponded to zero force). With this method, even if objects are placed on the plate during this 'zeroing'-time, the plate will only measure the net force produced.

4.2.2 Tekscan

4.2.2.1 General

As discussed, the desired system had to be flexible and conformable, yet robust. It must also be capable of measuring force at a high sampling frequency and threshold, but with minimal monetary cost. Lastly, it must be versatile to accommodate a wide range of applications. Compared to similar systems within the same price range, Tekscan (Boston, MA) sensors offered the best balance of these criteria. More specifically, the F-Scan Mobile system was chosen for further use primarily because its data logger allowed dynamic movements to be measured with minimal influence on an athlete's range of motion.

Each sensor, model 3000, is attached to a cuff connected to the data logger which can upload information to any computer (Fig 4.1). Individual sensors (insole) are 0.15 mm thick (0.007") and consist of 954 sensels (measuring points) with a pressure threshold of 862 kPa (125 psi). At its maximum sampling frequency of 500 Hz, the data logger is capable of capturing 15 seconds worth of data allowing 75 000 data points to be stored. Whilst this frequency may be considered too low for dynamic impact measurements, other systems capable of measuring at higher sampling frequencies were offset by inadequately low pressure thresholds and significantly higher costs. Moreover, most other systems capable of measuring at the adequate threshold could not provide continuous real-time measurements (Bachus et al., 2006).

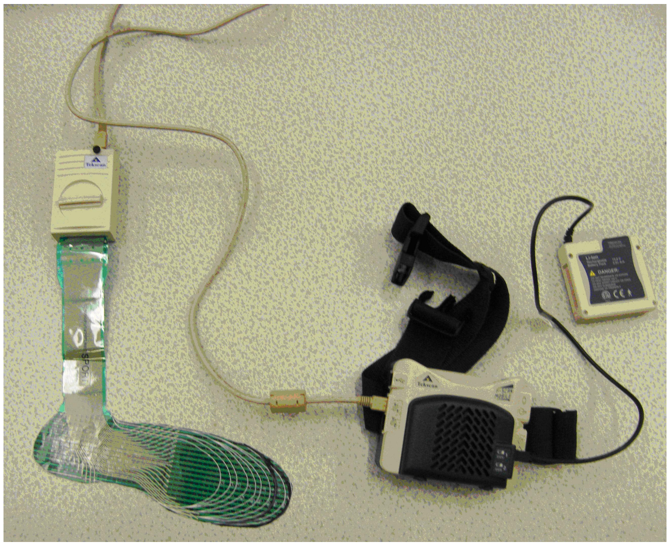

Figure 4.2 Tekscan data-logger with battery pack, socket and F-Scan sensor

F-Scan sensors consist of rows and columns of semi-conductive ink which intersect at points called 'sensels' (Fig 4.2, Table 4.1). Using piezoresistive technology, each sensel measures a change in resistance which is scaled to voltage and proportional to the force applied. In each frame, the force applied across the entire sensor is obtained through multiplexing. In this way, the sensor sweeps across the columns of the sensors and stores the values of force measured by each sensel within that column. However, data from each column can only be processed individually. As such, the duration of this process is a function of the sampling frequency and each sweep is completed once for every frame (i.e. a sampling rate of 500 Hz has a sweeping period of 2 ms). Therefore, in fast impacts where loads constantly change, measurements can be inaccurate since the spatial resolution is reduced to a single column every ~ 0.1 ms. In addition, this left the sensor prone to drift after an applied load (Otto et al., 1999).

Figure 4.2 Individual model 3000 sensor showing the matrix of sensels (www.tekscan.com)

Table 4.1 Summary of sensel dimensions

Total Sensels	Sensel Density (sensels/cm-2)	Columns			Row Width (mm)		
		Width (mm)	Spacing (mm)	Quantity	Width (mm)	Spacing (mm)	Quantity
954	3.9	2.5	5.1	21	2.5	5.1	60

Tekscan sensors are marketed as pressure sensors, but each is actually a sensor that provides force at each sensel and then uses its area to infer pressure data. It is intended to provide information about walking and running throughout the duration of foot strike while used in-shoe but its mobility (i.e. lack of cable connections during data collection) allow its uses to be extended to sprinting, jumping and kicking analysis when used as a traditional insole. Its use though, is not restricted to be used in-shoe; these sensors can measure force independently on any surface, but its performance has been found to be very sensitive to the specific contact surfaces (Luo et al., 1998; Morin et al., 2000) with potentially large errors in the calculation of contact areas (Drewniak et al., 2007). Nevertheless, these sensors have allowed researchers to measure surface abdominal forces (Johannsen & Schindler, 2007), which was an application similar to this research, or measure grip pressure in tennis rackets (Glynn, 2007) and golf clubs (Komi et al., 2007) with acceptable accuracy. With this increased freedom in the movements and combination of movements to be analysed, sensor calibration was important to decrease measurement errors.

4.2.2.2 Calibration

The recommended protocol requires each Tekscan sensor to be placed in an air bladder whilst applying two pressure values which encompass the expected range to be used. A regression curve, either linear or power, is fit between the two points and serves as the calibration to convert voltage to force. However, Pain et al. (2008) found that its low sampling frequency and multiplexing led to an under-estimation of force during a dynamic impact. Similarly, Sumiya et al. (1998), found a slow dynamic response of F-Scan sensors compared to force plates. Whilst calibrating each individual sensel would have removed inter-sensel variation, this was a time consuming exercise that likely would not have an effect on the magnitude of loads measured (Brimacombe et al., 2009). Instead, Morin et al. (2000) suggested that the best calibration procedure was the method which matched its intended use as close as possible. As such, the recommended Tekscan calibration was not conducted and a dynamic calibration using a deformable impactor was used in its place.

In a dynamic calibration, a single Tekscan sensor was placed flat on the Kistler plate with sampling rates set at 500 and 2000 Hz, respectively. Two different medicine balls, m = 3.9 and 10 kg, were chosen because of their difference in dynamic stiffness. Each was dropped onto a single sensor and force plate simultaneously, from multiple heights between 1.0 – 1.6 m, whilst measuring force with both systems. Each impact was plotted with the force plate values displayed as a function of the Tekscan raw data (Fig 4.3). Brimacombe et al. (2009) had suggested that a power function was the most accurate calibration curve type (particularly for large force ranges). However, using a power function for these data points produced a worse fit (i.e. lower R^2 fit). Moreover, this recommendation was based on the results from rigid impacts so it was unclear whether this would apply for impacts involving deformable objects. In fact, these authors argued that the performance of Tekscan sensors was unclear when used with compliant surfaces since the surface and sensor deformed at different rates. As such, these data points were linearly regressed against each other with a linear relationship fitted through the origin. These gradient lines (e.g. equation 1) served as the calibration factors for adjusting the raw Tekscan data to impact force data during all participant trials.

(1) $y = 0.1649 \cdot x$, where y=force in Newtons [N]
x=Tekscan raw data

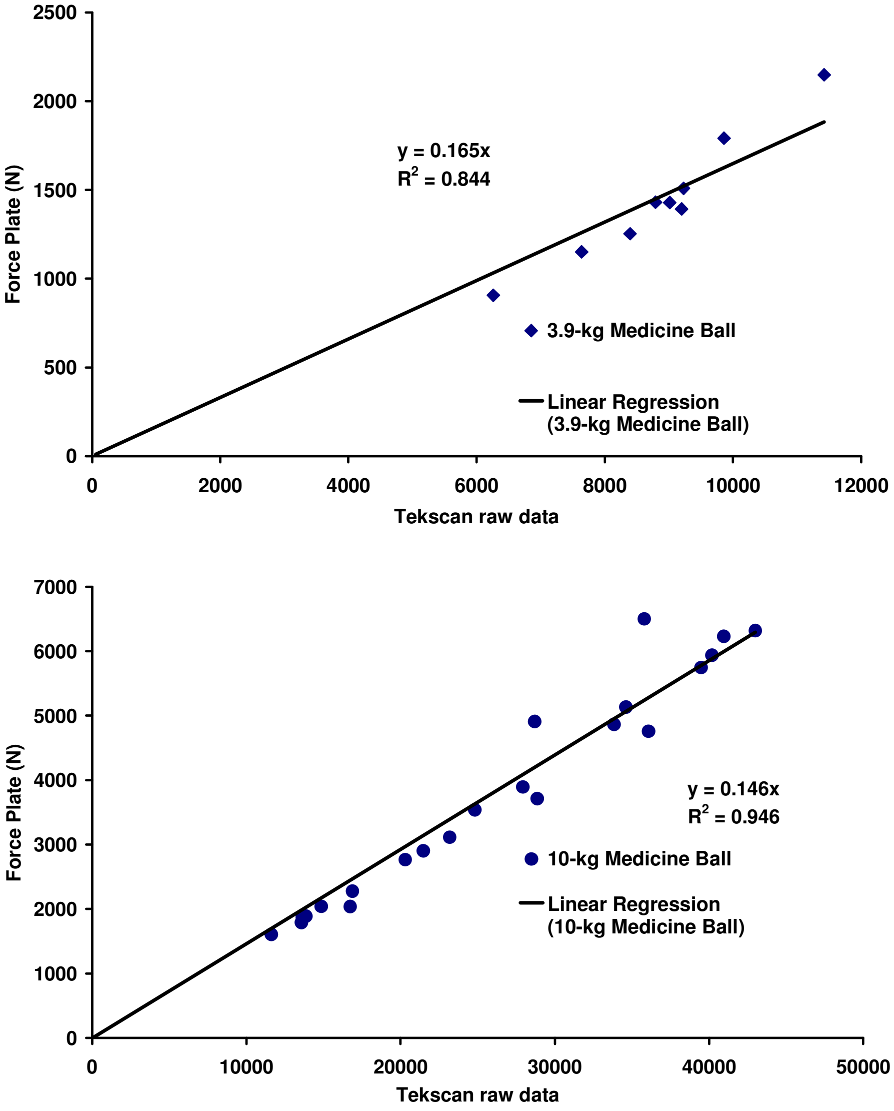

Figure 4.3 Tekscan calibration curves for 4-kg and 10-kg medicine ball.

Whilst it may be argued that these calibrations only created two discrete calibration curves, a paired t-test comparing the two regression curves did not show a significant difference ($p = 0.36$). In addition, the times to peak force between the two were similar at 12.8 ms and 11.7 ms for the 3.9-kg and 10-kg medicine balls, respectively, suggesting that medicine balls of mass within this range would also perform similarly. In subsequent experimental chapters, the calibration factor chosen was dependent on the curve which produced a similar range in force magnitude and time to peak force as these calibration curves.

It has been postulated that sensor performance degraded over time due to fatigue or age, but this effect had yet to be investigated (Polliack et al., 1998; Drewniak et al., 2006). As such, a small study was conducted to analyse how multiple impacts could influence the integrity of the calibration curve. Impacts using the same 3.9-kg medicine ball were conducted in 24 separate sets each consisting of 10 drops. After each set, a new calibration curve was constructed. Calibration curves were also constructed from merging two sets of drops and four sets of drops together. Table 4.2 shows the calibration coefficient resulting from each block of testing.

The general trend in calibration coefficients was that the first few sets of impacts showed a large variation but then stabilised as the coefficients slowly increased in magnitude with increasing number of impacts (Fig 4.4). It was difficult, however, to determine exactly when the original calibration could be considered to be unacceptable due to the natural variation in raw impact force measured by the Tekscan sensors. This was supported by the wide variation in R^2 values. Despite this uncertainty, sensors were changed every ~200 impacts to account for this change in performance with time. Before use, each sensor was individually calibrated in the same way described here as individual sensel and whole sensor performance could vary considerably (Brimacombe et al., 2009). Moreover, impacts were administered to each sensor prior to use to eliminate the variation in performance present in early impacts.

Table 4.2 Regression coefficients resulting from repeated impacts.

Trial (sets of 10)	Groups of 10		Groups of 20		Groups 40	
	Regression	R^2	Regression	R^2	Regression	R^2
1	0.1377	0.3504	0.1378	0.6093	0.1407	0.5734
2	0.1379	0.8061				
3	0.1438	0.7241	0.1438	0.5348		
4	0.1438	0.3239				
5	0.1296	0.7821	0.1415	0.4175	0.1452	0.5885
6	0.1577	0.4304				
7	0.1451	0.6924	0.1507	0.7215		
8	0.1573	0.7827				
9	0.1592	0.6648	0.1566	0.6805	0.1524	0.6287
10	0.1539	0.7133				
11	0.1477	0.419	0.1484	0.5981		
12	0.1493	0.7596				
13	0.1563	0.7921	0.155	0.7438	0.152	0.7016
14	0.1534	0.6717				
15	0.1544	0.5439	0.1494	0.6607		
16	0.1448	0.8555				
17	0.158	0.6419	0.1571	0.7217	0.1557	0.763
18	0.1562	0.7435				
19	0.1483	0.9054	0.1546	0.7773		
20	0.162	0.6793				
21	0.1543	0.5661	0.1552	0.6102	0.1553	0.555
22	0.156	0.6646				
23	0.1634	0.2004	0.1555	0.5907		
24	0.15	0.7659				

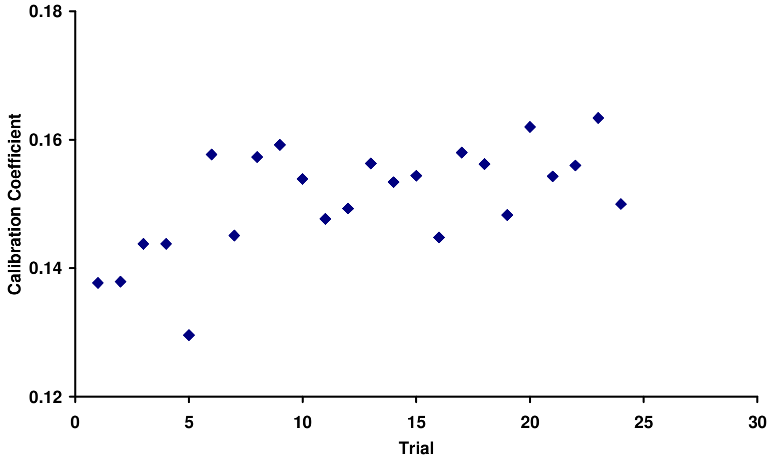

Figure 4.4 Calibration coefficient as a function of trial number.

To analyse the repeatability in Tekscan sensor calibrations, all trials were split into four equal groups and a repeated measures ANOVA was conducted. A significant difference between groups was found (F = 4.55, p = 0.019). Post-hoc analysis revealed that the first group of measurements was significantly different from the remaining three groups, which were not significantly different from each other. This suggested that the first few sets of impacts in the calibration of a new sensor should be discarded to account for this large variation in sensor performance. A 95% CI for all drops was also calculated to help account for variation in force measurement in future experimental sections (Fig 4.5).

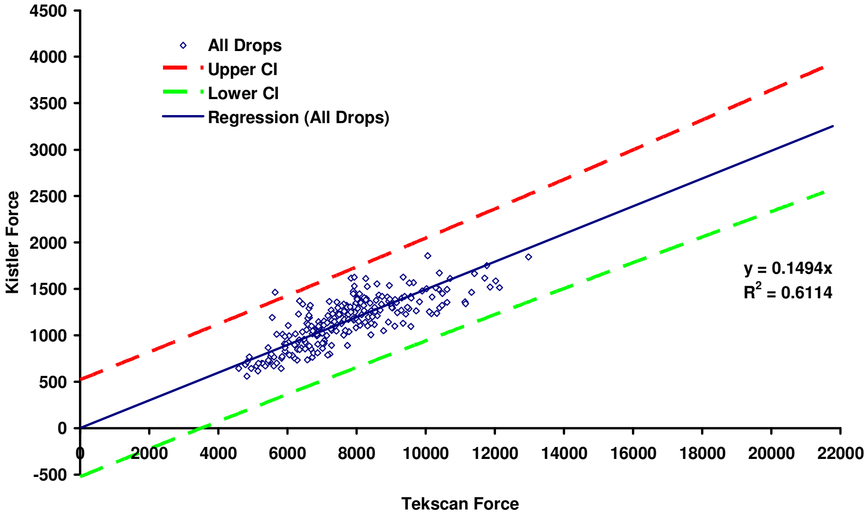

Figure 4.5 95% CIs for Tekscan sensor calibration.

4.2.3 Custom Force Plate (CFP)

4.2.3.1 General

The Custom Force Plate (CFP) is made of four 3-component ICP 260A01 force transducers (PCB Piezotronics, New York, USA) sandwiched at the corners of two 0.05 m-thick metal plates measuring 0.15 m long and 0.10 m wide. The specification sheet for each transducer is found in *Appendix A*.

Each transducer employs the same technology found within the Kister plate with a quartz crystal generating an electrostatic charge proportional to the input force. To ensure intimate contact, linearity and accuracy of the sensor, the crystals had to be pre-loaded to 22 239 N between the two plates. This was applied by tensioning the bolts between the two plates. The necessary tightening torque was found using the following equation (2):

(2) $$P_1 = \frac{M_t}{0.2b},$$ where

$P_1 = \text{pre} - \text{load}$
$\mathrm{M_t} = \text{torque}$
$b = \text{bolt diameter}$

This equation was re-arranged for M_t and the relevant variables were inputted to determine that the necessary tightening torque for the bolts was 35.6 Nm. This was applied using a torque wrench.

The charge produced by the transducers is routed through a Model 482A22 four-channel, line-operated signal conditioner (PCB Piezotronics, New York, USA) for analysis and recording purposes (Fig 4.6). The output is expressed in terms of voltage and is converted using its calibration certificate (*Appendix A*). The main use of the CFP was in trials where the force plate could not be used but rigid force measurements were necessary.

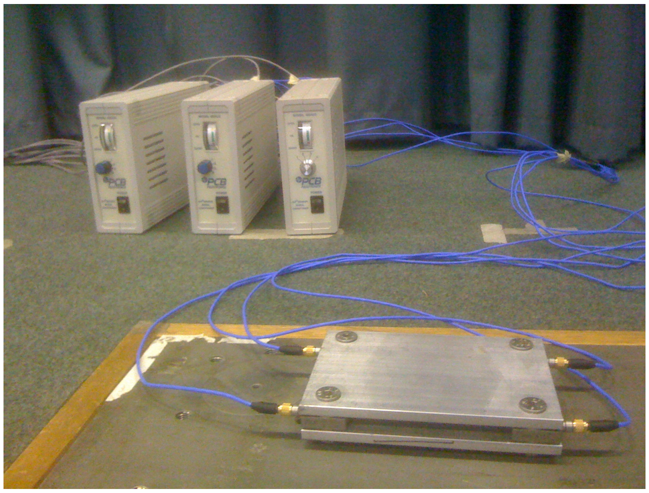

Figure 4.6 CFP linked to PCB signal conditioner which is routed to the Vicon box.

4.2.3.2 Calibration

Each sensor is individually calibrated by the manufacturer, PCB, in accordance to the National Institute of Standards and Technology (NIST). The sensor is placed in a hydraulic press while known forces are applied and recorded. Data points are collected at increasing 20% intervals of the known operating range and a best fit line through these points and the origin is plotted. If the calibration points are outside the specified linearity, then the sensor fails the calibration and is subsequently rejected. The manufacturer also reports a voltage decay at a rate of 1% per second, but as this research was interested in dynamic impacts only, it was not considered to be a major concern. The main characteristics of these transducers, including the sensitivity and linearity, are displayed in its calibration certificate (*Appendix A*). The coefficients used in this research are:

Sensitivity (z-axis) = 0.56 mv/N Range = 4.45 kN

Jaques (2008) performed a calibration using the manufacturer's recommended methodology to ensure that the correct sensitivity was used for each transducer. A Lloyds Model R10000 compression machine was used to apply loads of up to 250 kg at 3 mm·s^{-1} for up to 5 minutes. An exponential function was fit to the decaying voltage to account for this drift. Once the voltage was adjusted for drift, an average was taken of the contact over the first 0.5 s. The result of the different loads produced the calibration curves shown in Fig 4.7, which matched well comparably to the manufacturer's fit.

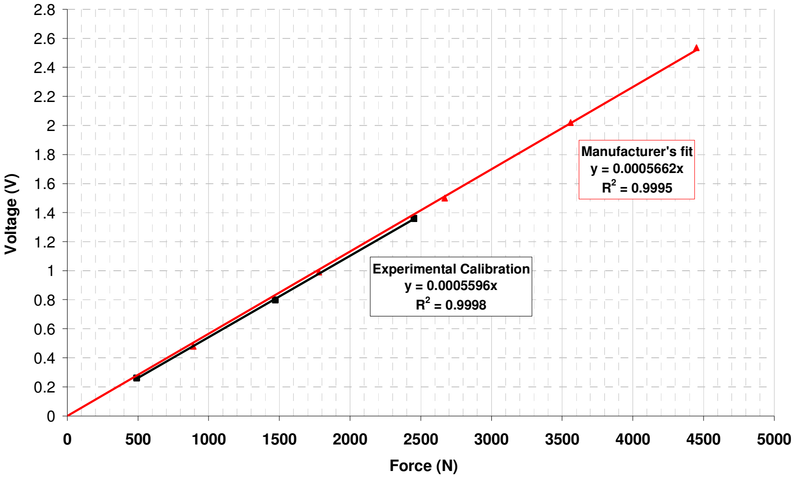

Figure 4.7 Comparison between calibration curves provided by the manufacture and developed experimentally (Jaques, 2008; modified, *with permission*)

4.3 Motion Analysis Systems

Motion analysis systems are necessary to collect information about the kinematics of movement. This research uses both an automatic motion capture system and a high-speed video camera.

4.3.1 Vicon

4.3.1.1 General

Vicon is a passive motion analysis system which tracks the location of opto-reflective markers in real-time using cameras equipped with infrared light-emitting diodes (LEDs). Each marker reflects this light relaying information about its position. With a single camera, the motion of a marker can be tracked in two-dimensions; if a marker is visible with at least two cameras, its position can be reconstructed in three-dimensions. The cameras used in this research are the MX-13 and T-20. The MX-13 can record 1280 x 1024 pixels full frame at rates up to 484 Hz, with a maximum speed of 10 kHz at lower resolution, whilst the T-20 can record 1600 x 1280 pixels full frame at rates up to 500 Hz (2000 Hz with reduced resolution). Specification sheets for both cameras are provided in *Appendix A*. The performance of each camera is ultimately dependent on the calibration and reconstruction parameters set within the Vicon Nexus Software.

The main advantage of this system is its versatility in motion capture. Using passive markers eliminates the need for leads or wires for batteries or data transport and, therefore, does not restrict the size of marker that can be used. Whilst this may lead to marker occlusion, particularly when using markers less than 14 mm in diameter, this can be offset by precise camera placement and careful consideration of the specific movements under analysis. Therefore, for each motion capture, it is possible to find the optimal camera settings and location for a set of cameras. The only caveat is that this system suffers under natural light conditions as the light spectrum creates too much noise for the system to accurately capture the reflected light.

Using the tracked marker positions present in a given frame, user-defined custom kinematic models can be constructed. Between frames, Nexus attempts to predict the movement of each marker to allow for almost completely automatic digitising. This prediction is based on the reconstruction parameters which help locate marker positions between frames based on the size of markers, the speed of the movement, the rigidity of the object analysed and the predicted radius of possible movement from the previous frame. Therefore, the reconstruction can be made specific for the desired movement to be analysed. Marker positions and joint angles can be exported into ASCII files and post-processed using other programs such as Microsoft Excel or Matlab.

4.3.1.2 Calibration

After the position, zoom and focus are properly adjusted for each camera, it is necessary to calibrate the system. This determines the accuracy of the reconstruction and consists of a static and dynamic component. The dynamic calibration tracks the movement of either a 3-marker or 5-marker wand and produces a 'camera residual' which measures the accuracy of the system as a function of the individual accuracies in each camera. Each camera's residual is the RMS value of the distance between two rays and is expressed in pixels. The first ray is taken from the centre of the strobe ring to the centroid of the marker whilst the second is the reflection of the light ray from the centroid of the marker to the camera lens. The overall mean residual is then calculated as the mean of all camera residuals. In general, Vicon recommends that this value should be less than 0.1% of the distance from the camera to the centre of the capture volume. The only caveat is that the residual does not have a physical meaning; that is, the residual represents a distance on the lens and does not correspond to a physical dimension in 3-space. However, using this value and the volume area, a rough estimate of accuracy can be obtained. The static calibration sets the origin and axis orientation for the capture volume by locating either a static L-frame or T-frame consisting of multiple markers at known distances apart. Average camera residuals are reported in each experimental section.

4.3.2 Phantom High-Speed Camera

4.3.2.1 General

The Phantom V4.1 (Vision Research, NJ, USA) high-speed camera can capture 1000 frames per second (pps) at its full screen resolution of 512 x 512 pixels. With decreased resolution, the sampling frequency could be further increased up to ~ 32 kHz, though the quality of the image also suffers. At each frequency and resolution, the exposure time can be adjusted to improve the quality of the image.

Footage from this camera is continuously stored within its memory until the trigger has been activated which specifies the precise one-second loop to be saved (.cin file). Whilst this one-second window could occur from a second before trigger up to one-second after trigger, the maximum amount of footage that can be stored at any one time is still just one second. All saved .cin files could then be digitised within the Phantom camera software allowing for simple two-dimensional position-time data to be obtained. The quality of digitising is a function of the resolution used to capture the video. Alternatively, .cin files can be converted into .avi files for processing with other compatible software, particularly those that allow digitising to be conducted sub-pixel. SimiMotion (Unterschleissheim, Germany) will be used to digitise high-speed footage as it provides 100 times the resolution by increasing the resolution in each axis by ten-fold.

4.3.2.2 Calibration

High-speed cameras do not require calibration provided that they are in working order and the zoom and focus are properly adjusted. However, to provide physical meaning to the obtained footage, the field of view itself must be calibrated. This is achieved by placing an object of known length in the same plane as the movement to be analysed and then digitising its ends. The total number of pixels measured between the two ends could then be related to the object's length to provide a calibration coefficient. This must be performed in both the horizontal and vertical directions as the resolutions are not always the same in both axes. If more than one camera is used to produce three-dimensional data, the cameras either must be set up perpendicular to each other or a Direct Linear Transform (DLT) must be used.

4.4 Summary

This chapter examined the basic technology and calibration procedures for the force measuring and motion analyses systems. The operation and performance of all systems was standardised except for the Tekscan. The Tekscan system was adapted for use within this research and this required that its technology and performance be scrutinised.

Chapter 5

Influence of Muscle Tension on Biomechanical Response

5.1 Chapter Overview

A review of past research into the influence of muscle tension on biomechanical response and injury prevention is presented. Test methods are presented; impacts were delivered on relaxed and tensed muscle and measurements of impact intensity were measured. Implications for injury identification, quantification and prevention and PPE design are discussed.

5.2 Introduction

Early studies using human volunteers showed that muscle tensing influenced the biomechanical response by increasing thoracic stiffness (Table 5.1). While impactors ranged from cylindrical plates (Stalnaker et al., 1973; Lobdell et al., 1973; Patrick, 1981) to diagonal belts (Backaitis & St. Laurent, 1986), all tests were kept to a non-injurious range. Studying the effects of muscle tension in more severe impacts though, was difficult because while it may be possible to stimulate muscle contraction electrically in a postmortem subject, human cadavers typically could not be obtained, screened, and prepared for testing prior to the onset of rigor mortis (Kent et al., 2003). Therefore, it remained largely unknown how muscle tensing and its effects would vary with impact velocity, level of chest deflection, degree of skeletal damage or respiratory state (Lobdell et al., 1973). In spite of this, the data obtained from volunteer tests were used to scale the response of human cadavers by shifting the biomechanical response curve upwards by 667 N, to account for the increase in stiffness caused by muscle tension (Neathery, 1974).

Table 5.1 Comparison of stiffness increases from muscle tension under different loadings.

Author	Test Loading	Average Thoracic Stiffness Relaxed (N/cm)	Tensed (N/cm)	% increase	% deflection
Lobdell et al. (1973)	Rigid Plate	70	236	337	11
Stalnaker et al. (1973)	Rigid Plate	403	1138	282	8
Patrick et al. (1981)	Rigid Plate	570	790	139	18
Backaitis & St. Laurent (1986)	Diagonal Belt	1336	1613	121	-

The main effect of muscle tensing was that it changed the kinetics of the impact without altering the gross kinematics (Pain & Challis, 2002), but its role in preventing injury was unclear. Pain & Challis (2002) investigated forearm impacts under three muscle conditions and found that tensing decreased the intersegmental tissue movement during impact leading to increased impact force and decreased time to peak force. Increased impact force was thought to increase internal stresses within the body leading to a greater injury potential (Crisco et al., 1996). In contrast, Crisco (1996) impacted the gastrocnemius of a rat and found that tensing decreased impact force with increased compression. This decrease in stiffness was caused by the increase in muscle cross-sectional area which reduced the contribution of the bone on the impact response by decelerating the impact before bone contact. Tensing has also been found to alter the stress distribution in the tissues causing a change in fracture mode (Funk, 2002). It also acted to pre-load the bones in compression leading to an overall increase in structural capacity (Nordsletten & Ekeland, 1993). This was supported by Kent et al. (2006), who suggested that tensing could influence the thoracic force-deflection response in two ways:

1) Through an increased cross-fibre modulus of the muscle tissue thus increasing the force required to deform the thorax; and
2) Through the generation of an isometric tensile force that pre-stressed the thoracic cage and underlying viscera.

However, Kent et al. (2003) argued that muscle tensing only affected the impact response at levels below the injury threshold and that the ribcage was primarily responsible for the elastic response of the thorax. This was further supported by Kent et al. (2006), who found a negligible difference in thoracic stiffness between tensed and relaxed muscle conditions as chest deflection approached 20% (Fig 5.1). This was significant because it was the level at which irreversible injury (i.e. rib fractures or organ lacerations and ruptures) was found to occur. At deflections greater than 20%, stiffness for both muscle states were similar. Therefore, it was argued that the uniform shift of 667 N to account for an increased stiffness should be ignored since it did not accurately account for effects in muscle tension as stiffness increased with increasing chest deflection, but occurred only at levels below the threshold for irreversible injury. However, this did not account for the shape of the response curve for each muscle state before the stiffness' converged. At all levels of deflection below 20%, the tensed muscle required more energy for a given deformation than the relaxed muscle (i.e. increased area under the F-d curve). It was likely that this influenced the occurrence of reversible injuries or reduced the discomfort at impact as subjective tolerances were kept below this threshold (Lobdell et al., 1973; Stalnaker et al., 1973; Patrick et al, 1981).

Figure 5.1 As deflection approached 20%, the increase in force from tensing became negligible, but the work required to deform the thorax increased (Kent et al., 2006).

Omitting muscle and the influence of muscle tension ignores a real set of possible injuries and masks the true impact response. While this may be a suitable simplification in automobile accidents, which were primarily interested in preventing life-threatening or catastrophic injuries, sports feature similar high-energy collisions which can cause muscle injuries and be just as debilitating to performance as a ‘catastrophic’ injury. In particular, athletes must prevent against muscle contusions which are caused by compression of the muscle against bone. Since tensing has shown to decrease the amount of compression for a given load (i.e. increased stiffness), it is likely that muscle tension played an important role in preventing soft tissue injuries. In running, tensing has been shown to reduce soft tissue injury by changing the coupling between soft tissue and bone (Wakeling & Nigg, 2000) and increased the damping of soft tissue vibrations (Wakeling et al., 2002). This could be important since prolonged vibrations can also affect soft tissue by reducing motor unit firing rates and muscle contraction force (Wakeling et al., 2002). Soft tissues were also found to account for up to 70% of energy dissipated within an impact (Pain & Challis, 2002) and could attenuate peak forces by up to 28% (Robinovitch et al., 1995). As such, it is clear that muscle tension has a role in changing human biomechanical response and may have the ability to reduce injury.

This chapter examines the effects of muscle tension on the human biomechanical response to impact and how this may influence the occurrence of subjective or low-intensity (i.e. contusion) reversible injuries. Furthermore, it looks to develop correlates that can be used to determine the occurrence of these selective types of injury. These results have implications for the design of higher biofidelity ATDs and Personal Protective Equipment (PPE), in particular those that aim to only reduce peak force.

5.3 Methods

5.3.1 Subjects

Seven physically active males provided informed voluntary consent to participate in this study in accordance with the protocol outlined by the Loughborough University Ethical Advisory Committee (*Appendix B*). Each was a martial artist who participated in either Mixed Martial Arts or Karate and trained at least four hours per week. Inertial parameters of the right leg for each subject were calculated using the model developed by Yeadon (1990). A list of all athletes appears in Table 5.2.

Table 5.2 Summary of athletes.

Subject	Age (years)	Height (m)	Mass (kg)	Sport
1	25	1.83	79.40	Mixed Martial Arts
2	20	1.69	76.00	Mixed Martial Arts
3	24	1.74	92.40	Mixed Martial Arts
4	25	1.76	82.00	Mixed Martial Arts
5	20	1.82	73.70	Mixed Martial Arts
6	38	1.75	95.10	Karate
7	39	1.75	84.00	Karate

Each athlete was instructed to sit in an upright posture with the weight of their right thigh resting on the middle of a bench (width = 0.5 m) whilst their right foot was planted on the ground. During each impact, the thigh was compressed between the impactor and bench. Bench height was adjusted until a resting external right knee angle of ~ 90° was achieved. The left knee was positioned off the side of the bench, just posterior and inferior to the right knee, to provide an unencumbered view of the impacted thigh. After a short warm-up, consisting of sub-maximal isometric knee extensions, each athlete performed a Maximum Voluntary Isometric (MVI) knee extension whilst the force generated was measured using an ankle strap instrumented to a load cell. Athletes were then asked to produce 60% MVI so that they would know how much effort to exert in tensed trials. The entire set-up is shown in Fig 5.2.

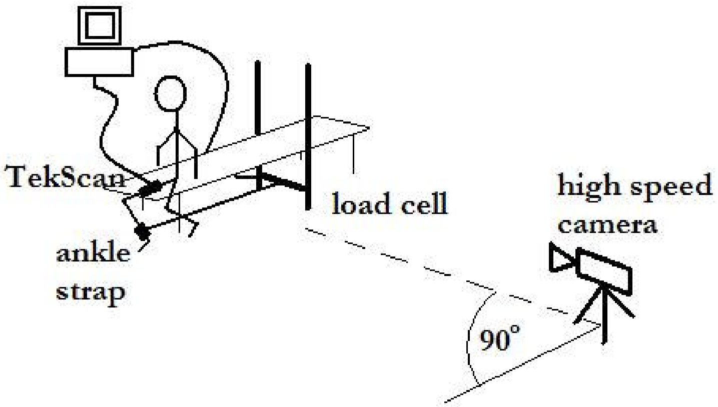

Figure 5.2 Experimental set-up showing load cell, ankle strap, high speed camera and Tekscan.

5.3.2 Trial Protocol

In each trial, a medicine ball was dropped from seven different drop heights ranging from 1.0 – 1.6 m (0.1 m increments) onto the specified target area of the thigh. Participants were instructed to either relax (no isometric knee extension) or tense (target knee extension at 60% MVI) their quadriceps muscles. After each trial, participants were asked to rate their level of discomfort experienced from the impact ranging from 0 (‘No Pain’) to 10 (‘Extreme Pain’) on a Borg CR10 pain scale. Impact force, contact time (CT) and time to peak force (TTPF) were obtained from force sensors while impactor inbound and outbound velocity in each trial were obtained from digitising high-speed video footage.

Each participant was subjected to 20 impacts spread over two sessions. This reduced muscle fatigue and bias of their perceived discomfort, particularly for the last impacts in each session. Drop heights were randomized, but care was taken to ensure that higher energy impacts were not administered in succession to allow for a period of recovery. Time between impacts was approximately 120 seconds and drop heights were withheld from each subject prior to each trial.

5.3.3 Instrumentation

Two Tekscan (Boston, MA) pressure insoles were wrapped around the quadriceps of the right thigh for each participant and secured with electrical tape. Sensors were orientated to maximize the surface measuring area, but limit the amount of overlap between the sensors and creasing and folding of the individual sensors. Sensors were set to record at 500 Hz.

A Phantom High Speed Camera (Wayne, NJ), operating at 2000 Hz, was set perpendicular to the bench to record the ball-thigh interaction. Camera position and settings were adjusted to record ten frames prior to and after impact and include a view of the right leg to allow qualitative observation of the impact (Fig 5.3).

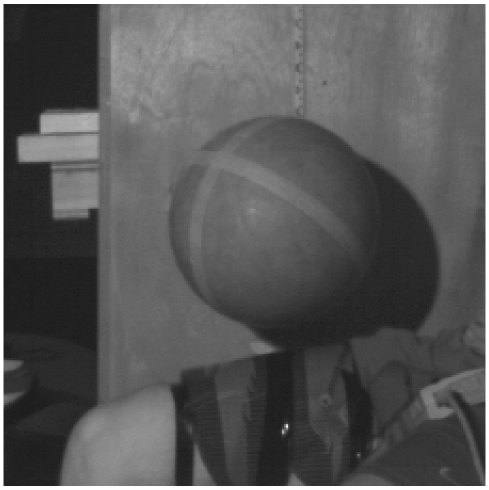

Figure 5.3 Sample frame taken from the Phantom high-speed camera.

5.3.4 Impactor Properties

A 3.9-kg medicine ball was used as the impactor in this study. Its dynamic impact properties were assessed by examining the amount of energy lost due to deformation during a rigid impact. The medicine ball was dropped vertically, between heights of 0.50 – 1.60 m, onto a Kistler force plate (f = 2000 Hz). The energy lost was calculated using the difference between drop and rebound heights determined from digitizing video footage obtained from a High Speed Camera (f = 1000 Hz). This value was plotted against the impact force and a power function was fit to the data. In participant trials, this curve was used to estimate the amount of energy lost during ball-thigh impacts based on the force measured by the Tekscan sensors.

5.3.5 Impact and Rebound Velocity

Impact and rebound ball velocities were determined by analysing the high-speed video footage of each drop. In each trial, the three frames prior to and after impact were digitized using SimiMotion (Unterschleissheim, Germany) software with each trial digitised three times. In each frame, a total of four points were digitized representing the top-, bottom-, left- and right-most extremes of the ball. These four points were averaged to determine the centre of the ball and changes in its position were used to calculate vertical and horizontal velocities. As only one camera was used, any oblique impacts were discarded from the trials. To ensure the correct impact conditions, knee extension forces (%MVI) and the deviations in drop heights (difference between the intended drop heights and that calculated by the impact velocity) were analysed.

5.3.6 Calculations and Statistics

Impact forces were converted to SI force units (i.e. Newtons) using the raw data in the linear Tekscan calibration curve equation (§ 4.2.2.2). Estimates of the energy absorbed in deforming the medicine ball were then calculated using the power curve described in § 5.2.3 and was based on the measured impact force. Energy absorbed by the thigh during impact was approximated using equation 5.1.

$$E_{absorbed} = \underbrace{\frac{1}{2}mv_{impact}^{2}}_{\text{impact energy}} - \underbrace{\frac{1}{2}mv_{rebound}^{2}}_{\text{rebound energy}} - E_{ball\ deformation} \qquad (5.1)$$

At each height, a t-test was conducted to determine the differences between relaxed and tensed impacts for force, energy absorption and perceived impact intensity. A pairwise t-test was also used to compare between muscle states. In addition, a repeated measures (RM) ANOVA was conducted to examine the main effects for height and muscle tension and the interaction between these two variables. Statistical significance was set at $\alpha = 0.05$.

5.3.7 Muscle Mass Estimation

Inertial parameters of the right thigh (mass, length and perimeter) were calculated for each athlete using the mathematical inertia model of Yeadon (1990). Using thigh mass, tissue masses were estimated as proportions of segmental body mass (Clarys et al., 1984; Clarys & Marfell-Jones, 1986). However, the composition of fat was reduced to 10% and 15%, respectively, to provide a more accurate representation of the athletic population. The excess mass was redistributed using two different methods (Wilson, 2003; Pain & Challis, 2002): the *All to Muscle* (ATM) method converted all excess mass directly to muscle, while the *Ratio* method calculated muscle and bone masses based on the original muscle-to-bone mass ratios. The new ratios for both methods appear in Table 5.3 and sample calculations appear in *Appendix C*.

Table 5.3 Ratios used for muscle mass estimation modified from Clarys et al. (1984).

15% Fat				**10% Fat**			
All to Muscle (ATM)		**Ratio**		**All to Muscle (ATM)**		**Ratio**	
Skin	5.4	Skin	5.4	Skin	5.4	Skin	5.4
Fat	15	Fat	15	Fat	10	Fat	10
Muscle	52.2	Muscle	48.74	Muscle	57.2	Muscle	52.45
Bone	13.5	Bone	16.96	Bone	13.5	Bone	18.25

Using the calculated thigh masses, an estimate of thigh muscle mass was obtained for both methods and averaged to provide an overall estimation of muscle mass within the thigh. Three correction factors based on the inertial parameters and muscle mass were proposed to help normalise the impact force, energy absorption and perceived impact intensity data to account for the variation in body types between athletes. Each corrective factor provided an estimate for the thigh thickness by relating either the mass or perimeter per unit length. However, as this section focuses on the influence of muscle tension, it was likely that the amount of muscle thickness per unit length was the most influential factor.

5.4 Results

5.4.1 Impactor Properties

The energy absorbed by the medicine ball during deformation was plotted as a function of impact force (Fig 5.4). A power curve was fit to the data to account for the visco-elasticity of the impactor; i.e. changes in impact velocity or impact force led to a non-linear change in impactor deformation. Using the equation of the power curve together with the impact force measured in subject trials, an estimate of the impactor deformation energy required for equation 5.1 in § 5.2.6 was obtained.

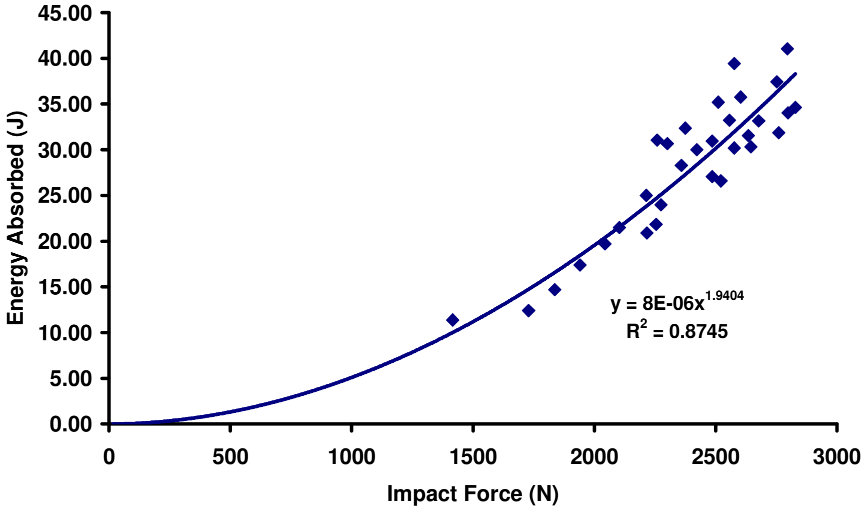

Figure 5.4 Energy required to deform the medicine ball during impact.

As impact force increased, the variance in residuals between the best fit power curve function and the data points showed a general increase. Whilst this increase may be caused by poor sensor performance and may exhibit heteroscedasticity, there were not enough data points in the low range to fully support this claim. More data points should be collected in the future to determine if this heteroscedastic relationship was truly present.

5.4.2 Impact Intensity Measurements

Average group peak forces with standard deviation error bars for all subjects were calculated at each drop height and compared (Fig 5.5). In general, peak forces were higher for the tensed condition than the relaxed condition at all drop heights except for 120 cm, though only impacts at 100 cm were found to be significantly different. On average, tensed impacts were 1.11 times greater than relaxed impacts, ranging from 0.98 – 1.24x.

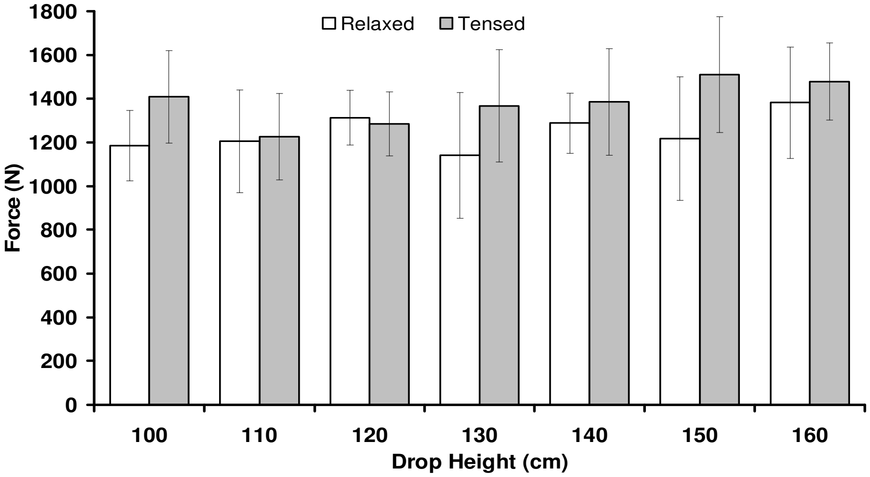

Figure 5.5 Average group impact force (± SD) at each individual drop height.

At all heights, the average energy absorbed in relaxed muscles were higher than tensed muscle, though significance was only found at 130 cm (Fig 5.6).

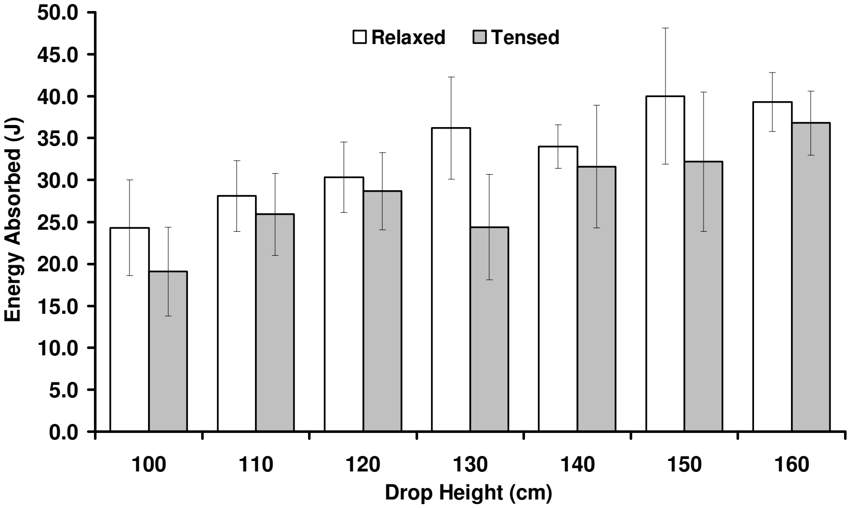

Figure 5.6 Average energy absorbed (± SD) by the thigh at each drop height

A comparison of all impacts using a pairwise t-test revealed that tensed impacts produced significantly greater impact forces whilst absorbing significantly less energy than relaxed impacts. This was supported by the RM ANOVA for impact force (F=32.616, p=0.029) and absorbed energy (F=28.62, p=0.033) across all drop heights. An interaction between muscle condition and drop height was not found for impact force (F=2.422, p=0.26) but was found for absorbed energy (F=5.372, p=0.007). This interaction can be seen in Fig 5.6; that is, the difference in energy absorbed between relaxed and tensed muscle was influenced by drop height.

Perceived impact intensities (mean ± SD) in tensed muscle (1.4 ± 0.8) were significantly lower than that of the relaxed muscle condition (4.2 ± 1.1). This relationship was examined further to determine if either force or energy absorbed could be used to predict perceived impact intensity (Fig 5.7). The relationship between force and perceived impact intensity seemed to depend on muscle state; in tensed muscle, force decreased with increasing perceived intensity, whilst the opposite trend was exhibited in the relaxed condition (i.e. higher force, higher perceived intensity). In contrast, thigh energy absorption seemed to be insensitive to muscle condition and correlated positively to perceived intensity.

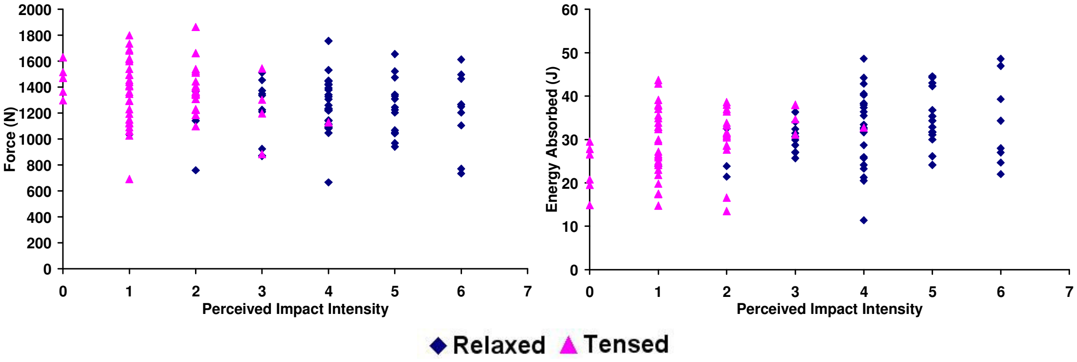

Figure 5.7 Plot of force and energy absorption as a function of perceived impact intensity

5.4.3 Impact Characteristics

Tensed impacts had significantly lower TTPF compared to relaxed impacts while CTs did not exhibit a statistical difference (Table 5.4). High-speed video footage revealed greater thigh deformations in the relaxed condition, while impactor deformations were greater in the tensed condition (Fig 5.8). While neither of these deformations was quantified for each athlete, the impact forces from each trial provided some insight into the energy absorbed by the medicine ball during impact. Higher forces, observed in tensed impacts, led to higher energy absorbed by the medicine ball, according to the regression curve displayed in § 5.3.1, and thus higher ball deformations. The medicine ball was not digitised during contact for all subjects and is examined further in the discussion.

Table 5.4 Impact characteristics for each drop height split into muscle condition

Height		Relaxed			Tensed	
	TTPF (ms)	CT (ms)	Comfort	TTPF (ms)	CT (ms)	Comfort
100	16.0 ± 2.1	43.8 ± 5.8	3.9	13.4 ± 1.5	43.4 ± 6.1	1
110	16.5 ± 1.7	45.5 ± 7.0	3.8	15.1 ± 2.3	45.7 ± 5.8	1
120	14.3 ± 2.7	46.0 ± 6.6	3.8	14.4 ± 2.3	42.2 ± 4.8	1
130	16.0 ± 2.4	47.8 ± 8.2	4.1	14.4 ± 2.3	45.6 ± 4.8	1.3
140	15.3 ± 1.0	39.3 ± 6.7	4.1	13.8 ± 2.4	43.6 ± 4.4	1.4
150	15.2 ± 1.7	44.0 ± 9.9	4.8	13.0 ± 3.9	41.7 4.1	1.5
160	14.9 ± 1.9	45.7 ± 8.9	4.9	13.4 ± 2.2	43.1 ± 5.3	1.7
Average	15.6 ± 2.0	44.6 ± 7.6	4.2	14.0 ± 2.4	43.7 ± 4.9	1.4

To ensure consistency between impacts, the amount of muscle contraction and the deviation in drop height was assessed. On average, the amount of muscle contraction for each subject in the tensed condition exceeded the target of 60% MVI (range 50.3 – 86.8%). A comparison of drop heights revealed a mean of 7.0 cm difference between the drop height calculated by impact velocity and the intended drop height for each trial (Table 5.5).

Table 5.5 Mean average (±SD) for MVI in voluntary contractions in tensed impacts and the overall variation in drop heights for all impacts separated by athlete.

Athlete	Percentage of MVI (%)		Deviation in Drop Heights (cm)
	Average	Standard Deviation	
1	60.5	6.2	4.0
2	72.7	5.8	4.5
3	60.0	6.2	6.7
4	72.9	8.7	6.2
5	70.2	4.1	6.0
6	59.6	7.3	10.8
7	59.1	2.6	8.1
Mean Average	65.0	5.8	7.0

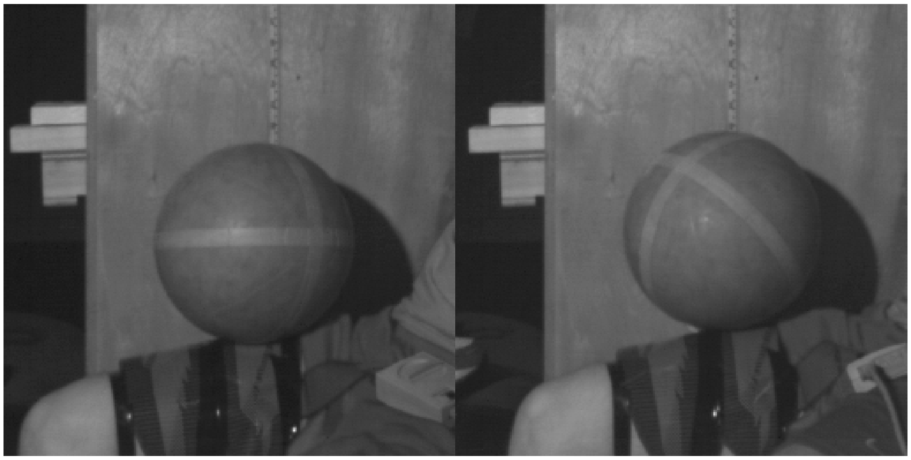

Frame Before Impact
Time: 0 ms

Frame Before Impact
Time: 0 ms

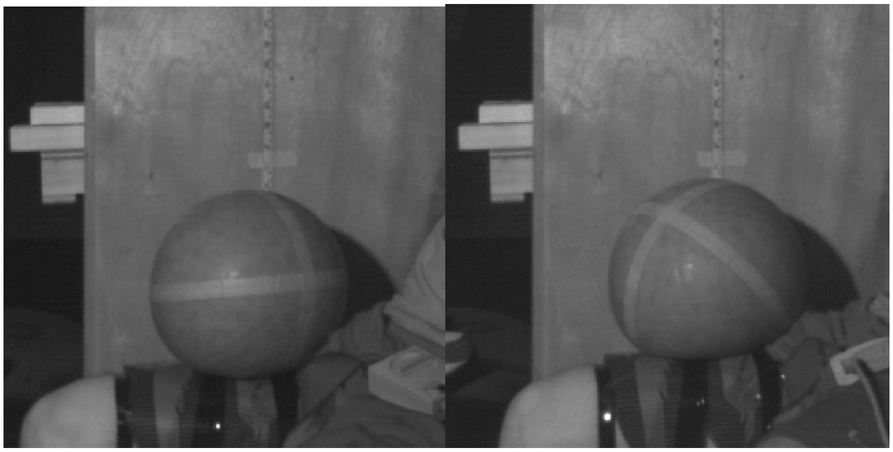

Maximum Compression
Time: 18.5 ms

Maximum Compression
Time: 17 ms

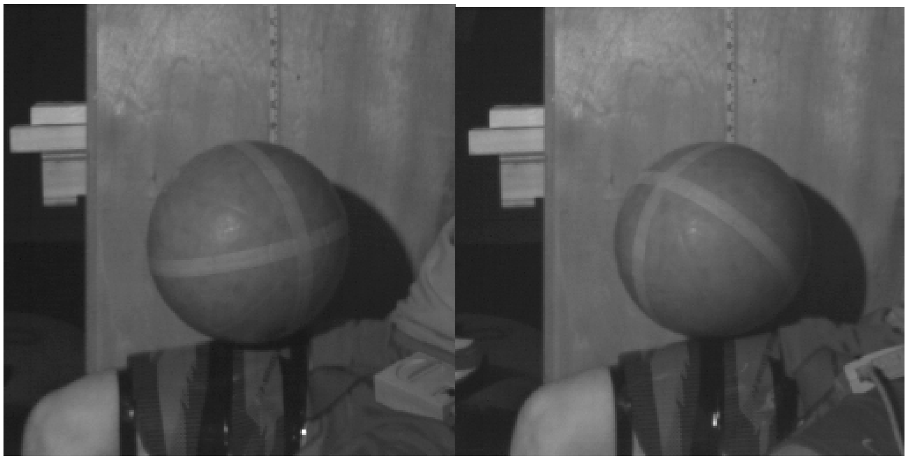

End of Impact
Time: 53 ms

End of Impact
Time: 39.5 ms

Figure 5.8 Representative trial from subject 1. Left sequence is relaxed while right is tensed.

5.4.4 Subject Normalisation

Subject-specific inertia parameters calculated using the Yeadon (1990) model are shown in Table 5.6. Using the thigh's mass, length and perimeter, two correction factors were developed to help normalise the original data. These were:

1) Thigh Mass/Thigh Length (M/L): provides an indication of overall thigh mass per unit length and a higher M/L ratio indicated greater thickness
2) Thigh Perimeter/Thigh Length (P/L): provides an indication of thigh volume and a higher P/L ratio indicated a greater volume and thickness

Of these two corrective factors, the M/L ratio was likely more relevant as this provided an indication of the amount of the thigh effective mass, which was more meaningful than just thigh volume. Higher effective masses are generally associated with higher impact stiffness so there was likely a systematic increase in impact force with increased M/L ratio that could be accounted for.

Table 5.6 Subject-specific inertia parameters obtained using Yeadon's model (1990) and possible athlete correction factors using thigh mass, length and perimeter.

			Thigh Inertial Parameters			**Possible Corrections**	
Athlete	**Height (m)**	**Mass (kg)**	**Mass [M] (kg)**	**Length [L] (m)**	**Perimeter [P] (m)**	**M/L**	**P/L**
1	1.83	79.40	11.84	0.495	0.558	23.92	1.13
2	1.69	76.00	10.25	0.390	0.573	26.28	1.47
3	1.74	92.40	12.11	0.404	0.600	29.98	1.49
4	1.76	82.00	10.76	0.405	0.564	26.57	1.39
5	1.82	73.70	9.89	0.410	0.515	24.12	1.26
6	1.74	90.30	13.49	0.438	0.582	30.81	1.33
7	1.75	84.00	12.96	0.434	0.585	29.86	1.35

Using the calculated thigh masses and the ratios displayed in Table 5.4, tissue masses for each individual, assuming 15% fat were calculated (Table 5.7). A third correction factor, the muscle mass-to-length (MML) ratio, was also calculated to help account for differences between subjects. This provided an indication of the muscle thickness per unit length. It was considered to be superior to the M/L and P/L ratios since the increase in effective mass caused from tensing was directly related to the amount of muscle mass in the thigh.

Table 5.7 Bone, fat and muscle ratios for 15% adipose.

Clarys et al. (1984) - 15%										
Subject	**All to Muscle**			**Constant Ratio**			**Average**			**Muscle / Length**
	Bone Mass	**Fat Mass**	**Muscle Mass**	**Bone Mass**	**Fat Mass**	**Muscle Mass**	**Bone Mass**	**Fat Mass**	**Muscle Mass**	
1	1.60	1.78	6.18	2.01	1.78	5.77	1.80	1.78	5.98	12.07
2	1.38	1.54	5.35	1.74	1.54	5.00	1.56	1.54	5.17	13.26
3	1.63	1.82	6.32	2.05	1.82	5.90	1.84	1.82	6.11	15.13
4	1.45	1.61	5.62	1.82	1.61	5.24	1.64	1.61	5.43	13.41
5	1.33	1.48	5.16	1.68	1.48	4.82	1.51	1.48	4.99	12.17
6	1.82	2.02	7.04	2.29	2.02	6.58	2.05	2.02	6.81	15.55
7	**1.75**	**1.94**	**6.76**	**2.20**	**1.94**	**6.32**	**1.97**	**1.94**	**6.54**	**15.07**

Perceived impact intensities were also plotted against the MML ratio for each individual (Fig 5.9). This showed that the perceived impact intensity was not only higher for relaxed muscle, but also increased with decreasing MML ratio (i.e. higher perceived intensity with less muscle mass per unit length).

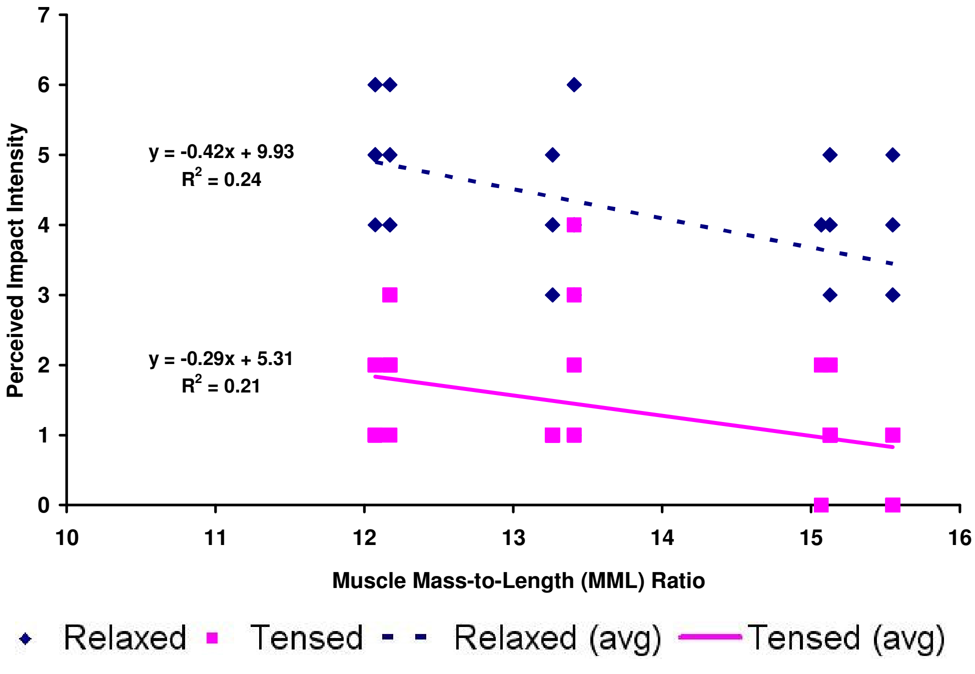

Figure 5.9 Perceived impact intensity plotted as a function of MML ratio for all subjects. Please note that the lines are only to show a negative correlation between perceived impact intensity and MML ratio, not to suggest a continuous mathematical relationship.

In § 5.4.2, peak forces were found to be significantly higher for tensed impacts across all impacts. To investigate whether subject differences influenced this result, force was compared to MML ratio for each muscle condition. Peak impact forces for relaxed and tensed impacts were plotted as a function of MML ratio at heights of 100, 130 and 160 cm (Fig 5.10). MML ratio did not appear to be an influential factor.

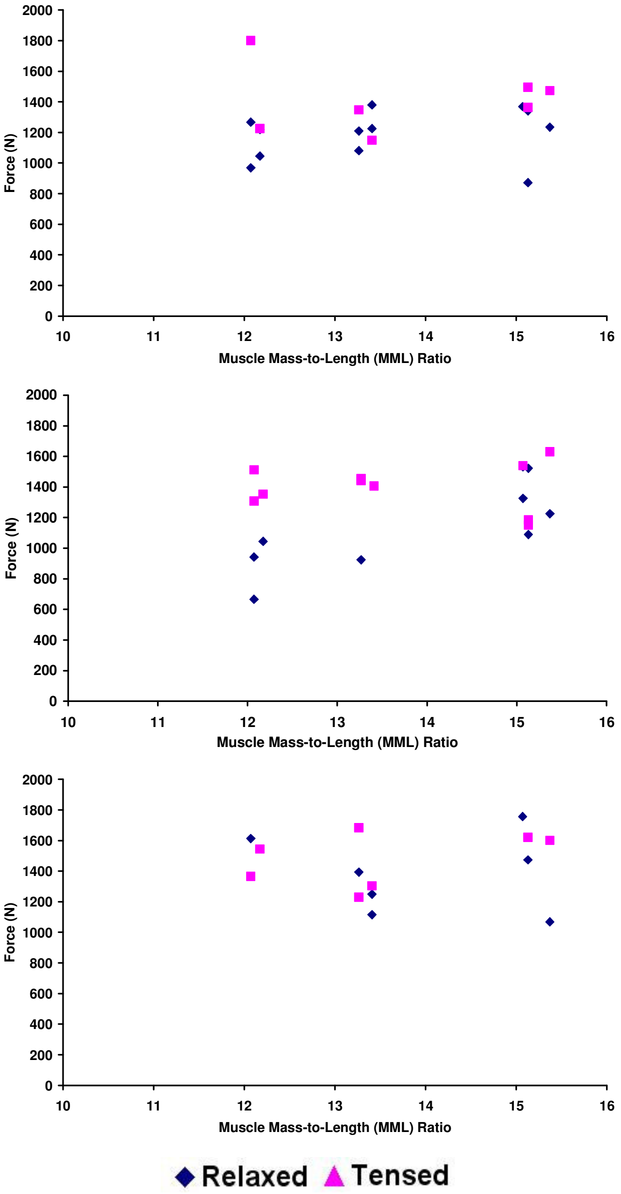

Figure 5.10 Force plotted as a function of MML ratio for drop heights of 100 cm (*top*), 130 cm (*middle*) and 160 cm (*bottom*).

5.5 Discussion

5.5.1 General

In the tensed condition, impact forces were, on average, 11% higher for all drop heights but the perceived intensity and energy absorbed were lower. Tensed impacts were also associated with lower CTs and significantly lower TTPF. These results compared favourably to Hrysomallis et al. (1996) which attributed the increased force and decreased TTPF in tensed conditions to a greater hardness or resistance to indentation (or deformation) of the thigh. These authors also observed a lower level of discomfort in tensed conditions and suggested that at low intensity impacts, higher peak decelerations of the striking mass may not cause higher levels of discomfort. It was also likely that the increased resistance caused shorter CTs, which has been shown to increase the threshold for physical injury (Bir et al., 2004), so it was assumed that this could have led to a slight increase in pain threshold as well. Whilst force was negatively correlated to discomfort in this study (Fig 5.7), it could not be used as a discomfort or pain predictor in this way; that is, higher forces did not lead to lower magnitudes of subjective injury. Kent et al. (2006) suggested that a *"higher force – less injury"* relationship would only hold at impact intensities where serious (either reversible or survivable) injury would not occur. Moreover, the authors proposed that the work (i.e. energy) in deforming the body provided more insight into any potential cause for all types of injury.

The energy absorbed by the thigh was estimated using the inbound and outbound velocities and assumptions about the impact properties of the impactor. At each drop height, the energy absorbed was greater in the relaxed condition and was positively correlated with perceived intensity for both muscle conditions. Incidentally, reducing energy absorption during impact had been identified as a preventative measure of injury causation in car crashes (Viano, 1987). As such, one of the likely functions of tensing was to reduce the amount of energy absorption which could lead to a decrease in actual injury (e.g. rib fracture). Whilst this was a better indicator of discomfort than force, the magnitudes of absorbed energy could not be compared without considering the drop height or impact velocity. For example, the energy absorbed in the tensed condition at 110 cm was higher than the relaxed condition at 100 cm, though the perceived intensity was less (1.0 versus 3.9). Since discomfort was likely caused by compression of soft tissue against bone, this implied that there was less compression in the tensed condition despite more absorbed energy. This supported Kent et al. (2006) which showed that more work (or energy) was required to deform the tissue when the muscle was tensed. Therefore, it was assumed that tensed muscle was also more effective at dissipating any excess absorbed energy and decreased the amount of soft tissue compression. Pain & Challis (2002) showed that when muscles were tensed, the effective mass of that limb would increase. With a greater anvil effective mass, the ratio between impactor-to-anvil mass would decrease resulting in less deformation and a more rigid impact. This has also been found to be the main contributing factor for an increase in impact forces (Viano, 1991) whilst decreasing deformation would decrease injury risk.

Velocities in this study ranged from 4.4 – 5.6 ms^{-1} (drop heights of 1.0 – 1.6 m) which were almost double the 3 m/s threshold at which compression had been shown to be the main predictor of injury (§ 2.3). At this velocity, impacts were likely to cause viscous injuries with the magnitude of deformation being more influential than the deformation velocity. Whilst energy can be computed using the product of force and deformation, the deformation of the thigh could not be estimated using the total energy absorbed and the peak force measured within each trial. This calculation requires peak deformation to occur at the same time as peak force, but past force-deformation relationships obtained from the literature indicated that peak force generally occurred before peak deformation. Regardless, without synchronised force- and energy-time histories, an estimate of peak compression could not be obtained. Digitisation of high-speed video footage was used to estimate inbound and rebound velocities and was qualitatively able to indicate less deformation in tensed muscle at each drop height (Fig 5.8). However, poor lighting in the trials during contact, particularly when the ball was in the foreground made it difficult to digitise the ball during contact. In spite of this, an attempt was made on the impacts of player 1 which revealed significantly lower deformations when tensed (Table 5.8). With less deformation and an almost 11% increase in impact force, a substantial increase in impact stiffness for tensed impacts was likely similar to the increases observed in Table 5.1. However, without more deformation data from other players, it was not possible to accurately determine the correlation between compression and/or stiffness on perceived impact intensity.

Table 5.8 Summary of impacts for player 1

Condition	Force (kN)	Energy Absorbed (J)	Deformation (cm)	Perceived Intensity
Relaxed	1.22 ± 0.28	34.0 ± 8.4	3.1 ± 0.3	5.4 ± 0.7
Tensed	1.31 ± 0.26	31.0 ± 9.0	2.0 ± 0.2	1.4 ± 0.5

Hrysomallis et al. (1996) had suggested that one of the roles of muscle tension was to stiffen the body leading to higher impact forces but less compression. Whilst this increased stiffness was also observed in this study, those authors did not account for the differences in the amount of muscle tissue present between subjects. Results of Crisco et al. (1996), which impacted the gastrocnemius muscle in rats, suggested that this variable had a major influence on the impact response. In relaxed muscle, there was insufficient muscle mass to decelerate the impactor before contacting the underlying bone leading to an increase in impact force. In contrast, tensed muscle increased the muscle cross-sectional area thus reducing the effect of the underlying bone and lowering impact forces. Whilst this force-deformation relationship contrasted to results shown in § 5.3.2 (i.e. higher forces in tensed muscle) these authors still reported less cases of contusion. Since Crisco et al. found tensing to decrease soft tissue injury risk regardless of the thickness of soft tissue at impact, the impact force, or the amount of compression, it was assumed that this relationship would hold for discomfort as well. This finding was supported in Fig 5.9 which showed lower perceived impact intensities for tensed muscle at all values of the MML ratio. This implied that the reduction in energy absorption and/or the effectiveness in energy dissipation were responsible for lower impact intensities in tensed muscle. It also proposed that at low levels of MML ratio, compression may not be the main injury mechanism or a good indicator of injury. Whilst other mechanisms suggested by Nordsletten & Ekelend (1993), Funk (2002) and Kent et al. (2006) were discussed in § 5.2, these did not apply as these were in reference to skeletal injuries whilst the onset of possible soft-tissue injuries were examined in this study.

In this study, a subjective metric (e.g. perceived impact intensity or discomfort) was used to infer an objective injury outcome (e.g. contusion). Since each appeared to share the same injury mechanism (e.g. energy absorption), it was thought to be a reasonable assumption. A caveat was that it was unclear to what extent muscle tension affected the transmission of pain stimuli. A pain stimulus is first detected by the nociceptors (pain receptors) which transmits this signal to the Central Nervous System (CNS). However, the CNS is also responsible for sending action potentials to the muscles during voluntary contraction. Gated Theory proposed that the CNS would be too busy processing the electrical signals associated with muscle contraction, a large fibre input, to properly assess the pain stimulus, a small fibre input. In this instance, the gate would be closed. In contrast, relaxed muscle would not produce any large fibre inputs to process meaning the gate for processing pain would be open. As such, the blocked pain stimuli may have led to the lower perceived intensities during the tensed muscle trials, though it was unclear whether this was more influential than the changes observed in the parameters measured here. Furthermore, whilst it may be argued that tensing of any body part will block the transmission of pain stimuli, it was also possible that these signals were compartmentalised by body part or region; that is, the transmission of pain stimuli may not be interrupted if the larger fibre input is rooted in another part of the body. Future work may determine if these parameters influenced the level of discomfort for or if it was caused by a blockage of pain stimuli.

Perceived impact intensities were also influenced by the MML ratio; higher MML ratios resulted in lower impact intensities for both tensed and relaxed muscle (Fig 5.8). This suggested that there was a systematic difference in perceived impact intensities based on the MML ratio. As such, it was hoped that the MML ratio could be used to explain any variance in forces shown with the standard deviation bars of Fig 5.5. However, when impact forces were separated by drop height and muscle condition and plotted as a function of MML ratio, a systematic trend was not observed (Fig 5.10). It is assumed that when there is no muscle (i.e. MML ratio = 0), the response of relaxed and tensed muscle would be the same since the bone would be responsible for generating the impact response. At low levels of MML ratio, tensed muscle would have enough effective mass to reduce impact forces, but relaxed muscle did not, a result which Crisco et al. (1996) eluded to. As the MML ratio increases, the influence of bone decreases as the impact response depends more on the soft tissue. This leads to a reduction in impact force until the response is entirely dependent on the soft tissue at which point the force plateaus. However, since tensed muscle is much stiffer, the rate at which force reduces is likely much slower and the plateau region would be higher than relaxed muscle. Moreover, as drop height increases, the rate of force attenuation would decrease and higher MML ratios are necessary to generate a plateau in force. Force magnitudes would also be higher due to the higher decelerations necessary to stop the impactor. This theoretical relationship is plotted in Fig 5.11; the linear curve, the rates of decrease in peak force and the force plateaus are chosen arbitrarily to illustrate the assumed dependence force had on MML ratio and muscle condition. Moreover, the range of MML ratios represented by these subjects and the real curve shape are unknown. Therefore, the theoretical difference expected between the two muscle states is unclear. This coupled with the variance associated with Tekscan sampling errors (§ 4.2) likely explained why this assumed relationship was not observed in Fig 5.10.

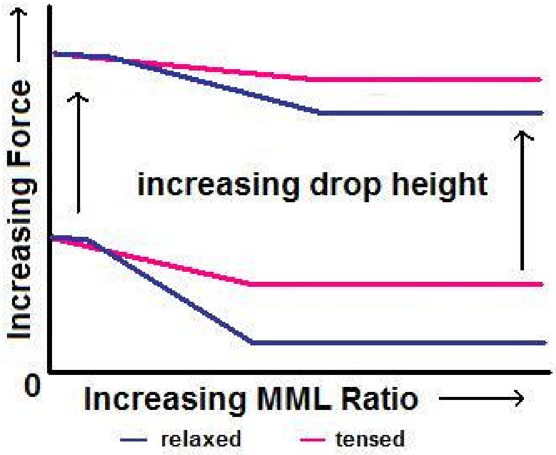

Figure 5.11 Theoretical force-MML ratio curve for tensed and relaxed muscle. Magnitudes of force and MML and and curve shape were arbitrary.

One of the primary outcomes of this research was the implications for PPE design. Forces were not found to correlate well with perceived impact intensity which implied that PPE should not be necessarily concerned with minimising peak impact force. Instead, PPE should concentrate on reducing energy absorption in the body or aiding its energy dissipation. Viano et al. (2000) suggested that PPE could spread the load, absorb part of the kinetic energy and/or increase the mass of the segment impacted. Whilst the importance of increased mass was supported by Martin et al. (1994), the potential mass of PPE was limited as an athlete's performance could not be hindered. However, increasing the effective mass was shown in these results to be a natural mechanism for protection achieved by tensing. As such, the response of PPE must account for the composition of the underlying body as they worked together in-series to develop the impact response (Pain et al., 2008). Furthermore, if future PPE was going to be subject-specific, the leg volume or MML ratio will be important, not only for fit and conformity, but for its affect on PPE requirements. For example, subjects of lower MML ratio will require PPE that increase the effective mass of the soft tissue more than subjects of higher MML. The method for how this may be obtained, however, was another study in itself and will not discussed be here.

Prior to this study, a pilot study was conducted to ensure that the impact intensity would not cause injury to any of the participants. Three medicine balls (masses = 1kg, 3.9 kg, 10 kg) were piloted, as was a 2-kg shot put, which was a similar impactor to that used in Hrysomallis et al. (1996). Both the 10-kg medicine ball and the shot put were found to be too stiff, while the compliance of the 1-kg was too low. As the majority of sporting impacts, save cricket balls, feature two deformable, viscoelastic objects colliding together, the 3.9-kg medicine ball was selected. Whilst this made estimating the energy absorbed more difficult, it provided more realistic impact interactions in terms of contact time and rate of force development and reduced the risk for serious injury. To further reduce the occurrence of severe injury, the thigh was chosen as the impact location due to the abundance of soft tissue. The maximum force measured in any trial (1.86 kN) was lower than the fracture tolerance of the tibia, which has less soft tissue covering than the femur, suggesting the likelihood for serious injury to the thigh was low. In addition, subjects were selected based on their assumed tolerance to impacts. As such, it was necessary that each subject have experience in a sport which relied heavily upon physical contact. This ensured that the impact intensity level would not be unfamiliar and that they would be able to distinguish between perceived intensities. Also, as these intensities were not high in comparison to competition impacts, there was less chance of actual or perceived injury with this group of athletes since their tolerance was theoretically higher. In addition, the time between impacts was at least 120 seconds to allow for recovery and the number of impacts was restricted to ten per session to reduce discomfort from fatigue.

5.6 Conclusion

This study showed that peak force was not the best indicator of subjective injuries and that another variable such as energy absorption or compression may be more appropriate. It also showed how subjective injury tolerances were influenced by muscle contraction and segmental muscle mass composition. These results provided implications for future PPE designs; that is, the protective function of PPE must be able to account for differences between (i.e. muscle mass) and within (i.e. muscle condition) athletes. As such, PPE may need to adapt during competition to either attenuate force and/or reduce energy absorption without undergoing permanent change to its structure to account for these physiological differences in muscle during a match or competition.

Chapter 6
Biofidelity of Human Surrogates

6.1 Chapter Overview

This chapter discusses the uses and limitations of current Anthropometric Test Dummies (ATDs) as anvils for analysing PPE performance. A commercially available martial arts training device is introduced and its biofidelity is examined. Modifications to the device are proposed and results for its biomechanical response are presented. The aim is to present an ATD which can be used as an anvil to determine impact intensities during a specific martial arts attack.

6.2 Introduction

Before athletic PPE can be commercially sold, it must first be tested by a set of British Standards (*BStan*). These tests examine the force transmitted through PPE garments onto an instrumented anvil when impacted with a rigid impactor. Typically, these anvils have taken the form of an Anthropometric Test Dummy (ATD). Independent research studies using this technique have tested football shin guard performance on a wooden leg (Philippens & Wismans, 1989; Lees & Cooper, 1995), the Hybrid III leg-form (Bir et al., 1995) and on composite bones (Francisco et al., 2000; Ankrah & Mills, 2003). Similarly, cricket leg guards have been tested using a rigid anvil (Hrysomallis, 1996) and baseball chest protectors have been evaluated using a Hybrid III dummy and a 3-Rib Chest Structure (3-RCS) (Bir & Viano, 1999; Viano et al., 2000). In each instance, the ATDs were designed to match a set of inertial parameters but not necessarily the material properties of the body part to be protected. This can lead to erroneous results as the size, inertia and elasticity of an ATD influenced the measurement of impact force (Falco et al., 2009). Instead, the materials were likely chosen to produce repeatable results and prolong the life of the ATD (i.e. resist break or fracture) rather than maximising biofidelity. Furthermore, the impact intensities that these tests were designed to match were based on theoretical calculation instead of experimental research. Therefore, there was potential that both the ATDs and impactors were unrealistic thus reducing *BStan* evaluations to a simple dynamic materials test between a rigid impactor and anvil.

Human-on-human collisions in sport typically do not involve two rigid bodies, but instead engage two visco-elastic bodies. As such, assessing PPE performance with rigid bodies does not provide a true measure of its capacity for injury protection. Pain et al. (2008) evaluated the effectiveness of rugby shoulder pads using *BStan* methods and *in vivo* during a rugby tackle. Whilst *BStan* methods showed a reduction in peak force (35%) which was similar to that found at the bony acromioclavicular joint (40%) when a shoulder pad was used, the surrounding soft tissue did not show an appreciable change. This was significant because injuries to the region were typically to the ligaments in the shoulder and not through skeletal fracture at the shoulder. Therefore, not only does the performance variable not reflect the injury mechanism, but the anvil used did not mimic the response of the majority of the area being protected.

The validity of a PPE evaluation would be greatly improved with a higher biofidelity anvil and/or impactor to produce more realistic test conditions. While using human subjects for both the anvil and impactor is ideal, this was not always possible particularly in instances where the possibility of serious injury existed. As such, studies have often substituted the human anvil for an ATD to measure impact intensities in sport, particularly in boxing. ATDs such as water-filled punching bags (Joch et al., 1981), padded metal targets suspended as a ballistic pendulum (Atha et al., 1985), the Hybrid III head-form (Walilko et al., 2005) and punching bags instrumented with tri-axial accelerometers (Smith et al., 2000) have been impacted with a human fist. However, it was not possible to compare results across studies due to the varying stiffness and damping coefficient of the shock-absorption layer (Pedzich et al., 2006). Moreover, since none of these ATDs were validated to *in vivo* impact responses, it was unclear how well it matched human response. Only Pierce et al. (2006) managed to measure punches during competition boxing by instrumenting the gloves and headgear with the *bestshot* system™ created by SensorPad Systems, Inc. (SPS; Norristown, PA).

Unfortunately, the development of a high biofidelity surrogate has been very difficult. Hrysomallis (2009) examined the performance of thigh protectors in cricket by constructing a surrogate thigh model using an instrumented stainless steel beam and Silastic ® 3483 rubber to represent the femur and surrounding soft tissue. This rubber was chosen based on matching the decelerations obtained by combining extrapolated results from impacts on human volunteers and similar, but higher intensity, impacts conducted on cadavers. However, this was a very complicated process and was only relevant because this ATD was validated specifically for this impact condition before testing the performance of the thigh protectors. Other ATDs, such as the Hybrid III and its constituent parts, were developed from force-deflection time-histories from very specific impacts (i.e. automobile) so their validity likely did not extend to human (sporting) impacts. Therefore, unless a direct comparison between the ATD and the *in vivo* response it was meant to replicate is conducted, it will be very difficult to compare results across studies and only within study comparisons can be made.

The extra-large version of the Body Opponent Bag (*BOBXL*) is a martial arts training device which consists of a head, torso and lower mid-section (Fig 6.1). Its outer layer is made of high-strength plastisol and its cavity is filled with durable urethane foam. It was designed to mimic the shape and size of a large male martial artist while having a 'human feel' to provide the proper amount of resistance when punched, kicked or grappled. However, it was unclear whether this translated to a biomechanical response which was of high biofidelity as its biofidelity has yet to be evaluated scientifically.

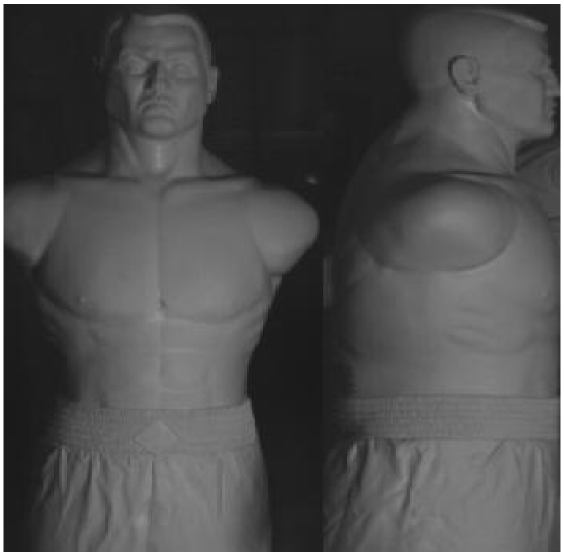

Figure 6.1 Front- and side-on view of *BOBXL*.

This chapter examines the biofidelity of *BOBXL* and determines if it can be modified to be used as a human surrogate for investigating the impact intensity of martial arts kicks. The biofidelity of subsequent modified versions of *BOBXL* are assessed by comparing their impact response to that measured *in vivo*. This provides a set of methodologies that can be easily implemented for the future pursuit of a higher biofidelity surrogate.

6.3 Pilot Testing

Prior to modification, it was necessary to determine the biofidelity of *BOBXL* in its recommended training position. The base was filled with 70 L of water and placed in the middle of a motion capture volume consisting of 11 Vicon MX cameras capturing at 250 Hz. Seven elite martial artists were each instructed to consistently perform ~ 60 kicks. Kicks were targeted to a designated area of *BOBXL*'s torso which had been instrumented with two F-Scan Tekscan sensors sampling at 500 Hz (Fig. 6.2). Opto-reflective markers were placed on *BOBXL* and the kicking leg to allow impact velocities and location to be calculated. Forces were normalised to account for differences in body mass.

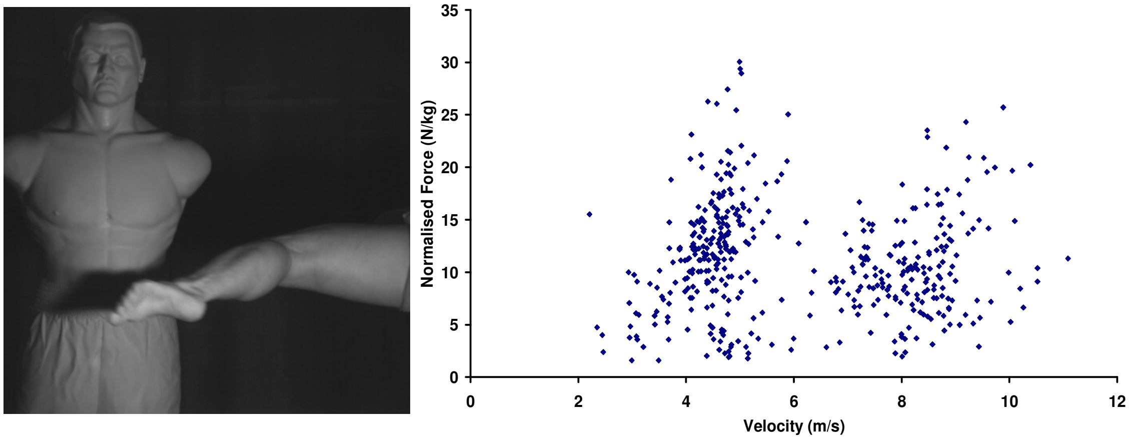

Figure 6.2. *Left:* Image taken from high-speed camera showing roundhouse kick
Right: Normalised Force-Velocity graph obtained from pilot test.

Despite normalising force, the results exhibited a large variation at all velocities. There were several issues which likely contributed to this finding:

1) *Sensor Response*: Sensors performed poorly on soft surfaces or when folded and/or creased

2) *Double impacts*: After initial contact, separation was observed between the foot and *BOBXL*. This was a result of the entire unit rocking due to an uneven base and from the high moment of force generated about the posterior edge of the base. Therefore, as the foot continued to follow through the target, a 'double impact' was produced.
3) *Sampling Frequency*: 500 Hz was likely too low to accurately capture the impact force, especially with the issue of multiplexing discussed in § 2.2.2
4) *Surface Stiffness*: response of surface material was visco-elastic with higher stiffness' at lower velocities. Local surface stiffness for *BOBXL* was higher than human surface stiffness. This difference in energy dissipative properties was likely the cause of the stinging feeling experienced when impacting *BOBXL*.

It was expected that impact force was related to impact velocity, but this relationship was not found in this pilot test. Whilst it was possible that a relationship may not actually exist, these model limitations did not allow a proper conclusion to be made. As such, modifications were proposed to address these issues and are discussed further in § 6.4.2.

6.4 Methods

6.4.1 Trial Protocol

Four male martial artists (31.2 yrs, height: 1.75 m, m: 80.2 kg, black belts), labelled S1 through to S4, were recruited for this study. Each provided consent in accordance with the Loughborough University Ethical Advisory Committee. Prior to data collection, each player performed a self-selected warm-up.

Impacts were produced using front-leg roundhouse kicks and the biomechanical response was measured using two separate anvil conditions: *in vivo* and custom ATDs (Table 6.1). The *in vivo* anvil condition used the abdominal region of an experienced and willing martial artist (S1), who was either padded or unpadded. Two martial artists (S3 and S4) were chosen to perform these impacts because of their extensive experience in sparring with S1. Each performed three set of kicks directly onto the unprotected abdomen of S1 (i.e. "*No Pad*"), whilst S3 also struck the protected abdomen (i.e. "*Pad*"). In each set (consisting of 5 or 6 kicks), players were instructed to increase the intensity of their kicks within and across each trial. That is, within a set, the intensity of the last kick was higher than the first and the first kick of set 2 was higher than the first kick of set 1.

Custom ATD impacts consisted of 10-15 kicks performed by all four players onto three different surrogate anvils. Each anvil (or model) was a modified version of *BOBXL* and is explained in § 6.4.3.

Table 6.1 Breakdown of conditions with anvils and impactors defined.

PART	CONDITION	ANVIL	IMPACTOR(S)
1	*In vivo*	S1	S3, S4
2	Custom ATDs	*BOBXL w/ Hogu*	S3
		BOBXL w/o Hogu	S3
		MBOBXL	S1, S2,S3,S4

Nine Vicon MX cameras were strategically positioned to capture up to eighteen opto-reflective markers in a single trial – eleven on the kicking leg, four on the hogu and three on the wall behind the ATD anvils (Fig 6.3).

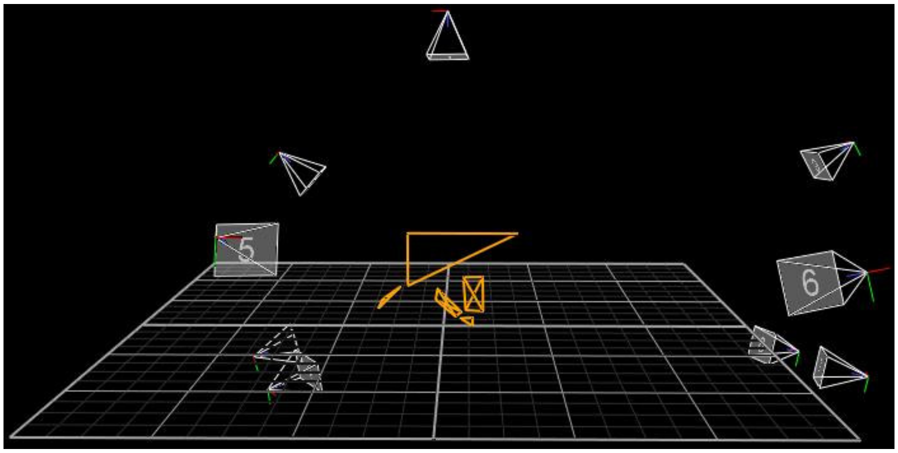

Figure 6.3 Nine camera Vicon MX system used to track 15 opto-reflective markers.

These markers were used to determine leg kinematics, impact velocity and impact location relative to the anvil surface (*Appendix D*). Surface impact forces, transmitted forces, contact times (CT) and times to peak force (TTPF) were measured with the Tekscan F-Scan sensors at 500 Hz and the CFP at 1000 Hz, respectively. The CFP was strapped to the torso of *BOBXL* while the force sensors were affixed to the outer face of the hogu using double-sided tape and electrical tape on its edges. In trials in which a hogu was not worn, force sensors were attached directly to the surface of *BOBXL* or onto a t-shirt worn by S1 resting over the abdominal region. Each system was calibrated using the methods outlined in § 4.

For clarity, *in vivo* impacts were identified by the impactor (either S3 or S4) and by the presence of padding on S1. For example, *S3, No Pad* referred to an impact delivered by S3 whilst S1 was unprotected. Meanwhile, custom ATD anvils were identified based on their modifications (*see* § 6.4.3).

6.4.2 Assessing Biofidelity

To determine the biofidelity of each surrogate anvil, impact responses from each custom ATD model were compared to impact responses from *in vivo* anvil trials. All impact forces were obtained using Tekscan sensors, its data was adjusted (*see* § 4.2.2) and normalised using each individual player's body mass. Normalised impact forces within each customised ATD condition were plotted as a function of impact velocity. A non-linear regression curve was fit to each set of data points and its equation and calculated R^2 value were provided. This produced an equation for each custom ATD model which could be used to predict the results from *in vivo* trials. The impact velocity measured for each *in vivo* impact was input into each of the three custom ATD models to obtain three separate predictions for normalised impact force. The effectiveness of each model (i.e. equation) for predicting the actual *in vivo* force was analysed in three ways. The first method calculated the root mean square error (RMSE) between model prediction and actual performance using equation 6.1.

$$\mathrm{RMSE}_{\mathrm{y}} = \sqrt{\frac{\sum_{i=1} \left(f(x_i) - y_i\right)^2}{n}} \tag{6.1}$$

The second method calculated the residuals (i.e. differences) between the model predictions and its actual value. A student's t-test conducted between the residuals of each model for the custom ATD condition determined which model was significantly better at minimising the differences between actual and predicted performance. For example, a t-test was conducted for the residuals of models 1 and 2, 1 and 3, and 2 and 3 for the *S3, No Pad* condition. The model which generated the lowest RMSE and average residual (particularly if significant) was considered to have the highest biofidelity.

The final method compared the confidence intervals (CIs) derived from each set of *in vivo* performance to each custom ATD model. Each set of *in vivo* performances was individually plotted and a non-linear regression curve was fit to each data set. Upper and lower bounds for the 95% CI were calculated using its regression equation and equations 6.2 through 6.4.

$$CI = t_{n-2} * SE_{y,x} * \sqrt{\frac{1}{n} + \frac{\left(x_i - \bar{x}\right)^2}{SS_x}} \tag{6.2}$$

$$SE_{y,x} = \sqrt{\frac{1}{(n-2)}\left[\sum\left(y - \bar{y}\right)^2 - \frac{\left[\sum\left(x - \bar{x}\right)\left(y - \bar{y}\right)\right]^2}{\sum\left(x - \bar{x}\right)^2}\right]} \tag{6.3}$$

$$SS_x = \sum\left(x_i - x\right)^2 \tag{6.4}$$

The custom ATD model which best fit the 95% CIs, for each set of *in vivo* kicks, provided support for the biofidelity of that particular model.

In addition to analysing the ‘impact force – impact velocity’ relationship, average CTs and TTPFs were calculated for each condition in the customised ATD impacts and compared to the results obtained from *in vivo* testing using a student’s t-test. As there were three comparisons for both CT and TTPF, a Bonferroni correction was used to ensure that a Type I error would not be made when comparing between groups. For all t-tests, significance was set at α = 0.05.

6.4.3 Customised ATD Impacts

To develop a higher biofidelity ATD, two modifications were implemented to BOBXL to create three custom ATD impact models. These modifications were:

Modification 1: The polyethylene base was set flush against the wall with high-density foam placed behind the torso to restrict the rocking movement. This created two anvils: *BOB w/ Hogu* (Model 1) and *BOB w/o Hogu* (Model 2).

Modification 2: The CFP was fixed to the torso of BOBXL so that when the adidas hogu was placed overtop, it provided a stiffer surface for the Tekscan sensor contact upon impact (Fig 6.4). The corners of the CFP were cushioned with high-density foam. This anvil was identified as *MBOBXL* (Model 3).

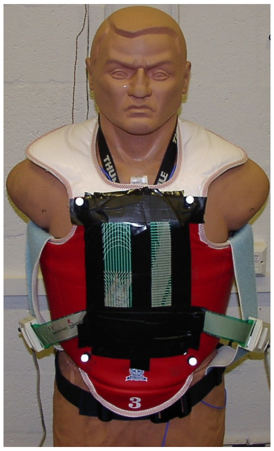

Figure 6.4 MBOBXL made from BOBXL with CFP, hogu and Tekscan sensors.

6.4.4 Impact Velocity

Foot velocity was measured by calculating the change in distance between the mid-point of the two toe markers (i.e. MTPJC) between successive frames in a local co-ordinate system (LCS). The LCS was created from three markers on the wall directly behind the customised ATD anvils and was orientated such that the z-axis was perpendicular to the surface of each anvil and parallel to the direction of the foot just prior to impact (similar to the process described in *Appendix E*). The transformation matrix required to convert the global co-ordinate system (GCS) to the LCS was used to transform the coordinates of the MTPJC into the LCS. This allowed changes in MTPJC location between frames in the LCS to be calculated and thus, instantaneous velocity to be calculated. Impact was identified using the frame in which any of the markers on each of the custom ATDs deviated from its stationary position. The instantaneous velocity before this marker movement was selected as the impact velocity. *MBOBXL* markers were not used to create the LCS because of their movement within and between trials.

6.5 Results

For each impact condition, mean impact forces and its overall range were summarised along with the corresponding range in impact velocities (Table 6.2). Whilst differences in impact intensities were found, the impact forces from each set of impacts were normalised to each player's body mass to more relevantly compare results. When collecting the kinematic data for each impactor, the mean average residuals were for the Vicon MX cameras were 0.142, 0.142, 0.115 and 0.189 (all units in pixels) for athletes 1 through 4, respectively.

Table 6.2 Summary of force and velocities for *in vivo* trials (condition 1) and customised ATD trials (condition 2).

Trial	Force (N)				Mean Velocity (ms^{-1})	
	Mean	S.D.	Min	Max	Min	Max
Condition 1: *in vivo*						
S3, No Pad	1158	358	414	1763	6.11	14.29
S3, Pad	988	396	112	1696	7.18	14.34
S4, No Pad	1087	435	304	1669	4.1	12.53
Condition 2: Custom ATDs						
BOB w/ Hogu	670	184	389	870	9.63	13.16
BOB w/o Hogu	766	316	321	1201	10.08	12.33
MBOBXL	1256	356	703	2235	9.49	13.55

For each custom ATD trial within condition 2, normalised forces from each set of kicks were individually plotted as a function of impact velocity. A regression curve was fit to each set of impact responses to produce three unique predictor models (Fig 6.5, *top*). These exact same regression curves were re-plotted and each impact from the *in vivo* condition was overlaid (Fig 6.5, *bottom*) with *in vivo* impacts separated for both "*No Pad*" trials and the single "*Pad*" trial. The regression equations for each predictor model are shown in Table 6.3 along with their calculated R^2 values. This table also displays calculated RMSE values obtained from comparing each custom ATD model to each set of *in vivo* impacts. RMSE values indicated how well each model could be used to predict the performance of *in vivo* impacts. Of the three custom ATD models, the lowest RMSE scored across all *in vivo* trials was model *MBOBXL*, despite having a low-strength R^2 value. Furthermore, all models were closest to predicting the *S3, Pad* trial as its RMSE values were the lowest among all trial types with respect to condition 1.

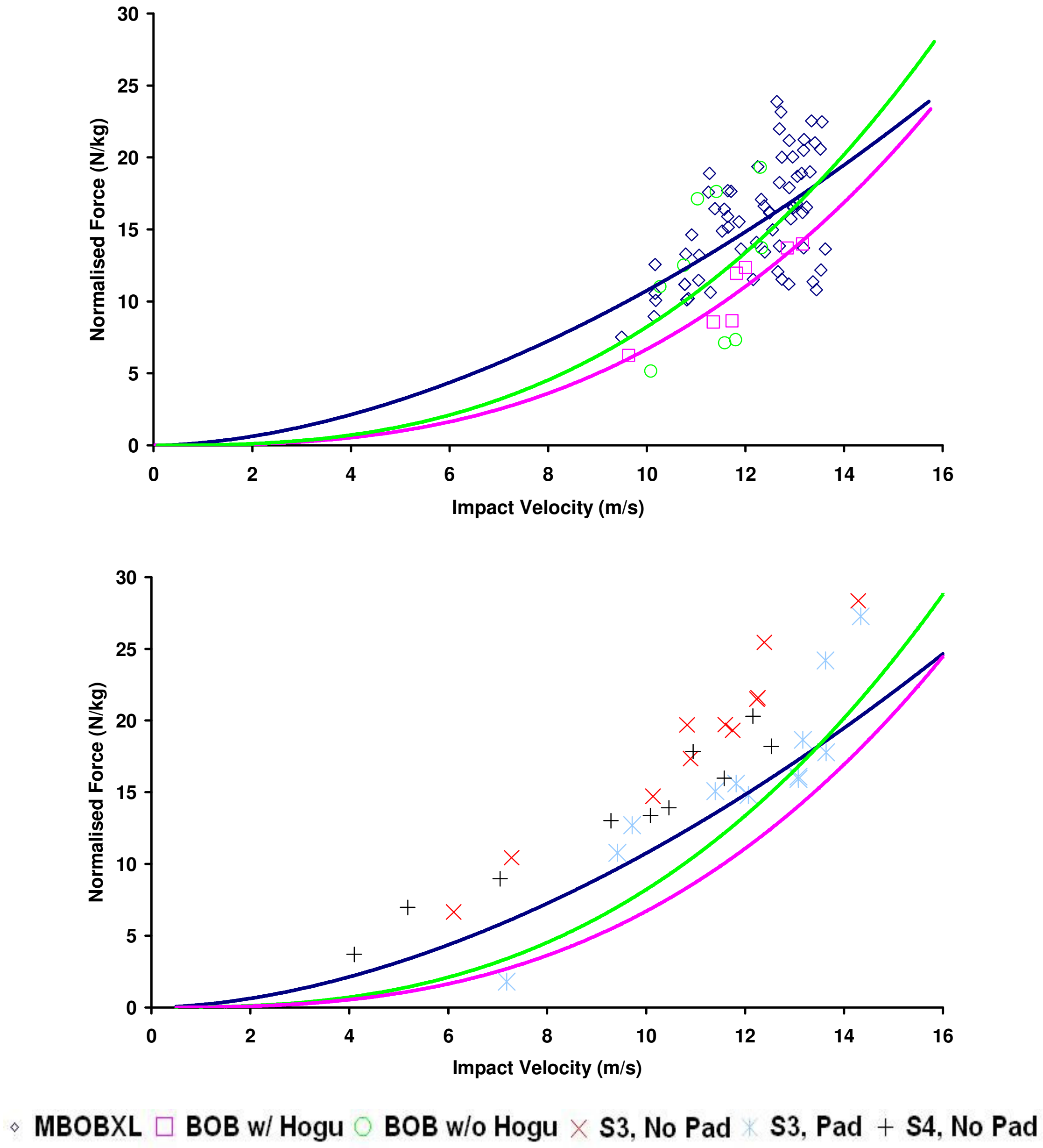

Figure 6.5 *Top:* Each roundhouse kick plotted for each condition to obtain regression lines. *Bottom:* Using regression lines from *top* to compare with *in vivo* impacts.

Table 6.3 Results for each surrogate with their regression line, R^2 value and RMSE values.

Model	Regression Equation	R-Squared	RMSE Values		
			S3, No Pad	***S3, Pad***	***S4, No Pad***
BOB w/ Hogu	$y = 0.01x^{2.76}$	0.87	9.54	3.31	5.29
BOB w/o Hogu	$y = 0.02x^{2.67}$	0.18	7.54	5.19	6.75
MBOBXL	$y = 0.18x^{1.77}$	0.36	6.10	3.08	3.35

The bottom graph in Fig 6.5 was also used to determine the residual; i.e. the average difference between model prediction and *in* vivo performance. All residuals indicated that each predictor model underestimated the impact forces obtained from *in vivo* trials (Table 6.4). Overall, the smallest residuals (in magnitude) were found using model *MBOBXL*, particularly when compared to the *S3, Pad* trial. This model was significantly better than model *BOB w/o Hogu* but not when compared to model *BOB w/ Hogu* for predicting all *in vivo* trials. The worst was model *BOB w/o Hogu* – its residuals magnitude was greatest, despite not being significantly worse than *BOB w/ Hogu*. Each customised ATD predictor model performed best when compared to the *S3, Pad* as each of these models had the smallest overall residual amongst all *in vivo* trials.

Table 6.4 Residuals (± SD) for each comparison between customised ATD and *in vivo* impacts; '-' indicated that the *in vivo* impacts were underestimated.

	in vivo **impacts**		
Customised ATD impacts	***S3, No Pad***	***S3, Pad***	***S4, No Pad***
BOB w/o Hogu	-9.31 ± 2.07	-4.39 ± 2.89	-6.55 ± 1.72
BOB w/ Hogu	-7.37 ± 1.60	-2.08 ± 2.69	-5.10 ± 1.46
MBOBXL	-5.76 ± 2.03*	-1.03 ± 3.03*	-3.12 ± 1.28*

* significance found between MBOBXL and all BOB w/o Hogu impacts at α = 0.05

The third evaluation method used each set of *in vivo* impacts to create three separate 95% confidence intervals (95% CIs). Each individual 95% CI was plotted (solid line) with each regression curve from the three predictor models (dashed lines) in Fig 6.6. All customised ATD models performed poorly when compared to the 95% CIs obtained from both padded *in vivo* trials (*S3, No Pad* and *S4, No Pad*). Similar to the measured residuals, each model was found to underestimate these two 95% CIs, particularly at velocities above ~ 4 m/s. The shapes of the models were also different to the shape of the 95% CIs that they were compared against. In contrast, the 95% CI of *S3, Pad* was able to capture the magnitude of all three predictor models at impact velocities below ~ 12.5 m/s, though the overall shape of the curves were still slightly different.

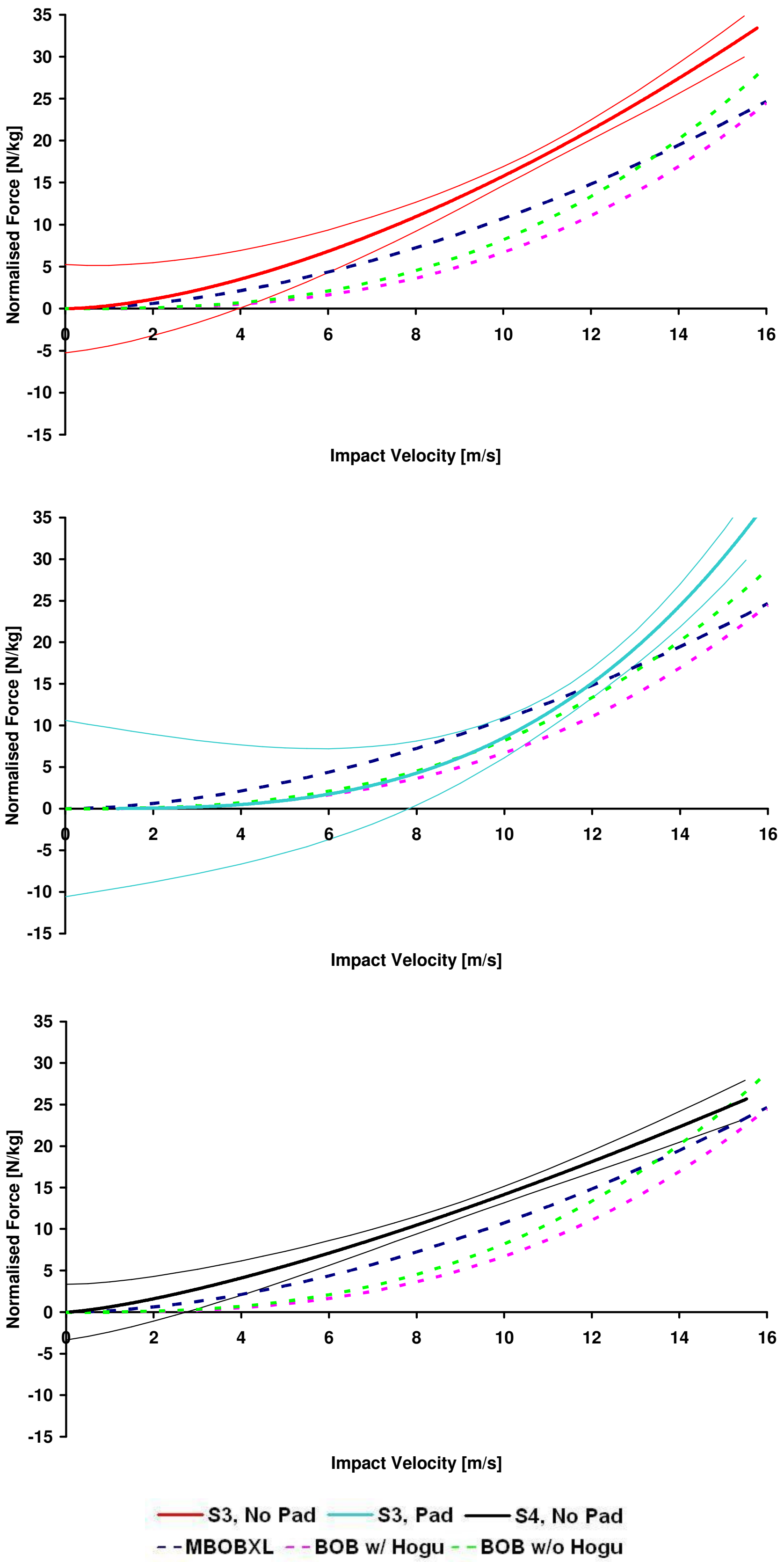

Figure 6.6 Confidence intervals for each *in vivo* trial with customised ATD impacts overlaid. From Top-Bottom: a) *S3, No Pad*; b) *S3, Pad*; c) *S4, No Pad*.

In both impact conditions, *in vivo* and customised ATDs, the highest average CTs occurred when hogus were not worn by either the human anvil or custom ATD (Table 6.5). Both *S3, No Pad* and *S4, No Pad* conditions not only had significantly higher CTs than the *S3, Pad* impacts, but were also significantly greater than models *BOB w/ Hogu* and *MBOBXL*. A comparison of the three custom ATD models did not reveal a significant difference.

Table 6.5 P-values (* denotes significance) for CT comparing custom ATD impacts to in vivo impacts with α = 0.05 (using Bonferroni Correction). CT reported as mean ± SD.

CONTACT TIMES (CT)				
	Actual	***S3, No Pad***	***S3, Pad***	***S4, No Pad***
Model	**Average ± SD**	47.4 ± 6.8	40.5 ± 9.4	49.2 ± 8.8
BOB w/Hogu	39.7 ± 3.1	0.01*	0.79	<0.001*
BOB w/o Hogu	42.9 ± 5.8	0.13	0.48	0.2
MBOBXL	40.3 ± 4.7	0.01*	0.96	<0.001*

In vivo conditions revealed that TTPF was significantly higher when the human anvil was unpadded, but was significantly lower than models *BOB w/ Hogu* and *BOB w/o Hogu* (Table 6.6). These two custom ATD models produced significantly higher TTPFs when compared to all *in vivo* impacts, whilst *MBOBXL* produced significantly lower TTPFs when compared to both unpadded *in vivo* trials. A significant difference in TTPF was not found between *MBOBXL* and the *S3, Pad* trial (p = 0.04).

Table 6.6 P-values (* denotes significance) for TTPF comparing custom ATD impacts to *in vivo* impacts with α = 0.05 (using Bonferroni Correction). TTPFs reported as mean ± SD.

TIMES TO PEAK FORCE (TTPF)				
	Actual	***S3, No Pad***	***S3, Pad***	***S4, No Pad***
Model	**Average ± SD**	8.4 ± 1.1	5.7 ± 1.4	8.8 ± 1.9
BOB w/Hogu	14.3 ± 1.8	0.00*	0.00*	0.00*
BOB w/o Hogu	14.7 ± 3.0	0.00*	0.00*	0.00*
MBOBXL	4.7 ± 1.0	0.00*	0.04	0.00*

A sample calculation for the RMSE and residual are shown in *Appendix F* along with the process used to create the 95% CIs.

.

6.6 Discussion

Previous studies have used sport-specific training devices to determine impact intensities or injury risk in impact sports, but very few, if any, have validated their surrogate by comparing it to human performance. Whilst it would be ideal to create a specific surrogate, such as Hrysomallis (2009), this was a costly process and still relied heavily upon assumptions such as the extrapolation of data. Instead, this chapter used a pilot study to help construct three ATD models which were modified versions of a martial arts training device, *BOBXL*. The performances of these models were compared to the human impact response using three separate evaluative measures. Of the three custom ATD models, *MBOBXL* was found to be the surrogate with the highest biofidelity for impact testing of roundhouse kicks. While this was categorically different than claiming full biofidelity for this anvil, further examination of its impact characteristics provided support there may be certain impact conditions for which this full biofidelity may apply.

MBOBXL impacts were found to have the lowest RMSE value when compared to each *in vivo* impact trial and its average residual was lower than the other two models at, or close to, significance. Since both of these variables were measures of how well the model estimated actual data, it provided evidence that this model had the highest biofidelity. While it may be argued that the RMSE and residual had very little physical meaning – especially since an acceptable tolerance level was not defined – the residual for *MBOBX*L was found to be within the variability of the *S3, Pad* data as shown in its 95% CI (Fig 6.6). This suggested that this particular model, *MBOBXL*, and this specific *in vivo* trial, *S3, Pad*, exhibited the most similar impact response. In addition to the force-velocity relationship, CTs and TTPFs were also not significantly different when comparing the impacts of *MBOBXL* and *S3, Pad*. Therefore, with similar impact forces, CT and TTPF, the overall impact energy measured in both conditions was also quite similar. As discussed in § 5, impact energy was more likely to be an indicator for injury than just force alone. As such, it was reasonable to assume that not only was the biofidelity of *MBOBXL* high, but that it could also be a good predictor of impact injury as a result of a roundhouse kick.

The 95% CIs were not only able to help support the biofidelity of *MBOBXL*, but may have also provided insight into the materials and impact properties of *BOBXL*. Each of the three predictor models underestimated the impact response of the two unpadded *in vivo* trials at velocities greater than ~ 4 m/s. This would be expected for both padded ATD models (*BOB w/ Hogu* and *MBOBXL*) as the hogus would act to reduce the acceleration of the foot at impact and spread a percentage of the load over a larger area. However, this also occurred for the unpadded ATD model, *BOB w/o Hogu*, suggesting that the dynamic impact stiffness of an unpadded *S1*, a human anvil, was much higher. As such, it was possible that a systematic or proportional difference existed between *the in vivo* and *BOB w/o Hogu* impacts. It is postulated that this increased stiffness may be similar to that found between a relaxed and tensed impact. In § 5, tensed muscle was shown to increase impact force by a factor of 1.11. Comparing the unpadded and padded *in vivo* trials to *BOB w/o Hogu* and *BOB w/ Hogu* trials, respectively, a slightly higher result was obtained (1.48). This suggested that part of the difference between ATD and in vivo impacts was attributed to *BOBXL* being more closely modelled to a relaxed human. It was also likely that the surface stiffness of *BOBXL*'s outer layer, high-strength plastisol, helped dissipate impact energy contributing to a lower impact force. Conversely, the impact response of *MBOBXL* matched the performance of the padded *in vivo* trials more closely (only a factor of 1.03 greater). If the impactor-hogu-anvil impact interaction was considered to be a system (in series) and the impact characteristics were similar for two different anvils, it was likely that the contributions of elastic, viscous and inertial forces were also similar meaning that this force was not achieved artificially (Kent et al., 2006). As such, it could be properly assumed that the two anvils were close enough to be interchangeable. It was expected that with the addition of the CFP, the increase in stiffness was akin to accounting for muscle tension to properly model human impact response.

While all three models underestimated actual performance in the unpadded *in vivo* trials, this did not occur in the padded condition. In fact, the 95% CI of *S3, Pad* was able to capture the predictions of all models suggesting that all were a good fit particularly *BOB w/o Hogu* which appeared to be an almost perfect match. This was counterintuitive as this would suggest that the *BOB w/o Hogu* could be used to model a padded human impact. Instead, this was more likely due to chance as the R^2 value for the regression curve was low (0.18) whilst RMSE and residuals were not the lowest compared to the other models. It was more likely that the adidas hogu was very effective at reducing peak forces in all padded conditions. This was observed when comparing padded and unpadded conditions within both *in vivo* and custom ATD impacts and thus it seemed coincidental that the impact forces from a padded *in vivo* impact matched the performance of an unpadded ATD.

This validation was based on the possible relationship between impact force and impact velocity. From Table 6.3, the explained variance for model *MBOBXL* was $R^2 = 0.36$ suggesting a relatively weak relationship between the two variables. However, this only proposed that the specific curve used to relate the variables was weak, not that the force-velocity relationship did not exist at all. In fact, if the impact profiles of each generated curve from each surrogate were examined, each showed a trend towards increased force with increased velocity. For objects in free-fall, this made sense – higher velocities resulted in higher peak decelerations at impact and, thus, higher forces. For human impacts, such as kicks, this was not as precise. If the leg were to swing freely just prior to impact, it was likely that this relationship would hold. However, if there was any hamstring activation prior to impact, this would actively begin to decelerate the foot leading to a decreased peak deceleration and contact time without significantly affecting the impact velocity. Conversely, if there was active quadriceps contraction during contact, this would have increased the peak deceleration and contact time also without affecting the impact velocity. In this study though, the players were asked to kick consistently so any affect of hamstring or quadriceps activation would have been present in every trial, thus leaving the general trend similar. The affect of muscle activation on the force-velocity relationship will be more thoroughly examined in a following section (§ 8).

The range of measured impact forces and impact velocities was shown in Table 6.2 to compare these impact intensities to those measured in other impact conditions reported in § 3. Condition 1, the *in vivo* impacts, had a force range of 112 – 1763 N at velocities between 4.1 – 14.34 ms^{-1} and condition 2, the custom ATD impacts, had a range of 321 – 2235 N at 9.49 – 13.55 ms^{-1}. Whilst the maximum velocities for both conditions were similar, these were on the low end of those reported within the literature (Table 3.17). The range in velocities for *in vivo* impacts was much greater which reflected one of the disadvantages of the *in vivo* condition as the number of impacts at high velocities had to be controlled to avoid subjective and reversible injury from occurring. Forces for both conditions were also found to be lower than reported for similar studies, though *in vivo* impact forces compared favourably to other studies which had used human volunteers (Table 3.16). Conversely, the low impact forces measured in the ATD impacts were likely a result of its dynamic impact properties as this was postulated to be a major influence on impact force (Falco et al., 2009). However, this only further highlighted the importance of a validated ATD. To help minimise systematic variation, all impact forces were normalised to each player's body mass. This had been shown to influence impact forces in roundhouse kicks (Pedzich et al., 2006).

MBOBXL was validated for the roundhouse kick, or Bandal Chagui, because it was found to be the most frequently used technique in Taekwondo (Lee, 1983). While there are other forms of attack, the roundhouse made up 50% of all attacks accounting for 89% of all points scored (Lee, 1988; as cited in Kim, unpublished masters). Furthermore, the roundhouse kick has been extensively researched in terms of technique (Hwang, 1987; Boey & Xie, 2002; Kim & Hinrichs, 2006; Tang et al., 2007; Nien et al., 2007), execution time (Tsai et al., 1999; Falco et al., 2009), impact force (Pedzich et al., 2006; O'Sullivan et al., 2007), and injury potential (Serina & Lieu, 1999; Chuang & Lieu, 1992) As such, it was logical to focus future research into this type of attack, particularly when analysing the performance of hogus in response to the roundhouse kick.

In all trials, impact forces were measured with the Tekscan F-Scan sensors. In spite of the issues discussed in § 4, this was the only method of obtaining *in vivo* impact forces. Whilst the CFP was capable of much more accurate readings in model *MBOBXL*, the forces were still taken from the Tekscan sensors for consistency between trials as the CFP was not present in every condition. It was also hoped that any issues with sampling frequency and multiplexing would be consistent between models and the errors would be consistent throughout all trials. Therefore, while the magnitude of the forces may not be exact, the relationship between *in vivo* and custom ATD impacts would still remain and the measures of CT and TTPF would still be legitimate.

6.7 Conclusion

Previous studies have used biomechanical surrogates to measure impact intensities observed within a given sport, but very few have taken the necessary steps to ensure their biofidelity. As such, values obtained from different studies could not be compared and were only valid for their specific set-up. To address this issue, this chapter presented a simple methodology which could be adopted by future studies. This methodology was shown to provide an objective comparison between biomechanical surrogates and the *in vivo* impact responses they attempted to mimic. More specifically, the *MBOBXL* model performed comparably to padded *in vivo* impacts and will be used as a surrogate for measuring the performance of TKD chest protectors, impact intensities in TKD and variations in kick execution in future sections.

Chapter 7

Evaluation of Hogu Performance

7.1 Chapter Overview

The functionality and design of chest protectors (i.e. hogus) are first discussed and existing performance requirements are introduced. Four commercially available hogus were tested with two separate anvils and two different impactor types to determine their influence on impact-protection performance. Individual hogu performances were found to be sensitive to both changes in anvil and impactor and the implications of this result were discussed.

7.2 Introduction

Since 1995, the World Taekwondo Federation (WTF) has regulated the use of sports PPE, particularly chest protection (i.e. hogus), during competition. Its intent was to reduce injuries and, as a result, introduce the sport into the 2000 Olympics. Its functionality as a protective garment, though, has never been properly assessed. This was likely due to the low incidences of chest injury whilst wearing a hogu during competition (§ 3.2.3). As such, there has not been a reason to doubt their effectiveness. However, in terms of performance, its overall design has come under scrutiny as it has been regarded as bulky and cumbersome. While it would be simple to reduce the weight of the existing material, either by volume or density, the trade-off between protection and performance would be unknown. Therefore, it has become increasingly necessary to scrutinize the existing methods of assessing hogu performance and introduce modifications to its technique to ensure its relevance.

The designs of all commercially available hogus are fundamentally the same. The outer material of each is a soft vinyl shell that wraps around the front and sides of the torso while the top of the shoulders are covered with two flaps that circle around the neck. The protection offered by each hogu is then a function of the type and density of the foam inserted within the shell. As such, hogus ranged from light (i.e. kwon) to heavy and bulky (i.e. adidas Electronic Body Protector or adidas EBP). However, an indication of which hogu offered the most protection does not exist, despite most being WTF-recognised. This is crucial as some competitors may be under-protected, while others may be restricting their range of motion unnecessarily. A summary of commercially available hogus is shown in Table 7.1. All are similarly priced except for the three automated scoring systems (adidas EBP, LaJust EIDSS and Daedo TK-Strike) which have been found to cost in excess of £300.

Table 7.1 Summary of commercially available hogus.

Hogu	**Insert Materials**	**Mass (kg)**
adidas	Rubber foam layer and strong sponge	0.90
daedo	Strong sponge	0.78
macho	Durable, high-density EVA foam	0.84
kwon	unpublished	0.66
adidas Electronic Body Protector (adidas EBP)	Consists of an inlay and sensor unit foam lined with air tubes to measure scoring **Inlay:** vulcanized PP/EPDM **Sensor Unit:** ABS (acrylonitrilebutadiene styrene) **Tubing:** FKM (fluorinated elastomer)	1.83
LaJust Electronic Impact Detection & Scoring System (EIDSS)	**Shock absorbing pad**: EVA (Ethylene Vinyl Acetate Copolymer **Surface:** vinyl or urethane-coated	-
Daedo TK-Strike Electronic Protector System	unpublished	1.5*

* all hogus were personally weighed, except for the Daedo TK-Strike

British Standards (*BStan*) requires that the impact-mitigating performance of each hogu is tested using a rigid impactor while measuring the force transmitted to the rigid anvil that the hogu is strapped to. Hogus are deemed adequate for competition if they can reduce the force transmitted to the rigid anvil such that it is less than 3 kN when subjected to an impact energy of 12 J. However, as Pain et al. (2008) discussed, this is not an accurate indicator of PPE performance. This is merely just a repeatable dynamic materials test which fails to consider the entire system in-series; that is, the performance of its insert materials depend on the impact properties of the anvil and impactor. Moreover, as separate anvils are not used to model the thorax and abdomen, it is unlikely that the impact properties of the anvil are accurate. In addition, the actual impact characteristics (e.g. impact velocity, contact area, etc) observed within TKD and the injury mechanisms (e.g. deformation) involved in potential chest injury are not considered. As such, the validity of *BStan* as a tool for assessing hogu performance is unclear.

Previous research in automobile, ballistics and sports impacts provided insight into the necessary protection performance characteristics required for each hogu as summarized in § 2 and § 3. As discussed, *BStan* requires the hogu to mitigate impact forces below 3 kN to be approved for competition. Compared to impact forces to the thorax and abdomen, this seemed reasonable as injuries had not been reported at or below this threshold. The velocity (3.1 ms^{-1}) of *BStan* impacts though, was much lower than those found in TKD kicks (13.9 – 18.0 ms^{-1}, though Tsai et al. (1999) reported velocities at 6.4 ms^{-1}). As such, it is unclear whether hogus will perform adequately with a change in loading rate. In addition, *BStan* does not specify parameters for viscous criterion (VC) or compression (C) of the anvil – both of which have been shown to be good indicators of injury at these velocities. It also does not discern between the differences in impact response between the thorax and abdomen. Examination of biomechanical response has revealed that the abdomen is considerably less stiff than the thorax and the onset of injury in each region has also been found to be different. In general, the threshold for irreversible injuries to the thorax occur at VC = 1.0 ms^{-1} and C = 34 %, and in the abdomen at VC = 1.4 ms^{-1} and C = 48 %. Since VC and C are difficult parameters to measure without the use of highly sophisticated ATDs, this study will focus only on the impact force response.

This section examines the influence of the anvil and impactor on hogu performance. It compares several different combinations of anvil and impactor including the traditional *BStan* method and moves towards evaluations that attempt to re-create competition-style impacts. It is hoped that the results from this research can be used to develop a more accurate and relevant method for the future evaluation of hogu performance.

7.3 Methods

7.3.1 Introduction

Four different hogus were tested with ten impacts delivered within each of three methods: *British Standards, Modified British Standards* and *Competition*. Three hogus were commercially available (adidas, kwon, adidas EBP) whilst the fourth was made by filling the soft vinyl shell of the adidas EBP with blue CF45 Confor foam (Fig 7.1). This Confor foam (Table 7.2) was cut into the same shape as the adidas EBP insert and the new hogu weighed 1.02 kg. In all methods, hogu surface forces were measured using Tekscan sensors at 500 Hz and each sensor was calibrated according to the procedure outlined in § 4. The three hogu evaluation methods are outlined below.

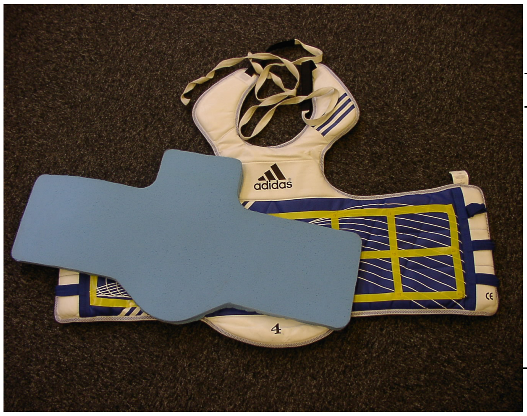

Table 7.2 Confor foam material properties.

Parameter	Test	Value
Density	ASTM D3574	93 kgm^{-3}
Thermal Conductivity	ASTM C177	0.04 Wkm^{-1}
Tensile Strength	ASTM D3574	125 kPa
Tear Strength	ASTM D3574	0.6 kN/m
Elongation	ASTM D3574	109%

Figure 7.1 Blue confor foam CF45 insert with adidas EBP shell.

7.3.2 Method 1: British Standards (BStan)

This test reproduced the method outlined by British Standards (*BStan*), BS EN 13277-1/2/3 (2000). Each hogu was placed on top of a Kistler force plate (*see § 4.1*), sampling at 1000 Hz, to measure the force transmitted through the hogu. A 2.72-kg shot put was dropped from 0.45 m to deliver 12 J of impact energy. The shot was modified to include a ring which attached to a custom electromagnetic dropping system (Fig 7.2). When triggered, the shot put would drop vertically onto the hogu. The overall set-up for this method is shown in Fig 7.3.

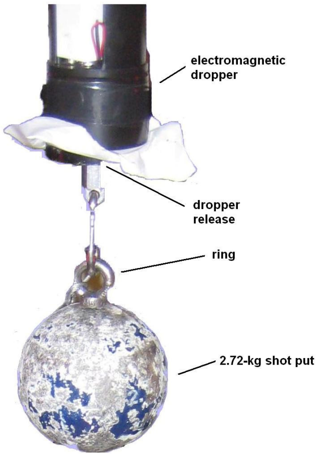

Figure 7.2 Diagram of electromagnetic dropper holding shot put before release.

7.3.3 Method 2: Modified British Standards (MBS)

Modified British Standards (*MBS*) tests altered *BStan* tests by evaluating the hogu on *MBOBXL*, the high biofidelity surrogate developed in § 6, instead of using a rigid anvil. Moreover, transmitted force was measured using the CFP at 1000 Hz collected by Vicon Nexus software and calibrated according to the procedure outlined in § 4. Similar to *BStan* tests, the shot put was released from 0.45 m above the hogu to produce 12 J of impact energy and the duration between impacts was set to 60 seconds. This set-up is also shown in Fig 7.3 (*middle*).

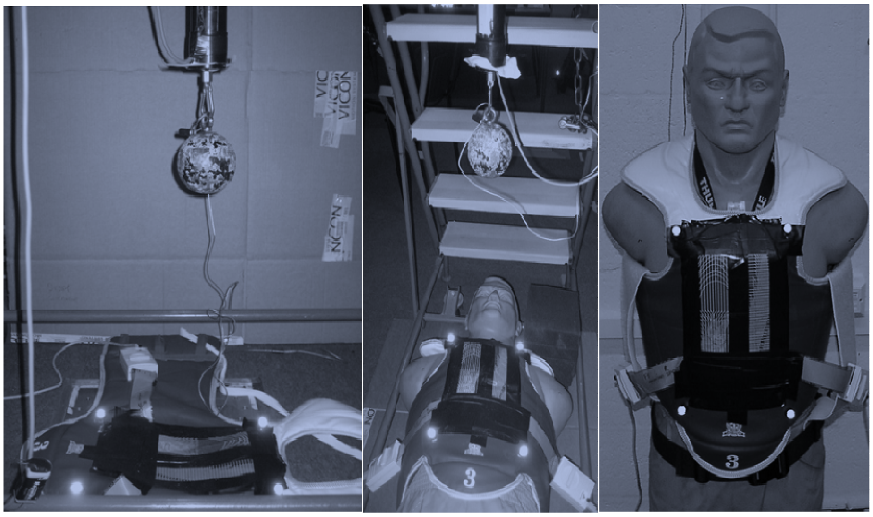

Figure 7.3 Set-up for each hogu evaluation method (*left to right*): *British Standards, Modified British Standards* and *Competition*.

7.3.4 Method 3: Competition

The *Competition* method changed the impactor from the rigid shot put to two elite martial artists (Table 7.3), each of whom performed front roundhouse kicks onto *MBOBXL*, the high biofidelity surrogate validated in § 6. Nine Vicon MX cameras were positioned to track the position of 5 opto-reflective markers placed on the kicking foot and 4 on the hogu at 250 Hz. Vicon Nexus software collected marker position data whilst simultaneously collecting transmitted force data via the CFP at 1000 Hz. Vicon cameras and the CFP were calibrated according to § 4 with residuals for all Vicon cameras also shown in Table 7.3. Foot markers were used to calculated impact velocity whilst the hogu markers provided information about the instant of impact and impact location (*Appendix E*). These calculations were identical to those performed in § 6. In total, each hogu was impacted with 10 to 15 kicks.

Table 7.3 Summary of both athletes (i.e. impactors).

Athlete	Age	Height	Mass	Mean Vicon Residual (pixels)
1	25	1.83	78.1	0.1423
2	37	1.75	94.5	0.1423

7.3.5 Analysis

A repeated-measures ANOVA was conducted for methods 1 and 2 to compare mean impact values across hogus using the force obtained from the Kistler plate and the CFP. A post-hoc analysis was used to reveal any differences between hogus. All statistics were computed using SPSS v17 software and significance set at $\alpha = 0.05$. This statistical analysis was not conducted in the *Competition* method because of the varying levels of velocity. Instead, the magnitudes of force were only compared within subject to determine trends in hogu performance and to examine whether these trends were similar to those found in the first two methods.

7.4 Results

7.4.1 Method 1: BStan

Of the four hogus tested, only the kwon failed to pass *BStan* tests as its average impact force exceeded the 3 kN threshold and it failed in all but one of its trials (Fig 7.4). Both the adidas EBP and confor hogus were able to comfortably reduce the peak force and the average transmitted force was significantly lower than the average surface force. The adidas hogu was close to failure (mean = 2.78 kN), but did not have a single trial in which the transmitted force exceeded the threshold. Both the adidas and kwon hogus had higher transmitted forces than surface forces.

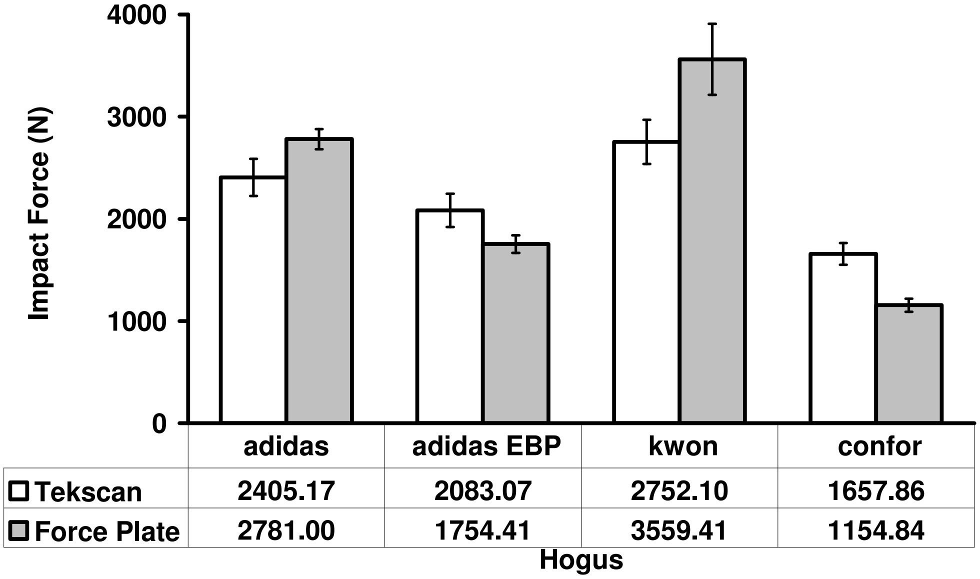

	adidas	adidas EBP	kwon	confor
☐ **Tekscan**	**2405.17**	**2083.07**	**2752.10**	**1657.86**
▨ **Force Plate**	**2781.00**	**1754.41**	**3559.41**	**1154.84**

Figure 7.4 Results for *BStan* method for all hogus with surface and transmitted force (±SD).

The repeated measures ANOVA revealed that the pad which offered the best protection using *BStan* methods was the confor insert hogu. It performed significantly better than the next best hogu, the adidas EBP, which in turn, produced significantly lower transmitted force than the adidas and kwon hogus. The kwon, which showed an average transmitted force greater than the 3 kN threshold, was significantly worse than all other hogus.

7.4.2 Method 2: Modified British Standards (MBS)

Using the *MBS* test, all hogus displayed an average transmitted force well below the 3 kN threshold (Fig 7.5). Moreover, there was not a single trial in which any hogu exceeded this limit and transmitted forces measured on the CFP were significantly lower than surface forces in all cases.

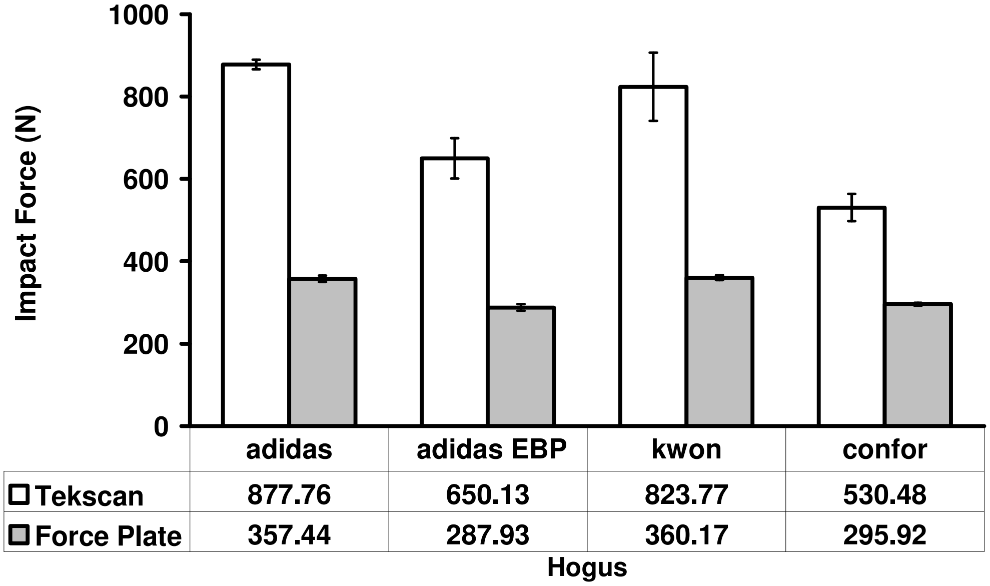

Figure 7.5 Results for MBS method for all hogus with surface and transmitted force (±SD).

The repeated measures ANOVA showed that both the confor and adidas EBP were equally the most effective hogu at dissipating the impact energy and reducing transmitted force. Both were significantly better than the adidas and kwon. Table 7.4 shows the p-values from each set of comparison between pads.

Table 7.4 Significance *p*-values from repeated measures ANOVA.

	adidas	adidas EBP	kwon	confor
adidas	--	0.001	0.986	0.001
adidas EBP	0.001	--	0.000	0.792
Kwon	0.986	0.000	--	0.001
confor	0.001	0.792	0.001	--

A comparison of CT and TTPF for both *BStan* and *MBS* methods showed significant differences between and within methods (Table 7.5). Between methods, *BStan* produced significantly higher TTPFs in all hogus but the kwon and significantly lower CTs for all hogus. Comparing the results within methods did not show a consistent trend for both tests, but it was clear that the performance of each hogu was dependent on the anvil. These differences revealed information about the impact characteristics of the two anvils and this disparity is examined further in the discussion.

Table 7.5 TTPF and CT for each hogu in *BStan* and *MBS* methods.

	BStan		***MBS***	
Hogu	**TTPF (ms)**	**CT (ms)**	**TTPF (ms)**	**CT (ms)**
Adidas	12 ± 2	21 ± 2	8 ± 1	70 ± 2
adidas EBP	14 ± 1	24 ± 1	8 ± 1	57 ± 14
Kwon	11 ± 1	18 ± 2	10 ± 1	90 ± 2
confor	15 ± 1	48 ± 7	22 ± 7	85 ± 4

7.4.3 Method 3: Competition

Average surface and transmitted impact forces for each hogu are separated for each athlete in Fig 7.6.

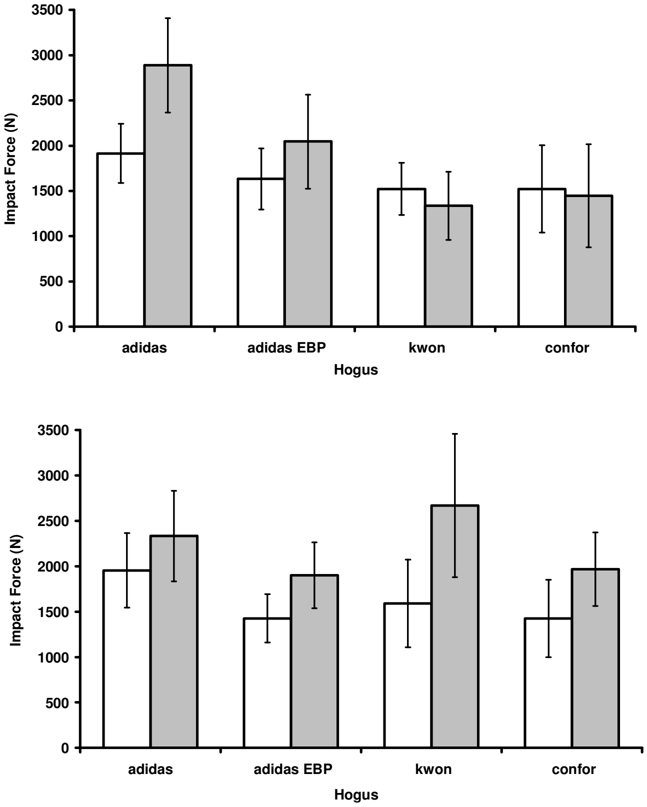

Figure 7.6 Results for *Competition* method for subject 1 (top) and subject 2 (bottom). Tekscan forces in white whilst CFP forces in grey.

For athlete 1, all hogus except the adidas (range: 2.01 – 3.65 kN) were able to maintain the impact forces within all trials to below the 3 kN threshold. Impact velocities between hogus were not significantly different and the range of velocities across all trials was 11.98 – 15.17 ms^{-1}. Table 7.6 summarises the impact characteristics for each hogu.

Table 7.6 Impacts summary for athlete 1.

Hogu	Foot Velocity (m/s)	Tekscan Force (kN)	Tekscan CT (ms)	TTPF	CFP Force (kN)	CFP CT (ms)
Adidas	14.23 ± 0.58	1.92 ± 0.33	42 ± 3	3 ± 0	2.89 ± 0.52	42 ± 5
adidas EBP	13.97 ± 0.66	1.63 ± 0.34	41 ± 4	3 ± 0	2.05 ± 0.52	45 ± 2
Kwon	13.45 ± 0.61	1.52 ± 0.29	83 ± 27	2 ± 0	1.34 ± 0.38	59 ± 5
confor	14.05 ± 0.54	1.52 ± 0.48	92 ± 22	5 ± 1	1.45 ± 0.57	48 ± 6

Conversely, the performance of athlete 2 suggested that the kwon (range: 1.80 – 4.18 kN) did not provide adequate protection. Impact velocities across all trials ranged from 14.69 – 17.90 ms^{-1}. Table 7.7 summarises the impact characteristics for each hogu.

Table 7.7 Impacts summary for athlete 2.

Hogu	Foot Velocity (m/s)	Tekscan Force (kN)	Tekscan CT (ms)	TTPF (ms)	CFP Force (kN)	CFP CT (ms)
Adidas	15.57 ± 0.58	1.95 ± 0.41	43 ± 3	2 ± 0	2.33 ± 0.50	36 ± 2
adidas EBP	16.75 ± 0.26	1.41 ± 0.27	50 ± 20	2 ± 0	1.90 ± 0.36	32 ± 4
Kwon	16.34 ± 0.67	1.59 ± 0.48	105 ± 20	2 ± 0	2.67 ± 0.79	31 ± 5
confor	16.71 ± 0.64	1.74 ± 0.42	108 ± 4	2 ± 0	1.00 ± 0.40	35 ± 4

For each athlete, CTs for the adidas and adidas EBP were significantly lower than both the kwon and confor hogus. Moreover, CTs for the adidas and adidas EBP were similar as were the CTs for the kwon and confor. These trends were also observed in the *MBS* method. TTPF for all hogus were found to be significantly lower for the *Competition* method when compared to either *BStan* or *MBS* methods, but an overall trend was not found.

7.5 Discussion

The aim of this chapter was to examine the performance of commercially available hogus using three different evaluation methods. Despite the large selection of hogus available, these three were selected as they were the most commonly used according to Gary Hall at UK TKD. The adidas EBP was the thickest and heaviest (and at the time, the only automated scoring hogu) whilst the kwon was the thinnest and lightest. The adidas hogu was selected because of its popularity at the British TKD championships in 2007 when this research began. The blue confor foam, while not currently used as an insert within a hogu, was selected to determine if it could serve as a substitute for the foams currently used. In general, the confor performed the best in all three tests, while the adidas EBP was the most effective amongst the commercially available hogus. Both the adidas and kwon were unable to mitigate impact forces as it failed in at least one condition to keep transmitted forces below the 3 kN threshold.

In *BStan* methods, the kwon hogu was rejected since the average transmitted force was higher than 3 kN. While it was likely that the thickness and/or density of the foam was insufficient enough to decelerate the rigid shot put before contacting the rigid anvil, MBS provided contrasting results arguing that the kwon was a very effective hogu. The magnitude of impact forces in *MBS* tests were ~ 10% of the threshold despite using the same impactor with the same mass and dropped from the same height to produce the same energy upon impact. This led to two observations. First, the performance of the hogu was very sensitive to the anvil, which agreed well with Pain et al. (2008); that is, the performance of the hogu was dependent on the materials in-series with the line of impact. When rested on a rigid force plate, the threshold was exceeded, but when worn by the more compliant, deformable, and high-biofidelity *MBOBXL*, impact forces were significantly reduced. Secondly, the impact parameters – 12 J of impact energy with a 2.72-kg shot put – were unlikely to produce a true measure of hogu performance due to its loading rate and overall intensity. At impact, the velocity of the shot put was ~ 3 ms^{-1} – less than 25% of the average velocity measured in the *Competition* method. As such, the hogu would perform differently since the impact characteristics of the materials within the hogu are rate-dependent. Moreover, hogu performance was expected to be further affected by the low impact forces generated in *MBS* methods which were nearly one-sixth the force measured in the *Competition* method, despite the use of the same high-biofidelity surrogate. At these magnitudes of force, the impact would not be considered a 'point-scoring blow' nor would there be concern for injury so it would seem impractical to use this impact condition for hogu performance testing. Instead, the impact parameters for *BStan* tests were likely chosen to artificially produce impact forces which were close to the threshold for injury and had been observed within the sport.

BStan and *MBS* were both found to inaccurately measure hogu performance, but there was evidence to suggest that the *Competition* method did not suffer from these same issues. The main difference between these methods was through the replacement of the rigid impactor with an actual elite martial artist. This ensured that the interaction at impact was more realistic in terms of the impactor velocity, mass and material properties. Whilst the shot put impacts reached ~ 3 m/s, impact velocities for both subjects ranged from 11.9 – 17.9 ms^{-1} comparing well with the 13.9 – 18 ms^{-1} measured previously in expert martial artists (Serina & Lieu, 1991; Pieter & Pieter, 1995; Boey & Xie, 2002; Kim & Hinrichs, 2006; O'Sullivan et al., 2009). Using an actual kick also eliminated most of the major difficulties in matching the mass or *effective* mass of the kicking leg at impact. This is an important detail because mass-time histories, and subsequently the impact energy-time histories, were constantly changing throughout the duration of impact so it would be difficult to model using a single impactor. Furthermore, differences in material impact properties also affected the mass and overall impact intensity. In *BStan* and *MBS* methods, all energy from the impactor was transferred to the hogu and/or anvil as the impactor was not deformable. However, energy is lost through the joints (Zhang et al., 2000) and soft tissue (Pain & Challis, 2001; Pain & Challis, 2002) during the impact of a kick. Since rate of loading and energy are indicators for injury, it is vital to match these parameters as closely as possible.

In the *Competition* method, the adidas EBP and confor hogus consistently maintained impact forces below the 3 kN threshold while the adidas hogu was at or near failure for both athletes. Conversely, the overall performance of the kwon was unclear; impacts delivered by the first athlete suggested that it was the most effective hogu while S2 implied that it was the worst. This contradiction in results was likely explained by the impact attenuation properties of the kwon hogu. For each hogu, significantly higher velocities were recorded for S2 compared to S1. From § 6, this suggested that higher impact and transmitted forces would also be observed. However, only the kwon showed a significant difference in transmitted impact response suggesting that its dynamic impact properties were the most sensitive to changes in loading rate. Therefore, with increasing impact velocity, the kwon seemed less likely to have enough sufficient mass to decelerate the impactor and/or spread the load. This seemed sensible since it was the lightest and thinnest hogu with material properties likely similar to the adidas hogu. Whilst fatigue could contribute to the difference in impact response (since the kwon was the last hogu tested for athlete 1), impact velocities within subject for all hogus were not significantly different suggesting that this was unlikely.

Viano et al. (2000) suggested that one of the functions of chest protectors was to increase the local mass of the chest since the impactor would have to accelerate the effective mass of the hogu to a common velocity before transferring its energy into the anvil. As such, it would not be surprising if the heaviest hogu was also the most effective protector. Whilst this held true for the commercially available hogus tested here, the blue confor was an exception. The mass of the confor hogu was the third highest yet far outperformed the more massive adidas EBP. In addition, the ability of the confor to wrap around any body shape meant that it offered other advantages over the commercial hogus aside from just increased protection such as the potential for increased comfort and mobility. Furthermore, it showed that it was possible to improve upon the existing commercial designs to create a light and conformable hogu without compromising its capacity for protection.

The performance variable used in all methods was the transmitted impact force with an impact threshold of 3 kN as outlined by *BStan* tests. Whilst surface forces were measured concomitantly in this study, transmitted forces were used as it was assumed that they would provide a better indication of the stress levels experienced by the human body beneath the hogu at impact. While this may have been true, it was also chosen in this study since it provided a more accurate evaluation. Surface forces were measured with Tekscan sensors and results from *BStan* and *Competition* methods suggested that there were possible issues with under-sampling and multiplexing (see § 4) which would lead to under-estimated impact forces. The magnitude of this under-estimation can be approximated using the 95% CIs shown in Fig 4.5. This helps to explain the variance in Tekscan force measurements and the reason for the larger transmitted forces when compared to the surface forces. These issues were likely exacerbated by the use of a rigid impactor to evaluate the hogus instead of the more compliant medicine ball used to calibrate the sensors. Though the forces from each trial were calibrated using TTPFs, the load-transfer mechanism of each impactor was likely to be different. These reasons would help justify the surface forces being lower than the transmitted forces in those two methods, which was highly counter-intuitive. In contrast, this may not have occurred in the *MBS* method because of the compliance in the anvil used which led to decreased stress levels. This difference in anvil compliance also accounted for the wide range in maximum impact forces (3.48 – 9.01 kN) measured for roundhouse kicks within the literature (see Table 3.16) This range of forces was similar to the range which had been reported for injury to the chest and abdomen (Table 2.6, 2.7) suggesting that the 3 kN threshold could actually be based upon the causation of injury. Therefore, it was important that hogus be able to mitigate forces below this level, but using impact conditions that more realistically mimicked human response.

7.6 Conclusion

This chapter has shown that the performances of TKD hogus were extremely dependent on the impactor and anvil used in its assessment. Current methods provide reliable and consistent impacts but do not realistically mimic the impact characteristics observed in competition TKD. As such, it may be necessary to construct or develop a more realistic impactor and anvil device to ensure that hogus in TKD are properly assessed. Whilst this will ensure that TKD athletes receive the proper protection, this type of evaluation can be performed for any piece of protective equipment to ensure its functionality.

Chapter 8

Determining Human Impactor Variation

8.1 Chapter Overview

This chapter continues to examine the importance of a human or human-like impactor. Front-leg roundhouse kicks were performed whilst leg kinematics and characteristics at impact were recorded. This data was used to determine the variability of roundhouse kicks and establish the reliability of using a human impactor. The data was also used in the modelling of this movement for future impact testing.

8.2 Introduction

The importance of having a consistent impactor, particularly in chest and abdominal impacts, has been thoroughly addressed within car crash literature. Impactor type and size and impact velocity have all been shown to have a significant role in altering the human biomechanical impact response. Moreover, impact location had a major influence over impact responses in the chest, due to the varying stiffness' of the ribs and pressure of the heart and lungs, and in the abdominal region due to the overlapping of the ribs (Viano et al., 1989) and overall asymmetry and proximity of the abdominal organs. This influence was often limited in cadaver and ATD testing, where rigid impactors were mechanically controlled to produce specific impact conditions in terms of velocity, energy or location. However, when using human participants, these parameters cannot be controlled. Human impacts are not rigid and the impact intensities created with a punch or kick would not be merely dependent on just the velocity at impact, but on the amount of muscle activation in the attacking limb as well (Tsaousidis & Zatsiorsky, 1996). As such, it would be difficult to determine the cause of a change in impact response without further examination of the human impactor itself.

Of the numerous forms of attack in TKD, the roundhouse kick was a logical choice for further study because of its popularity and success at scoring a point. Lee (1988) found that it accounted for 50% of all attacks and resulted in 89% of all total points scored in male competition TKD, whilst Kim & Kim (1997) reported that 79% of females preferred this technique (Kim, unpublished masters). The roundhouse kick is a multi-planar skill where the leg travels in an arc with the knee chambered (i.e. most flexed) followed by quick knee extension while striking the opponent with the metatarsal part of the extended foot (Falco et al., 2009). It is a fast unloading movement that exhibits a proximal-to-distal sequence in which the thigh accelerates due to flexion and abduction of the hip while the trunk rotates creating angular momentum as the lower leg lags behind (Putnam, 1993; Kukkiwon, 1995). As the thigh decelerates, momentum is conserved as the shank and foot accelerate. In its most simple form, this movement is a prime example of the kinetic link principle and is akin to the crack of a whip. Movement begins with a twist of the torso and stance leg, continues through the thigh and then down the long flexible chain of links, finally ending in the least massive distal segment (foot). This strategy, used also in throwing and other forms of kicking, allows maximal velocity to be obtained by the end effector.

The majority of research into TKD kicks has focused mainly on differentiating between types of kick (Tsai et al., 1999; Kong et al., 2000; Lan et al., 2000; Kim & Hinrichs, 2006) and how to maximise velocity and/or force in each (Sorensen, 1996; Boey & Xie, 2002; Pedzich et al., 2006; Falco et al., 2009; O'Sullivan et al., 2009). However, the importance of each kick within competition TKD was rarely discussed; that is, how the objective of the kick, in terms of scoring points, may influence its co-ordination. Whilst the co-ordination and timing of different types of kick in football has been well researched (Davids et al., 2002; Barfield et al., 2002, Apriantono et al., 2006; Manolopoulous et al., 2006; Van der Kamp, 2006; Kellis & Katis, 2007), research in TKD has only focused on maximum velocity kicks (Tsai et al., 1999; Boey & Xie, 2002; Kim & Hinrich, 2006; Tang et al., 2007). However, in competition, these kicks can be delivered in two ways; 'hard' kicks aimed to inflict the most pain or damage in an opponent whilst 'fast' kicks created fast point-scoring opportunities. Kong et al. (2000) suggested that the back-leg was generally used to produce the highest impact intensity and the front-leg for scoring quickly, but did not discuss how the co-ordination of each leg could change to achieve the hard or fast kicks.

Hard and fast kicks both exhibit proximal-to-distal sequences so the initiation of these movements at the torso and hip are similar. As the knee exits the chambered position, though, the execution of each was likely different to reflect the intent of each kick. Fast kicks aimed to reduce the overall movement time and it was expected that this was achieved through a high level of hamstring (i.e. biceps femoris) activation prior to impact to stop and quickly retract the leg. This hamstring activity would reduce the impact velocity, the effective mass of the leg and contact time leading to less impact force and energy transferred to the target. In contrast, muscle activity in hard kicks was expected to contribute to the leg's acceleration through contact until maximum force or maximum energy transfer was achieved. In competition, though, the velocity of these kicks can appear to be quite similar even though the impact intensity or injury potential of each was likely different. As such, an in-depth investigation into both of these kicks was necessary to not only determine kick variability, but to help identify the difference between kicks during competition.

The speed-accuracy trade-off would suggest that increased impact velocity would lead to decreased accuracy during a kick (Fitts, 1954). However, this did not account for learned skills developed through repetition. Latash (1998) suggested that repeated movements would have a relatively high variability of individual joint trajectories but a low variability of endpoint trajectory. Moreover, Roosen (2008) reviewed literature into the variability in human movement and found that as force produced increased, the variability in force decreased whilst spatial accuracy increased. This suggested that not only may hard kicks deliver the most damage, but may do so with the greatest accuracy. As such, a thorough examination of the front-leg roundhouse kick was conducted using the validated surrogate developed in § 6. The main focus of this research was to:

1) Establish parameters that could be correlated to impact force;
2) Determine the reliability of using a human impactor; and
3) Obtain leg kinematics which could be used as input into a mathematical or mechanical model for future research.

8.3 Methods

8.3.1 General

Nine physically active participants (male, 24.3 ± 7.4 years, 78.2 ± 11.5 kg, 1.77 ± 0.06 m) provided informed voluntary consent to participate in this study in accordance to the protocol outlined by the Loughborough University Ethical Advisory Committee (*Appendix B*). Each participant was a martial artist player with at least a 1st dan black belt. A summary of all players appears in Table 8.1.

Table 8.1 Summary of players involved in this study.

Players	Age (yrs)	Mass (kg)	Height (m)	Mean Vicon Residual (pixels)
1	36	90.3	1.741	0.1423
2	24	80.1	1.881	0.1423
3	21	62.2	1.725	0.1150
4	20	70.3	1.756	0.1047
5	19	63.4	1.700	0.1047
6	19	92.9	1.835	0.1729
7	19	72.8	1.760	0.1990
8	23	88.1	1.784	0.1990
9	38	83.5	1.750	0.1895

8.3.2 Trial Protocol

After a self-selected warm-up, including several practice kicks, each player performed 9 sets of roundhouse kicks with their self-selected front leg. All impacts were administered onto a target area on the torso area of MBOBXL. Surface and transmitted impact forces were measured with Tekscan F-Scan sensors at 500 Hz and the Custom Force Plate (CFP) at 1000 Hz, respectively. Tekscan sensors were calibrated according to the method outlined in § 4.2.2.2. CFP raw data was collected using the Vicon Nexus software which simultaneously tracked marker trajectories of the leg, MBOBXL and the wall behind the surrogate anvil using nine MX cameras at 250 Hz to obtain kinematic data (Fig 8.1). In total, there were 11 markers on the kicking leg, 4 on MBOBXL and 3 on the wall (Fig 8.2). Mean residuals for all Vicon cameras for each player is also shown in Table 8.1. Kinematic data was used to calculate impact location and velocity, as well as joint angle-time histories for the hip, knee and ankle joints. Impact velocity was calculated using the method described in § 6.4.3.3.

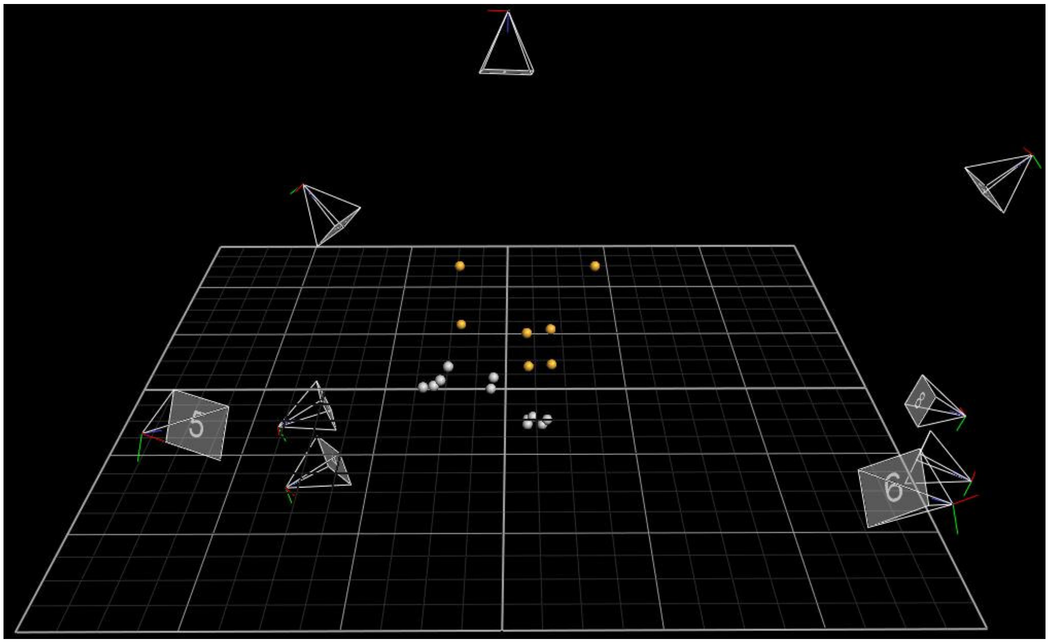

Figure 8.1 Screen-shot of capture volume including all 9 MX cameras and markers on the wall, MBOBXL and TKD player.

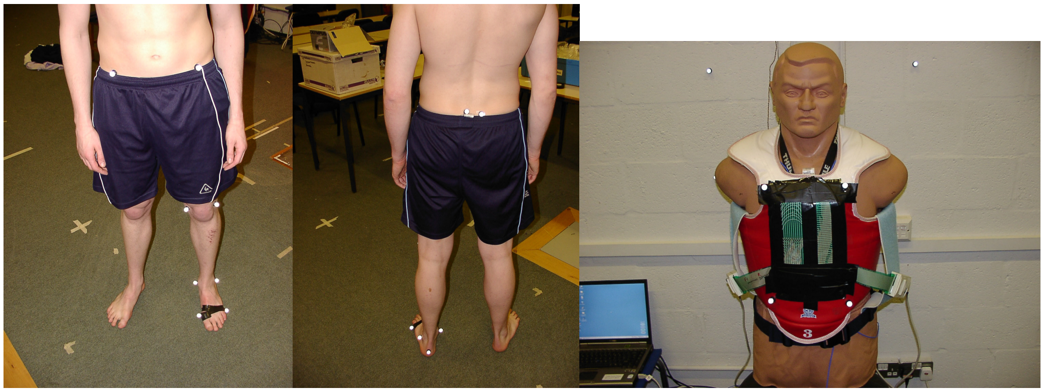

Figure 8.2 Marker locations on the leg, MBOBXL and wall.

8.3.3 Kick Trials

Each set of 5 or 10 kicks were comprised of either only *consistent* kicks or a *mixed* trial of *fast* and *hard* kicks. In the *consistent* trial, players were allowed to select their own exertion level but told to focus on making each kick as identical as possible in terms of its velocity, force and location. In *mixed* trials, players were instructed to either kick *hard*, producing as much force as possible, or *fast*, striking as quickly as possible and minimising contact time. The first instruction, which indicated the kick type, was provided before the start of each set and each subsequent instruction was provided when the previous kick finished (i.e. kicking leg returned to the ground). Players were also told to not hesitate between instructions though the reaction time – the time between instruction and the initiation of movement – and the overall movement time was not measured. The order of kicks in the mixed set was randomised, but a total of 20 kicks of each type were performed.

8.3.4 Determining Kick Location & Consistency

Similar to the calculation of impact velocity, a local co-ordinate system (LCS_{MBOBXL}) was established using the four *MBOBXL* markers. The origin was set as the bottom left marker and a grid, the x-y plane, was created using the bottom right and top left markers and a series of cross-products. These calculations set the orientation of the x-axis as horizontal while the y-axis was vertical. While only 3 markers were necessary for this procedure, the fourth was used in the event that one of the other markers became occluded during a trial. The procedure for establishing the LCS_{MBOBXL} is outlined in *Appendix E*. At the first instant when the *MBOBXL* markers deviated from their static position, the location of the mid-point between the two toe markers, MTPJC, was plotted on this plane to provide the impact location.

Kick locations were averaged for each player and kick type to determine overall kick locations. Kick consistency was assessed using the standard deviations in x- and y- coordinates. These co-ordinates were used to form a rectangular box where its size would indicate its consistency with a smaller box indicating a more consistent kick.

8.3.5 Kinematic Analysis of Kick

Joint angles for the hip, knee and ankle were obtained in the plane of flexion-extension for each kick type (i.e. *consistent*, *hard* and *fast*). In each successful kicking trial – one in which force was measured on the CFP and all markers on the leg could be reconstructed reliably – the frame of first contact was identified and normalised for each kick type and player. This allowed trials of different length (with respect to time) to be combined and a mean to be calculated for each joint angle at each moment in time. A group mean of each joint angle for all subjects was then calculated using the individual means (i.e. a mean of group means). These angles were analysed to help qualitatively describe the differences between kick types. Quantitative analysis was conducted in § 9.5.3.

8.3.6 Statistical Analysis

A repeated-measures ANOVA was conducted for each player to analyse the difference between types of kick in terms of its velocity, force, contact time (CT) and time to peak force (TTPF). Correlation analysis was also performed to determine the strength of the relationship between impact force and velocity. Significance was set at α = 0.05. Performances between individual athletes were not compared against each other.

8.4 Results

8.4.1 Impact Force & Velocity

Comparing all conditions, *hard* kicks were shown to produce the highest mean impact force, CTs and impact velocities (Table 8.2). All displayed impact forces were obtained from the CFP data.

Table 8.2 Mean impact characteristics for each athlete separated by condition; variables include: velocity, force, contact time (CT) and time to peak force (TTPF).

Players	**1**	**2**	**3**	**4**	**5**	**6**	**7**	**8**	**9**
Consistent									
Vel (m/s)	8.2	12	8.9	8	5.3	12.5	14	11.8	7.2
Force (kN)	0.9±0.1	1.3±0.2	0.7±0.1	0.6±0.3	0.3±0.1	2.0±0.4	2.3±0.4	1.3±0.4	0.5±0.1
CT (ms)	30	39	27	44	39	50	45	42	33
TTPF (ms)	4	3	3	5	6	3	3	3	6
Hard									
Vel (m/s)	12.3	13.1	12.1	9.9	8.2	11.6	14.6	13.2	11.6
Force (kN)	1.7±0.5	1.8±0.3	1.2±0.4	0.7±0.2	0.5±0.2	1.7±0.4	2.3±0.5	1.6±0.3	1.4±0.3
CT (ms)	39	41	37	42	42	44	45	43	37
TTPF (ms)	3	3	3	5	4	3	3	3	5
Fast									
Vel (m/s)	7.8	11	8.8	7.2	4.7	7.1	12.7	10.1	9.5
Force (kN)	0.5±0.1	0.7±0.2	0.5±0.3	0.4±0.1	0.2±0.1	0.5±0.2	1.2±0.4	0.9±0.2	0.6±0.2
CT (ms)	24	36	26	37	32	35	40	36	29
TTPF (ms)	3	4	3	6	9	6	4	5	5

Each kick type was statistically compared to the other two kick types to make three paired comparisons in total (Table 8.3). The '+' symbol was used to indicate that the first kick type in the pair was significantly greater for that particular parameter. For example, the impact velocity for player one’s *hard* kick was significantly greater when compared to the *consistent* kick. Conversely, the ‘- ‘symbol indicated a significantly lower difference whilst ‘NS’ indicated that significance was not found between the two kick types. In general, *hard* kicks had the highest impact force when compared to *consistent* and *fast* kicks. A significant difference was not found in CT between *hard* and *consistent* kicks, but both were significantly higher than fast kicks. TTPFs were not consistently different across any of the three kick types.

Table 8.3 Statistical comparison between each style of kick in terms of impact velocity, force, contact time (CT) and time to peak force (TTPF). Significance was set at α = 0.05.

Players	**1**	**2**	**3**	**4**	**5**	**6**	**7**	**8**	**9**
Hard - Consistent									
Vel (m/s)	+	+	+	+	+	NS	+	+	+
Force (kN)	+	+	+	+	+	NS	NS	+	+
CT (ms)	+	NS	+	NS	NS	NS	NS	NS	+
TTPF (ms)	NS	NS	NS	NS	-	NS	NS	NS	NS
Hard – Fast									
Vel (m/s)	+	+	+	+	+	+	+	+	+
Force (kN)	+	+	+	+	+	+	+	+	+
CT (ms)	+	NS	+	+	+	+	NS	+	+
TTPF (ms)	NS	+	NS	NS	-	NS	NS	-	NS
Consistent – Fast									
Vel (m/s)	NS	+	NS	+	NS	+	+	+	+
Force (kN)	+	+	NS	+	+	+	+	+	NS
CT (ms)	+	+	NS	+	+	+	NS	+	+
TTPF (ms)	+	-	NS	NS	NS	-	NS	NS	NS

Mean impact forces for each player and kick type were plotted as a function of mean impact velocity (Fig 8.3). A regression curve was fit to each type of kick with its equations and R^2 values shown. An additional regression curve was also fitted to all kicks, irrespective of type and player. At velocities < ~10 m/s, all kick types performed similarly. Above this value, fast kicks were shown to produce significantly lower impact forces. As such, two regression curves were fit to the data comprising of all kicks to reflect this change in the impact force – impact velocity relationship (Fig 8.4). RMSE and residual values for these regression curves were calculated with respect to the ‘S3, Pad’ condition in § 6.5. The RMSE was 2.38 and the residual was -0.48 ± 2.45 whilst the *MBOBXL* trial, which used the same anvil but with a smaller sample size, was 3.08 and -1.03 ± 3.03, respectively. Therefore, the larger sample provided additional support to show that the MBOBXL was an anvil of acceptable biofidelity.

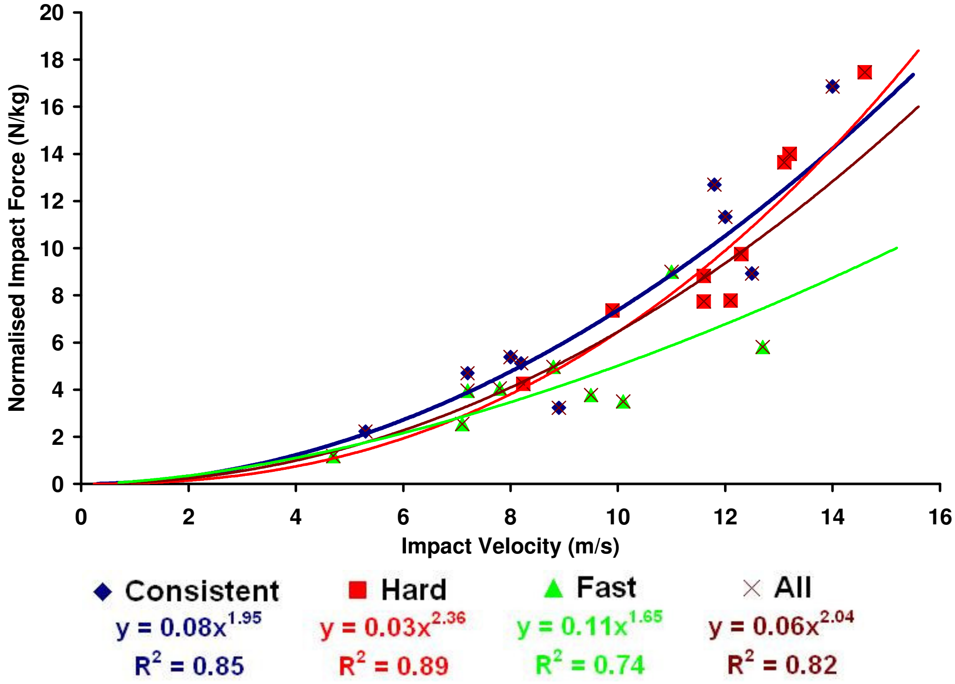

Figure 8.3 Normalised mean impact force for each player as a function of impact velocity and separated by kicking condition. Regression equations with corresponding R^2 values are provided.

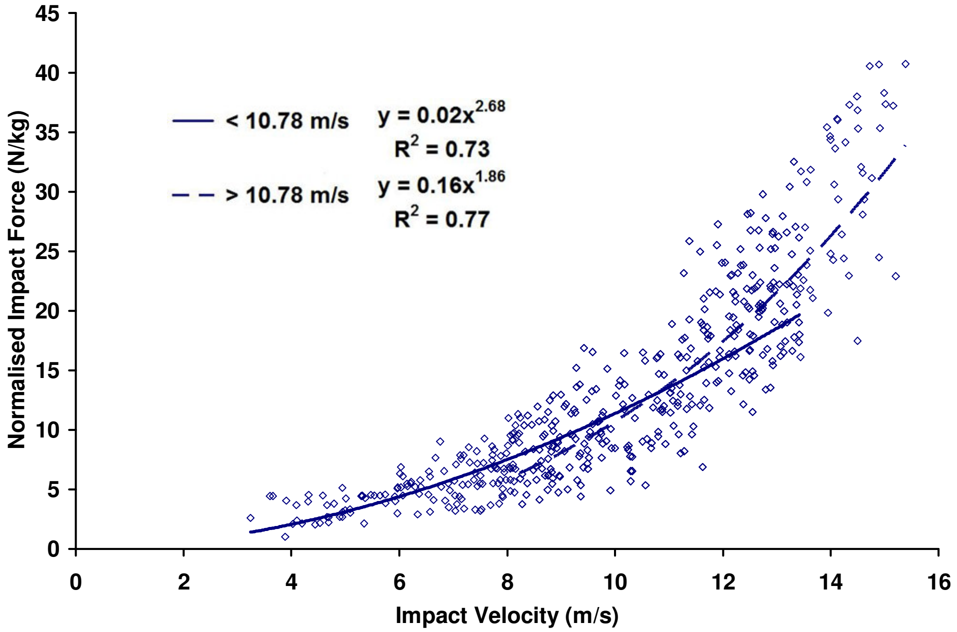

Figure 8.4 Plot of the relationship between impact velocity and normalised impact force for a combination of *hard* and *consistent* kicks for all TKD players.

8.4.2 Impact Location

For each player, all kicks – separated by type – were plotted on an x-y grid derived from the LCS_{MBOBXL} and displayed similarly to that shown in Fig 8.5. The origin of the grid represented the bottom left marker on *MBOBXL* whilst the bottom left corner of the CFP was situated approximately 25 mm along the x-axis and 100 mm up the y-axis.

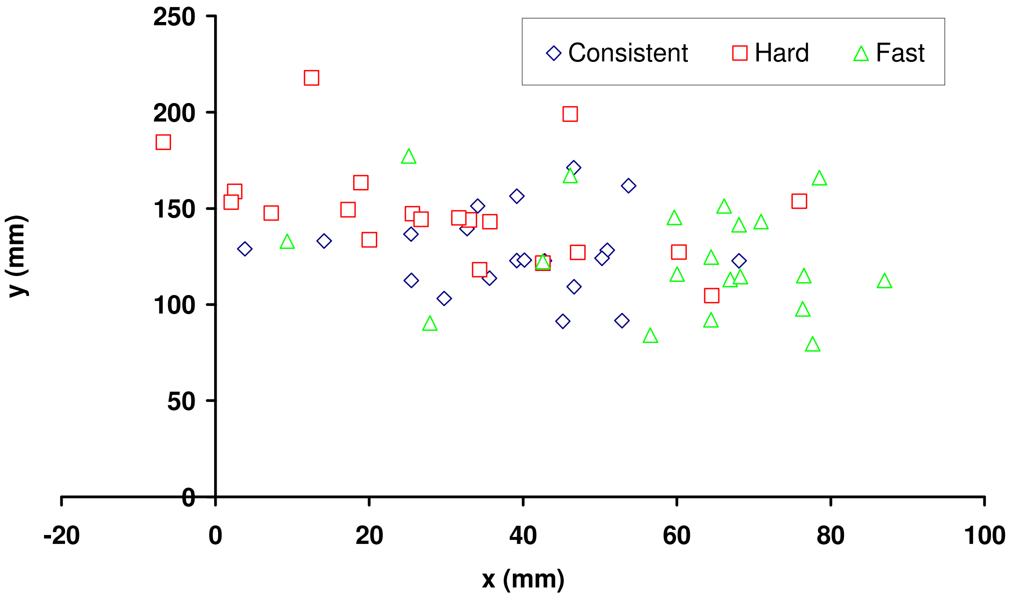

Figure 8.5 Sample plot of kick location obtained for player 1. The origin is set at the bottom left marker placed of MBOBXL.

Mean kick locations for each subject are displayed in Table 8.4. In general, hard kicks had the highest impact location, but this was not observed consistently amongst all athletes.

Table 8.4 Mean kick locations for each player organised by kick type.

Players	Impact Location (mm)					
	Consistent		Hard		Fast	
	x	y	x	y	x	y
1	38.8	127.2	29.9	149.2	59.6	124.3
2	26.3	116.8	18.9	116.3	14.2	109.2
3	170.0	156.9	179.3	181.8	193.1	180.5
4	64.3	114.2	39.6	124.3	55.6	137.3
5	171.6	152.1	157.6	220.1	161.1	215.0
6	194.5	108.8	191.8	101.8	213.1	124.0
7	201.4	145.8	205.4	121.0	197.6	93.0
8	1.8	131.3	21.4	146.3	16.9	108.8
9	222.3	125.9	246.1	155.0	233.2	151.7

8.4.3 Kick Consistency

Kick consistency for each player is shown in Table 8.5. The most consistent impact was the *consistent* kick as it had the lowest area of deviation for most players. For players whose *consistent* kick did not have the least amount of variation, *fast* kicks were their most consistent and was considered the second most consistent amongst the group. The least consistent was easily the *hard* kick which showed over 80 mm of vertical deviation in 2 players, and only 2 players were able to maintain a vertical deviation of less than 35 mm. In contrast, only 2 athletes had higher than 35 mm vertical deviation in the *consistent* kick and only 3 in the *fast* kick.

Table 8.5 Kick consistency for each subject separated by trial. Consistency was assessed by using the area bounded by the standard deviation in kick location.

Players	**Impact Consistency (mm)**					
	Consistent		**Hard**		**Fast**	
	x	**y**	**x**	**y**	**x**	**y**
1	10.2	18.8	21.9	27.0	20.0	28.4
2	10.4	29.2	22.7	29.9	25.9	30.0
3	14.1	18.4	23.9	47.1	23.4	25.7
4	22.6	31.0	39.2	43.2	27.2	33.7
5	20.5	42.4	40.7	38.9	19.7	40.1
6	25.8	44.8	49.4	82.7	38.2	38.2
7	18.6	20.7	29.2	37.3	21.8	43.9
8	22.4	30.5	19.8	91.6	16.1	20.8
9	13.4	26.4	35.2	39.1	40.0	24.2

8.4.4 Kinematic Analysis of the Kick

Of the nine players which provided force-velocity data, only five were able to provide reliable joint kinematics due to marker occlusion. Using this data, mean joint angle data for each kick type were calculated and compared individually for the hip, knee and ankle (Fig 8.6). In addition, hip, knee and ankle angles for the *hard* kick were displayed on the same plot to show the co-ordination between joints (Fig 8.7). Three phases were identified and an interpretation of the angle changes between each phase is discussed in the following. A schematic showing the relationship between joint angles and each leg segment at three key moments (identified by a number) and phases (time between moments) is also provided (Fig 8.8).

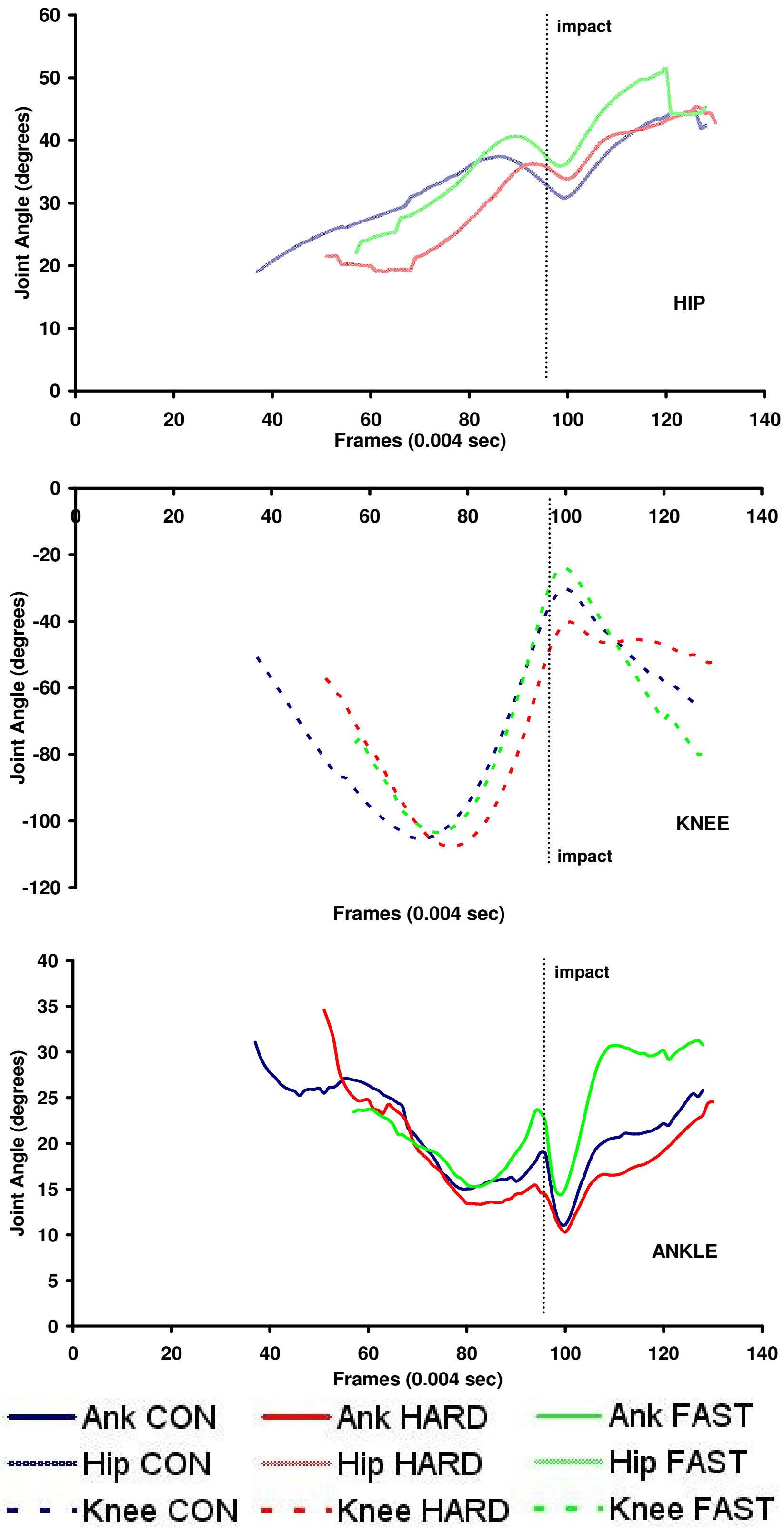

Figure 8.6 Mean hip, knee and ankle angle for all players separated by *consistent, hard* and *fast* kicks.

The first moment highlighted the transition of the knee from flexion to extension. Hip flexion, which had started at the initiation of the kick, continued throughout this moment and phase whilst the ankle underwent slight dorsi-flexion until plantar-flexing just prior to impact. Ankle dorsi-flexion was likely a passive movement as a consequence of the proximal-to-distal sequencing observed in a kick (Putnam, 1993), but plantar-flexion was likely active as the foot prepared for impact.

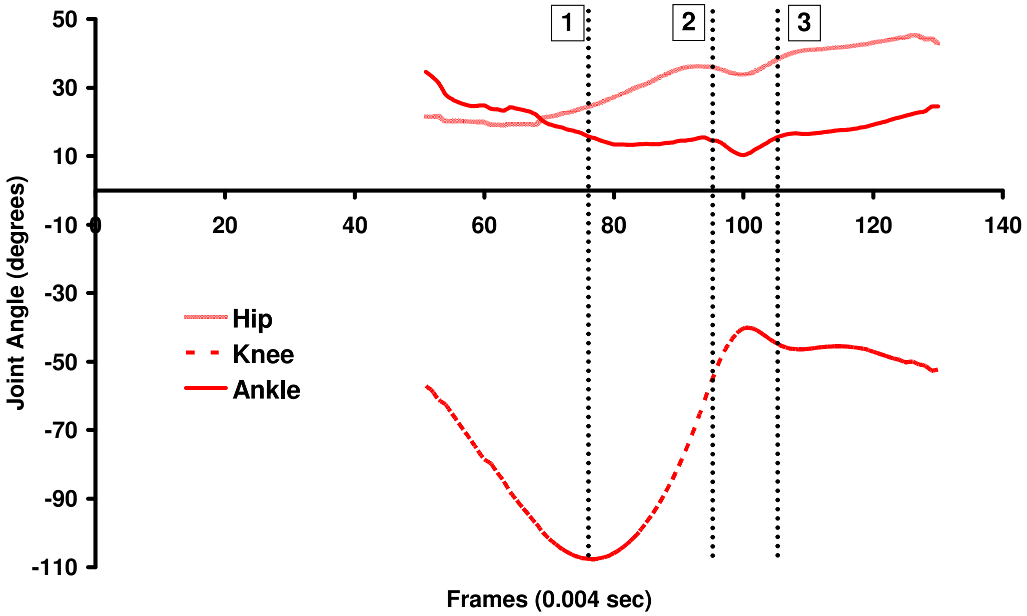

Figure 8.7 Plot of all hip, knee and ankle joint angles for an average hard kick

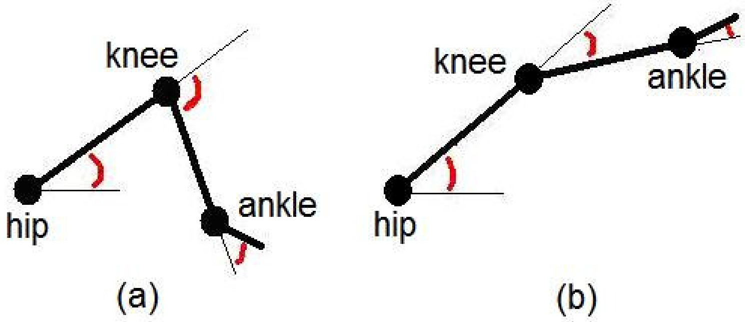

Figure 8.8 Schematic showing the relationship between joint angles and limb segments at two instances of Fig 8.7; (a) Phase 1, (b) mid-contact

The second moment marked the beginning of impact and the contact phase. During the first half of this contact phase, knee flexion continued and was coupled with what appeared to be hip extension. Instead, it was likely that the hip was always actively flexing but the whip-like movement of the shank and foot forced the hip into a small amount of passive hip extension. At the ankle, the magnitude of the impact force, offset from the ankle joint, created a large moment causing rapid dorsi-flexion. The rate of this dorsi-flexion was a function of the active and passive stiffness at the ankle. In the second half of the contact phase, the ankle returned to its pre-impact angle likely as a result of its passive stiffness, whilst hip flexion ‘resumed’ and the knee began to flex. The cause of knee flexion was either due to the same magnitude of force creating a large moment around the knee (greater than the generated knee torque) or from the activation of the hamstrings actively retracting the knee.

The third moment marked the end of the contact phase and provided insight into the difference in execution for each kick type. For *hard* kicks, it appeared that the knee flexion post-impact was initiated by the moment caused by the impact force since the hip continued to flex with small changes in knee angle. Whilst the hip continued to flex for *consistent* and *fast* kicks, there were large changes in knee angle which suggested that this was caused by active muscle contraction. This qualitative analysis of the overall kick kinematics will be examined more thoroughly in § 8.4.

8.5 Discussion

In § 6, it was proposed that a relationship between impact force and velocity for a TKD roundhouse kick existed. However, the explained variance obtained ($R^2 = 0.36$) did not provide overwhelming confidence that the variables were, in fact, correlated. In spite of this, the discussion in that chapter provided rationale for why a correlation between the two variables may actually exist. As such, this chapter examined this potential relationship in more depth and attempted to determine differences in impact characteristics when the objective of the kick was varied. Results showed that impact velocity could be used to reliably predict impact force in the roundhouse kick with separate mathematical relationships obtained for both hard and fast kicks. The hard kick displayed the highest average impact velocity and, subsequently, the highest average impact force but was also the most inconsistent kick in terms of the variation in impact location.

The reliability of the impact force-impact velocity relationship in this chapter was substantially higher than that measured in § 6 with all R^2 values greater than or equal to 0.74. These were achieved with a much larger data set providing more confidence that these relationships occurred by more than chance alone. As such, it was reasonable to assume that impact velocity was an appropriate predictor of impact force and at a given velocity, particularly when greater than ~10 ms^{-1}, the force of a *hard* kick would be greater than that of a *fast* kick, as shown in Fig 8.3. This was logical given the objective of each kick type as discussed in the introduction. *Hard* kicks tried to recruit as much effective mass during impact whilst maintaining the highest possible velocity. Players have often been instructed to imagine the finishing point of the kick as being just beneath the impact surface, thus allowing the hip to continue extending through impact. Mean knee joint angles in Fig 8.6 supported this theory as the knee at impact was the least extended in *hard* kicks affording the quadriceps more mechanical advantage to produce additional energy during contact. The lower amounts of knee flexion in *hard* kicks during impact suggested that this was a passive movement, whilst *fast* kicks seemed to exhibit an active flexing of the knee post-impact. Therefore, the execution of a *fast* kick may show higher joint velocities at the hip and knee to decrease movement time, but hamstring activation just prior to impact will decrease the angular velocity of the shank. Kong et al. (2000) suggested that this event may be a reflex contraction of the hamstrings to protect the knee joint before the leg is fully extended. Reducing the velocity of the shank would lead to decreased foot velocities and decreased effective mass recruited throughout the impact. Furthermore, with the shank returned to the chamber position quicker, contact times were reduced and the leg was unable to impart more impact energy onto the anvil. As such, impact force was likely a function of both impact velocity and contact time, which may help to differentiate between *hard* and *fast* kicks.

In novice competitors, body mass was found to be a significant and positive correlate for impact force (Pedzich et al., 2006; Falco et al., 2009). Pedzich et al. (2006) further suggested that this correlation effect may be linear amongst novice players. While the players involved in this study were all experts, all impact forces were normalised to each individual player's body mass to diminish the effects of body mass on impact force in this study. This may have erroneously assumed that the increases in body mass led to a linear increase in impact force (as shown in novices), but there was not enough data collected to make a more accurate assumption. Moreover, it was considered better to account for some of the variation in impact force than use the raw data which clearly would have been affected by this trend.

Mean peak impact forces for all players ranged from 0.5 – 2.3 kN for *hard* kicks. This was considerably lower than the range of 3.48 – 9.01 kN which had been summarised from previous literature and reported in Table 3.8. Whilst this disparity could be accounted for by the difference in anvils used, these roundhouse kicks were executed with the back leg. Kong et al. (2000) showed that maximum linear velocity at the ankle were much higher for back leg kicks (26.26 ± 8.83 ms^{-1}) compared to front-leg kicks (18.83 ± 5.81 ms^{-1}). Since higher velocities have been shown to increase impact force, it can be assumed that the forces measured in this chapter were artificially low due to the kicking leg chosen. Pilot work conducted with the UK TKD squad provided further support for this claim. Using the same set-up, including the human anvil, described in § 6 for *in vivo* kicks, players were able to generate up to 2.4 kN on front-leg kicks and 4.1 kN on back-leg kicks when impacting a human anvil. Whilst impact velocities were not measured, this showed the disparity between the executions of both kicks.

The regression curve equations for each kick type were all modelled using a power function, with powers ranging from 1.65 for *fast* to 2.36 for *hard* kicks, up to 16 ms^{-1} (Fig 8.3). Each curve was not extrapolated beyond this value because that would assume that these equations would continue to hold at all velocities. Instead, it was likely that the best-fit curve for the “impact velocity – impact force” relationship would consist of multiple curves as shown in Fig 8.4. In that plot, two curves were fit to the data with a higher slope for the velocities above ~10.78 ms^{-1}. This value was obtained arbitrarily as it was the point at which both regression curves crossed in Fig 8.4. As such, without any measures of velocities at magnitudes greater than 16 ms^{-1}, it would be impossible to predict whether the slope would increase, decrease or plateau, especially if those velocities were not attainable due to human limitation.

In previous research, impact force and velocity were found to depend on kick height with lower kicks recording a higher force and velocity than higher ones (O’Sullivan et al., 2009). In this study, hard kicks had the highest mean impact location as well as the highest impact force and impact velocity. The largest overall difference in impact average height occurred with player 5's hard kick almost 130 mm higher than player 7's fast kick. However, such a comparison was invalid due to differences in player height and leg length, as well as the location of their back (i.e. plant) leg relative to the target. Whilst the data could have been normalised to each players height and/or leg length, it was not necessary to determine the actual impact location, but to analyse the difference and variation between kicks within each subject. Examining the variation of impact location within-subjects revealed a difference of only ~68 mm, with all kicks executed at a height set at their own discretion. As such, it would not be expected that impact height would significantly influence the impact force in this condition. As for the kick execution distance, Falco et al. (2009) found that for experts, impact height did not lead to a significant difference in impact force, so it was assumed that this was not a factor in this study.

The kick with the least amount of variance in impact location was the *consistent* kick, which was expected. All martial artists in this study were of an elite level (1st dan or higher) and this confirmed that each were capable of making any necessary compensatory changes during the kick to ensure that similar forces and impact locations were achieved. Comparing the other two kicks showed that the *fast* kick was slightly worse than the *consistent* kick, but far out-performed the *hard* kick. This was likely because *fast* kicks were practiced more because of the advantages it offered in competition TKD. Players can execute this kick with a faster total movement time thus creating quicker scoring opportunities whilst returning the leg back into position for another attack or movement sooner (O'Sullivan et al., 2010). As such, being precise with the impact location was paramount when executing such a kick. In contrast, a *hard* kick focused more on maximising force rather than impact precision. It was also possible that since the end-point in a *hard* kick was theoretically below the impact surface, there was not as much focus on the consistency of initial impact locations as long as the point at which maximal force generated was consistent. Nien et al. (2007) was able to show that the performance of roundhouse kicks improved when players could see a visual target.

For all players, the upper and lower bounds of force increased with increased velocity (Fig 8.4), whilst *consistent* and *fast* kicks had lower kick location variance than *hard* kicks (Table 8.4). While fatigue, which can affect the intersegmental co-ordination leading to a decreased accuracy and velocity (Apriantono et al., 2006; Kellis et al., 2006; Jordet et al., 2007), may have been an influential factor, all trials were randomised in an attempt to minimise this effect. Furthermore, the volume of kicks performed in this study was less than that experienced in a regular training session. Determining this variance was important because it was necessary to have a consistent impact when examining impacts to the chest and abdominal region. Impact responses in this region are overly sensitive due to the complex structure of the underlying organs, bones and musculature. Without a consistent impact, it would be difficult to determine which body parts were absorbing the impact without having individual measurement devices on each. As such, it may be more useful to develop a biofidelic mechanical impactor which can provide controlled impacts. Enough data was captured in this research to calculate leg kinematics and to determine the contribution of each joint angle change on the final kick velocity. This will be examined further in the next section. An immediate application for this impactor was that it would provide a more accurate method for assessing hogu performance as discussed in §7.

One of the main applications of establishing an impact force-velocity relationship was that it provided another means of collecting impact data from TKD competition non-invasively. Normally, this would be an arduous task as sensors would need to be embedded within the TKD garment or hogu in order to make the required impact measurements. This would test a sensor's ability to transmit numerous streams of data wirelessly whilst being robust enough to withstand the actual impact. However, data in this section showed that multiple regression equations could be developed to approximate impact force from impact velocity and contact time, if necessary. Regression parameters can be easily obtained by reconstructing the footage of at least 2 high-speed cameras (or even 50-Hz cameras) and digitised. This is a technique that was originally used, and with good accuracy, to obtain kinematics for sports such as gymnastics or athletics. Using impact forces from competition TKD, a hogu can be developed to consistently record score automatically. Currently, points in TKD are awarded when a powerful blow is delivered and are determined based on the opinion of four corner judges. However, it is unclear what is meant by 'powerful' as points could be based on the assumed kick velocity or impact force, the sound at impact and/or the victim's response.

8.6 Conclusion

In front-leg roundhouse kicks, impact force was found to depend on impact velocity and contact time. This "impact force – impact velocity" relationship provided a means for obtaining impact data non-invasively in competition TKD. Consistency between kicks was found to be dependent on the motivation for each kick with *fast* kicks outperforming *hard* kicks. If the injury potential or the performance of PPE was to be determined, it would be necessary to develop a more consistent impactor. The impact characteristics and joint kinematics at the hip, knee and ankle presented within this chapter can then assist in the future modelling of the impactor to produce the desired impact consistency.

Chapter 9

Development of a Computer Simulation Model of an Impactor

9.1 Chapter Overview

This chapter begins with an overview of previous mechanical and computer-simulation models for different types of kick. A mechanical martial arts kicking robot constructed in parallel to this research is presented. Mechanical components of this robot are combined along with kinematics from human performance to calculate parameters for a single-segment computer simulation model of a roundhouse kick and are outlined. Using the motor and human inertia parameters, a multi-segment model is presented and its potential construction investigated. Performances between simulation models are compared to determine the efficacy of each in mimicking human performance.

9.2 Introduction to Kicking Models

9.2.1 Mechanical Models of Soccer Kicks

Simple, rigid-mass surrogate models of a kicking leg have been used extensively within research. Mechanical replicas of the foot have been modelled as a rounded cylinder (British Standards), a single mass on a pendulum (Bir et al., 1995) and tubes covered in rubber (Francisco et al., 2000), whilst the kicking leg has been modelled as a series of water-filled cylinders (Serina & Lieu, 1991; Chuang & Lieu, 1992). Each of these impactors was designed to match the energy of the impact which, as discussed in § 7, could lead to incorrect impact intensities. The main flaws of this assumption were the differences in loading rate and the effective mass at impact. Using human impactors, though, was also limited as the variation in their performance made it difficult to determine the cause of changes in impact response as found in § 8. As such, a balance between the two methods is necessary to advance research in this field.

More complex models have also been designed and constructed. Schempf et al. (1995) used a combination of active and spring-assisted actuator modules at multiple joints to control a three-segment kicking leg based on kick performances measured by Plagenhoef (1971) and the inertia of a 70th-percentile male (Fig 9.1, *left*). Whilst the multi-segment model could produce realistic joint angles and angular velocities, its complexity in trying to replicate human movement ultimately made it almost impossible to keep in working order. As such, this model could not be trusted to provide reliable results. In contrast, a soccer kicking robot was also developed by the Sports Technology Institute (STI) at Loughborough University (Fig 9.1, *right*). This model consisted of two connected beams with a nylon end effector actuated with a motor at a joint representing the hip. Its design was based on the inertia of a 50th percentile male and stress analyses to provide the highest strength to weight ratio for the materials used in its construction. Its simplicity, particularly in actuation, and robustness allowed this model to provide consistent and repeatable impacts at velocities similar to human kicks and thus has been used more often the multi-segment model.

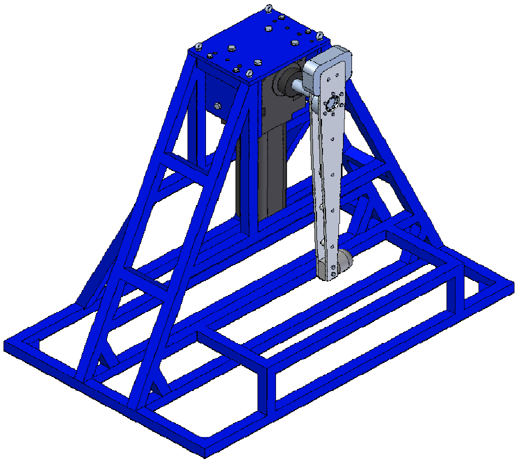

Figure 9.1 Two mechanical models; **(**left): Three-segment kicking robot (Schempf et al., 1995); (right): single segment kicking robot developed by STI (Loughborough University)

9.2.2 Mathematical Models of Martial Arts Kicks

Serina & Lieu (1991) produced a mathematical model of TKD kicks based on human performance[4]. Its aim was to determine the injury potential of the thrust and swing kicks in TKD. Each kick was filmed from above and digitised at the hip, knee and ankle to determine joint kinematics and linear end effector velocity. Swing kicks were modelled as a lower leg and foot rotating about the knee (knee velocities were negligible) whist thrust kicks were modelled as a slider-crank linkage with the foot represented by a point mass at the end of the leg (Fig 9.2). Each limb was modelled as a water-filled cylinder with the same diameter as the average of that limb segment. Quasi-static force of the kicking leg was also measured to determine the maximum muscle force that could be exerted during the contact time of each kick. Using the motion and force of a kick, in conjunction with the impact force, kinetic input (i.e. effective mass) was derived to drive the Lobdell chest model to determine injury potential. Unfortunately, accuracy of the calculated effective mass (i.e. based on equivalent energies) was unknown, thus making the conclusions about injury potential inconclusive. In spite of this, it showed the value of impactor models that were based on actual human performance.

Figure 9.2 Model of thrust kick and swing kick (Chuang & Lieu, 1992).

Doke & Kuo (2005) created a simple mathematical model of a karate front kick using a two-segment model with hip and knee joints to examine the effects of activation and co-ordination on kick performance. Each joint was actuated using a simple Hill-type muscle model and were activated using an adjustable, constant activation level during flexion and extension phases. Co-ordination of the joints was controlled by two timings; one to determine the change from flexion to extension of the knee and another for the change from flexion to extension of the hip. Their results, while not validated, were shown to resemble observations from experimentation providing support that simple kick models could provide insight into kick execution or performance.

---

[4] Subsequently adopted in a parametric study by Chuang & Lieu (1992)

9.2.3 Chapter Aims

The aim of this chapter was to develop a single-segment (1-SM) and a three-segment (3-SM) computer simulation model of the roundhouse kick. Model *1-SM* was based on a mechanical robot in co-development (discussed in § 9.3) but was not validated to its performance as this was beyond the scope of this particular research. Instead, *1-SM* was used to validate the overall modelling procedure and help develop a suitable anvil. Components of *1-SM* were then used in conjunction with the kinematics from i*n vivo* kicking data collected in § 8 to design model *3-SM*. This model was intended to improve upon the mechanical robot and, as such, its feasibility for future construction was investigated.

9.3 Mechanical Model of a Roundhouse Kick

9.3.1 Overview

Walker (unpublished thesis) designed and constructed a single-segment mechanical model (Fig 9.3) as part of the SCUTA project (§ 1.2) The aim of this model was to provide more realistic impacts, in terms of the effective mass of the kicking leg and impact velocity, for the performance testing of existing TKD hogus. Its overall design was similar to the STI kicking robot and consisted of two tapered beams made of high strength aerospace grade aluminium alloy 7075-T6 connected by vertical struts. On its proximal end, a motor was attached to the leg whilst an end effector made of nylon was used to impact the anvil. This anvil was housed within a frame that was adjoined to the frame of the kicking robot.

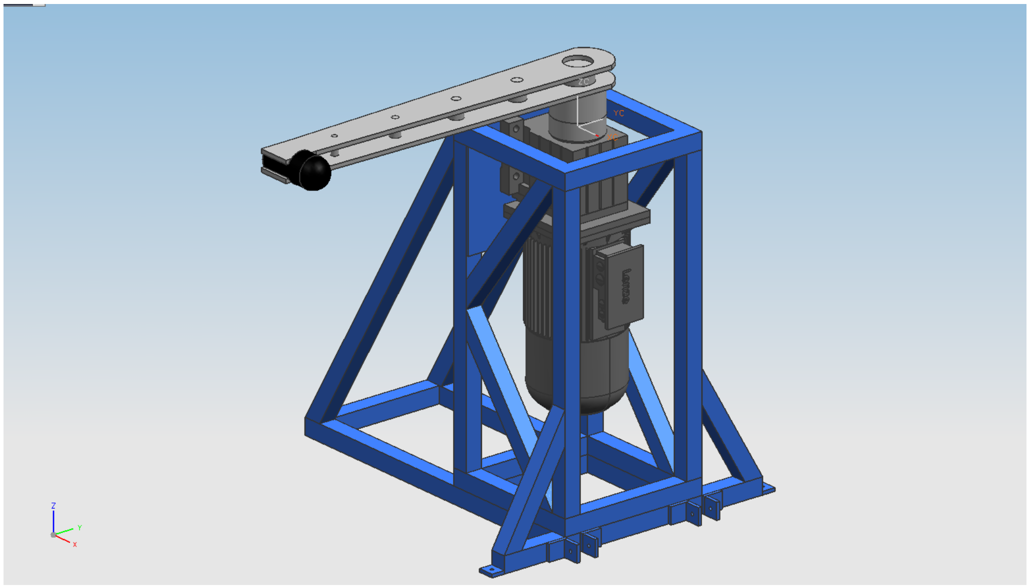

Figure 9.3 CAD of kicking robot (Walker, unpublished thesis).

Leg mass, length and moment of inertia were based on the anthropometric data of a 50th percentile male and a 95th percentile male. These parameters were obtained using formulas derived by Dempster (1955) and Winter (1990). Lengths and masses of the thigh, shank and foot were calculated and input into equation 9.1 to calculate the MoI for each segment about its CG. The overall MoI about the hip was calculated using the parallel-axis theorem.

$$I_{CG} = mk^2 \qquad (9.1)$$

Where, m = segment mass
k = radius of gyration[5]

Using the calculated segmental masses, tissue distributions (i.e. bone, muscle and fat) were estimated according to Clarys et al. (1984) and Clarys & Marfell-Jones (1986) assuming 15% body fat (Table 9.1). This technique was similar to that used in § 5.2.7 and calculations for these parameters are shown in *Appendix C*.

---

[5] Calculated using the segment lengths and Dempster's tables (Winter, 1990)

Table 9.1 Inertial parameters summarised for a 50th and 95th percentile male.

	Whole Body			
Measurements	**50th Percentile**		**95th Percentile**	
Mass (kg)	77		100	
Height (m)	1.78		1.88	
	Segment			
Measurements	**50th Percentile**		**95th Percentile**	
	Inertia			
Inertia about CG (kg·m^3)	3.04		4.41	
	Lengths			
Thigh (m)	0.44		0.46	
Shank (m)	0.44		0.46	
Foot (m)	0.27		0.29	
Masses	***Bone only***	***All Tissues***	***Bone Only***	***All Tissues***
Thigh (kg)	1.17	7.70	1.52	10.00
Shank (kg)	0.55	3.58	0.71	4.65
Foot (kg)	0.17	1.12	0.22	1.45
Total	*1.89*	*12.40*	*2.45*	*16.10*

The mass of the rigid mechanical leg was set at 12.4 kg though bony mass (i.e. rigid) was found to represent only 1.89 kg. This simplification allowed the total leg mass and MoI to be correct whilst providing sufficient strength to maximise the strength-to-weight ratio of the leg. The additional inertial parameters were provided to allow:

1) extra mass (3.7 kg) to be rigidly attached to model the leg to a 95th percentile male with similar MoI;
2) for the feasibility of designing a higher biofidelity single-segment model based on bony and soft tissue masses to be investigated; and
3) for the design and construction of future multi-segment models.

Motor requirements were determined using these inertial parameters and the maximum theoretical impact velocity (Table 9.2). These values were over-specified to ensure that the motor was not at full capacity while in use. In addition, two constraints placed on the motor stemmed from the interaction between the leg and anvil. First, the travel or the total angular distance of the leg had to be equal to or less than 270° before impact to prevent contact with the anvils' housing unit (Fig 9.4). Secondly, the motor must be compatible with a mechanism that will allow it to be freely-rotating at impact to ensure that the generated torque would not crash the motor or fracture the leg. This constraint was also put in place to prolong the longevity of the kicking leg and anvil.

Table 9.2 Maximum motor requirements (adopted from Walker, unpublished thesis)

Leg Length (m)	0.95
Leg Inertia (kg·m^{-3})	6
Leg Mass (kg)	12.4
Linear Velocity (m·s^{-1})	20
Range of Motion (º)	270
Contact Conditions	freely rotating

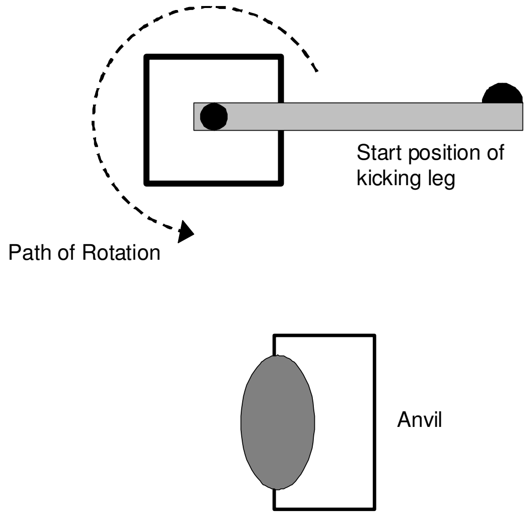

Figure 9.4 Schematic of the interaction between kicking robot and anvil. (Walker, unpublished thesis)

A Lenze 9.2-kW geared servo-motor was selected to drive the kicking leg system. It was capable of rotating the rigid leg to a maximum rotation velocity of 254 rpm (equivalent to an end effector velocity of ~ 25 ms^{-1}) with a torque limiter installed to prevent failure of the motor and kicking leg at impact.

The anvil system consisted of a housing frame, catching frame, support tower and anvil (Figure 9.5). The housing frame was joined to the frame of the kicking leg and was the main support structure for the anvil system. The catching frame, through the use of dampers, was used to decelerate the anvil when impacted and ensured that the anvil did not contact the housing frame. At the base of the housing frame, a universal joint was mounted to allow movement of the 0.5-m support tower atop of which rested the anvil. The anvil was a surrogate torso which TKD hogus were mounted on and impact tested. It was a stadium solid (length = 0.4 m, radius 0.1 m, height = 0.6 m) but actually consisted of a steel cylindrical inner tube (radius = 0.15 m) with an aluminium shell. This shell could be rotated into two configurations to allow hogus to be tested in front-on and side-on impacts. Transmitted force was measured using Newton's 2nd law with acceleration obtained from three tri-axial accelerometers housed within the cylindrical inner tube. The overall mass of the torso (m = 100 kg) and its distance from the universal joint meant that the anvil could be considered as a freely suspended mass.

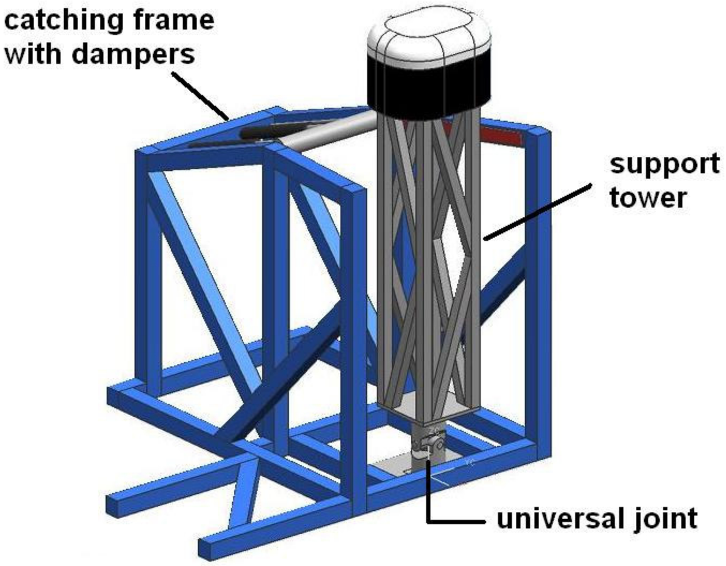

Figure 9.5 Design of mechanical anvil (Walker, unpublished thesis).

9.3.2 Mechanical Model Discussion

The aim of the single-segment mechanical leg was to improve upon the biofidelity of the impactor during *BStan* tests. The development of this model was based on research presented within this section but the physical building and testing of the model was conducted by Walker (unpublished thesis) who was a member of the SCUTA research project. These improvements were thought to create a more realistic effective mass and velocity at impact whilst maintaining the impact consistency in terms of velocity, accuracy and contact area present within current procedures. Despite these adjustments, its biofidelity was not maximised particularly for the effective mass. These limitations are discussed below.

One of the main limitations of the mechanical kicking robot was that it was composed entirely of rigid mass. This design afforded the leg with the proper strength to deliver impacts within the specified safety tolerance. However, rigidly attaching soft tissue to form a model has been found to increase impact force by almost 200% in a drop landing model (Pain & Challis, 2006). Whilst this suggested that the effective mass of soft tissue was much lower than its actual mass, the specific amount was unclear. In a straight-armed palm impact, Pain & Challis (2002) found soft tissues in the forearm continued to decelerate up to 0.0125 seconds post-impact due to its inertia and viscoelastic connections to bone while the heel of the palm came to a complete stop. As whole-body decelerations remained the same (palm did not move post-impact), changes in force from the 'loose' to 'stiff' condition would have resulted from the change in effective mass caused by tissue movement during contact. Soft tissue movement post-impact may act to increase force (through an increased effective mass), but was also more adept at reducing force and dissipating impact energy. The degree of force reduction and energy dissipation and transfer though, was found to be dependent on the stiffness of the muscle at impact. In a TKD roundhouse kick, this uncertainty in soft tissue contribution on impact force was further exacerbated by the fact that the soft tissue motion did not occur in the same direction as the foot at impact.

Another limitation of this model was that it essentially replicated a straight-legged kick despite the movement being much more complex. Previous kinematic investigation into roundhouse kicks, including § 8, has shown that each lower limb segment had its own angular and linear velocity at impact. That is, it has been found to be a co-ordination of limb segments combining to produce linear momentum at impact. Serina & Lieu (1989) found that the relative velocity of the ankle and foot to be much greater than the knee at impact and thus decided that the linear momentum at impact would be generated by the shank and foot only. In contrast, the mechanical leg would convert its rotational momentum into linear momentum of the anvil at impact. This was likely to lead to higher impact forces but its exact influence was unknown.

The material and shape of the end effector were also limitations of this model. The current half-circular end effector was made of nylon, a material more compliant than the steel which comprised the rest of the leg. However, it was still much too stiff to account for the passive stiffness at the hip, knee and ankle joints. This simplified design may have been reasonable in soccer kicks since the compliance in the ball was much larger than the compliance in the ankle and foot

(Tsaouidis & Zatsiorsky, 1996), but that did not apply for this movement. This increased stiffness would have likely led to impacts of shorter contact time and time to peak force whilst increasing impact force. The current shape of the end effector was based on the STI kicking robot instead of anthropometric or experimental data. Whilst the exact influence of this difference in shapes is unknown, changes in loading condition (including impactor surface area) have been shown to change the biomechanical response (§ 2). As such, the end effector shape should be matched as closely as possible.

In spite of the likelihood in producing higher impact forces due to these limitations (which ultimately result in higher effective mass), its performance was offset by its simplicity. This model only had one input – motor torque – and was able to create consistent impacts at velocities comparable to competition TKD. It was for this same reason that the STI soccer kicking robot was used more than the complicated, three-segment Schempf (1995) model. However, it is likely that it is possible to still keep the simplicity but improve upon these limitations.

9.4 General Simulation Model Parameters

9.4.1 Constraints from the Mechanical Model

As discussed, the main aim of this chapter was to develop two computer simulation models (*1-SM* and *3-SM*) to first model the mechanical kicking robot and then provide means of improving it. As such, certain parameters from the kicking robot or the feasibility in building one were used to produce constraints on both simulation models. First, the motor employed in simulation was modelled after the Lenze 9.2 kW motor and disengaged just prior to impact. This imposed a restriction on the maximum torque that could be delivered to the kicking leg thus preserving the longevity of the leg. Second, the angular distance of the limb attached to the motor for both simulation models was restricted to 270° (equivalent to a leg starting position of -90°) to prevent contact with the housing unit of the anvil. Lastly, only passive mechanical components (i.e. spring-dampers) could be used in the actuation of each joint to reduce the complexity of the model.

9.4.2 Computer Simulation Anvil

Whilst a multi-layered model could be constructed to represent each part of the human body or *MBOBXL*, this was a complex and timely process. As such, it was not necessary to generate an impact response for the anvil which was of high biofidelity. However, it was vital to design an anvil which allowed the impactor to mimic human-like performance and to generate a reasonable impact response. To satisfy these requirements, it implied that the anvil had to create a non-rigid impact to absorb most of the impact energy yet create enough stiffness and resistance to have the leg retract passively (a protection mechanism to prolong the life of the mechanical leg). These constraints simplified the design and allowed the anvil to be built as an overall system and not a summation of individual parts.

The anvil consisted of two rectangular cubes of varying mass and thickness connected by a linear spring (Fig 9.6). The larger cube (x-y-z: 0.35 x 0.125 x 0.4 m, m: 80 kg) was the 'rigid' surface and represented the whole body mass whilst the smaller cube (x-y-z: 0.35 x 0.05 x 0.4 m, m: 5 kg) acted as a 'deformable' outer surface. This lighter outer surface was attached to the larger surface with a linear spring (k = 200 Nm^{-1}, c = 100 Nsm^{-1}) and was constrained to move only in the y-axis (i.e. direction of impact). Stiffness was set to allow for an acceptable amount of 'deformation' whilst damping was set to ensure that most of the energy from the kick was absorbed by the anvil and not returned back to the foot. These parameters were also set to visually match the performance of *in vivo* kicks; that is, to ensure that the leg did not rebound immediately off the anvil at contact.

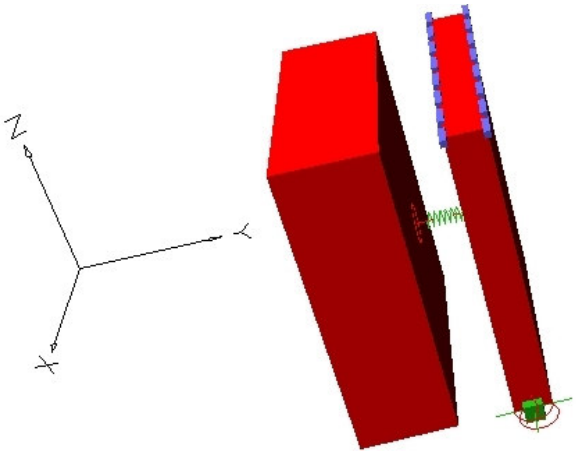

Figure 9.6 Schematic of the anvil used for the 1-SM and 3-SM kicks.

The location of the anvil was referenced relative to the axis of rotation for the motor. From the legs' starting position at 0°, the anvil was placed 0.89 m from the motor axis in the direction away from the knee along the length of the thigh. The surface of the anvil must then be displaced 0.07 m forward against the anticipated direction of impact. This forward distance was instituted to ensure that the kicking leg did not first contact the housing frame of the anvil (if the existing frame size had to increase). Whilst anvil location would not affect the kinematics of the leg pre-impact, it would have an affect on the time of impact and the orientation of the leg at impact. As such, this parameter was also adjusted iteratively with other leg parameters until the overall kinematics were close to matching the recorded human performance. This distance was not measured during *in vivo* kicks so it is unknown how closely this matched human preference or performance.

9.5 Single-Segment Model (*1-SM*)

9.5.1 Design & Model Parameters

The final design of *1-SM* was a single segment leg similar to the leg shown in Fig 9.3 with the same mass and MoI as the mechanical leg. At the hip, a revolute motor was used to drive the leg until it was disengaged just prior to impact. At this moment, a revolute joint allowed the leg to swing freely to create a passive impact. A semi-circular (radius = 0.05 m) impactor made of nylon was used to model the end effector and was placed 0.1 m from the distal end.

For 1-SM, its main performance constraint was its end effector velocity. Impact velocities were calculated using the method outlined in § 6.4.3.3 and the results for each TKD player shown in § 8.3.1. The range in velocities reported was 9.49 – 15.87 ms^{-1} for these athletes, which was slightly less than the 11.9 – 17.62 ms^{-1} which had been previously reported (Table 3.16). To encompass the full range of maximum velocities exhibited from each athlete in § 8, three different velocities were chosen for matching: 12, 14 and 16 ms^{-1}.

Since leg length was constant (~0.78 m from motor to middle of end effector) during the entire movement, the only parameters which needed to be specified were the motor torque and its time of activation from time zero (i.e.

Activation Time). The results of these parameters in generating the three velocities are shown in Table 9.3. Whilst there were other combinations of torque and activation times that could provide the desired angular velocities (and impact velocities), torques were minimised where possible to reduce the power necessary for each impact. This was achieved by setting longer activation times.

Table 9.3 Model parameters for the 1-Segment (*1-SM*) model.

Desired Velocity (m/s)	Angular Velocity (°/sec)	Torque (Nm)	Activation Time (ms)
12	837	63	< 0.39
14	983	97	< 0.354
16	1090	135	< 0.321

9.5.2 Performance

Performance of *1-SM* was evaluated by its impact velocity, impact forces, and internal stresses produced within the leg. Since this model was only dependent on angular velocities, it was capable of producing velocities up to 25 ms^{-1} with the power of the motor from the mechanical leg being the limiting factor. At impact, forces were measured between the contact surface of the end effector and the anvil's lighter outer surface as well as stress analysis (i.e. FE-analysis) of the leg. Whilst these cannot be compared to the results from the kicking robot (data has yet to be collected), impact forces generated from *1-SM* were compared against *3-SM*. Moreover, trends in FE-analysis were also compared between both simulation models. These results are discussed in § 9.6.2.

9.5.3 Discussion

The aim of *1-SM* was to replicate the kinematic performance of the mechanical kicking robot. Whilst this model will suffer from the same limitations discussed in § 9.3.2, it was conducted to validate the modelling procedure and not the mechanical model itself. This was mainly achieved through the examination of high stress concentration areas within the leg at impact. Another aim of the model was that it aided in future developments of a single-segment kicking robot as changes to the existing design could be implemented and tested much quicker. These amendments included, but were not limited to: changing the leg design, adding wobbling masses or changing the end effector.

Similar to the mechanical robot, *1-SM* was composed entirely of rigid mass which was thought to produce erroneously high effective mass. Ideally, the rigid mass would be reduced to the bony mass of the leg to be modelled and the remaining leg mass would be composed of wobbling masses whilst creating the proper moment of inertia. Rather than experimentally determining which materials were suitable, computer simulation would allow different materials of higher strength-to-weight ratios to be examined with stress analysis to provide theoretical characteristics with which future leg materials could be composed. In addition, it would allow investigation into how wobbling masses could be added to replicate soft tissue movement and how they could be attached to the leg to produce the correct moment of inertia.

The compliance of the end effector has also been identified as a limitation of this model. It has been proposed that its compliance could be increased through the addition of one or more linear spring-dampers. This would help to dissipate part of the impact energy but also create a change in the co-ordination of effective mass during impact. Computer simulation would allow different combination of spring-dampers to be tested before the actual model was reconstructed.

9.6 Three-Segment Model (*3-SM*)

9.6.1 Design & Model Parameters

The final *3-SM* design consisted of a motor and revolute joint to represent the hip and spring dampers and revolute joints to control movement at the knee and ankle. The motor was responsible for initiating leg movement and was disengaged to create a passive impact similar to *1-SM*. At the knee, its angle was initially fixed before freely rotating about a revolute joint. As the hip rotated, the entire leg system attempted to conserve angular momentum which led to passive flexion at the knee. Further rotation turned this passive knee flexion into passive knee extension. This was coupled with the activation of a rotational spring-damper to help increase the knee angular velocity prior to impact. Activation of a rotational spring-damper at the ankle, which up until now had been fixed, was made just prior to contact to simulate the joint stiffness at impact.

Parameter values for each mechanical component at each joint combined to produce kinematics to match the performance of measured *in vivo* kicks. This included not only their individual performance characteristics, but also its absolute and relative joint activation time. Each parameter was obtained iteratively, generally from proximal-to-distal, as its performance was dependent on the settings of another parameter. The general strategy was to first set the motor torque until at least ~100° of passive knee flexion was generated. Using the amount of passive extension, initial hip angle, and spring-damper parameters at the knee were determined. Parameters at the ankle were last to be examined.

The kinematic performance of *in vivo* kicks were summarised using the average joint angle-time histories of the hip, knee and ankle found in § 8.3.4 for hard kicks only. These were used to calculate overall angle changes, angular velocities and relative joint activation timings at each joint. Whilst the overall joint angle change was just the difference between maximally flexed and extended positions for a given joint, angular velocities were calculated in two ways. The *Average joint angular velocity* was calculated as the overall change in extension angle divided by the total duration of time necessary for that movement to occur. In contrast, the *Maximum joint angular velocity* was calculated using the greatest rate of change for knee extension angle between any two frames. These values are displayed in Table 9.4.

Table 9.4 Joint angles and overall knee angle change in hard kicks measured from § 8

		Hip			**Knee**		
Subject	**Mean Impact Velocity**	**Angular velocity (°/s)**		**Overall Angle Change**	**Angular velocity (°/s)**		**Overall Angle Change**
		Average	**Maximum**		**Average**	**Maximum**	
1	12.3	-	-	-	945.13	1604.05	71.83
2	13.1	218.15	425.92	20.07	699.00	1367.00	69.90
3	12.1	221.85	462.57	20.41	726.18	1411.93	55.19
7	14.6	100.71	499.46	17.3	837.83	1395.06	50.27
9	11.6	215.08	414.42	24.95	698.25	1343.85	55.86
Average	*12.7*	*184.46*	*458.97*	*20.68*	*742.43*	*1424.39*	*56.43*

Comparing the average angular velocities to previously obtained literature values showed the knee was in the middle of the range, whilst the hip was lower than any value previously reported (Table 9.5). This was likely due to differences in the kicking leg investigated; though all were roundhouse kicks, Nien et al.

(2007) and O'Sullivan et al. (2009) studied the back-leg whilst the front-leg was examined here. The lower hip angular velocities observed in this study were not unexpected as the back-leg roundhouse generated higher impact velocities. This was supported by the smaller range in velocities for the hard kicks found here, 9.49 – 15.87 ms^{-1}, versus the 11.9 – 17.62 ms^{-1} which had been previously reported for back leg kicks (Table 3.16). The execution of back leg kicks allowed the foot to generate higher velocities through a twist of the planted foot and a subsequent larger twist of the torso. It was also expected that the distance of the anvil would affect the impact velocity, but this parameter was not examined (Falco et al., 2009). In terms of the overall joint angle change, only the knee had been reported in previous literature. The ~ 56° change in angle observed here was within the range found by Kong et al. (2000) which reported 67.6 ± 22.9°.

Table 9.5 Summary of joint angular velocities of roundhouse kick from literature.

Study	Maximum Angular Velocity		
	Hip	Knee	Ankle
Kong et al. (2000)		913.29 ± 308	
Nien et al. (2007)	-533.21 ± 79.06	1736.86 ± 321.53	999.86 ± 200.7
O'Sullivan et al. (2009)	693 ± 115	1586 ± 181	

Relative joint activation timings referred specifically to the time at which the clutch should engage (at the hip) and the knee and ankle spring-dampers should be activated to create the proximal-to-distal chain exhibited in a roundhouse kick. This was achieved by re-examining the combined plot of hip, knee and ankle angles as a function of time (Fig 8.8). As this plot was normalised to impact, joint angles were used to determine a *local* activation time – a time relative to the frame of impact – for each joint; e.g. the local activation time for the knee would specify when the knee joint changed from flexion to extension relative to the frame of impact. However, the local timings of hip, knee and ankle activation (or de-activation) were dependent on the values of motor torque and the rotational spring-damper characteristics; that is, a change in one of these parameters led to the adjustment of another. As such, the determination of each parameter could not be achieved individually and had to be obtained iteratively. Whilst these times were determined locally each had to be specified *globally* (relative to each segment's starting position at time zero). Local activation timings ensured that the proper kinematics were achieved during execution, whilst the global activation time was responsible for the actual programming of the movement.

All relevant characteristics for each parameter are displayed in Table 9.6. The initial knee angle was set to 0° (i.e. straight) to generate passive knee flexion whilst the ankle was fixed at 15° dorsi-flexion to maintain its pre-impact angle. Significant stiffness and damping was placed at the knee and ankle to ensure that their joints did not hyper-extend during or after impact.

Table 9.6 **Characteristics for each mechanical** component in 3-SM along with key performance measures at the knee and hip.

Velocity (m/s)			**12.1**	**14.0**	**16.0**
Hip		**Initial Angle (°)**	-175	-180	-180
		Maximum Hip Angular Velocity (°/s)	782	870	936
		Hip Angular Velocity at Impact (°/s)	64.9	41.9	179
	Torque	**Value (N·m)**	56	70	82
		Active (s)	< 0.49	< 0.42	< 0.38
	Revolute	**Active (s)**	> 0.48	> 0.41	> 0.37
Knee		**Initial Angle (°)**	0	0	0
		Maximum change in knee angle (°)	58.8	62.6	69.7
		Time between knee flexion & impact (ms)	86	79	79
		Knee Angular Velocity (°/s)	1730	1870	2350
	Fixed	**Active (s)**	< 0.12	< 0.12	< 0.115
	Revolute	**Active (s)**	always	always	always
	Spring	**Resting Length (°)**	-5	-5	-5
		Spring Constant (N·m/°)	11.5	19	22
		Damper (N·m·s/°)	0.31	0.31	0.31
		Active (s)	> 0.431	> 0.4	> 0.367
Ankle		**Initial Angle (°)**	15	15	15
	Fixed	**Active (s)**	< 0.402	< 0.395	< 0.361
	Spring	**Resting Length (°)**	10	10	10
		Spring Constant (N·m/°)	10	10	10
		Damper (N·m·s/°)	1	1	1
		Active (s)	> 0.401	> 0.395	> 0.360

Maximum hip and knee angular velocities were slightly higher than literature reported values (Table 9.5) but were almost twice the magnitude as the average of all players observed in § 8 (Table 9.4). This discrepancy, particularly in the hip, existed as this joint had a much larger angular distance to travel in a restricted amount of time to maintain the co-ordination timing at the knee. In addition, it helped compensate for the lack of linear translation at the hip in generating linear velocity at the foot.

9.6.2 Performance

In § 8.3.4, three moments were identified to help describe the co-ordination and execution of a hard front-leg roundhouse kick and this plot is re-shown here (Fig 9.7, 9.8). In brief, moment 1 indicated the transition between flexion and extension of the knee whilst the hip continued in extension. Moment 2 highlighted the beginning of impact and occurred, on average, 76 ms after the start of moment 1. Lastly, moment 3 marked the end of contact and began the retraction (i.e. knee flexion) of the leg.

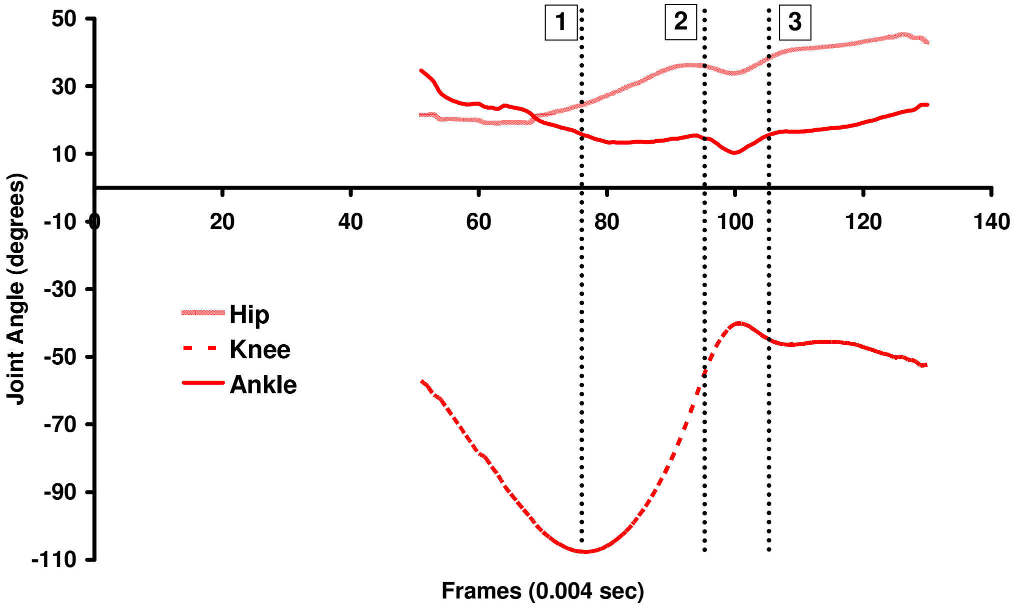

Figure 9.7 Plot of all hip, knee and ankle joint angles for an average hard kick (Fig 8.7

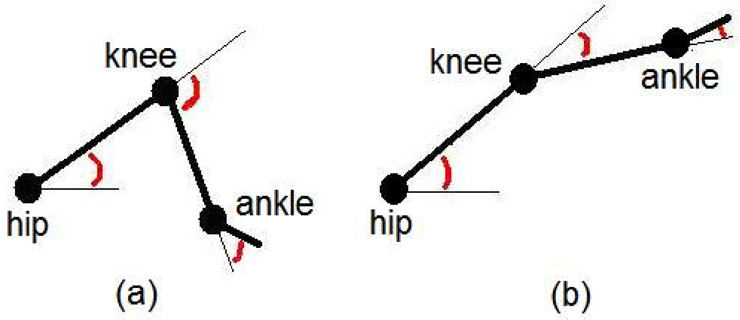

Figure 9.8 Schematic showing the relationship between joint angles and limb segments at two instances of Fig 8.7; (a) Moment 1 and (b) mid-contact

The joint angle-time plot from *in vivo* kicks was compared to the hip and knee joint angles produced by the 3-SM (Fig 9.9, 9.10). Throughout the entire movement, hip angles were found to be different between *in vivo* and simulation performances. This disparity was mainly a function of the starting position for each model. *In vivo* kicks were performed by the front leg meaning that the hip only had to undergo ~ 20° of extension before impact. In contrast, *3-SM* had to extend ~180° before making contact. As such, not only was the overall change in angle different at all times, but the angular velocities were also much higher than the average hip angular velocity reported in human kicks (~460°). Moreover, the fixed hip joint of 3-SM meant that the linear velocity of the hip was zero. In contrast, knee angles were quite similar from 0.8 s prior to maximum knee flexion up until just after contact.

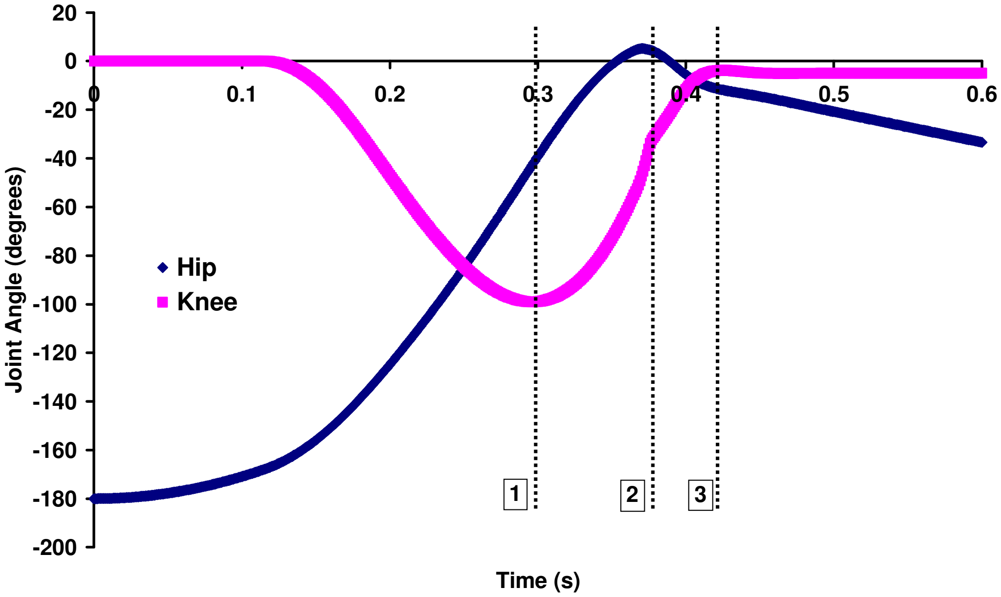

Figure 9.9 Plot of hip and knee angles during a 16 ms^{-1} kick by the *3-SM* kicking robot. Ankle joint angle not included as it was held to 15° dorsi-flexion until moment 2.

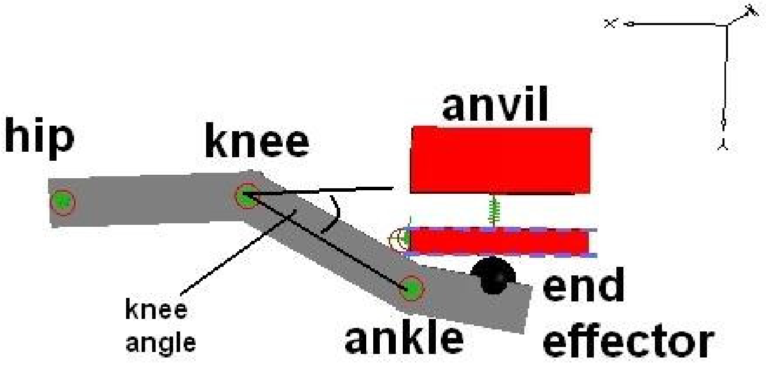

Figure 9.10 Schematic of 3-SM with anvil just prior to impact. Hip angle not shown as it is virtually zero (~4.2°) at impact.

For *in vivo* kicks, the knee started straight (i.e. 0°), flexed ~ 110° to reach maximum flexion, extended from moments 1 and 2 by ~ 56° and underwent gradual flexion post-impact. Similarly, the model exhibited ~ 100° of knee flexion and between 58.8 – 69.7° of knee extension before impact depending on the impact velocity. Slight differences in time were also observed with the model spending between 79 – 86 ms between moments 1 and 2 compared to 76 ms in human performance. However, angular velocities were not affected as the longer duration knee extension was offset by slightly larger knee extension angles. In general, pre-impact kinematics were reasonably matched, but the passive impact generated meant that post-impact kinematics could not be controlled. Whilst this helped prolong the life of the leg and anvil and helped retract the leg, this led to considerably shorter contact times as hip flexion continued post-impact.

Despite the disparity in kinematic performance at the hip, there was evidence to suggest that *3-SM* was an acceptable model. Serina & Lieu (1991) found that the linear velocity at the hip and knee was 3% and 7%, respectively, of the toe velocity at impact. Similarly, Nien et al. (2007) reported maximum hip and knee linear velocities were ~ 18% and ~ 47%, respectively, of the maximum toe velocity. Whilst this latter study found greater percentages, these were maximums and it was likely that these occurred well before impact as shown by the decrease in angular velocity at the hip in Fig 9.7. In the *3-SM* model, the hip was fixed so linear hip velocity was zero. Hip angular velocity was ~ 3.1 $\text{rad}\cdot\text{s}^{-1}$, which equated to a linear velocity at the knee of ~ 1.3 ms^{-1} or 8.4 % of the linear velocity at the toe for a 16 ms^{-1} kick. Moreover, the maximum hip angular velocity was 16.3 $\text{rad}\cdot\text{s}^{-1}$, equivalent to 7.17 ms^{-1} or 44.8% of a 16 ms^{-1} kick. As such, these results did not differ much from the Serina & Lieu (1991) and Nien et al. (2007) studies providing evidence that this model could be considered acceptable.

9.6.3 Comparison: 1-SM and 3-SM

As this model had similar kinematics to an *in vivo* roundhouse kick, the impact forces produced between *1-SM* and *3-SM* were compared which allowed the influence of the straight-legged design to be investigated as mentioned in § 9.3.2. Whilst both models were constructed of rigid parts, the effective mass for each model was inevitably different despite the same leg mass and end effector impact velocity. In the 16 ms^{-1} kick, the 1-SM had a large mass (12.4-kg leg) moving at an angular velocity of 1090 °/s. This produced up to 40% larger forces than the 3-SM which essentially had a lighter mass (4.7-kg shank and thigh) moving at a knee angular velocity of 2350 °/s at impact (Table 9.7). As impact velocity for each model was the same, higher forces and longer TTPF for *1-SM* indicated a higher effective mass compared to 3-SM. This showed that *3-SM* would, in fact, be an upgrade over *1-SM* in obtaining a realistic response as it was able to decrease the force magnitude at similar impact velocities. This decreased magnitude was expected due to the different timings of the rigid masses used, as discussed throughout this chapter, and the impact properties of the anvil which had a significant influence on the forces measured as discussed in § 5. In addition, the low TTPF indicated that a more compliant end effector was necessary to generate a more realistic response. As such, it was inappropriate to compare the impact forces measured between *in vivo* kicks and simulation models in too much detail and only relevant to compare the performances between *1-SM* and *3-SM* as the anvils were the same.

Table 9.7 Comparison of impact forces and time to peak force between 1-SM and 3-SM

Velocity (m/s)	**Single Segment (1-SM)**		**Three Segment (3-SM)**	
	Impact Force (N)	**TTPF (ms)**	**Impact Force (N)**	**TTPF (ms)**
12	5620	3	4400	1
14	6380	3	4540	1
16	6810	3	4850	1

In addition to comparing impact forces generated between models, FE-analysis was performed to determine the difference in stress concentrations between the two models. To validate the procedure, FE-analysis was first performed on *1-SM* (Figure 9.11). The highest stresses were found at the time of peak impact force and were located in the distal half of the leg. Similar to a cantilever beam with end loading, high levels of tensile stress found on the side nearest the anvil and high compressive stresses on the opposite side. Stresses at the support were minimised by allowing the leg to passively retract using a revolute joint. This provided support that the software produced reasonable results and allowed a similar analysis to be conducted for *3-SM.*

In *3-SM*, the magnitude of peak stresses throughout the leg were much lower than *1-SM*. This was likely due to the lower impact forces generated as a result of the compliance from the end effector and ankle and knee joints (i.e. spring-dampers). The largest stresses were observed in the shank which experienced the same tensile and compressive stresses observed in 1-SM. Surprisingly, large stresses were not found at the connection point between segments as the discontinuity in geometry at the joint has generally been found to be an area of high stress concentration. Whilst the mesh in the area of the discontinuity may not be accurate, it was more likely that the direction of impact (i.e. normal to the foot) and the freely rotating joints would not cause large shearing stresses at the joints.

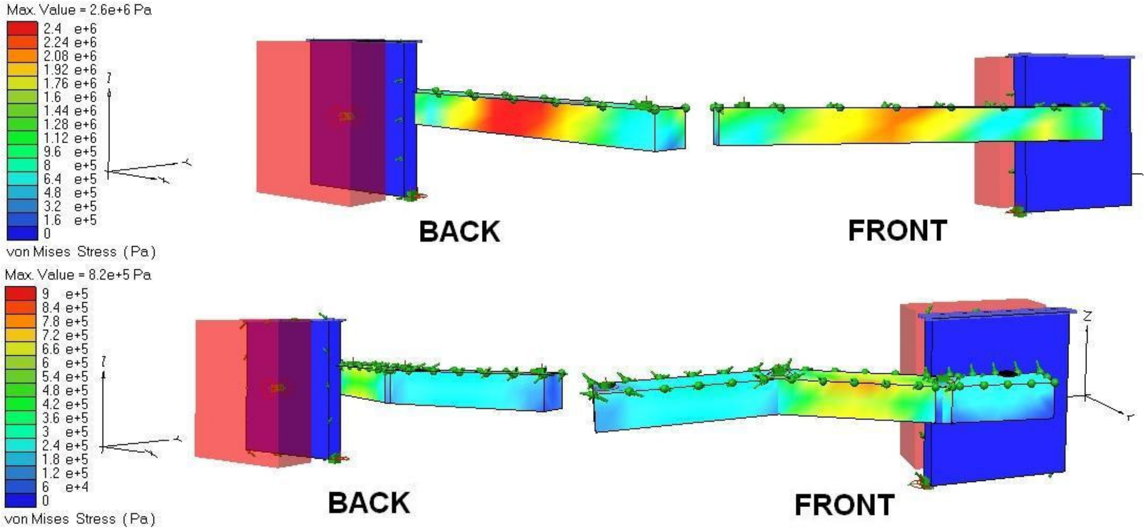
Max. Value = 2.6e+6 Pa
2.4 e+6
2.24 e+6
2.08 e+6
1.92 e+6
1.76 e+6
1.6 e+6
1.44 e+6
1.28 e+6
1.12 e+6
9.6 e+5
8 e+5
6.4 e+5
4.8 e+5
3.2 e+5
1.6 e+5
0
von Mises Stress (Pa)
BACK
FRONT
Max. Value = 8.2e+5 Pa
9 e+5
8.4 e+5
7.8 e+5
7.2 e+5
6.6 e+5
6 e+5
5.4 e+5
4.8 e+5
4.2 e+5
3.6 e+5
3 e+5
2.4 e+5
1.8 e+5
1.2 e+5
6 e+4
0
von Mises Stress (Pa)
BACK
FRONT

Figure 9.11 FE-analysis for 1-SM (*top*) and 3-SM (*bottom*) showing each side of the leg.

9.6.4 Discussion

Similar to *1-SM*, this model improved upon the impactor used in *BStan* tests by adjusting the effective mass whilst maintaining consistency in impact velocity, contact area and impact location. However, *3-SM* had some distinct advantages over *1-SM*. First, the multi-segment, multi-joint design offered an improvement upon the effective mass. Whilst each segment was still rigid, the sequential limb movement meant that the inertia of the entire leg did not act at impact. Second, the overall system was more compliant due to the knee and ankle joint stiffness modelled using the rotational spring-dampers. This ensured that at impact all energy was not imparted onto the anvil and also helped in reducing the effective mass. Lastly, it allowed the role of each limb and joint in generating impact intensity to be investigated; that is, to adjust the co-ordination of the limbs to determine its influence on impact intensity.

Despite improvements introduced within *3-SM*, it was still unclear exactly how well this model performed relative to the actual kick performance. Whilst kick kinematics were greatly improved, a computer model of *MBOBXL* was not designed so any impact characteristics obtained within the software could not be directly compared to the results summarised in § 8. Instead, the implications of its design on impact intensities would have to be examined theoretically. First, using rigid masses instead of wobbly soft tissue mass found *in vivo* would increase the impact intensity through increased effective mass and decreased energy dissipation. However, the extent of this phenomenon was unclear in a rotational impact, particularly with multiple joints and segments. Second, the parameters of the spring-dampers were designed to produce correct kinematics pre-impact, but it was unknown how closely they matched the stiffness during contact. This would have a pronounced effect on the contribution of proximal segments on effective mass as it would help to dissipate part of the impact energy. As such, it was possible that the spring-dampers could offset the exclusion of soft tissue and *3-SM* may be a more effective model than the results have shown.

One of the major limitations of this model was that it took a multi-planar movement and simplified it into a single plane. As such, parameters such as hip adduction and rotation, which have been found to significantly contribute to the initiation of this kick, were not modelled. Whilst a multi-planar robot would be ideal, it would be significantly more complicated and may never reach the desired level of accuracy. This model was similar to Serina & Lieu (1991), which also only modelled this movement in the plane of flexion-extension, but this model included the movement about the hip and of the thigh instead of simplifying it to just knee extension. Whilst this model (Fig 9.8, 9.9) was unable to match the hip angles and hip angular velocities during the three outlined phases outlined within human performance (Fig 9.6, 9.7), this was only a function of the starting position of the leg or the angular distance in which the leg had to travel. In addition, it was also affected by the constraints presented by the motor. The motor required the leg to start from rest and was driven by constant torque increasing hip angular velocity at a constant rate. In order for the motor to produce the required angular velocity within the same angular distance as a human kick (~ 17°), it would have to be extremely powerful. As cost was a design constraint, it would not have been possible to obtain a motor which could accelerate the 3-SM could at the same rate of a human kick.

A simplification of *3-SM* was that the ankle was fixed to 15° plantar-flexion through the duration of the kick except for just prior to impact. It was assumed that this would not have an effect on the overall kinematics and was designed in this way for ease. This seemed like an acceptable simplification since the ankle angle didn't seem to exhibit much change until just prior to impact. In this way, the ankle joint was not wholly ignored allowing its passive joint stiffness to contribute towards the compliance of the kicking robot at impact.

9.7 Conclusion

Using inertial parameters and anthropometric data of average individuals, a multi-segment (*3-SM*) model, based solely on mechanical components, was designed to match the kinematics of *in vivo* roundhouse kicks. Whilst *1-SM* and *3-SM* were not compared to the performance of a physical model, analysis showed that this model would help reduce impact forces through an improvement in the effective mass of the kicking leg model. In addition, internal stresses were also found to decrease in the *3-SM* suggesting that it may be feasible to construct a leg with these parameters to improve upon future hogu tests even further beyond the mechanical leg presented. Future work should look to perform a proper validation using results from § 8 and techniques presented in this section.

Chapter 10

Conclusion

10.1 Chapter Overview

Overall research aims are reviewed from § 1. Research questions posed in § 1 are also presented and then addressed with reference to major findings obtained in § 5 - § 9 through experimentation. Limitations for the overall research are examined. Finally, implications of this research and future directions are discussed.

10.2 Research Aims

The main aims of this research were to:

1) Collate impact intensity, injury risk and injury prevalence data from automobile, ballistics and sport research with specific reference to injury mechanisms, human impact responses and personal protection.
2) Examine factors which influenced the human biomechanical response
3) Examine the biofidelity of current testing techniques for obtaining impact intensities and assessing Personal Protective Equipment (PPE) performance in Tae Kwon Do (TKD).
4) Present methods of improving anvil and impactor properties to generate more realistic impact characteristics

These aims were addressed in each experimental chapter, § 5 - § 9, and focused on impacts in sports as a whole with particular attention paid to roundhouse kicks in TKD.

10.3 Research Questions

The following reviews the research questions posed in § 1 and references specific findings from each experimental chapter to discuss how these questions were addressed.

Q1. *How do the impact properties of a human anvil change its biomechanical response and predictions for injury?*

During impact, human anvils change material impact properties to reflect relaxed or tensed muscle. Previous research has focused on the effects of these muscle states for serious injuries (i.e. fractures) and found that, in spite of large increases in stiffness, it did not influence the occurrence of reversible or lethal injuries. However, this ignored an athlete's discomfort to impact and common injuries such as contusions which can be as detrimental to performance as more 'serious' injuries. In § 5, a deformable impactor was dropped onto relaxed and tensed muscle *in vivo*. Across the group of athletes, tensed muscle was found to increase impact force by ~ 11%. Soft tissue deformation was also found to decrease with one player exhibiting a ~ 33% reduction. As such, this supported the claim from previous research of an increased stiffness with muscle tension. This increased stiffness was positively correlated to a decrease in perceived impact intensity (mean was 3 levels lower on the Borg CR10 pain scale) and energy absorption (~ 10% decrease across all impacts for the entire group). As the injury mechanism for perceived intensity and soft tissue injury was likely similar (i.e. deformation), it was suggested that tensed muscle had a role in injury prevention. Moreover, it was thought that tensed muscle was more adept at dissipating impact energy whilst the increased stiffness not only reduced deformation but also changed the ratio of compliance between the anvil and impactor causing more impact energy to be absorbed by the impactor. A larger soft tissue thickness, expressed as a muscle mass to length ratio, was also found to decrease the risk for soft tissue injury in relaxed and tensed muscle.

Q2. What effect does test equipment (i.e. impactor, anvil) have on the assessment of Personal Protective Equipment (PPE) performance, specifically hogus?

In § 7, limitations of the current methodology (i.e. rigid anvil and impactor) for assessing the performance of hogus were discussed. The main argument was that colliding bodies act in-series and include any materials (including PPE) sandwiched in between during impact. As such, PPE performance is dependent not only on its specific material properties, but also on the ratio of compliances between the anvil and impactor. Since the main focus of this research was on human collisions (i.e. deformable bodies), the anvil and impactor needed to also reflect this compliance.

Using existing (i.e. *BStan*) methods, hogus were found to deform in a point-elastic manner whilst performance, measured in terms of transmitted force, was found to correlate positively with hogu mass. Heavier hogus (adidas EBP, confor) were found to produce nearly half the transmitted force than lighter-weighted hogus (adidas, kwon). When the rigid anvil was replaced with a high-biofidelity anvil in method *MBS*, hogu performance improved through an increase in effective mass as the deformable anvil and hogu worked in-series. This highlighted the importance of using a representative anvil as transmitted forces reduced nearly ten-fold despite the use of the same rigid impactor. In the *Competition* method, the high biofidelity anvil and an *in vivo* impactor were used to provide more realistic impact characteristics by eliminating the need to match the effective mass and impact velocity of the kicking leg. Though impact forces were within the same range as *BStan* methods, TTPFs were 75% shorter and CTs were twice as long suggesting the impact energy and the energy absorbed was significantly different. As energy absorption has been identified as a likely mechanism for reducing injury, it would be important that hogus are tested at the correct impact conditions. The *Competition* method was also able to show the sensitivity of hogu performance to loading rate as velocities were roughly six times higher for the *in vivo* impactor. These results showed the importance of testing condition on hogu performance and advocated that impact characteristics should match *in vivo* performances as closely as possible.

Q3. How can the surrogate mechanical anvil and/or impactor be improved to produce an impact of higher biofidelity?

Mechanical anvils generally match the size, shape, mass and kinematics of humans, but not an *in vivo* impact response. Similarly, martial arts training devices have similar size and shape, but are designed with much greater compliances to protect the athlete whilst not necessarily producing realistic impact responses. However, surrogate mechanical anvils can be improved by closely matching their dynamic impact properties to *in vivo* performances. In § 6, elite martial artists performed front roundhouse kicks onto a human anvil (*in vivo*) and three different surrogate anvils (modified versions of a martial arts training device, *BOBXL*) whilst recording force and impact velocity. Model *MBOBXL*, which consisted of a restricted base, increased thoracic stiffness and an overlying hogu, was found to most minimise the RMSE and residual values when compared to *in vivo* impacts delivered to a human anvil sporting the same hogu. In addition, *MBOBXL* performance was found to lie within the 95% CI created by the range of *in vivo* impacts. This provided support that *MBOBXL* could be a suitable replacement for the human anvil and be used in future testing. Whilst the biofidelity of this anvil was not fully maximised, this procedure produced a simple technique that could be applied to any sport so long as there were *in vivo* impacts to compare against the surrogate anvil impacts. It was suggested that the impactor type used for the validation procedure should reflect the intended use of the anvil; that is, if roundhouse kicks are to be examined, the matching of biomechanical responses should be validated specifically for that attack.

The mass and impact velocity of existing rigid impactors have often been arbitrarily chosen to produce a level of pre-determined impact energy. However, impacts such as roundhouse kicks are co-ordinated movements of multiple leg segments which change effective mass and compliance throughout the duration of impact. As such, a single mass often produced artificially high impact forces (when tested with a rigid impactor) and low impact velocities. Whilst using a human impactor would eliminate the need of a surrogate, human impacts were found to be inconsistent. Standard deviations for parameters such as impact velocity, force and location were found in § 8 to be as high as 0.97 ms^{-1}, 0.5 kN and 91.6 mm, respectively, when players performed a kick in which the main aim was to inflict the most damage. A simple improvement to the classic rigid impactor was first obtained in a single segment leg by examining peak kick velocities and attempting to match inertial parameters for a 50th and 95th percentile male (§ 9). Whilst this ensured correct loading rates, the effective mass was still shown to be too high. As such, data on impact force, contact time (CT) and time to peak force (TTPF) collected in § 8 was used to ensure that impact energies at the prescribed loading rates were more correct. The co-ordination of three masses (akin to the thigh, shank and foot) and using the same inertial parameters would then provide a model which could further improve the rigid model. This design would serve as a compromise between the rigid and human impactors and may become an integral part of future impact testing.

Q4. *Can the impact intensity of a roundhouse kick be obtained with non-invasive modes of measurement during competition?*

A caveat of obtaining impact intensities in an artificial or controlled environment was that these measurements may not have been indicative of impacts most commonly found in competition. However, obtaining these intensities was an inherently difficult task as any measurement device could not be found to harm or hinder the movement of the athlete. Throughout this research, it had been hoped that research within WP6 would have been successful at embedding sensors into a TKD hogu. However, this proved to be unsuccessful due to issues associated with spatial accuracy, signal transmission and robustness. As these issues were speculated at the start of the project, another method for obtaining impact intensities non-invasively was sought. In § 8, multiple high-strength (all > 0.70) relationships were formed between impact force and impact velocity, measured using a 3-D motion analysis system. Whilst this passive motion analysis cannot be used during competition, a similar analysis can be conducted using multiple 50-Hz video cameras – a technique that has been employed in other research to obtain kinematics in sports non-invasively. Whilst there would be little reason to suggest that this technique would be inadequate for this analysis, this process should be validated to assess its reliability in future work.

10.4 Research Limitations

The primary aim of this research was to examine how human impact responses (and their relationship with injury) have been measured in previous research and to propose improvements upon current techniques to increase its biofidelity. Whilst this showed the novelty of this research, the method for obtaining these measurements remained one of its primary limitations. This and other research limitations are discussed in the following.

In § 1, *impact intensity* was defined as the measure of a mechanical variable which related to a probability for injury with higher intensities indicating a higher probability. However, injuries could not be instigated, particularly *in vivo*, due to the underlying ethical issues associated. This was problematic as the mechanisms and probability for injury had to be inferred and not observed directly. Whilst cadavers or animal models have been used in similar research to generate injury, this option was not readily viable. As such, the focus was not on creating impact models but on improving the biofidelity of existing surrogates particularly at low impact intensities (i.e. no injuries caused). Impact intensities measured using these models were then related to existing literature to infer injury probability or PPE performance. As such, it was still unclear how closely these new models would be to an *in vivo* injury model. Instead, it served to lessen the gap between the classic artificial rigid test and a fully *in vivo* injury model.

Measuring these impact intensities introduced another major limitation in this research. The Tekscan F-Scan Mobile system was used as it was found to have the greatest balance between force threshold, sampling frequency, durability, cost and portability (§ 4). However, it was still unable to perform reliably in this research as shown in its inability to produce a consistent calibration curve (§ 4), its variability when used on deformable objects (§ 6) and low sampling frequency and multiplexing (§ 7). Whilst the CFP was more reliable at measuring force, its rigid structure meant that it could not be used on deformable surfaces as it would automatically change the impact properties of the impact area. In fact, its use on deformable structures also limited the types of variables (i.e. acceleration or deformation) that could be reliably measured. Part of the SCUTA project was to develop novelty impact intensity measuring devices which would be embedded into existing PPE, but research is still ongoing. As such, the reliability of results was more a function of the lack in technology instead of poor methodologies.

In § 8, the kinematics of a roundhouse kick were examined to develop an "*impact force – impact velocity"* relationship and for use as input into a mechanical model designed to produce more consistent impacts. Joint kinematics were analysed (i.e. projected) only in the horizontal plane with velocities and forces taken in an axis perpendicular to the anvil surface within that plane. As such, out-of-plane movement, such as hip abduction, which may have contributed to the generation of these velocities or forces were not included. This meant that the joints in a planar model would have to compensate for the lack of out-of-plane movement to produce similar characteristics at impact. Whilst this may have been an unacceptable simplification, a planar model was much easier to design and control than the multi-planar model described in § 9. Another limitation with these measurements was the size of the target area and CFP. Any oblique or off-centre impact, with respect to the force sensor or CFP, was discarded as these results would show similar impact velocities with potentially significantly less force. This would further exacerbate the variation in force measurement beyond just the inadequacies of the equipment. However, the impact location could not be verified to account for this phenomenon until a thorough analysis was conducted. As such, each player may not have had the same number of kicks analysed for each type as their number of kicks was fixed complicating the statistical analyses.

10.5 Future Directions

10.5.1 Product Design Specification (PDS)

One of the main motivational factors of this research was to aid in the development of custom-tailored, impact mitigating PPE (§ 1.2). As such, each review and experimental chapter can be used as input into PPE design with a specific focus on TKD hogus. Existing literature from the automotive, ballistics and sport industry were collated to determine possible injuries, injury mechanisms and injury tolerances to the chest an abdomen. An in-depth look into human and surrogate anvils, as well as human and surrogate impactors provided insight into methods of testing future PPE performance. In addition, impact parameters such as force, velocity, CT and TTPF were obtained to provide measures of protection performance. However, as this was only conducted for a roundhouse kick, it can and must be extended out to other forms of attacks in TKD or for other PPE such as shin guards or cricket leg guards to ensure that their designs and protection reflect the types of impacts found in their respective sport.

10.5.2 Automated Scoring in TKD

The subjectivity of scoring in competition TKD has long been a point of debate. Currently, points in TKD are awarded when a powerful blow is delivered and are determined based on the opinion of four corner judges. However, it is unclear what is meant by 'powerful' as points could be based on the assumed kick velocity or impact force, the sound at impact and/or the victim's response. To reduce this subjectivity, a threshold can be established by assigning each impact with a value of '0' for non-scoring impacts and a '1' for point-scoring blows. All impact forces or velocities can then be plotted as a function of their respective value, '0' or '1', and a logistic curve can be fitted to the data. This would provide an objective threshold to distinguish between point and non-point scoring blows during competition. Moreover, this procedure could be conducted at all age levels and weight categories to determine adjusted thresholds for scoring. In addition, this would also provide an indication for the most common impact intensities observed during competition.

10.5.3 Multi-segment Kicking Robot

Using the model developed (or the modelling procedure) outlined in § 9, amendments to the existing mechanical robot can be explored. Materials of greater strength-to-weight ratio can be trialled to produce different leg shapes and ways of attaching wobbling masses or elastically attaching rigid masses. Different end effector designs and materials can also be examined further to provide greater compliance at impact These amendments will help improve upon the current mechanical testing techniques by improving upon the effective mass whilst maintaining the impact velocity used in the mechanical robot. This can then be coupled with future high-biofidelity anvils to help determine injury potentials or assess the performance of PPE.

REFERENCES

AGEL, J ET AL. (2007). Descriptive Epidemiology of Collegiate Men's Soccer Injuries: National Collegiate Athletic Association Injury Surveillance System, 1988-1989 Through 2002-03. *Journal of Athletic Training*, 42 (2), 270-277.

AHERNE, B. (2006). UK TKD Championships: Personal INTERVIEW. Loughborough University, Oct 2006.

ANKRAH, S & MILLS, NJ. (2002). Ankle protection in Football shin guards. In: *The Engineering of Sport 4*, Ed. S. Ujihashi & SJ Haake, 128-135.

ANKRAH & MILLS, NJ. (2003). Performance of football shin guards for direct stud impacts. *Sports Engineering*, 6, 1-14.

ANKRAH & MILLS, NJ. (2003a). Analysis of ankle protection in football. *Sports Engineering*, 6, 1-12.

APRIANTONO, T ET AL. (2006). The effect of muscle fatigue on instep kicking kinetics and kinematics in association football. *Journal of Sports Sciences*, 24(9), 951-960.

ATHA, J ET AL. (1985). The damaging punch. *British Medical Journal*, 291, 1756- 1757.

BACHUS ET AL. (2006). Measuring contact area, force, and pressure for bioengineering applications: Using Fuji Film and TekScan systems. *Medical Engineering & Physics*, 28, 483-488.

BACKAITIS, SH & ST-LAURENT, A. (1986). Chest Deflection Characteristics of Volunteers and Hybrid III Dummies. *30th Stapp Car Crash Conference*. SAE Paper 861884, 157-166.

BARFIELD, WR ET AL. (2002). Kinematic instep kicking difference between elite female and male soccer players. *Journal of Sports Science and Medicine*, 1, 72-79.

BECKMAN, DL ET AL. (1970). Thoracic force deflection studies in living and embalmed primates. *J Biomechanics*, 3, 551-555.

BEDEWI, PG. (2001). A review of biomechanics in automotive safety. *Int. J. Vehicle Design*, 26(4), 407-429.

BEIS, K ET AL. (2007). Taekwondo techniques and competition characteristics involved in time-loss injuries. *Journal of Sports Science and Medicine*, 6 (CSSI-2), 45-51.

BIR, CA & VIANO, DC. Biomechanical Predictor of Commotio Cordis in High-Speed Chest Impact. *The Journal of Trauma: Injury, Infection and Critical Care*, 47 (3), 468-473.

BIR, C & ECK, J. (2005). Preliminary Analysis of Blunt Ballistic Impacts to the Abdomen. In: *IUTAM Symposium on Impact Biomechanics: From Fundamental Insights to Applications*. Wayne State University: Michigan, 25-32.

BIR, CA ET AL. (1995). An analysis and comparison of soccer shin guards. *Clinical Journal of Sports Medicine*, 5 (2), 95-99.

BIR, CA ET AL. (2004). Development of biomechanical response corridors of the thorax to blunt ballistic impacts. *Journal of Biomechanics*, 37, 73-79.

BLUM, H. (1977). Physics and the art of kicking and punching. American *Journal of Physics*, 45 (1), 61-64.

BODEN, BP ET AL. (1999). Tibia and fibula fractures in soccer players. *Knee Surg.*, 7, 262-266.

BOEY, LW & XIE, W. (2002). Experimental investigation of turning kick performance of Singapore National Taekwondo players. *XX ISBS Conference*, 302-305.

BRIMBACOMBE, JM ET AL. (2009). Effect of Calibration Method on Tekscan Sensor Accuracy*. Journal of Biomechanical Engineering*, 131, 1-4.

BROOKS, JHM & FULLER, CW. (2006). The influence of methodological issues on the results and conclusions from epidemiological studies of sports injuries. *Sports Med*, 36 (6), 459-472.

BS 6183-1:2000. Protective equipment for cricketers – Part 1: General Requirements, *British Standards*, London.

BS 6183-3: 2000. Protective equipment for cricketers – Part 3: Leg protectors for batsmen, wicket keepers and fielders, and thigh, arm and chest protectors for batsmen, *British Standards*, London.

BS EN 13277-1: 2000. Protective equipment for martial arts – Part 1: General requirements and testing methods, *British Standards*, London.

BS EN 13277-3: 2000. Protective equipment for martial arts – Part 3: Additional requirements and test methods for trunk protectors, *British Standards*, London.

BS EN 13061: 2001. Protective Clothing – shin guards for association football players, *British Standards*, London.

BURKE, DT ET AL. (2003). Effect of implementation of safety measures in tae kwon do competition. *Br. J. Sports Med.*, 37, 401-404.

BUSH, IS & CHALLENER, SA. (1989). An assessment of criteria for the prediction of contusion injury under non-penetrating thoracic impact. *1989 Proceedings of IRCOBI*, 111-122.

CASWELL, SV & DEIVERT, RG. (2002). Lacrosse helmet designs and the effects of impact forces. *Journal of Athletic Training*, 37 (2), 164-171.

CATTERMOLE, HR et al. (1996). The footballer's fracture. *Br J Sports Med.*, 30, 171-175.

CAVANAUGH, JM ET AL. (1986). Lower Abdominal Tolerance and Response. *30th Stapp Car Crash Conference*. SAE Paper 861878, 41-63.

CAVANAUGH, JM ET AL. (1990). Biomechanical Response and Injury Tolerance of the Thorax in Twelve Sled Side Impacts. *34th Stapp Car Crash Conference*. SAE paper 902307, 23-38.

CAVANAUGH, JM ET AL. (1996). Abdominal Injury and Response in Side Impact. *40th Stapp Car Crash Conference*. SAE Paper 962410, 1-16.

CHAPON, A. (1984). Thorax and upper abdomen: anatomy, injuries and possible mechanism of injury. In: *The Biomechanics of Impact Trauma: Proceedings from course given at International Centre for Transportation Studies*. Amalfi, Italy, May 30 – June 4, 251-275.

CHIU, P-H ET AL. (2007). Designing a measurement system for Taekwondo training. XXI ISB Conference, *Journal of Biomechanics*, 40 (Suppl. 2), S619.

CHUANG, TY & LIEU DK. (1992) A Parametric Study of the Thoracic Injury Potential of Basic Taekwondo Kicks. *Journal of Biomechanical Engineering*, 114, 346-351.

CLARYS, JP ET AL. (1984). Gross Tissue Weights in the Human Body By Cadaver Dissection. *Human Biology*, 56 (3), 459-473.

CLARYS, JP & MARFELL-JONES, MJ. (1986). Anthropometric Prediction of Component Tissue Masses in the Minor Limb Segments of the Human Body. *Human Biology*, 58 (5), 761-769.

CRISCO, JJ ET AL. (1996). Maximal contraction lessens impact response in a muscle contusion model. *J. Biomechanics*, 29(10), 1291-1296.

DAVIDS, K ET AL. (2000). Understanding and measuring coordination and control in kicking skills in soccer: Implications for talent identification and skill acquisition. *Journal of Sports Sciences*, 2000, 18, 703-714.

DAVIS, RB. ET AL. (1991). A gait analysis data collection and reduction technique. *Human Movement Science*, 10, 575-587.

DEMPSTER, WT. (1955). Space requirements of the seated operator (WADC TR 55-159). Dayton, OH: *Wright-Patterson Air Force Base*.

DOERER, JJ ET AL. (2007). Evaluation of Chest Barriers for Protection Against Sudden Death Due to Commotio Cordis. *The American Journal of Cardiology*, 99, 857-869.

DOKE, J & KUO , AD. (2005). A simple mathematical model of karate front kick. *XXth Congress of ISB*, Paper 0648.

DREWKNIAK, EI ET AL. (2006). Accuracy of contact area measurements with thin-film pressure sensors. *Proceedings of the 30th meeting of the American Society of Biomechanics*. Blacksburg, Virginia, Abstract 114.

DREWNIAK, EI ET AL. (2007). Accuracy of circular contact area measurements with thin-film pressure sensors. *Journal of Biomechanics*, 40, 2569-2572.

DVORAK, J ET AL. (2007). Medical Report from the 2006 FIFA World Cup Germany™. *Br. J. Sports Med*, 1-13.

DUMA, S ET AL. (2005). Non-censored rib fracture data from dynamic belt loading tests on the human cadaver thorax. *Enhanced Safety of Vehicles*, Paper 05-0360, 1-15.

ELHAGEDIAB, AM & ROUHANA, SW. (1998). Patterns of abdominal injury in frontal automotive crashes. *Enhanced Safety of Vehicles*, Paper 98-S1-W-26, 327-37.

ELIAS, SR. (2001). 10-year trend in USA Cup soccer injuries: 1988-1997. *Medicine & Science in Sports & Exercise*, 359-367.

EPPINGER, R ET AL. (1999). Development of Improved Injury Criteria for the Assessment of Advanced Automotive Restraint Systems – II. A Report for: *National Highway Traffic Safety Administration*.

FALCO, C ET AL. (2009). Influence of the distance in a roundhouse kick's execution time and impact force in Taekwondo. *Journal of Biomechanics*, 42 (3), 242-8.

FAYON, A ET AL. (1975). Thorax of 3-Point Belt Wearers During a Crash. *19th Stapp Car Crash Conference*. SAE Paper 751148,

FERGENBAUM, MA ET AL. (2003). Assessment of pressure measurement Systems on flat surfaces. *Proceedings of the 27th meeting of the American Society of Biomechanics*. Toledo, Ohio, Abstract 268.

FITTS, PM. (1954). The information capacity of the human motor system in controlling the amplitude of movement. *Journal of Experimental Psychology*, 47(6), 381-391.

FORBES, PA ET AL. (2006). Multi-scale human body model to predict side impact thoracic trauma. *IJCrash*, 11(3), 203-216.

FORET-BRUNO, JY ET AL. (1978). Correlations Between Thoracic Lesions and Force Values Measured at the Shoulder of 92 Belted Occupants Involved in Real Accidents. *22nd Stapp Car Crash Conference*. SAE Paper 780892, 271-292.

FRANCISCO, AC ET AL. (2000). Comparison of Soccer Shin Guards in Preventing Tibia Fracture. *Am. J. Sports Med.*, 28, 227-233.

FULLER, CW ET AL. (2006). Consensus statement on injury definitions and data collection procedures in studies of football (soccer injuries). *Br. J. Sports Med.*, 40, 193-201.

FUNK, JR ET AL. (2002). The Axial Injury Tolerance of the Human Foot/Ankle Complex and the Effect of Achilles Tension. *Journal of Biomechanical Engineering*, 124, 750 – 757.

FUNK, JR ET AL. (2004). The Effect of Tibial Curvature and Fibular Loading on the Tibia Index. *Traffic Injury Prevention*, 5, 164-172.

GIZA, E. (2005). Injuries in women's professional soccer. *Br.J. Sports Med.*, 39 (4), 212-216.

GIZA, E & MICHELI, LJ. (2005). Soccer Injuries. *Med Sport Sci.*, 49, 140-169.

GLYNN, J. (2007). An investigation of elbow loading in one-handed tennis backhand groundstrokes using computer simulation. Unpublished Doctoral Thesis, *Loughborough University*.

GRIMAL, Q ET AL. (2004). Finite element study of high-speed blunt impact on thorax: linear elastic considerations. *International Journal of Impact Engineering*, 30, 665-683.

HARDY, WN ET AL. (2001). Abdominal impact response to rigid-bar, seatbelt and airbag loading. *45th Stapp Car Crash Conference*. SAE Paper 2001-22-0001, 1-32.

HAWKINS, RD & FULLER, CW. (1999). A prospective epidemiological study of injuries in four English professional football clubs. *Br. J. Sports Med*, 33, 196-203.

HAWKINS, RD ET AL. (2001). The association football medical research programme: an audit of injuries in professional football. *Br. J. Sports Med.*, 35, 43-47.

HEINER, AD & BROWN, TD. (2001). Structural properties of a new design of composition replicate femurs and tibias. *Journal of Biomechanics*, 34, 773-781.

HRYSOMALLIS, C ET AL. (1996). Drop tests on relaxed and tensed musculature. *Biomechanics – 1st Australasian Conference*, Sydney.

HRYSOMALLIS, C. (2009). Surrogate thigh model for assessing impact force attenuation of protective pads. *Journal of Science and Medicine in Sport*, 12: 35-41.

JACOBSON, I & TEGNER,Y. (2007). Injuries among Swedish female elite football players: a prospective population study. *Scand J Med Sci Sports*, 17, 84-91.

JAQUES, HP. (2008). Determining and modelling the forces exerted by a trampoline suspension system. Unpublished M.Phil. Thesis, *Loughborough University*.

JANDA , DH ET AL. (1992). An analysis of preventative methods for baseball-induced chest impacts. *Clinical Journal of Sports Medicine*, 2, 172- 179.

JOCH, W ET AL. (1981). Biomechanical analysis of punching in boxing. In: *Biomechanics VII-A*, Eds. A. Morecki, K. Fidelius, K. Kdizor & A. Wit. Baltimore, MD: University Park Press, 343-349.

JOHANNSEN, H & SCHINDLER, V. (2007). Development and assessment of a surface abdominal sensor. *Enhanced Safety of Vehicles*. Paper 07-0365, 1-15.

JONES, MD ET AL. (1995). Postmortem electrical excitability of skeletal muscle: preliminary investigation of an animal model. *Forensic Science International*, 76, 91-96.

JORDET, G ET AL. (2007). Kicks from the penalty mark in soccer: The roles of stress, skill and fatigue for kick outcomes. *Journal of Sports Sciences*, 25(2), 121-129.

JUNGE, A ET AL. (2004). Soccer injuries during FIFA tournaments and the Olympic Games 1998-2001. In: Communications to the 5th World Congress on Science and Football. *Journal of Sports & Exercise Sciences*, 22 (6), 588.

KALLIERIS, D ET AL. (1982). Comparison of three-point belt and air bag knee bolster systems: Injury Criteria and injury severity at simulated frontal collisions. *1982 IRCOBI Proceedings*, 166-183.

KALLIERIS, D ET AL. (1998). Prediction of thoracic injuries in frontal collisions. *Enhanced Safety of Vehicles*, Paper 98-S7-O-04, 1550-63.

KAZEMI, M & PIETER, W. (2004). Injuries at a Canadian National Taekwondo Championships: a prospective study. *BMC Musculoskeletal Disorders*, 5, 22.

KAZEMI, M ET AL. (2005). Pre-competition habits and injuries in Taekwondo athletes. BMC *Musculoskeletal Disorders*, 6, 26-35.

KELLIS, E ET AL. (2007). Effects of an intermittent exercise fatigue protocol on biomechanics of soccer kick performance. *Scand J Med Sci Sports*, 16, 334-344.

KENT, RW & CRANDALL, JR. (2001). Boundary condition effects on thoracic deformation response to anterior impact loading. *Bioengineering Conference*, 50, 797-798.

KENT, R & CRANDALL, J. (2003). International harmonization of side impact standards: vehicle design and thoracic injury criteria trends. *Int. J. Vehicle Design*, 32, 1, 158-171.

KENT, R & PATRIE, J. (2005). Chest deflection tolerance to blunt anterior loading is sensitive to age but not load distribution. *Forensic Science International*, 149, 121-128.

KENT, RW ET AL. (2001). The Influence of Superficial Soft Tissues and Restraint Condition on Thoracic Skeletal Injury Prediction. *45th Stapp Car Crash Conference*. SAE Paper 2001-22-0008, 183-204.

KENT, RW ET AL (2002). Radiographic Detection of Rib Fractures: A Restraint-Based Study of Occupants in Car Crashes. *Traffic Injury Prevention*, 3, 49-57.

KENT, R ET AL. (2003). Muscle Tetanus and Loading Condition Effects on the Elastic and Viscous Characteristics of the Thorax. *Traffic Injury Prevention*, 4, 297-314.

KENT, R ET AL. (2004). Thoracic response to dynamic, non-impact loading from a hub, distributed belt, diagonal belt, and double diagonal belts. *48th Stapp Car Crash Conference*. SAE Paper 2004-22-0022, 495-519.

KENT, RW ET AL. (2006). The role of muscle tensing on the force-deflection response of the thorax and a reassessment of frontal impact thoracic biofidelity corridors. *Proc. IMechE*, 220, 853-868.

KIM, YK. (1995). Effect of practice on pattern changes: roundhouse kick in taekwondo. Unpublished Masters Thesis, *Korea Advanced Institute of Science & Technology*, Taejon, Korea.

KIM, YK & HINRICHS, RN. (2006). Biomechanical classification of taekwondo kicks. *XXX ASB Conference*, paper 239.

KIMPARA, H ET AL. (2006). Effect of Assumed Stiffness and Mass Density on he Impact Response of the Human Chest Using a Three-Dimensional FE Model of the Human Body. *Journal of Biomechanical Engineering*, 126, 772-776.

KING, AI. (2000). Fundamentals of Impact Biomechanics: Part I – Biomechanics of the Head, Neck, and Thorax. *Annu. Rev. Biomed*. Eng., 2, 55-81.

KING, AI. (2001). Fundamentals of Impact Biomechanics: Part 2 – Biomechanics of the Abdomen, Pelvis and Lower Extremities. *Annu. Rev. Biomed. Eng.*, 3, 27-55.

KING, AI. (2004). Injury Biomechanics from Head to Foot. In: *Vehicle Crashworthiness and Occupant Protection*. Eds. Prasad, P & Belwafa, JE. Southfield, MI: 269-333.

KOMI, ER ET AL. (2007). Evaluation of thin, flexible sensors for time-resolved rip force measurement. *IMechE*, 221, 1687-1699.

KONG, P-W et al. (2000). Difference betwen taekwondo roundhouse kick executed by the front and back leg – a biomechanical study. *XVIII ISBS Conference*, 268-272.

KROELL, CK ET AL. (1971). Impact Tolerance and Response of the Human Thorax. *15th Stapp Car Crash Conference*. SAE Paper 710851, 85-103.

KROELL, CK ET AL. (1974). Impact Tolerance and Response of the Human Thorax II. *18th Stapp Car Crash Conference*. SAE Paper 741187, 383-413.

KROELL, CK ET AL. (1981). Interrelationship of Velocity and Chest Compression in Blunt Thoracic Impact to Swine. *25th Stapp Car Crash Conference*. SAE Paper 811016, 549-579.

KUKKIWON. (1995). The manual of Taekwondo. Seoul, Korea: Korea Taekwondo Federation.

L'ABBE, RJ ET AL. (1982). An experimental analysis of thoracic deflection response to belt loading. *1982 Proceedings of IRCOBI*, 184-193.

LAN, YC ET AL. (2000). The kinematic analysis of three taekwondo kicking movements. In: *Proceedings of XVIII International Symposium on Biomechanics in Sports*, 1, 277-280.

LATASH, ML. (1998). Neurophysiological Basis of Movement. Champaign, IL: Human Kinetics.

LAU, IV & VIANO, DC. (1986). The Viscous Criterion – Bases and Applications of an Injury Severity Index for Soft Tissues. *30th Stapp Car Crash Conference*. SAE Paper 861882, 123-142.

LAU, IV & VIANO, DC. (1988). How and When Blunt Injury Occurs – Implications to Frontal and Side Impact Protection. *32nd Stapp Car Crash Conference*. SAE Paper 881714, 81-100.

LAU, IV ET AL. (1993). Mechanism of injury from air bag deployment loads. *Accid. Anal. & Prev.*, 25(1), 29-45.

LEARY, T & WHITE, JA. (2000). Acute injury incidence in professional county club cricket players. *Br. J. Sports Med.*, 34, 145-147.

LEE, M ET AL. (1994). Ribcage Compressibility in living subjects. *Clin. Biomech.*, 9, 379-380.

LEE, SK. (1983). Frequency analysis of the Taekwondo techniques used in a tournament. *Journal of Taekwondo*, 46, 122-130.

LEES, A & NOLAN, L. (1998). The biomechanics of soccer: a review. *Journal of Sports Science*, 16, 211-234.

LEES, A & COOPER, S. (1995). The shock attenuation characteristics of soccer shinguards. In: *Sport Leisure and Ergonomics*, 130-135.

LENEHAN, B ET AL. (2003). Tibial shaft fractures in amateur footballers. *Br. J. Sports Med*, 37, 176-178,

LINK, MS ET AL. (1998). An experimental model of sudden death due to low-energy chest-wall impact (commotion cordis). *New England Journal of Medicine*, 338 (25), 1805-1811.

LINK, MS ET AL. (2001). Impact directly over the cardiac silhouette is necessary to produce ventricular fibrillation in an experimental model of commotion cordis. *Journal of the American College of Cardiology*, 37, 649-654.

LINK, MS ET AL. (2002). Reduced Risk of Sudden Death From Chest Wall Blows (Commotio Cordis) with Safety Baseballs. *Pediatrics*, 109, 873-877.

LINK, MS ET AL. (2003). Upper and lower limits of vulnerability to sudden arrhythmic death with chest-wall impact (commotio cordis). *Journal of the American College of Cardiology*, 41, 99-104.

LINK, MS. (2003). Mechanically induced sudden death in chest wall impact (commotio cordis): Review . *Progress in Biophysics & Molecular Biology*, 82, 175-186.

LINK, MS & MARON, BJ. (2005). Sudden cardiac death caused by innocent chest wall blows: Editorial. *Ital Heart J*, 6 (4), 281-283.

LOBDELL, TE ET AL. (1973). Impact response of the human thorax. In: *Human Impact Response: Measurement and Stimulation*. Eds. King, WF & Mertz, HJ. Plenum Press: New York, 201-245.

LUO, ZP ET AL. (1998). Validation of F-Scan pressure sensor system: A technical note. *Journal of Rehabilitation Research*, 35(2), 186-191.

MANOLOPOULOS, E ET AL. (2006). Effects of combined strength and kick coordination training on soccer kick biomechanics in amateur players. *Scand J Med Sci Sports*, 16, 102-110.

MANSINGH, A ET AL. (2006). Injuries in West Indies cricket 2003-2004. *Br J Sports Med*, 40, 119-123.

MARTIN ET AL. (1994). The relationship between mass and acceleration for mpacts on padded surfaces. *Journal of Biomechanics*, 27, 361-364.

McINTOSH, AS & McCRORY, P. (2000). Impact energy attenuation performance of football headgear. *Br. J. Sports Med*. 34, 337-341.

McINTOSH, AS ET AL. (2005). Impact Injury In Sport. In: *IUTAM Symposium on Impact Biomechanics*. Eds. M.D. Gilchrist. Netherlands: Springer, 231-246.

MILLER, MA. (1989). The biomechanical response of the lower abdomen to belt restraint loading. *J. Trauma*, 29, 1571-1584.

MILLS, PJ & HOBBS, CA. (1984). The Probability of Injury to Car Occupants in Frontal and Side Impacts. *28th Stapp Car Crash Conference*. SAE Paper 841652, 223-235.

MOHR, M ET AL. (2007). Geometry of human ribs pertinent to orthopaedic chest-wall reconstruction. *Journal of Biomechanics*, 40, 1310-1317.

MORGAN, RM ET AL. (1986). Side Impact – The Biofidelity of NHTSA's Proposed ATD and Efficacy of TTI. *30th Stapp Car Crash Conference*. SAE Paper 861877, 27-40.

MORIN, EL ET AL. (2000). Calibration Issues of Tekscan Systems for Human Pressure Assessment. Presented at the RTO Specialists' Meeting on: *Soldier Mobility: Innovations in Load Carriage System Design and Evaluation*, RTO MP-056. Kingston, Canada, **24**, 1-7.

NAHUM, AM. (1973). Chest Trauma. In: *Biomechanics and Its Application to Automotive Design*. Society of Automotive Engineers, Inc: Detroit, MI, 1-7

NATIONAL GEOGRAPHIC. (2006). Fight Science (J. Brenkus, Director). In J. Brenkus (producer), *Fight Science*. USA

NEATHERY, RF. (1974). Analysis of Chest Impact Response Data and Scaled Performance Recommendations. *18th Stapp Car Crash Conference*. SAE Paper 741188, 459-493.

NEWMAN, D. (2003) A prospective survey of injuries at first class counties in England and Wales 2001 and 2002 seasons. In: *2nd World Congress of Science and Medicine in Cricket*. Eds R.A.Stretch, 83-84.

NICHOLLS, RL ET AL. (2004). Impact injuries in baseball: prevalence, aetiology, and the role of equipment performance. *Sports Med*, 34 (1): 17-25.

NIEN, Y-H ET AL. (2007). The kinematics of target effect during roundhouse kick in elite taekwondo athletes. *XXI ISB Conference*, paper 0709.

NORDSSLETTEN, L & EKELAND, A. (1993). Muscle Contraction Increases the Structural Capacity of the Lower Leg: An In Vivo Study in the Rat. *Journal of Orthopaedic Research*, 11, 299-304.

NYQUIST, G ET AL. (1985). Tibia bending strength and response. *29th Stapp Car Crash Conference*. SAE Paper 851728, 99-112.

O'SULLIVAN, D ET AL. (2009). Measurement and comparison of Taekwondo and Yongmudo turning kick impact force for two target heights. *Journal of Sports Science and Medicine*, 8, 13-16.

ORCHARD, JW ET AL. (2002). Injuries in Australian cricket at first class level 1995/96 to 2000/01. *Br J Sports Med*, 36, 270-275.

ORCHARD, JW ET AL. (2005). Methods for injury surveillance in international cricket. *Br. J. Sports Med.*, 39, 22-28.

ORCHARD, JW ET AL. (2005). Cricket Australia Injury Report 2005. *Cricket Australia*.

OTTO, JK ET AL. (1999). Static and Dynamic Response of a Multiplexed-array Piezoresistive Contact Sensor. *Experimental Mechanics*, 39(4), 317-323.

PAIN, MTG & CHALLIS, JH. (2001). The role of the heel pad and shank soft tissue during impacts: a further resolution of a paradox. *Journal of Biomechanics*, 34 (3), 327-33.

PAIN, MTG & CHALLIS, JH. (2002). Soft Tissue Motion During Impacts: Their Potential Contributions to Energy Dissipation. *Journal of Applied Biomechanics*, 18, 231-242.

PAIN, MTG & CHALLIS, JH. (2006). The influence of soft tissue movement on ground reaction forces in drop landings. *Journal of Biomechanics*, 39, 119-124.

PAIN, MTG ET AL. (2008). In vivo determination of the effect of shoulder pads on tackling forces in rugby. *Journal of Sports Sciences*, 26 (8), 75-82.

PAPPAS, E. (2007). Boxing, wrestling and martial arts related injuries in emergency departments in the United States, 2002-2005. *Journal of Sports Science and Medicine*, 6(CSSI-2), 58-61.

PATRICK, LM ET AL. (1965). Force on the human body in simulated car crashses. *9th Stapp Car Crash Conference*. SAE Paper 650961, 237-259.

PATRICK, LM. (1981). Impact Force-Deflection of the Human Thorax. *25th Stapp Car Crash Conference*. SAE Paper 811014, 471-495.

PEDZICH, W ET AL. (2006). The comparison of the dynamics of selected leg strokes in taekwondo WTF. *Acta of Bioengineering and Biomechanics*, 8 (1): 1-9.

PENROSE, T ET AL. (1976). Release velocities of fast bowlers during a cricket test match. *Australian Journal for Health, Physical Education and Recreation*, 71 (suppl), 2-5.

PHILLIPENS, M & WISMANS, J. (1989). Shin guard impact protection. *Proceedings of the IRCOBI Conference*, 650-676.

PHILLIPS, JS ET AL. (1998). Injury surveillance in Taekwondo and judo during physiotherapy coverage of the 7th All Africa Games. *SA J Phys*, 57, 32-34.

PIERCE, J ET AL. (2006). Direct measurement of punch force during six professional boxing matches. *Journal of Quantitative Analysis in Sports*, 2 (2), Article 3.

PIETER, F & PIETER, W. (1995). Speed and force of selected taekwondo techniques. *Biology of Sport*, 12 (4), 257-266.

PIETER, W ET AL. (1995). Injury situation and injury mechanism at the 1993 European Taekwondo Cup. *H Hum Mov Stud.*, 28, 1-24.

PIETER, W ET AL. (1999). Injuries in adult American Taekwondo athletes. In: *Proceedings of 5th IOC World Congress on Sport Sciences*, Sydney:Australia.

POLLIACK, AA ET AL. (1998). Scientific characterization of the Rincoe socket nd Tekscan f-socket interface pressure measurement systems: implications or clinical utility. Rehabilitation R&D Progress Reports, 2.

PUTNAM, CA. (1993). Sequential motion body segments in striking and throwing skills: descriptions and explanations. *J Biomechanics*, 40, 125-136.

RAHNAMA, N ET AL. (2002). Injury risk associated with playing actions during competitive soccer. *Br J Sports Med*, 36, 354-359.

RAHNAMA, N ET AL. (2007). Incidence of injury between guest and host football teams. *Journal of Sports Science and Engineering*, 1, 189-195.

RIDELLA, SA & VIANO, DC. (1990). Determining Tolerance to Compression and Viscous Injury in Frontal and Lateral Impacts. *34th Stapp Car Crash Conference*. SAE paper 902330, 349-356.

ROBERTS, JC ET AL. (2005). Modeling Non-penetrating Ballistic Impact on a Human Torso. *John Hopkins APL Technical Digest*, 26 (1), 84-92.

ROBERTS, JC ET AL. (2007). Computational and experimental models of the Human torso for non-penetrating ballistic impact. *Journal of Biomechanics*, 40, 125-136.

ROBINOVITCH, SN ET AL. (1995). Force Attenuation in Trochanteric Soft Tissues During Impact from a Fall. *Journal of Orthopaedic Research*, 13, 956-962.

ROOSEN, A. (2008). Skill reproduction in a reduced time-frame by martial athletes. *Unpublished Doctoral Thesis*, Loughborough University

ROUHANA, SW. (1987). Abdominal Injury Prediction in Lateral Impact – An Analysis of the Biofidelity of the Euro-SID abdomen. *31st Stapp Car Crash Conference*. SAE Paper 872203, 95-104.

SCHEMPF, H ET AL. (1995). Roboleg: a robotic soccer-ball kicking leg. *International Conference on Robotics & Automation*, 2, 1314-1318.

SCHNEIDER, LW. (1992). Development of an advanced ATD thorax for improved injury assessment in frontal car crash environments. *36th Stapp Car Crash Conference*. SAE Paper 922520, 129-156.

SERINA, ER & LIEU, DK ET AL. (1991). Thoracic injury potential of basic competition taekwondo kicks. *J. Biomechanics*, 24 (10), 951-960.

SHAW, JM ET AL. (2006). Oblique and Lateral Impact Response of the PMHS Thorax. *50th Stapp Car Crash Conference*. SAE Paper 2006-22-0007, 147-167.

SHERMAN, D ET AL. (2005). Evaluation and quantification of bruising. *XXth Congress of ISB*. Cleveland, Ohio: USA, 700.

SMITH, MS & HAMILL, J. (1985). Selected karate and boxing glove impact characteristics during the punch. In: *Biomechanics in Sports II*. Eds. J. Terauds & J.N. Barnham. Del Mar, CA: Academic Publishers.

SMITH, MS ET AL. (2000). Development of a boxing dynamometer and its punch force discrimination efficacy. *Journal of Sports Sciences*, 18, 445-450.

SNYDER, RG. (1973). Techniques for Establishing Tolerances to Impact. In: Biomechanics and Its Application to Automotive Design. Society of Automotive Engineers, Inc: Detroit, MI, 1-19.

SORENSEN, H ET AL. (1996). Dynamics of the martial arts high front kick. *Journal of Sports Sciences*, 14, 483-495.

STALNAKER, RL ET AL. (1973). Human torso response to blunt trauma. In: Human Impact Response: Measurement and Stimulation. Eds. King, WF & Mertz, HJ. Plenum Press: New York. 181-199.

STALNAKER, RL ET AL. (1973a). Side impact tolerance to blunt trauma. *17th Stapp Car Crash Conference*. SAE Paper 730979, 377-408.

STALNAKER, RL ET AL. (1979). Modification of Part 572 dummy for lateral impact according to biomechanical data. *23rd Stapp Car Crash Conference*. SAE Paper 791031, 841-872.

STITZEL, JD ET AL. (2003). Defining Regional Variation in the Material Properties of Human Rib Cortical Bone and Its Effect on Fracture Prediction. *47th Stapp Car Crash Conference*. SAE Paper 2003-22-0012, 243-265.

STITZEL, JD ET AL. (2004). Predicting fractures due to blunt impact: a sensitivity analysis of the effects of altering failure strain of human rib cortical bone. *IJCrash*, 9(6), 633-642.

STRETCH, RA. (2003). Cricket injuries: a longitudinal study of the nature of injuries to South African cricketers. *Br J Sports Med*, 37, 3, 250-253.

STRETCH, RA ET AL. (1998). The force absorption and rebound characteristics of cricket batting pads at four impact velocities. In: *From Community Health to Elite Sport: Proceedings of the 3rd Annual Congress of the ECSS*. Liverpool:UK, 465.

STRETCH, RA ET AL. (2000). A review of batting in men's cricket. *Journal of Sports Sciences*, 18, 931-949.

SUMIYA, T ET AL. (1998). Sensing stability and dynamic response of the F-Scan in-shoe sensing system: A technical note. *Journal of Rehabilitation Research and Development*, 35(2), 192-200.

TALANTIKITE, Y ET AL. (1998). Human Thorax Behaviour for Side Impact: Influence of Impact Masses and Velocity. *Enhanced Safety of Vehicles*. Paper 98-S7-O-03, 1542-1549.

TANG, W-T ET AL. (2007). The kinematics characteristics of preferred and non-preferred roundhouse kick in elite taekwondo athletes. *XXI ISB Conference*, Paper 0708.

TORTORA, GJ & GRABOWSKI, SR. Muscle Tissue. In: *Principles of Anatomy and Physiology: 10th Edition*. John Wiley & Sons: New York, 273-307.

TROSEILLE, X ET AL. (2002). Abdominal Response to High-Speed Seatbelt Loading. 46th Stapp Car Crash Journal, SAE Paper 2002-22-0004, 71-79.

TSAI, YJ ET AL. (1999). The biomechanical analysis of taekwondo attack movements. Paper presented at ISB XVII Congress, Calgary, Canada, pp 938.

TSAOUSIDIS, N & ZATSIORSKY, V. (1996). Two types of ball-effector interaction and their relative contribution to soccer kicking. *Human Movement Science*, 15, 861-876.

VAN EE, CA ET AL. (2000). Quantifying Skeletal Muscle Properties in Cadaveric Test Specimens: Effects of Mechanical Loading, Postmortem Time, and Freezer Storage. *Journal of Biomechanical Engineering*, 122, 9-14.

VAN LOOCKE, M ET AL. (2005). Three dimensional passive properties of muscle tissue incompression. *IUTAM Symposium on Impact* Biomechanics. Ed: Gilchrist, MD. Springer, Netherlands, 313-320.

VERRIEST, J-P. (1984). Thorax and upper abdomen: kinematics, tolerance levels and injury criteria. In: *The Biomechanics of Impact Trauma: Proceedings from course given at International Centre for Transportation Studies*. Amalfi, Italy, May 30 – June 4, 251-275.

VIANO, DC. (1987). Evaluation of the Benefit of Energy-Absorption Material in Side Impact Protection: Part I. *31st Stapp Car Crash Conference*. SAE Paper 872212, 185-203

VIANO, DC. (1989). Biomechanical Responses and Injuries in Blunt Lateral Impact. *33rd Stapp Car Crash Conference*. SAE Paper 892432, 113-142.

VIANO, DC. (2001). Chest and Abdomen Injury Biomechanics. *Crashworthiness: energy management and occupant protection*. Eds. Ambrosio, JAC. Springer, New York: 415-425.

VIANO, DC & King, AI. (2000). Biomechanics of Chest and Abdomen Impact. *The Biomechanical Engineering Handbook*. Eds Bronzino, JD. Springer, Germany, 24-1-24-12.

VIANO, DC & LAU, IV. (1988). A viscous tolerance criterion for soft tissue injury assessment. *Biomechanics*, 21 (5), 387-399.

VIANO, DC ET AL. (1977). Comparative thoracic impact response of living and sacrificed porcine siblings. *21st Stapp Car Crash Conference*. SAE Paper 770930, 627-709.

VIANO, DC ET AL. (1989a). Biomechanics of injury in lateral impacts. *Accid. Anal. & Prev.,* 21 (6), 535-551.

VIANO, DC ET AL. (1989b). Biomechanics of the human chest, abdomen, and pelvis in lateral impact. *Accid. Anal. & Prev.*, 21 (6), 553-574.

VIANO, DC ET AL. (2000). Prevention of commotio cordis in baseball: an evaluation of chest protector. *J Trauma*, 49 (6), 1023-8.

WAKELING, JM & NIGG, BM. (2001). Modification of soft tissue vibrations in the leg by muscular activity. *J. Appl. Physiol.*, 90, 412-420.

WAKELING, JM ET AL. (2002). Muscle activity damps the soft tissue resonance that occurs in response to pulsed and continuous vibrations. *J. Appl. Physiol.*, 93, 1093-1103.

WALKER, PJ. (in progress). Mechanical and Computer Simulation of Personal Protective Equipment Performance. Unpublished doctoral thesis, Loughborough University.

WALILKO, TJ ET AL. (2005). Biomechanics of the head for Olympic boxer punches to the face. *Br. J. Sports Med*, 39, 710-719.

WARD, EE ET AL. (2005). Modeling the effects of blast on the human thorax using high strain rate viscoelastic properties of human tissue. In: IUTAM *Symposium on Impact Biomechanics: From Fundamental Insights to Applications*. Editor: MD Gilchrist, Publisher: Springer, Dordrect, The Netherlands, 17-24.

WEINSTOCK, J ET AL. (2006). Failure of Commercially Available Chest Wall Protectors to Prevent Sudden Cardiac Death Induced by Chest Wall Blows in an Experimental Model of Commotio Cordis. *Pediatrics*, 117 (4), 656-662.

WILSON, C. (2003). Optimisation of performance in running jumps. Unpublished Doctoral Thesis, Loughborough University.

WINTER, DA. (1990). Biomechanics and motor control of human movement. New York: John Wiley & Sons, Inc.

WOODS, C ET AL. (2003). The Football Association Medical Research Programme: an audit of injuries in professional football: an analysis of ankle sprains. *Br. J. Sports Med.,* 37, 233-238.

WONG, P & HONG, Y. Soccer injury in the lower extremities. *Br. J. Sports* Med, 39, 473-482.

WONG, C ET AL. (2010). Finite element analysis of tibial fractures. Danish Medical Bulletin, 57 (5), 1-4.

YANG, J. (1997). Mathematical simulation of knee responses associated with leg fracture in car-pedestrian accidents. *IJCrash*, 2 (3), 259-271.

YEADON, MR. (1990). The Simulation of Aerial Movement – II. A Mathematical inertial model of the human body. J. Biomechanics, 23 (1), 67-74

YOGANANDAN, N ET AL. (1997). Impact biomechanics of the human thorax-abdomen complex. IJCrash, 2 (2), 219-228.

ZEMPER, ED & PIETER, W. (1988). Injury rates during the 1988 Olympic Team Trials for Taekwondo. *Br J Sports Med*, 23, 161-164.

ZETARUK, MN. (2005). Injuries in martial arts: a comparison of five styles. *Br. J. Sports Med*, 39, 29-33.

ZETOU, E ET AL. (2006). Injuries in Taekwondo Athletes. Department of Physical Education and Sport Sciences, *Aristotle University of Thessaloniki*, Greece.

ZHANG, SN ET AL. (2000). Contributions of lower extremity joints to energy dissipation during landings. *Medicine & Science in Sports & Exercise*, 32 (4), 812-819.

ZHOU, Q ET AL. (1996). Age Effects on Thoracic Injury Tolerance. *40th Stapp Car Crash Conference*. SAE Paper 962421, 137-148.

APPENDIX A

MEASUREMENT SYSTEMS SPECIFICATIONS

A1. Kistler 9281B12 Specification Sheet: Part 1

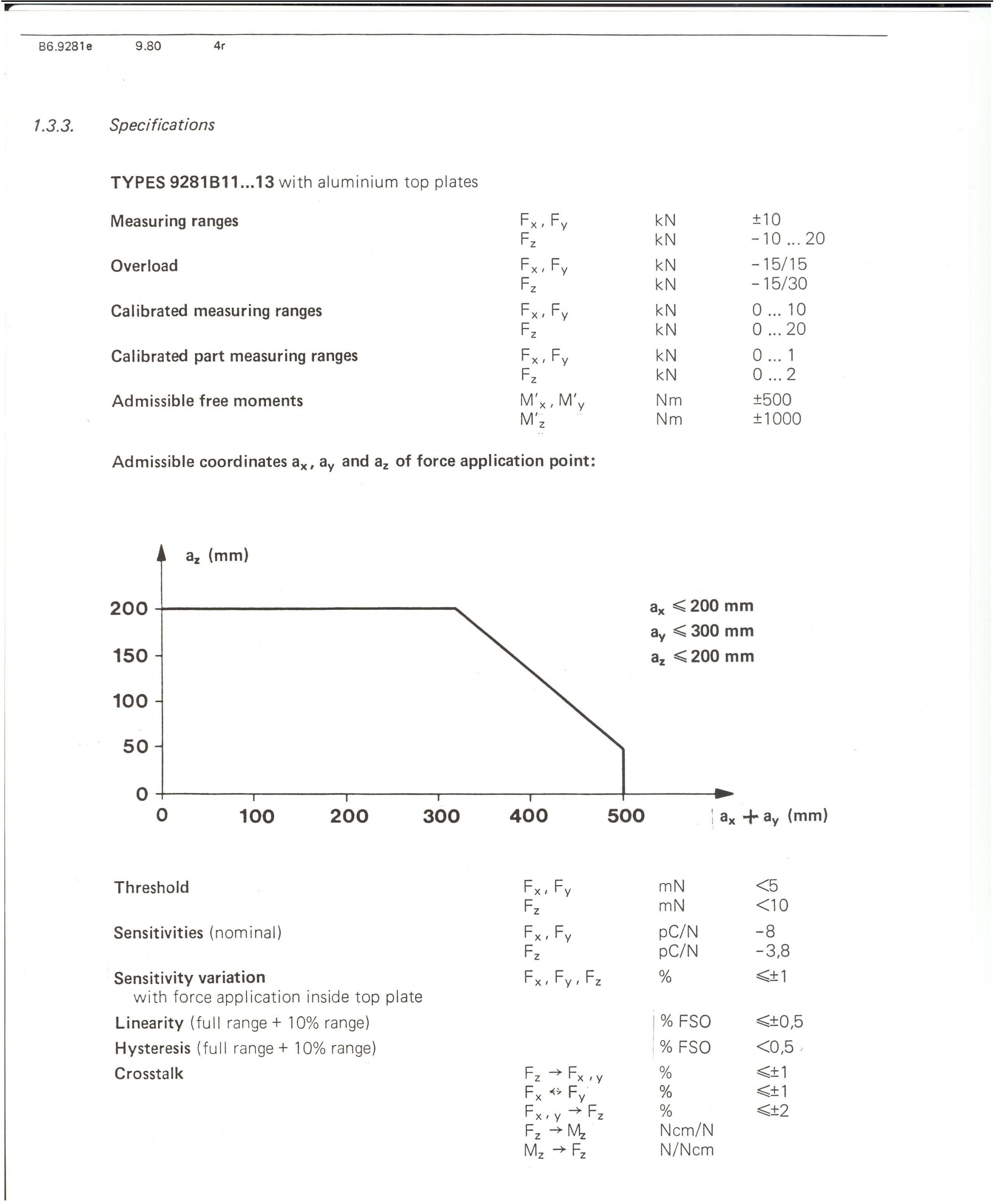

B6.9281e 9.80 4r

1.3.3. *Specifications*

TYPES 9281B11...13 with aluminium top plates

Measuring ranges	F_x, F_y	kN	±10
	F_z	kN	−10 ... 20
Overload	F_x, F_y	kN	−15/15
	F_z	kN	−15/30
Calibrated measuring ranges	F_x, F_y	kN	0 ... 10
	F_z	kN	0 ... 20
Calibrated part measuring ranges	F_x, F_y	kN	0 ... 1
	F_z	kN	0 ... 2
Admissible free moments	M'_x, M'_y	Nm	±500
	M'_z	Nm	±1000

Admissible coordinates a_x, a_y and a_z of force application point:

a_z (mm)
200
150
100
50
0
0
100
200
300
400
500
$a_x + a_y$ (mm)
$a_x \leqslant 200$ mm
$a_y \leqslant 300$ mm
$a_z \leqslant 200$ mm

Threshold	F_x, F_y	mN	<5
	F_z	mN	<10
Sensitivities (nominal)	F_x, F_y	pC/N	−8
	F_z	pC/N	−3,8
Sensitivity variation with force application inside top plate	F_x, F_y, F_z	%	≤±1
Linearity (full range + 10% range)		% FSO	≤±0,5
Hysteresis (full range + 10% range)		% FSO	<0,5
Crosstalk	$F_z \rightarrow F_{x,y}$	%	≤±1
	$F_x \leftrightarrow F_y$	%	≤±1
	$F_{x,y} \rightarrow F_z$	%	≤±2
	$F_z \rightarrow M_z$	Ncm/N	
	$M_z \rightarrow F_z$	N/Ncm	

A2. Kistler 9281B12 Specification Sheet: Part 2

			9281B11 9281B12	9281B13
Natural frequency	x axis	Hz	≈900	≈950
	y axis	Hz	≈800	≈850
	z axis	Hz	≈850	≈700
Rigidity	x axis	N/µm	≈900	≈900
	y axis	N/µm	≈1000	≈1000
	z axis	N/µm	≈400	≈200
	($a_x = a_y = 0$)			
Mean error of a_x and a_y	Δa_x	mm		
	Δa_y	mm		
Insulation resistance (per channel)		TΩ	>10	
Capacitance (per channel)		pF	630	
Operating temperature range		°C	-20 ... 70	
Tightening torque for fixing screws M12 x 25		Nm	90	
Weight (without mounting frame)		kg	42	
Material: top plate 9421B11...13		AC100B		
frame		St37 galvanized		
preload elements		stainless steel		
mounting frame 9423		St37 galvanized		

TYPES 9281B21...23 with steel top plates

Measuring range A	F_x, F_y	kN	±10
	F_z	kN	-10 ... 20
Overload	F_x, F_y	kN	-15/15
	F_z	kN	-15/30
Measuring range B	F_x, F_y	kN	±20
	F_z	kN	-20 ... 40
Overload	F_x, F_y	kN	-25/25
	F_z	kN	-25/50
Calibrated measuring range	F_x, F_y	kN	0 ... 20
	F_z	kN	0 ... 40
Calibrated part measuring range	F_x, F_y	kN	0 ... 2
	F_z	kN	0 ... 4
Admissible free moments	M'_x, M'_y	Nm	±500
	M'_z	Nm	±1000

Admissible coordinates a_x, a_y and a_z of the force application point:

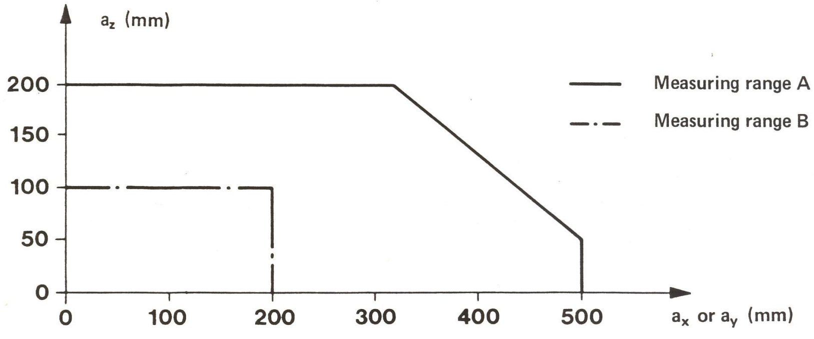

A3. Kistler Type 9865 8-Channel Charge Amplifier Specification Sheet: Part 1

Measure & Analyze – MCA

KISTLER

1 ... 2

8-Kanal-Ladungsverstärker
Amplificateur de charge à 8 canaux
8-Channel Charge Amplifier

9865E

Die Hauptanwendung des 8-Kanal-Ladungsverstärkers Typ 9865E liegt, zusammen mit KISTLER Messplattformen, in der Biomechanik.

Daneben findet der Typ 9865E allgemeine Verwendung als universeller, kostengünstiger Mehrkanal-Ladungsverstärker, insbesondere, wenn Ansteuerung und Datenverarbeitung mit einem Rechnersystem erfolgen.

L'amplificateur de charge à 8 canaux type 9865E est utilisé ensemble avec les plateformes de mesure de KISTLER en premier lieu pour des applications en biomécanique.

De plus, le type 9865E est employé comme amplificateur de charge à plusieurs canaux universel et économique, surtout lorsque le contrôle et le traitement des données s'effectuent avec un ordinateur.

The 8-channel charge amplifier Type 9865E is, together with the KISTLER force plates, mainly used in biomechanics.

Moreover, the Type 9865E is used as a universal, economically priced multichannel charge amplifier, especially if control and data processing are implemented with a computer system.

- Alle Funktionen sind fernsteuerbar
  Toutes les fonctions peuvent être télécommandées
  All functions can be remote controlled
- Modularer Aufbau, Elektronik auf 6 steckbaren Europakarten
  Construction modulaire, électronique sur 6 cartes-Europe enfichables
  Modular design, electronics on 6 plug-in Euro-Cards
- CE-konform als elektromedizinisches Gerät
  Conforme au CE comme instrument électromédical
  Conforming to CE as an electromedical instrument

8-Channel Charge Amplifier
Type 9865E
KISTLER

Technische Daten	Données techniques	Technical Data*		
Anzahl Messkanäle	**Number de canaux de mesure**	**Number of measuring channels**		8
Gruppe I	Groupe I	Group I	–	$X_{1,2}$ $X_{3,4}$ $Y_{1,4}$ $Y_{2,3}$
Gruppe II	Groupe II	Group II	–	Z_1 Z_2 Z_3 Z_4
Messbereiche	**Gammes de mesure**	**Measuring ranges**	Range 1	± 1'000 pC
(Umschaltung in zwei Gruppen	(Commutation en 2 groupes	(Switching in 2 groups	Range 2	± 5'000 pC
zu je 4 Kanalen)	à 4 canaux chacune)	with 4 channels each)	Range 3	±10'000 pC
			Range 4	±50'000 pC
Ausgangsspannung, wahlbar	**Tension de sortie**, au choix	**Output voltage**, selectable	V	±5 / ±10
Ausgangsstrom	**Courant de sortie**	**Output current**	mA	≤±5
Ausgangswiderstand	**Impédance de sortie**	**Output impedance**	Ω	10
Obere Grenzfrequenz (-3dB)	**Fréquence limite supérieure** (-3dB)	**Upper cut-off frequency** (-3dB)	kHz	≈10
Untere Grenzfrequenz	**Fréquence limite inférieure**	**Lower cut-off frequency**		
Schaltbar (Zeitkonstante)	Commutable (Constante de temps)	Switchable (Time constant)		
Bereiche 1'000 / 5'000 pC	Gammes 1'000 / 5'000 pC	Ranges 1'000 / 5'000 pC	s	≈ 10
Bereiche 10'000 / 50'000 pC	Gammes 10'000 / 50'000 pC	Ranges 10'000 / 50'000 pC	s	≈100
Fehler, alle Kanale	**Erreur**, tous les canaux	**Error**, all channels	% FS	<1
Rauschen, am Ausgang	**Bruit de fond**, à la sortie	**Noise**, at output	mV_{rms}	<2
Drift (Operate)	**Dérive** (Operate)	**Drift** (Operate)	pC/s	<±0,07

* In all Kistler documents, the decimal sign is a comma on the line (ISO 31-0:1992).

A4. Kistler Type 9865 8-Channel Charge Amplifier Specification Sheet: Part 2

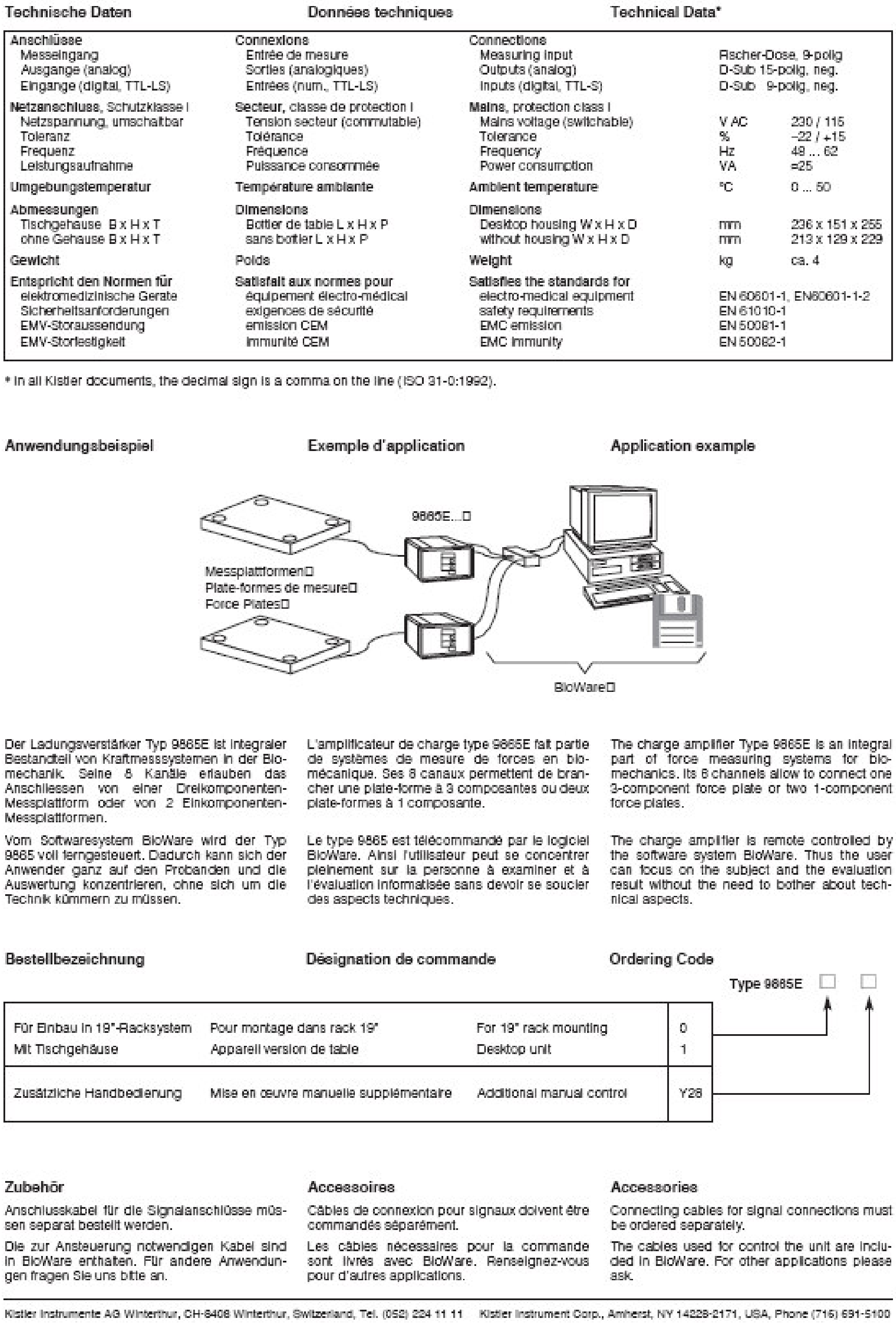

Technische Daten	Données techniques	Technical Data*		
Anschlüsse	**Connexions**	**Connections**		
Messeingang	Entrée de mesure	Measuring input	Fischer-Dose, 9-polig	
Ausgange (analog)	Sorties (analogiques)	Outputs (analog)	D-Sub 15-polig, neg.	
Eingange (digital, TTL-LS)	Entrées (num., TTL-LS)	Inputs (digital, TTL-S)	D-Sub 9-polig, neg.	
Netzanschluss, Schutzklasse I	**Secteur**, classe de protection I	**Mains**, protection class I		
Netzspannung, umschaltbar	Tension secteur (commutable)	Mains voltage (switchable)	V AC	230 / 115
Toleranz	Tolérance	Tolerance	%	–22 / +15
Frequenz	Fréquence	Frequency	Hz	48 ... 62
Leistungsaufnahme	Puissance consommée	Power consumption	VA	≈25
Umgebungstemperatur	**Température ambiante**	**Ambient temperature**	°C	0 ... 50
Abmessungen	**Dimensions**	**Dimensions**		
Tischgehause B x H x T	Boîtier de table L x H x P	Desktop housing W x H x D	mm	236 x 151 x 255
ohne Gehause B x H x T	sans boîtier L x H x P	without housing W x H x D	mm	213 x 129 x 229
Gewicht	**Poids**	**Weight**	kg	ca. 4
Entspricht den Normen für	**Satisfait aux normes pour**	**Satisfies the standards for**		
elektromedizinische Gerate	équipement électro-médical	electro-medical equipment	EN 60601-1, EN60601-1-2	
Sicherheitsanforderungen	exigences de sécurité	safety requirements	EN 61010-1	
EMV-Storaussendung	emission CEM	EMC emission	EN 50081-1	
EMV-Storfestigkeit	immunité CEM	EMC immunity	EN 50082-1	

* In all Kistler documents, the decimal sign is a comma on the line (ISO 31-0:1992).

Anwendungsbeispiel **Exemple d'application** **Application example**

Der Ladungsverstärker Typ 9865E ist integraler Bestandteil von Kraftmesssystemen in der Biomechanik. Seine 8 Kanäle erlauben das Anschliessen von einer Dreikomponenten-Messplattform oder von 2 Einkomponenten-Messplattformen.

Vom Softwaresystem BioWare wird der Typ 9865 voll ferngesteuert. Dadurch kann sich der Anwender ganz auf den Probanden und die Auswertung konzentrieren, ohne sich um die Technik kümmern zu müssen.

L'amplificateur de charge type 9865E fait partie de systèmes de mesure de forces en biomécanique. Ses 8 canaux permettent de brancher une plate-forme à 3 composantes ou deux plate-formes à 1 composante.

Le type 9865 est télécommandé par le logiciel BioWare. Ainsi l'utilisateur peut se concentrer pleinement sur la personne à examiner et à l'évaluation informatisée sans devoir se soucier des aspects techniques.

The charge amplifier Type 9865E is an integral part of force measuring systems for biomechanics. Its 8 channels allow to connect one 3-component force plate or two 1-component force plates.

The charge amplifier is remote controlled by the software system BioWare. Thus the user can focus on the subject and the evaluation result without the need to bother about technical aspects.

Bestellbezeichnung **Désignation de commande** **Ordering Code**

Type 9865E ☐ ☐

Für Einbau in 19"-Racksystem	Pour montage dans rack 19"	For 19" rack mounting	0
Mit Tischgehäuse	Appareil version de table	Desktop unit	1
Zusätzliche Handbedienung	Mise en œuvre manuelle supplémentaire	Additional manual control	Y28

Zubehör

Anschlusskabel für die Signalanschlüsse müssen separat bestellt werden.

Die zur Ansteuerung notwendigen Kabel sind in BioWare enthalten. Für andere Anwendungen fragen Sie uns bitte an.

Accessoires

Câbles de connexion pour signaux doivent être commandés séparément.

Les câbles nécessaires pour la commande sont livrés avec BioWare. Renseignez-vous pour d'autres applications.

Accessories

Connecting cables for signal connections must be ordered separately.

The cables used for control the unit are included in BioWare. For other applications please ask.

Kistler Instrumente AG Winterthur, CH-8408 Winterthur, Switzerland, Tel. (052) 224 11 11 Kistler Instrument Corp., Amherst, NY 14228-2171, USA, Phone (716) 691-5100

A5. Kistler 9281B12 Calibration Sheet

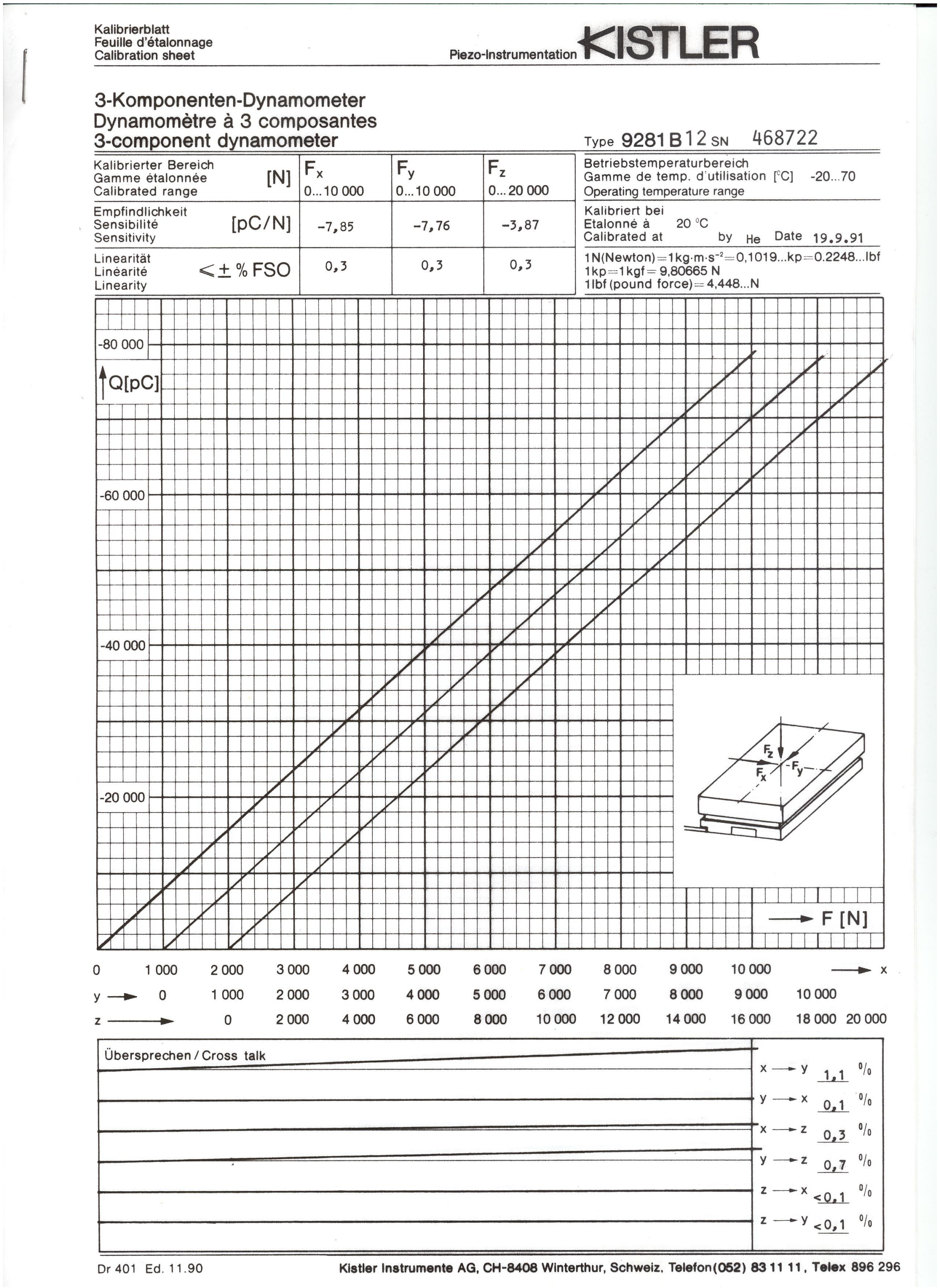

Kalibrierblatt
Feuille d'étalonnage
Calibration sheet

Piezo-Instrumentation **KISTLER**

3-Komponenten-Dynamometer
Dynamomètre à 3 composantes
3-component dynamometer

Type 9281 B 12 SN 468722

		F_x	F_y	F_z
Kalibrierter Bereich Gamme étalonnée Calibrated range	[N]	0...10 000	0...10 000	0...20 000
Empfindlichkeit Sensibilité Sensitivity	[pC/N]	-7,85	-7,76	-3,87
Linearität Linéarité Linearity	<± % FSO	0,3	0,3	0,3

Betriebstemperaturbereich
Gamme de temp. d'utilisation [°C] -20...70
Operating temperature range

Kalibriert bei
Etalonné à 20 °C
Calibrated at by He Date 19.9.91

1 N(Newton) = 1 kg·m·s⁻² = 0,1019...kp = 0.2248...lbf
1 kp = 1 kgf = 9,80665 N
1 lbf (pound force) = 4,448...N

-80 000
Q[pC]
-60 000
-40 000
-20 000
F [N]
F_z
F_x
$-F_y$
0 1 000 2 000 3 000 4 000 5 000 6 000 7 000 8 000 9 000 10 000 x
y 0 1 000 2 000 3 000 4 000 5 000 6 000 7 000 8 000 9 000 10 000
z 0 2 000 4 000 6 000 8 000 10 000 12 000 14 000 16 000 18 000 20 000
Übersprechen / Cross talk

x → y 1,1 %
y → x 0,1 %
x → z 0,3 %
y → z 0,7 %
z → x <0,1 %
z → y <0,1 %

Dr 401 Ed. 11.90

Kistler Instrumente AG, CH-8408 Winterthur, Schweiz, Telefon (052) 83 11 11, Telex 896 296

A6. ICP 260A01 Force Transducer Specification Sheet

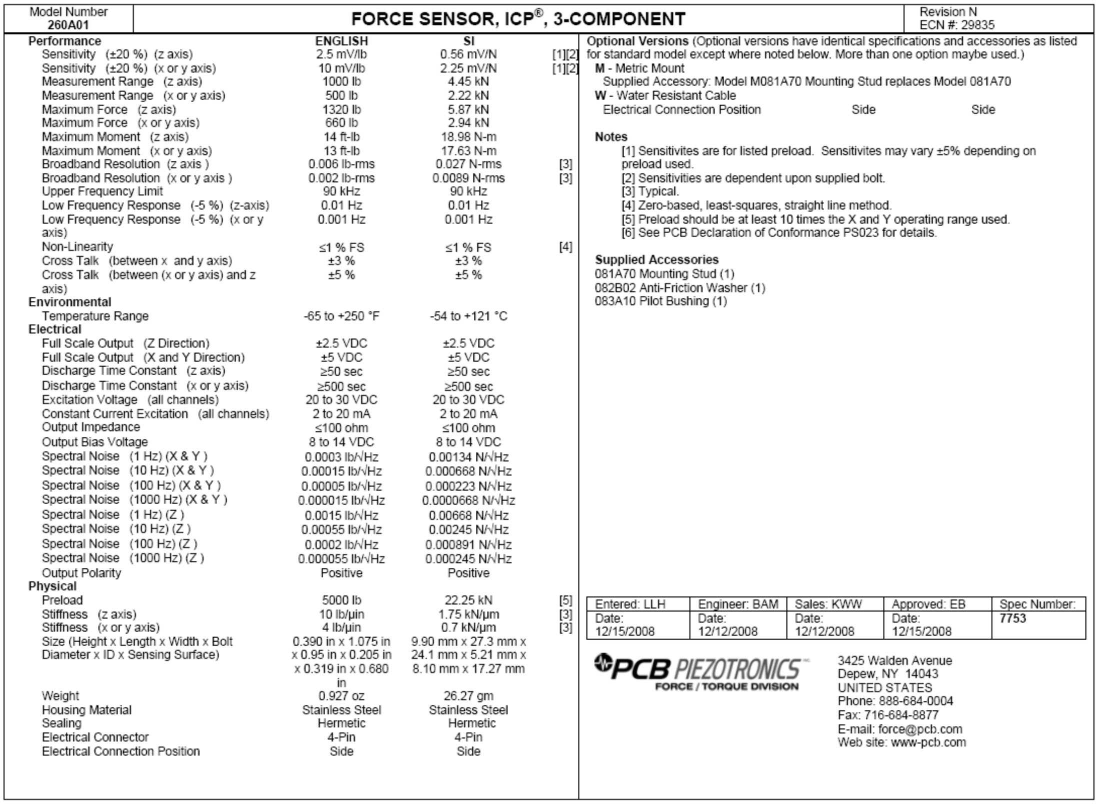

Model Number **260A01**	**FORCE SENSOR, ICP®, 3-COMPONENT**	Revision N ECN #: 29835

	ENGLISH	**SI**	
Performance			
Sensitivity (±20 %) (z axis)	2.5 mV/lb	0.56 mV/N	[1][2]
Sensitivity (±20 %) (x or y axis)	10 mV/lb	2.25 mV/N	[1][2]
Measurement Range (z axis)	1000 lb	4.45 kN	
Measurement Range (x or y axis)	500 lb	2.22 kN	
Maximum Force (z axis)	1320 lb	5.87 kN	
Maximum Force (x or y axis)	660 lb	2.94 kN	
Maximum Moment (z axis)	14 ft-lb	18.98 N-m	
Maximum Moment (x or y axis)	13 ft-lb	17.63 N-m	
Broadband Resolution (z axis)	0.006 lb-rms	0.027 N-rms	[3]
Broadband Resolution (x or y axis)	0.002 lb-rms	0.0089 N-rms	[3]
Upper Frequency Limit	90 kHz	90 kHz	
Low Frequency Response (-5 %) (z-axis)	0.01 Hz	0.01 Hz	
Low Frequency Response (-5 %) (x or y axis)	0.001 Hz	0.001 Hz	
Non-Linearity	≤1 % FS	≤1 % FS	[4]
Cross Talk (between x and y axis)	±3 %	±3 %	
Cross Talk (between (x or y axis) and z axis)	±5 %	±5 %	
Environmental			
Temperature Range	-65 to +250 °F	-54 to +121 °C	
Electrical			
Full Scale Output (Z Direction)	±2.5 VDC	±2.5 VDC	
Full Scale Output (X and Y Direction)	±5 VDC	±5 VDC	
Discharge Time Constant (z axis)	≥50 sec	≥50 sec	
Discharge Time Constant (x or y axis)	≥500 sec	≥500 sec	
Excitation Voltage (all channels)	20 to 30 VDC	20 to 30 VDC	
Constant Current Excitation (all channels)	2 to 20 mA	2 to 20 mA	
Output Impedance	≤100 ohm	≤100 ohm	
Output Bias Voltage	8 to 14 VDC	8 to 14 VDC	
Spectral Noise (1 Hz) (X & Y)	0.0003 lb/√Hz	0.00134 N/√Hz	
Spectral Noise (10 Hz) (X & Y)	0.00015 lb/√Hz	0.000668 N/√Hz	
Spectral Noise (100 Hz) (X & Y)	0.00005 lb/√Hz	0.000223 N/√Hz	
Spectral Noise (1000 Hz) (X & Y)	0.000015 lb/√Hz	0.0000668 N/√Hz	
Spectral Noise (1 Hz) (Z)	0.0015 lb/√Hz	0.00668 N/√Hz	
Spectral Noise (10 Hz) (Z)	0.00055 lb/√Hz	0.00245 N/√Hz	
Spectral Noise (100 Hz) (Z)	0.0002 lb/√Hz	0.000891 N/√Hz	
Spectral Noise (1000 Hz) (Z)	0.000055 lb/√Hz	0.000245 N/√Hz	
Output Polarity	Positive	Positive	
Physical			
Preload	5000 lb	22.25 kN	[5]
Stiffness (z axis)	10 lb/µin	1.75 kN/µm	[3]
Stiffness (x or y axis)	4 lb/µin	0.7 kN/µm	[3]
Size (Height x Length x Width x Bolt Diameter x ID x Sensing Surface)	0.390 in x 1.075 in x 0.95 in x 0.205 in x 0.319 in x 0.680 in	9.90 mm x 27.3 mm x 24.1 mm x 5.21 mm x 8.10 mm x 17.27 mm	
Weight	0.927 oz	26.27 gm	
Housing Material	Stainless Steel	Stainless Steel	
Sealing	Hermetic	Hermetic	
Electrical Connector	4-Pin	4-Pin	
Electrical Connection Position	Side	Side	

Optional Versions (Optional versions have identical specifications and accessories as listed for standard model except where noted below. More than one option maybe used.)

M - Metric Mount

Supplied Accessory: Model M081A70 Mounting Stud replaces Model 081A70

W - Water Resistant Cable

Electrical Connection Position	Side	Side

Notes

[1] Sensitivites are for listed preload. Sensitivites may vary ±5% depending on preload used.
[2] Sensitivities are dependent upon supplied bolt.
[3] Typical.
[4] Zero-based, least-squares, straight line method.
[5] Preload should be at least 10 times the X and Y operating range used.
[6] See PCB Declaration of Conformance PS023 for details.

Supplied Accessories

081A70 Mounting Stud (1)
082B02 Anti-Friction Washer (1)
083A10 Pilot Bushing (1)

Entered: LLH	Engineer: BAM	Sales: KWW	Approved: EB	Spec Number:
Date: 12/15/2008	Date: 12/12/2008	Date: 12/12/2008	Date: 12/15/2008	**7753**

PCB PIEZOTRONICS
FORCE / TORQUE DIVISION

3425 Walden Avenue
Depew, NY 14043
UNITED STATES
Phone: 888-684-0004
Fax: 716-684-8877
E-mail: force@pcb.com
Web site: www-pcb.com

A7. Model 482A22 Signal Conditioner Specification Sheet

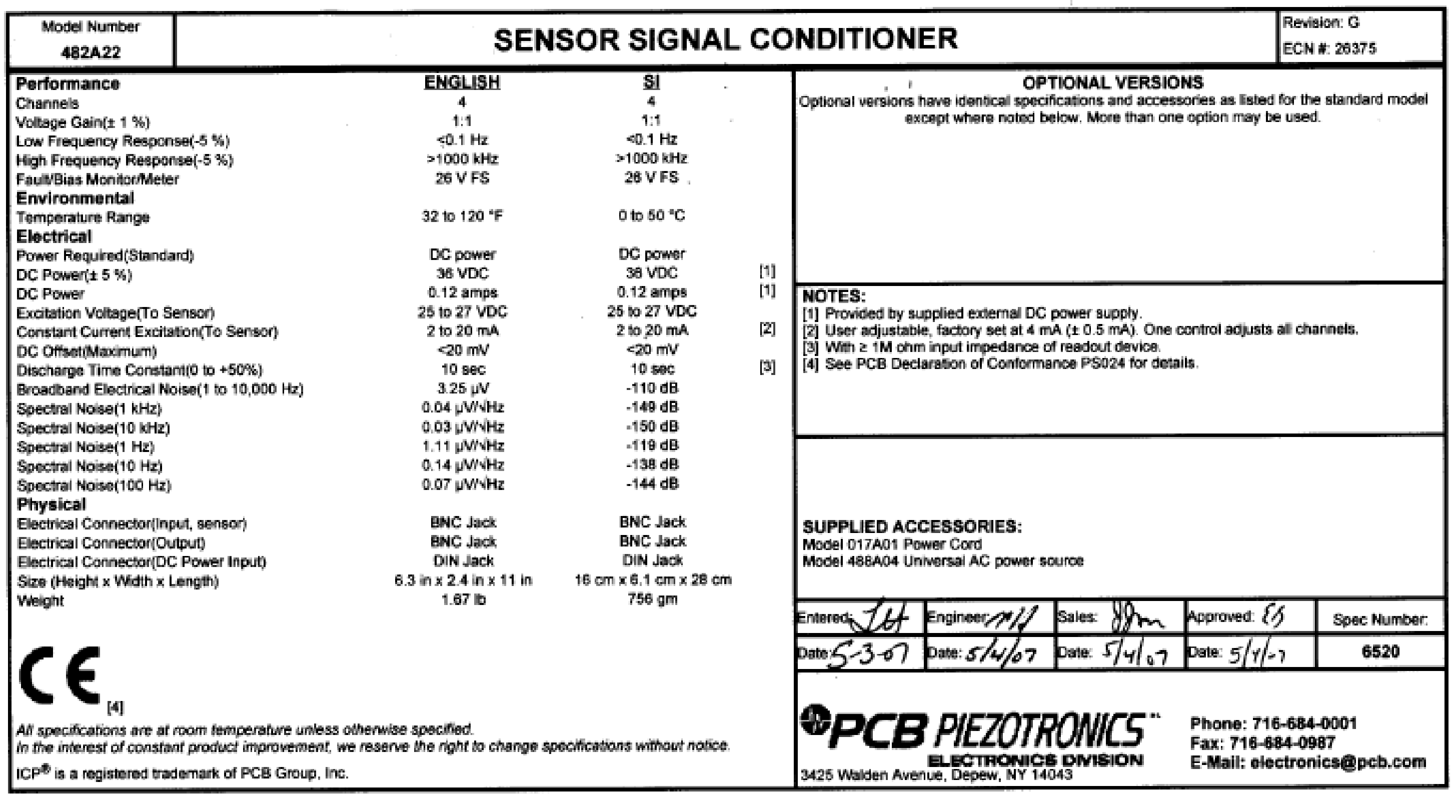

Model Number 482A22	SENSOR SIGNAL CONDITIONER	Revision: G ECN #: 26375

Performance	ENGLISH	SI	
Channels	4	4	
Voltage Gain(± 1 %)	1:1	1:1	
Low Frequency Response(-5 %)	<0.1 Hz	<0.1 Hz	
High Frequency Response(-5 %)	>1000 kHz	>1000 kHz	
Fault/Bias Monitor/Meter	26 V FS	26 V FS	
Environmental			
Temperature Range	32 to 120 °F	0 to 50 °C	
Electrical			
Power Required(Standard)	DC power	DC power	
DC Power(± 5 %)	36 VDC	36 VDC	[1]
DC Power	0.12 amps	0.12 amps	[1]
Excitation Voltage(To Sensor)	25 to 27 VDC	25 to 27 VDC	
Constant Current Excitation(To Sensor)	2 to 20 mA	2 to 20 mA	[2]
DC Offset(Maximum)	<20 mV	<20 mV	
Discharge Time Constant(0 to +50%)	10 sec	10 sec	[3]
Broadband Electrical Noise(1 to 10,000 Hz)	3.25 μV	-110 dB	
Spectral Noise(1 kHz)	0.04 μV/√Hz	-149 dB	
Spectral Noise(10 kHz)	0.03 μV/√Hz	-150 dB	
Spectral Noise(1 Hz)	1.11 μV/√Hz	-119 dB	
Spectral Noise(10 Hz)	0.14 μV/√Hz	-138 dB	
Spectral Noise(100 Hz)	0.07 μV/√Hz	-144 dB	
Physical			
Electrical Connector(Input, sensor)	BNC Jack	BNC Jack	
Electrical Connector(Output)	BNC Jack	BNC Jack	
Electrical Connector(DC Power Input)	DIN Jack	DIN Jack	
Size (Height x Width x Length)	6.3 in x 2.4 in x 11 in	16 cm x 6.1 cm x 28 cm	
Weight	1.67 lb	756 gm	

CE [4]

All specifications are at room temperature unless otherwise specified.
In the interest of constant product improvement, we reserve the right to change specifications without notice.

ICP® is a registered trademark of PCB Group, Inc.

OPTIONAL VERSIONS

Optional versions have identical specifications and accessories as listed for the standard model except where noted below. More than one option may be used.

NOTES:

[1] Provided by supplied external DC power supply.
[2] User adjustable, factory set at 4 mA (± 0.5 mA). One control adjusts all channels.
[3] With ≥ 1M ohm input impedance of readout device.
[4] See PCB Declaration of Conformance PS024 for details.

SUPPLIED ACCESSORIES:

Model 017A01 Power Cord
Model 488A04 Universal AC power source

Entered:	Engineer:	Sales:	Approved:	Spec Number:
Date: 5-3-07	Date: 5/4/07	Date: 5/4/07	Date: 5/4/-7	6520

PCB PIEZOTRONICS™
ELECTRONICS DIVISION
3425 Walden Avenue, Depew, NY 14043

Phone: 716-684-0001
Fax: 716-684-0987
E-Mail: electronics@pcb.com

A8. Vicon MX13 Camera Specification Sheet

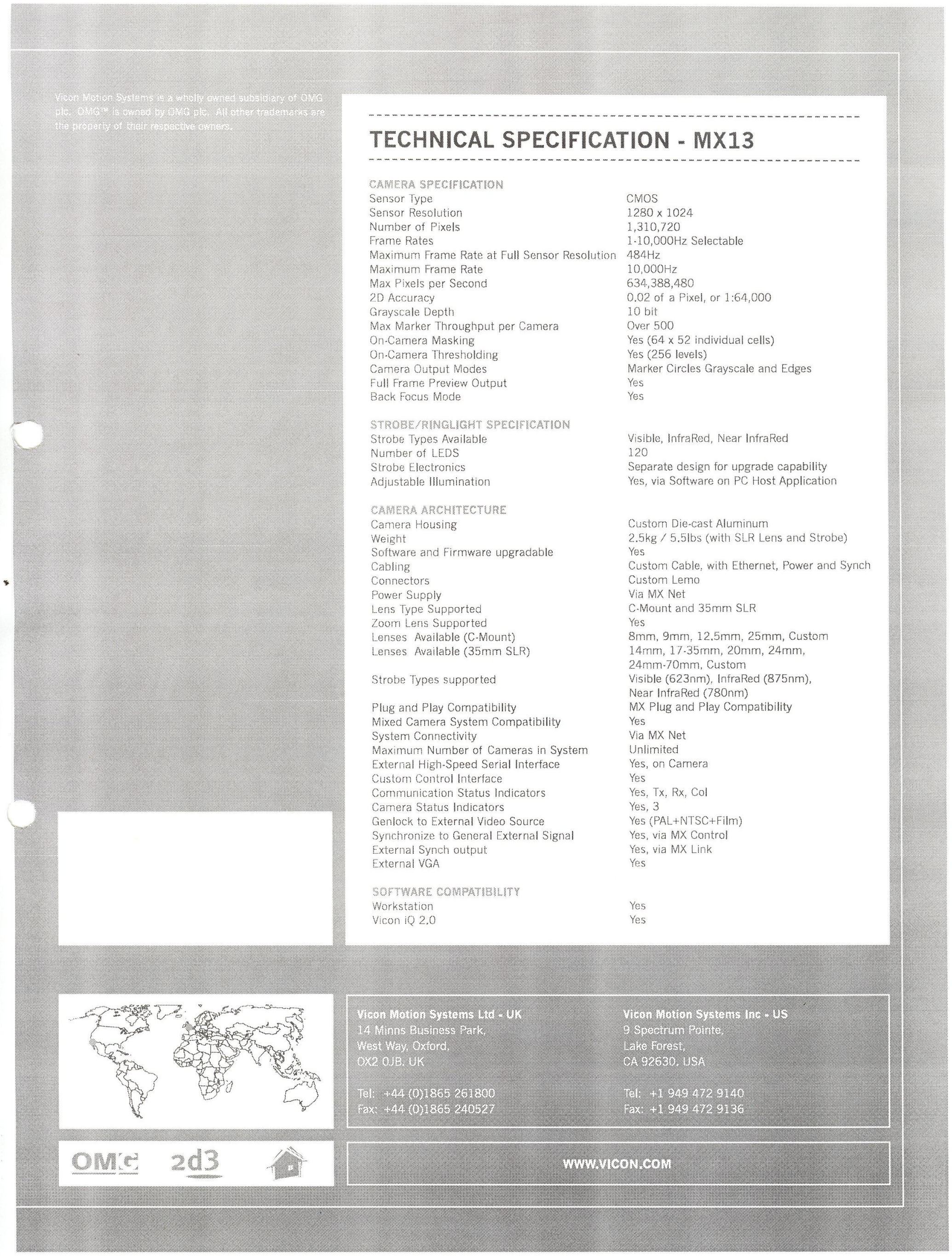

Vicon Motion Systems is a wholly owned subsidiary of OMG plc. OMG™ is owned by OMG plc. All other trademarks are the property of their respective owners.

TECHNICAL SPECIFICATION - MX13

CAMERA SPECIFICATION

Sensor Type	CMOS
Sensor Resolution	1280 x 1024
Number of Pixels	1,310,720
Frame Rates	1-10,000Hz Selectable
Maximum Frame Rate at Full Sensor Resolution	484Hz
Maximum Frame Rate	10,000Hz
Max Pixels per Second	634,388,480
2D Accuracy	0.02 of a Pixel, or 1:64,000
Grayscale Depth	10 bit
Max Marker Throughput per Camera	Over 500
On-Camera Masking	Yes (64 x 52 individual cells)
On-Camera Thresholding	Yes (256 levels)
Camera Output Modes	Marker Circles Grayscale and Edges
Full Frame Preview Output	Yes
Back Focus Mode	Yes

STROBE/RINGLIGHT SPECIFICATION

Strobe Types Available	Visible, InfraRed, Near InfraRed
Number of LEDS	120
Strobe Electronics	Separate design for upgrade capability
Adjustable Illumination	Yes, via Software on PC Host Application

CAMERA ARCHITECTURE

Camera Housing	Custom Die-cast Aluminum
Weight	2.5kg / 5.5lbs (with SLR Lens and Strobe)
Software and Firmware upgradable	Yes
Cabling	Custom Cable, with Ethernet, Power and Synch
Connectors	Custom Lemo
Power Supply	Via MX Net
Lens Type Supported	C-Mount and 35mm SLR
Zoom Lens Supported	Yes
Lenses Available (C-Mount)	8mm, 9mm, 12.5mm, 25mm, Custom
Lenses Available (35mm SLR)	14mm, 17-35mm, 20mm, 24mm, 24mm-70mm, Custom
Strobe Types supported	Visible (623nm), InfraRed (875nm), Near InfraRed (780nm)
Plug and Play Compatibility	MX Plug and Play Compatibility
Mixed Camera System Compatibility	Yes
System Connectivity	Via MX Net
Maximum Number of Cameras in System	Unlimited
External High-Speed Serial Interface	Yes, on Camera
Custom Control Interface	Yes
Communication Status Indicators	Yes, Tx, Rx, Col
Camera Status Indicators	Yes, 3
Genlock to External Video Source	Yes (PAL+NTSC+Film)
Synchronize to General External Signal	Yes, via MX Control
External Synch output	Yes, via MX Link
External VGA	Yes

SOFTWARE COMPATIBILITY

Workstation	Yes
Vicon iQ 2.0	Yes

Vicon Motion Systems Ltd - UK
14 Minns Business Park,
West Way, Oxford,
OX2 0JB, UK

Tel: +44 (0)1865 261800
Fax: +44 (0)1865 240527

Vicon Motion Systems Inc - US
9 Spectrum Pointe,
Lake Forest,
CA 92630, USA

Tel: +1 949 472 9140
Fax: +1 949 472 9136

WWW.VICON.COM

A9. Vicon T20 Camera Specification Sheet: Part 1

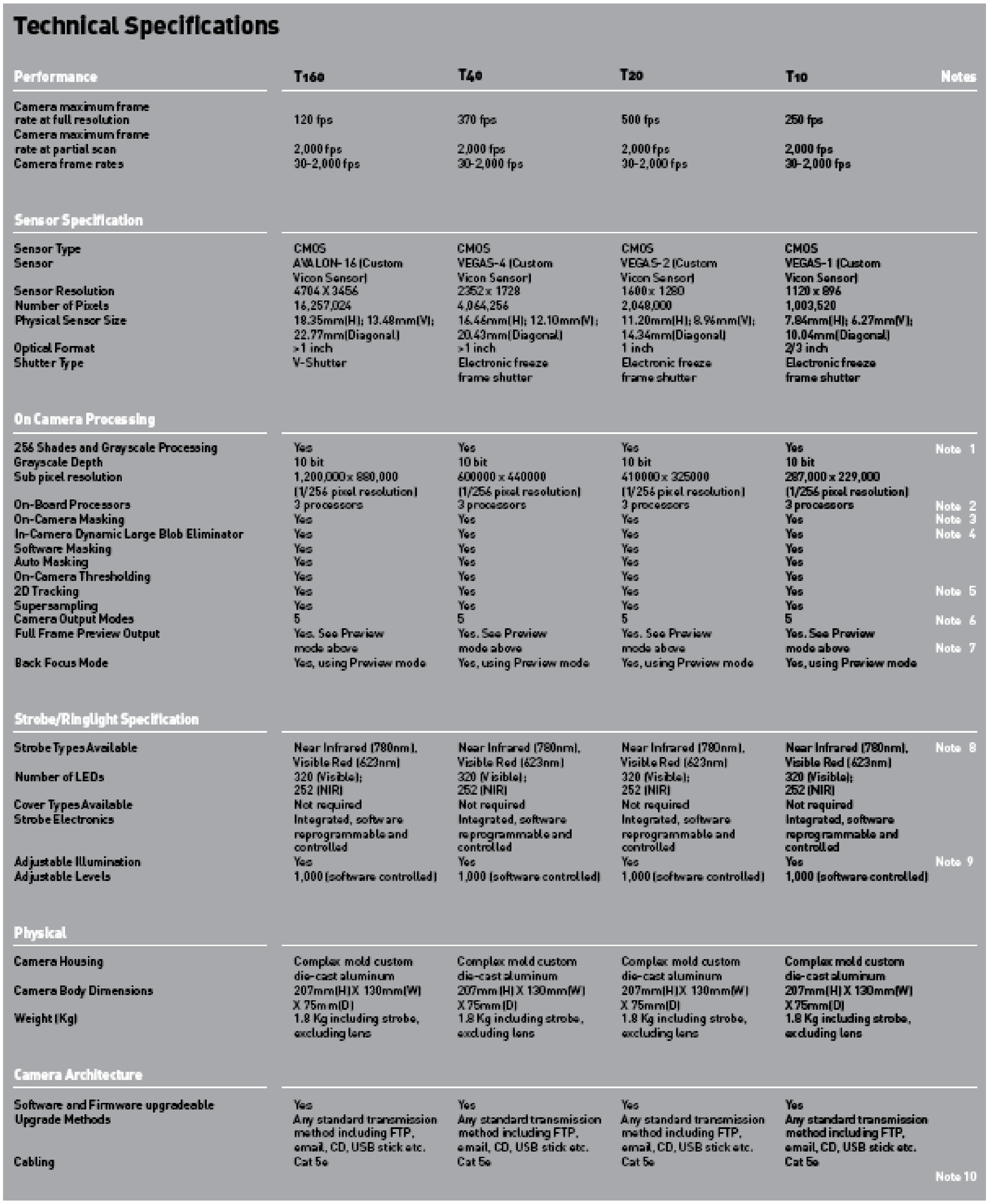

Technical Specifications

Performance	T160	T40	T20	T10	Notes
Camera maximum frame rate at full resolution	120 fps	370 fps	500 fps	250 fps	
Camera maximum frame rate at partial scan	2,000 fps	2,000 fps	2,000 fps	2,000 fps	
Camera frame rates	30-2,000 fps	30-2,000 fps	30-2,000 fps	30-2,000 fps	
Sensor Specification					
Sensor Type	CMOS	CMOS	CMOS	CMOS	
Sensor	AVALON-16 (Custom Vicon Sensor)	VEGAS-4 (Custom Vicon Sensor)	VEGAS-2 (Custom Vicon Sensor)	VEGAS-1 (Custom Vicon Sensor)	
Sensor Resolution	4704 X 3456	2352 x 1728	1600 x 1280	1120 x 896	
Number of Pixels	16,257,024	4,064,256	2,048,000	1,003,520	
Physical Sensor Size	18.35mm(H); 13.48mm(V); 22.77mm(Diagonal)	16.46mm(H); 12.10mm(V); 20.43mm(Diagonal)	11.20mm(H); 8.96mm(V); 14.34mm(Diagonal)	7.84mm(H); 6.27mm(V); 10.04mm(Diagonal)	
Optical Format	>1 inch	>1 inch	1 inch	2/3 inch	
Shutter Type	V-Shutter	Electronic freeze frame shutter	Electronic freeze frame shutter	Electronic freeze frame shutter	
On Camera Processing					
256 Shades and Grayscale Processing	Yes	Yes	Yes	Yes	Note 1
Grayscale Depth	10 bit	10 bit	10 bit	10 bit	
Sub pixel resolution	1,200,000 x 880,000 (1/256 pixel resolution)	600000 x 440000 (1/256 pixel resolution)	410000 x 325000 (1/256 pixel resolution)	287,000 x 229,000 (1/256 pixel resolution)	
On-Board Processors	3 processors	3 processors	3 processors	3 processors	Note 2
On-Camera Masking	Yes	Yes	Yes	Yes	Note 3
In-Camera Dynamic Large Blob Eliminator	Yes	Yes	Yes	Yes	Note 4
Software Masking	Yes	Yes	Yes	Yes	
Auto Masking	Yes	Yes	Yes	Yes	
On-Camera Thresholding	Yes	Yes	Yes	Yes	
2D Tracking	Yes	Yes	Yes	Yes	Note 5
Supersampling	Yes	Yes	Yes	Yes	
Camera Output Modes	5	5	5	5	Note 6
Full Frame Preview Output	Yes. See Preview mode above	Yes. See Preview mode above	Yes. See Preview mode above	Yes. See Preview mode above	Note 7
Back Focus Mode	Yes, using Preview mode	Yes, using Preview mode	Yes, using Preview mode	Yes, using Preview mode	
Strobe/Ringlight Specification					
Strobe Types Available	Near Infrared (780nm), Visible Red (623nm)	Near Infrared (780nm), Visible Red (623nm)	Near Infrared (780nm), Visible Red (623nm)	Near Infrared (780nm), Visible Red (623nm)	Note 8
Number of LEDs	320 (Visible); 252 (NIR)	320 (Visible); 252 (NIR)	320 (Visible); 252 (NIR)	320 (Visible); 252 (NIR)	
Cover Types Available	Not required	Not required	Not required	Not required	
Strobe Electronics	Integrated, software reprogrammable and controlled	Integrated, software reprogrammable and controlled	Integrated, software reprogrammable and controlled	Integrated, software reprogrammable and controlled	
Adjustable Illumination	Yes	Yes	Yes	Yes	Note 9
Adjustable Levels	1,000 (software controlled)	1,000 (software controlled)	1,000 (software controlled)	1,000 (software controlled)	
Physical					
Camera Housing	Complex mold custom die-cast aluminum	Complex mold custom die-cast aluminum	Complex mold custom die-cast aluminum	Complex mold custom die-cast aluminum	
Camera Body Dimensions	207mm(H) X 130mm(W) X 75mm(D)	207mm (H) X 130mm(W) X 75mm (D)	207mm(H) X 130mm(W) X 75mm(D)	207mm(H) X 130mm(W) X 75mm(D)	
Weight (Kg)	1.8 Kg including strobe, excluding lens	1.8 Kg including strobe, excluding lens	1.8 Kg including strobe, excluding lens	1.8 Kg including strobe, excluding lens	
Camera Architecture					
Software and Firmware upgradeable	Yes	Yes	Yes	Yes	
Upgrade Methods	Any standard transmission method including FTP, email, CD, USB stick etc.	Any standard transmission method including FTP, email, CD, USB stick etc.	Any standard transmission method including FTP, email, CD, USB stick etc.	Any standard transmission method including FTP, email, CD, USB stick etc.	
Cabling	Cat 5e	Cat 5e	Cat 5e	Cat 5e	Note 10

A10. Vicon T20 Camera Specification Sheet: Part 2

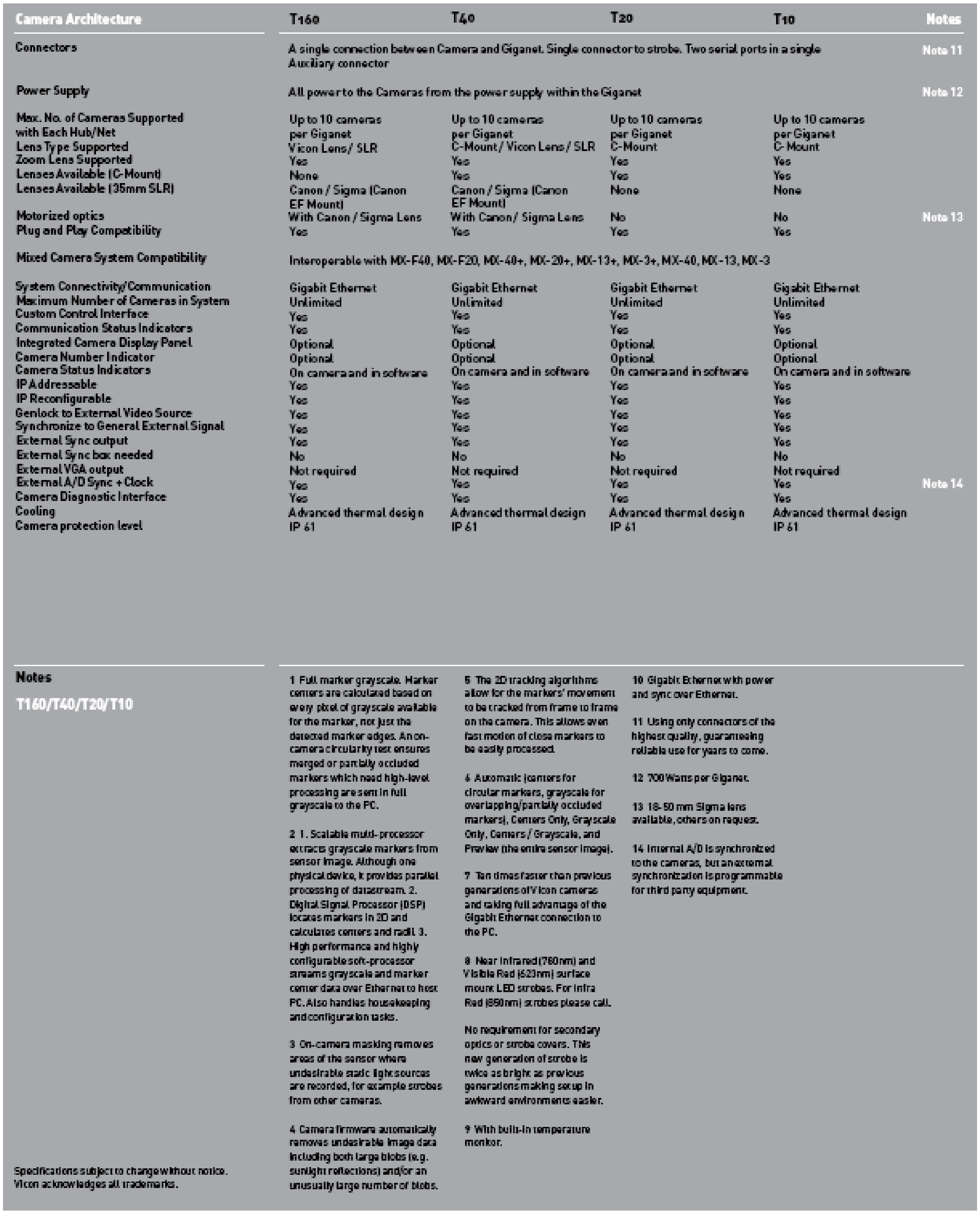

Camera Architecture	T160	T40	T20	T10	Notes
Connectors	A single connection between Camera and Giganet. Single connector to strobe. Two serial ports in a single Auxiliary connector				Note 11
Power Supply	All power to the Cameras from the power supply within the Giganet				Note 12
Max. No. of Cameras Supported with Each Hub/Net	Up to 10 cameras per Giganet	Up to 10 cameras per Giganet	Up to 10 cameras per Giganet	Up to 10 cameras per Giganet	
Lens Type Supported	Vicon Lens/ SLR	C-Mount / Vicon Lens / SLR	C-Mount	C-Mount	
Zoom Lens Supported	Yes	Yes	Yes	Yes	
Lenses Available (C-Mount)	None	Yes	Yes	Yes	
Lenses Available (35mm SLR)	Canon / Sigma (Canon EF Mount)	Canon / Sigma (Canon EF Mount)	None	None	
Motorized optics	With Canon / Sigma Lens	With Canon / Sigma Lens	No	No	Note 13
Plug and Play Compatibility	Yes	Yes	Yes	Yes	
Mixed Camera System Compatibility	Interoperable with MX-F40, MX-F20, MX-40+, MX-20+, MX-13+, MX-3+, MX-40, MX-13, MX-3				
System Connectivity/Communication	Gigabit Ethernet	Gigabit Ethernet	Gigabit Ethernet	Gigabit Ethernet	
Maximum Number of Cameras in System	Unlimited	Unlimited	Unlimited	Unlimited	
Custom Control Interface	Yes	Yes	Yes	Yes	
Communication Status Indicators	Yes	Yes	Yes	Yes	
Integrated Camera Display Panel	Optional	Optional	Optional	Optional	
Camera Number Indicator	Optional	Optional	Optional	Optional	
Camera Status Indicators	On camera and in software	On camera and in software	On camera and in software	On camera and in software	
IP Addressable	Yes	Yes	Yes	Yes	
IP Reconfigurable	Yes	Yes	Yes	Yes	
Genlock to External Video Source	Yes	Yes	Yes	Yes	
Synchronize to General External Signal	Yes	Yes	Yes	Yes	
External Sync output	Yes	Yes	Yes	Yes	
External Sync box needed	No	No	No	No	
External VGA output	Not required	Not required	Not required	Not required	
External A/D Sync + Clock	Yes	Yes	Yes	Yes	Note 14
Camera Diagnostic Interface	Yes	Yes	Yes	Yes	
Cooling	Advanced thermal design	Advanced thermal design	Advanced thermal design	Advanced thermal design	
Camera protection level	IP 61	IP 61	IP 61	IP 61	

Notes

T160/T40/T20/T10

1 Full marker grayscale. Marker centers are calculated based on every pixel of grayscale available for the marker, not just the detected marker edges. An on-camera circularity test ensures merged or partially occluded markers which need high-level processing are sent in full grayscale to the PC.

2 1. Scalable multi-processor extracts grayscale markers from sensor image. Although one physical device, it provides parallel processing of datastream. 2. Digital Signal Processor (DSP) locates markers in 2D and calculates centers and radii. 3. High performance and highly configurable soft-processor streams grayscale and marker center data over Ethernet to host PC. Also handles housekeeping and configuration tasks.

3 On-camera masking removes areas of the sensor where undesirable static light sources are recorded, for example strobes from other cameras.

4 Camera firmware automatically removes undesirable image data including both large blobs (e.g. sunlight reflections) and/or an unusually large number of blobs.

5 The 2D tracking algorithms allow for the markers' movement to be tracked from frame to frame on the camera. This allows even fast motion of close markers to be easily processed.

6 Automatic (centers for circular markers, grayscale for overlapping/partially occluded markers), Centers Only, Grayscale Only, Centers / Grayscale, and Preview (the entire sensor image).

7 Ten times faster than previous generations of Vicon cameras and taking full advantage of the Gigabit Ethernet connection to the PC.

8 Near Infrared (780nm) and Visible Red (623nm) surface mount LED strobes. For Infra Red (850nm) strobes please call.

No requirement for secondary optics or strobe covers. This new generation of strobe is twice as bright as previous generations making setup in awkward environments easier.

9 With built-in temperature monitor.

10 Gigabit Ethernet with power and sync over Ethernet.

11 Using only connectors of the highest quality, guaranteeing reliable use for years to come.

12 700 Watts per Giganet.

13 18-50 mm Sigma lens available, others on request.

14 Internal A/D is synchronized to the cameras, but an external synchronization is programmable for third party equipment.

Specifications subject to change without notice.
Vicon acknowledges all trademarks.

APPENDIX B

SUBJECT CONSENT FORMS

DATA ACQUISITION FOR THE ANALYSIS OF HUMAN MOVEMENTS
LAY SUMMARY

The study comprises a biomechanical analysis of the human response to impact. This analysis requires:

- Kinetic (i.e. force) and kinematic (velocity) measurements
- Subject-specific inertia and strength parameters
- Subjective ratings of impact intensities

This data will provide detailed information about current techniques used by humans to protect themselves against injury. The subject-specific parameters will be used to compare segment masses, in particular muscle mass, between subjects. Strength parameters will be used to distinguish between relaxed and tensed muscle states. While kinematic analysis will be performed to determine the mechanical impact intensity, subjects will be asked to rate their perception of the intensity. There will be absolutely no risk of injury during the trials as the level of impact will be less than that experienced in a regular contact training session.

The kinematic and kinetic data will be obtained through:

- A single high speed camera to obtain impactor velocities.
- A rig attached to a force plate used to measure joint forces.
- Thin film pressure sensors to measure impact force

The subject specific parameters will be obtained from:

- Anthropometric measurements of your preferred leg

Data will be acquired in the biomechanics research facilities in the University or in other research laboratories. Any data collection session will last no longer than 45 minutes, with the subject actively involved for only a fraction of the total time:

Actual performance of movements:	10 minutes
Anthropometric measurements:	10 minutes
Strength measurements:	2 minutes

A medical history questionnaire and full written consent will be required from the parent (if the subject is under the age of 18) or the subject prior to participation in the study.

DOCUMENTS WHEN SUBJECTS ARE AT LEAST 18 YEARS OF AGE

- INFORMATION FOR SUBJECTS
- PRE-SELECTION MEDICAL QUESTIONNAIRE
- INFORMED CONSENT FORM (SUBJECT)

INFORMATION FOR SUBJECTS

The study in which you have been invited to participate will involve a biomechanical analysis of human movement. The study will be divided into two parts; firstly, lengths, widths and circumferences of a body segment (i.e. leg) will be measured. It will also be necessary to take additional measurements to estimate your strength characteristics during various activities (i.e. knee extension). The measurement procedures will be described and demonstrated in advance. The data collected will be used to help increase our understanding of the mechanics of human movements.

The second part will require a video recording to be taken of you performing selected human movements. You will only be asked to perform movements that you are familiar with and feel comfortable performing such as those listed:

- Running
- Jumping
- Walking
- Carrying, bags rucksacks, books etc
- Ball skills
- Bat, racquet stick skills
- Throwing
- Kicking

You will perform the data collection in a suitable environment. The risk of injury during the data collection will be minimal since we will only ask you to perform movements with which you are familiar and comfortable. It is considered that no increased risks, discomforts or distresses are likely to result from the data collection of human movements above those associated with the normal performance of those movements.

The information obtained from the study will be collected and stored in adherence with the Data Protection Act. Whilst certain personal and training information will be required, you will be allocated a reference number to ensure that your identity and personal details will remain confidential. Video recordings will be stored in the video analysis room to which access is restricted to members of the biomechanics research team. The video images will be digitised and only the numerical values will be used in published work, not the images themselves. On occasion video images may be required. In such and instance we will seek your written permission to use such images and you are perfectly free to decline. Video recordings will be kept for three years after publication of the study. If you agree to take part in the study, you are free to withdraw from the study at any stage, with or without having to give any reasons. If you have any questions, concerns or general comments, please free to contact me:

Felix Tsui mmft2@lboro.ac.uk 07767796129

PRE-SELECTION MEDICAL QUESTIONNAIRE

LOUGHBOROUGH UNIVERSITY
DEPARTMENT OF PHYSICAL EDUCATION, SPORTS SCIENCE AND RECREATION MANAGEMENT

Please read through this questionnaire, BUT DO NOT ANSWER ANY OF THE QUESTIONS YET. When you have read right through, there may be questions you would prefer not to answer. Assistance will be provided if you require it to discuss any questions on this form. In this case please tick the box labelled "I wish to withdraw" immediately below. Also tick the box labelled "I wish to withdraw" if there is any other reason for you not to take part.

	tick appropriate box
I wish to withdraw	☐
I am happy to answer the questionnaire	☐

If you are happy to answer the questions posed below, please proceed. Your answers will be treated in the strictest confidence.

1. Are you at present recovering from any illness or operation? YES/NO*

2. Are you suffering from or have you suffered from or received medical treatment for any of the following conditions?

a. Heart or circulation condition YES/NO*
b. High blood pressure YES/NO*
c. Any orthopaedic problems YES/NO*
d. Any muscular problems YES/NO*
e. Asthma or bronchial complaints YES/NO*

3. Are you currently taking any medication that may affect your participation in the study? YES/NO*

4. Are you recovering from any injury? YES/NO*

5. Are you epileptic? YES/NO*

6. Are you diabetic? YES/NO*

7. Are you allergic to sticking plasters? YES/NO*

8. Do you have any other allergies? If yes, please give details below
YES/NO*

……………………………………………………………………………………………
…………………………………………………………………………………………
……………………………………………………………………………………………

9. Are you aware of any other condition or complaint that may be affected by participation in this study? If so, please state below;

……………………………………………………………………………………………
…………………………………………………………………………………………
……………………………………………………………………………………………
…………………………………………………………………………………………

* Delete as appropriate

INFORMED CONSENT FORM (SUBJECTS)

PURPOSE
To determine the role of muscle tension in impacts.

PROCEDURES
The kinematic and kinetic data of human movements will be obtained using:

- A high-speed camera
- A force plate
- Thin-filmed pressure sensors

ACTIVITIES
Possible activities of which only those to be undertaken will be listed

- Isometric knee extension
- Muscle Tensing

A number of trials will be requested with suitable breaks to minimise fatigue and boredom.

The subject specific parameters will be obtained from:

- Anthropometric measurements (using tape measures and specialist anthropometers)
- Isokinetic strength measurements

During the measurements two researchers will be present, at least one of whom will be of the same sex as you.

QUESTIONS
The researchers will be pleased to answer any questions you may have at any time.

WITHDRAWAL
You are free to withdraw from the study at any stage, with or without reason.

CONFIDENTIALITY
Your identity will remain confidential in any material resulting from this work.

I have read the outline of the procedures which are involved in this study, and I understand what will be required by me. I have had the opportunity to ask for further information and for clarification of the demands of each of the procedures and understand what is entailed. I am aware that I have the right to withdraw from the study at any time with no obligation to give reasons for my decision. As far as I am aware I do not have any injury or infirmity which would be affected by the procedures outlined.

Name …………………………………………

Signed ………………………………………… (subject) Date
……………………………
In the presence of:
Name …………………………………………

APPENDIX C

SOFT TISSUE RATIOS

The following explains how muscle and bone masses were calculated for § 5.2.7 and § 9.3. In Clarys et al. (1984), tissue weights as a percentage of body weight were found for skin (5.4%), adipose (28.4%), muscle (38.8%) and bone (13.5%). However, the percentage of adipose tissue was very high especially for an athlete, which was assumed to typically have no more than 10-15% body fat. As such, this extra adipose mass would have to be redistributed into a new combination of muscle and bone mass. This was conducted using an *All-To-Muscle (ATM)* and a *Ratio* method. The *All-To-Muscle* (ATM) method converted all excess adipose directly to muscle whilst the *Ratio* method kept the ratio between muscle and bone constant.

For example, assuming 15% body fat, the adjusted tissue percentages would be:

Tissue	Original	All To Muscle (ATM)	Ratio
Skin	5.4	5.4	5.4
Fat	28.4	15	15
Muscle	38.8	52.2	48.74
Bone	13.5	13.5	16.96

As both methods were likely the extremes for the redistribution of tissue masses, these values were averaged to provide a final proportion of tissue relative to whole body mass.

APPENDIX D

VICON BODYBUILDER CODE

```
{* VICON CODE for Kicking Variation Trials - RIGHT LEG *}
{*---------------------------------------------------------*}

{*** Define all optional points ***}

OptionalPoints(BLWall,TLWall,TRWall)
OptionalPoints(BLDummy,TLDummy,TRDummy,BRDummy)
OptionalPoints(RPSI,LPSI,LASI,RASI)
OptionalPoints(LKnee,MKnee,LAnk,MAnk)
OptionalPoints(Heel,MTMJ,LTMJ)

{*** DISPLAY AXIS (of each joint centre) MACRO ***}
{*'100' is the length of each axis*}
{*================================================*}

MACRO DisplayAxes (ASeg)
ASeg#O = ASeg(0)
ASeg#X = ASeg(0)+100*ASeg(1)
ASeg#Y = ASeg(0)+100*ASeg(2)
ASeg#Z = ASeg(0)+100*ASeg(3)
OUTPUT(ASeg#O,ASeg#X,ASeg#Y,ASeg#Z)
ENDMACRO



{*** HIP JOINT CENTRE ***}
{*Need Leg Length First and save as PARAM*}
{*=============================================*}

If $Static==1 then
```

```
MP_LegLength=DIST(RASI,LKnee)+DIST(LKnee,LAnk)
PARAM(MP_LegLength)
EndIf

{*** USE DAVIS ET AL. 1991 ***}

If $Static==0 then

SACR = (LPSI+RPSI)/2
PELF = (LASI+RASI)/2

Pelvis = [PELF,RASI-LASI,PELF-SACR,zxy]

RATD = 0.1288*MP_LegLength-48.56
LATD = RATD

MarkerDiameter=14
C = MP_LegLength*0.115-15.3
InterASISDist = DIST(LASI,RASI)
aa = InterASISDist/2
mm = MarkerDiameter/2
COSB = 0.951
SINB = 0.309
COST = 0.880
SINT = 0.476
COSTSINB = COST*SINB
COSTCOSB = COST*COSB

RHJC = {C*COSTCOSB-(RATD+mm)*SINB, C*COSTSINB-(RATD+mm)*COSB, -C*SINT+aa}*Pelvis
LHJC = {C*COSTCOSB-(LATD+mm)*SINB, C*COSTSINB-(LATD+mm)*COSB, C*SINT-aa}*Pelvis
HJC = (RHJC+LHJC)/2
```

```
OUTPUT(RHJC,LHJC,HJC)

{*** KNEE AND ANKLE JOINT CENTRES ***}

KneeJC = (LKnee+MKnee)/2
AnkJC = (LAnk+MAnk)/2
OUTPUT(KneeJC,AnkJC)

{*** LIMB SEGMENTS ***}

MTJJC = (LTMJ+MTMJ)/2
Foot = [AnkJC,MTJJC-AnkJC,LAnk-AnkJC,XYZ]
DisplayAxes(Foot)
OUTPUT(MTJJC)

{* Tibia *}
Tibia = [KneeJC,AnkJC-KneeJC,LAnk-AnkJC,XYZ]
DisplayAxes(Tibia)

{* Femur *}
Femur = [RHJC,KneeJC-RHJC,LKnee-KneeJC,XYZ]
DisplayAxes(Femur)


{*** JOINT ANGLES ***}

HipAngle = -<Pelvis,Femur,zyx>
KneeAngle = -<Femur,Tibia,zyx>
AnkleAngle = -<Tibia,Foot,zyx>

OUTPUT(HipAngle,KneeAngle,AnkleAngle)

EndIf
```

APPENDIX E

CALCULATION OF IMPACT ACCURACY

The following is an example calculation of the methodology used to obtain the local co-ordinate system (LCS) used to determine kick accuracy. This method was also used in the calculation of impact velocity but the dummy markers were replaced with the wall markers when calculating the LCS.

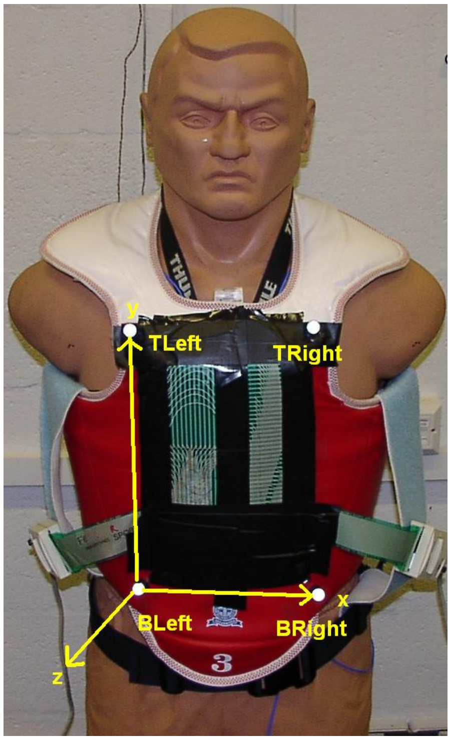

Dummy Marker Locations

(Global Co-ordinates shown)

BLDummy: (-141.861, 153.057, 158.147)
TLDummy: (-172.297, 142.923, 467.264)

TRDummy: (-168.384, 343.052, 476.65)

BRDummy: (-142.235, 362.545, 155.144)

Step 1. Set origin to BLDummy (i.e. bottom left marker)

Step 2. Establish x-axis using the vector between BRDummy and BLDummy markers and convert to a unit vector.
x-axis unit vector: (0.0194, 0.9987, 0.0471).

Step 3. Obtain a second vector from TLDummy and BLDummy and calculate the cross product of this vector and the x-axis unit vector.

This produces the z-axis unit vector.

z-axis unit vector: (0.9949, - 0.0239, 0.0972)

Step 4. Calculate the cross product between the x-axis unit vector and the z-axis unit vector.

This produces the y-axis unit vector.

y-axis unit vector: (-0.982, 0.449, 0.9941)

Step 5. Combine the three unit vectors into a transformation matrix. This matrix will convert co-ordinates from the Global Co-ordinate System (GCS) to the Local Co-ordinate System (LCS).

$$\underbrace{\begin{bmatrix} 0.0194 & -0.0982 & 0.9949 \\ 0.9987 & -0.0449 & -0.0238 \\ 0.0471 & 0.9941 & 0.0972 \end{bmatrix}}_{\mathit{Transformation\ matrix}} \begin{bmatrix} x_{GCS} \\ y_{GCS} \\ z_{GCS} \end{bmatrix} = \begin{bmatrix} x_{LCS} \\ y_{LCS} \\ z_{LCS} \end{bmatrix}$$

Step 6. Convert the co-ordinates of the midpoint of the foot into LCS at the moment of the first marker movement on the anvil.

APPENDIX F

CALCULATION OF RMSE, RESIDUALS AND 95% CONFIDENCE INTERVALS (95% CIs)

This section covers the calculation of Root Mean Square Error (RMSE), residuals and 95% Confidence Intervals (CIs) used in § 6 for the comparison of impact responses between custom ATDs and in vivo anvils.

Root Mean Square Error (RMSE) and Residual

A sample calculation of the RMSE and residual between the custom anvil, *MBOBXL,* and the in vivo trial, *S3 Pad*, are shown here.

The equation of the regression curve produced from MBOBXL impacts was used as its predictor model. This equation is:

$$y = 0.18x^{1.77}$$

Inputting each impact velocity obtained from the *S3, Pad* trial, a prediction of normalised impact force was obtained (*see* Table).

S3, Pad Trial Data			**Evaluation**		
Force (N)	**Normalised Force (N/kg)**	**Impact Velocity (m/s)**	**Prediction (N/kg)**	**RMSE**	**Residual**
111.97	1.80	7.18	5.99	17.54	4.19
670.65	10.78	9.42	9.67	1.23	-1.11
937.46	15.07	11.40	13.55	2.33	-1.53
1000.78	16.09	13.08	17.27	1.39	1.18
1696.36	27.27	14.34	20.31	48.45	-6.96
789.87	12.70	9.72	10.22	6.13	-2.48
920.64	14.80	12.07	14.98	0.03	0.18
971.43	15.62	11.82	14.44	1.39	-1.18
1106.31	17.79	13.64	18.59	0.65	0.81
990.72	15.93	13.08	17.27	1.79	1.34
1505.04	24.20	13.63	18.57	31.66	-5.63
1159.91	18.65	13.17	17.48	1.37	-1.17
		Overall		**3.08**	**-1.03**

The RMSE was calculated using equation 6.1 shown here:

$$\mathrm{RMSE}_y = \sqrt{\frac{\sum_{i=1} \left(f(x_i) - y_i\right)^2}{n}} \qquad (6.1)$$

In basic terms, the individual RMS column in the above table was the difference between the prediction and normalised force squared. The overall value at the bottom of the column sums up each individual RMSE, divides by the number of measurements and takes the square root.

In contrast, the residual calculates the difference between the predicted and actual normalised forces. This provides an idea of the direction of the prediction (i.e. higher or lower). This column was also averaged to provide an average residual.

95% Confidence Intervals (95% CIs)

A sample calculation of the CIs for the *S3, Pad* trial are shown here. A regression curve was first fit to the data of *S3, Pad*.

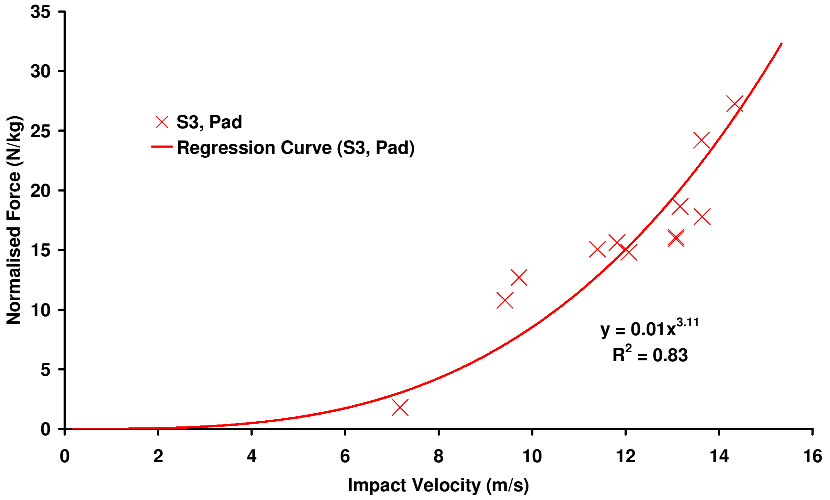

Using the same *S3, Pad* trial data in the table above, its 95% CI was calculated using equations 6.2 through to 6.4. These are shown again here:

$$CI = t_{n-2} * SE_{y,x} * \sqrt{\frac{1}{n} + \frac{\left(x_i - \bar{x}\right)^2}{SS_x}} \qquad (6.2)$$

$$SE_{y,x} = \sqrt{\frac{1}{(n-2)}\left[\sum\left(y-\bar{y}\right)^2 - \frac{\left[\sum\left(x-\bar{x}\right)\left(y-\bar{y}\right)\right]^2}{\sum\left(x-\bar{x}\right)^2}\right]} \tag{6.3}$$

$$SS_x = \sum\left(x_i - x\right)^2 \tag{6.4}$$

The width of the CI was dependent on the specific velocity used, but certain parameters were fixed such as:

$n = 12$

$SE_{y,x} = 2.78$

$\bar{x} = 11.88$

$\bar{y} = 15.89$

$SS_x = 49.83$

$t_{n-1} = 2.23$

These values were used, either directly or indirectly to solve for the 95% CI for the *S3, Pad* impact trials. At each velocity, the upper bound was created by adding the CI to the regression curve shown above, whilst the lower bound was created by subtracting the CI from the regression curve. This was conducted from 0 – 16 m/s for each *in vivo* impact trial to help produce 95% CIs shown in Figure 6.6.